Personal Exposure to Contaminant Sources in Ventilated Rooms

by

Henrik Brohus

This thesis is accepted for the degree of Doctor of Philosophy at the Faculty of Engineering and Science, Aalborg University, Denmark. Defended publicly at Aalborg University April 24, 1997.

Supervisor:
Peter V. Nielsen, Professor, Aalborg University, Denmark

Adjudication Committee:
P.O. Fanger, Professor, Technical University of Denmark, Denmark
Lars Olander, Professor, National Institute of Working Life, Sweden
Per Heiselberg, Associate Professor, Aalborg University, Denmark

ISSN 0902-7953 R9741

Henrik Brohus
Personal Exposure to Contaminant Sources in Ventilated Rooms
Ph.D.-Thesis
ISSN 0902-7953 R9741
Printed by Kolding Trykcenter, Denmark

Aalborg University
Department of Building Technology and Structural Engineering
Sohngaardsholmsvej 57
DK-9000 Aalborg
Denmark

Phone: +45 9635 8539
Fax: +45 9814 8243
E-mail: i6hb@civil.auc.dk
Web: www.civil.auc/i6/klima

Preface

This thesis is submitted in accordance with the conditions for attaining the Danish Ph.D.-degree.

It represents the end of my Ph.D.-study at Aalborg University, Department of Building Technology and Structural Engineering with Prof. Peter V. Nielsen as supervisor.

This research was supported financially by the Danish Technical Research Council (STVF) as part of the research programme “Healthy Buildings”, 1993 - 1997.

I wish to express my gratitude to Prof. Peter V. Nielsen for his guidance and for giving me the opportunity to fulfil this work.

My thanks also extend to Prof. P. Ole Fanger, Dr. Geo Clausen, Dr. Henrik Knudsen, Dr. Jan Pejtersen and the rest of the staff at the Laboratory of Heating and Air Conditioning for their hospitality and support during my stay at the Technical University of Denmark.

I would like to thank colleagues and members of the technical staff for their valuable assistance during the study. Especially, I want to thank Torben Christensen and Carl Erik Hyldgård for assistance in the laboratory, Bente Jul Kjærgaard for linguistic support, Norma Hornung for the drawings, and Dr. Kjeld Svidt for passing remarks on the work.

Finally, I want to thank my beloved family for their patience and support.

Henrik Brohus

February 1997

Abstract

Exposure models usually treat the indoor environment as well-mixed compartments without concentration gradients. However, in practice concentration gradients will occur, for instance, in the vicinity of contaminant sources or in the case of displacement ventilation.

When a person is located in a room where concentration gradients prevail, the local concentration distribution may be changed significantly and thus the personal exposure.

Three different tools for personal exposure assessment are presented. They are all able to consider the local influence of persons in ventilated rooms where concentration gradients prevail:

- the Breathing Thermal Manikin
- the Computer Simulated Person
- the Trained Sensory Panel

The tools are applied on the two major room ventilation principles, namely the displacement principle and the mixing principle. This is done in order to examine the tools and to investigate how the exposure assessment is influenced when concentration gradients and persons are considered.

A personal exposure model for a displacement ventilated room is proposed.

Two new quantities describing the interaction between a person and the ventilation are defined.

The findings clearly stress the need for an improved exposure assessment in cases where a contaminant source is located in the vicinity of persons.

It is also shown that it is not sufficient to know the local concentration level of an empty room, the local impact of a person is distinct and should be considered in the exposure assessment.

Contents

Chapter 1

Introduction

1.1. Importance of the indoor climate

In the industrial countries people spend the major part of their time in an indoor environment. Many people spend more than 90% of their time in an artificial climate i.e., offices, factories, public buildings, homes, transport vehicles etc. (Turiel, 1985; Awbi, 1991).

This fact stresses the importance of a healthy and comfortable indoor climate both regarding thermal comfort, indoor air quality, and other parameters constituting the indoor climate perceived by the occupants. In this thesis, the matter in question is the air quality.

Indoor air pollution

The indoor air is a complex mixture of outdoor air and different kinds of pollutants generated in the indoor environment. The outdoor air quality may vary from one location to another depending on possible outdoor contaminant sources, e.g. exhaust air from neighbouring buildings´ ventilation system, discharge from industrial processes, traffic etc.

Indoor air pollution (IAP) comes from the outdoor air, building materials, furniture and equipment, man and his activities. IAP may be inorganic pollutants (CO_2, CO, SO_2, NO_x etc.), organic pollutants (volatile organic compounds etc.), particulate matter, fibres, environmental tobacco smoke, radon, and different biological agents (house dust mites, fungi, and bacteria etc.). (McCarthy et al., 1991; Maroni et al., 1995).

Indoor environmental problems

Numerous cases of health complaints among employees in office buildings have occurred since the early 1970s. The complaints can be divided into two categories "those characterised by a generally clinical picture for which a specific cause has been identified, and those in which affected workers reported nonspecific symptoms occurring only during the time they were at work" (ECA, 1991). The first category is defined as the "building-related illness" (BRI) and the second category is defined as the "sick building syndrome" (SBS). Symptoms reported in SBS include mucous membrane and eye irritation, cough, chest tightness, fatigue, headache and malaise (Maroni et al., 1995).

A recent study on the indoor air quality in 56 European office buildings in nine countries reported that 30% of the occupants perceived the air as unacceptable although the average ventilation rate was way above existing national ventilation standards (Fanger, 1995).

Occupational health problems

While office workers are usually exposed to a larger number of indoor air pollutants at a low concentration, industrial workers may be exposed to fewer contaminants but at a higher concentration level. Serious health problems may occur if the workers are not sufficiently protected against exposure to the contaminants found in the industry.

1.2. Personal exposure assessment

The fact that many people spend the major part of their time in an artificial indoor environment, where they are subject to various contaminant sources, emphasises the importance of a proper exposure assessment.

Concentration gradients in ventilated rooms

When personal exposure in a ventilated room is to be determined one may choose to perform a series of measurements or to use a model for calculation. Both approaches may lead to erroneous results if they are not treated properly.

Exposure models usually treat the indoor microenvironments as well mixed compartments where the concentration of a certain component is found by a simple mass balance (Maroni et al., 1995). When the ventilated room is addressed the air is thus regarded as being fully mixed which implies that no concentration gradients exist.

Rodes et al. (1991) summarise various measurements from the literature and state that there may be considerable deviations between measurements using personal exposure monitors (PEM) and microenvironmental monitors (MEM). Typical PEM/MEM ratios were found in the interval from 1.58 to 13.40.
In practice concentration gradients will occur, for instance in the vicinity of contaminant sources and also in case of displacement ventilation, where contaminant stratification with considerable gradients is utilised to improve the ventilation effectiveness (Brohus and Nielsen, 1996b).

Interaction between a person and the environment

When a person is located in a ventilated room where concentration gradients prevail, the local concentration field may be changed significantly and thus the personal exposure. The reason is the local change in the flow field caused by the presence of the person, e.g. due to:

… the *excess surface temperature* of the human body generates a convective ascending air current along the body. This convective flow may entrain a contaminant in the lower part of the room and transport it to the breathing zone. In that way a person may be exposed to a concentration deviating substantially from the general concentration in the breathing zone height in other parts of the room.

… a person may locally act as an *obstacle* to the general flow field. For instance, if the person is exposed to a flow field coming from behind a wake is generated in

front of the person. This wake may entrain contaminant from a distance exceeding half a metre.

… when a person is *moving* the local flow field and the local contaminant field may change significantly. The effect of the ascending air flow in the human boundary layer will decrease according to the movements. The movements may also affect the general flow field and, therefore, indirectly the local field and thus the personal exposure.

If more persons are located near each other they may also affect the flow field and, furthermore, the exhalation from one person may penetrate another person's breathing zone and cause exposure (Bjørn and Nielsen, 1995; 1996).

Improved exposure models

The previous discussion raises a need for exposure models which are able to consider the local effect of persons located in ventilated rooms where concentration gradients prevail.

1.3. Definitions

Ventilation effectiveness

To describe the efficiency of an air distribution system, different quantities are commonly used. The mean ventilation effectiveness, $\bar{\varepsilon}$, is defined as

$$\bar{\varepsilon} = \frac{c_R}{\bar{c}} \tag{1.1}$$

where c_R is the concentration in the return opening and $\bar{c}$ is the mean concentration in the room. The ventilation effectiveness in the occupied zone, ε_{oc}, is given by

$$\varepsilon_{oc} = \frac{c_R}{c_{oc}} \tag{1.2}$$

where c_{oc} is the mean concentration in the occupied zone. Here, the occupied zone is defined as the area up to 1.8 m above floor level.

The local ventilation index, ε_P, is defined as

$$\varepsilon_P = \frac{c_R}{c_P} \tag{1.3}$$

where c_P is the concentration at a point in the room.

A new ventilation effectiveness will here be defined: the personal exposure index, designated ε_e

$$\varepsilon_e = \frac{c_R}{c_e} \tag{1.4}$$

where c_e is the concentration of inhaled contaminant. The personal exposure index expresses the effectiveness actually experienced by a person in the ventilated room. The new quantity and its use is discussed in more detail below.

Equations (1.1) to (1.4) assume that the supply air is uncontaminated.

Concentration, exposure and dose

Before the topic “personal exposure” is further discussed, it may be convenient to clarify the differences between the concepts of concentration, exposure and dose.

Exposure requires, strictly speaking, the simultaneous occurrence of two events: a pollutant concentration at a particular place and time, and the presence of a person at that place and time (Sexton and Ryan, 1988). Expressed in another way, exposure is defined as the event during which a person comes into contact with a pollutant.

Dose occurs when the pollutant actually crosses the physical boundary of a person. consequently, there can be an exposure without a dose but there cannot be a dose without an exposure (Ott, 1985). This implies that persons exposed to the same level may receive different doses if the pulmonary ventilation varies due to different activity levels (Tjelflaat, 1992; Brohus and Nielsen, 1994b).

The concentration of inhaled contaminant, c_e, corresponds to the exposure of a person. It represents the event during which a person is in contact with a pollutant. Subsequently c_e is designated "exposure" as well as "concentration of inhaled contaminant".

To compare the exposure and the concentration, c_P, measured at a "neutral" point at the breathing zone height, both quantities should in theory be determined at the same location, but in case of c_P without the local influence of the person (movements, convective boundary layer flow, etc.). In this way the difference between ε_e and ε_P is due solely to the person´s presence. The importance of making this distinction will appear clearly in the following chapters.

In practice, c_P is measured at the breathing zone height outside the thermal boundary layer some distance away from the person. Alternatively, the person in question is temporarily moved while measuring c_P at the point of interest.

The dose rate, $\dot{m}_e$, is found by

$$\dot{m}_e = \dot{m}_{res} c_e \tag{1.5}$$

where

$\dot{m}_e$ = Dose rate of inhaled contaminant (kg/s)
$\dot{m}_{res}$ = Pulmonary ventilation (kg/s), see equation (2.28)
c_e = Personal exposure (kg/kg)

The dose, m_{ed}, is found by integration

$$m_{ed} = \int_{\tau_s}^{\tau_e} \dot{m}_{res} c_e \, d\tau \tag{1.6}$$

where

m_{ed} = Dose of inhaled contaminant (kg)
τ = Time (s)
τ_s = Start time (s)
τ_e = Stop time (s)

If the dose is modelled the time integral may approximately be divided into N finite time steps, $\Delta\tau$

$$m_{ed} = \sum_{i=1}^{N} \dot{m}_{res,i} c_{e,i} \Delta\tau_i \tag{1.7}$$

In this case $c_{e,i}$ may be found as a steady-state personal exposure for each of the time intervals.

1.4. Aims and scope

The aim of the present work is to investigate the topic: personal exposure to contaminants in ventilated rooms. Both the concentration gradients and the local influence of a person will be considered when the personal exposure is assessed.

Different tools for exposure assessment are introduced and applied on the two major ventilation principles, the displacement principle and the mixing principle.

It is also the aim to gain more knowledge regarding the importance of considering the local influence of the person, and to develop and apply new and improved exposure models.

Only personal exposure due to gaseous contaminants (or smaller particles < 10 μm) is considered, where the exposure takes place solely in connection with the respiration.

Most of the results arise from steady-state conditions even though some measurements include the transient behaviour of real people.

Chapter 2

Tools for personal exposure assessment

2.1. Introduction

In Chapter 1 the importance of a proper exposure assessment was stated together with the need for tools which are able to include the local influence of persons in ventilated rooms where concentration gradients prevail.

This chapter will present three different tools for personal exposure assessment which are all able to consider the local influence of a person in different ways:

1. A Breathing Thermal Manikin which is a heated full-scale model of a person equipped with an artificial lung to simulate respiration. Tracer gas is used to simulate contaminant dispersion.

2. A Computer Simulated Person which is a numerical model of a person applied in Computational Fluid Dynamics, where the flow field and the contaminant transport are simulated.

3. A Trained Sensory Panel which is a group of persons trained to judge the air quality in comparison with references with known levels of perceived air quality.

In the following each of the three tools is presented together with the theoretical background, and in Chapter 3 and Chapter 4 the tools are applied in case of displacement ventilation and mixing ventilation, respectively.

2.2. Breathing Thermal Manikin

2.2.1. Introduction

In this Chapter 2.2. the Breathing Thermal Manikin will be introduced.

As mentioned in Chapter 1 the heat transfer between a person and the surrounding environment may exert a significant influence on the personal exposure, mainly due to the ascending air current along the person caused by the excess surface temperature compared with the surrounding air.

The respiration may also influence the exposure and, especially, the dose.

In the subsequent chapter the different modes of heat transfer from persons are described with special emphasise on the convective and radiative heat loss. Then the topic of respiration is shortly introduced and, finally, the Breathing Thermal Manikin is described together with the procedure applied when the manikin is used for personal exposure assessment.

2.2.2. Heat transfer from persons

2.2.2.1. Modes of heat transfer

A person produces heat according to the metabolism which depends on the activity level. The heat production is either stored in the body or it is dissipated to the environment through the skin and through the respiratory system. The different modes of heat transfer are summarised in Figure 2.1.

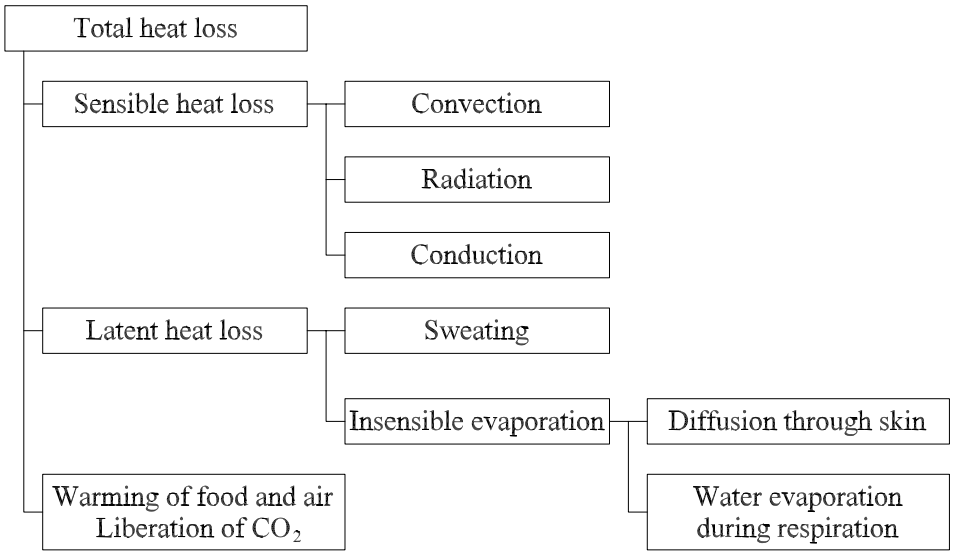

Figure 2.1. Modes of heat transfer from a person. The net amount of heat, i.e. the metabolic energy subtracted the amount of useful mechanical work, is either stored or transferred to the environment.

If the amount of energy for warming of food and air and for liberation of CO_2 is ignored, the human energy balance may be expressed as (ASHRAE, 1993)

$$M - W = Q_{sk} + Q_{res} + S_{body} \tag{2.1}$$

where

M = Rate of metabolic heat produced (W/m^2)
W = Rate of mechanical work accomplished (W/m^2)
Q_{sk} = Total rate of heat loss through skin (W/m^2)
Q_{res} = Total rate of heat loss through respiration (W/m^2)
S_{body} = Rate of heat storage in body (W/m^2)

The heat loss through the skin and the heat loss through the respiratory system may be expressed by the following two equations

$$Q_{sk} = C + R + K + E_{sk} \tag{2.2}$$

where

C = Rate of convective heat transfer from skin (W/m^2)
R = Rate of radiative heat transfer from skin (W/m^2)
K = Rate of conductive heat transfer from skin (W/m^2)
E_{sk} = Rate of total evaporative heat loss from skin (W/m^2)

Here, $C + R + K$ is known as the sensible heat loss from the skin or the clothing.

$$Q_{res} = C_{res} + E_{res} \tag{2.3}$$

where

C_{res} = Rate of convective heat loss from respiration (W/m^2)
E_{res} = Rate of evaporative heat loss from respiration (W/m^2)

If the energy balance is steady-state the storage term, S_{body}, will be zero. In this work only the steady-state heat balance will be considered.

The four modes of heat transfer involved in the energy balance above are conduction, convection, radiation, i.e. sensible heat, and evaporation, i.e. latent heat, which will be shortly described in turn.

Heat is a transfer of energy from places where the temperature (i.e. the internal energy) is high to places where the temperature is lower. When heat passes through solids or through fluids which are not moving the process is called conduction. Heat transfer by conduction takes place when part of the skin or the clothing of a person touches a surface, i.e. from the soles of the feet to the shoes, or when the person is in direct contact with a bed or a chair. Usually, conduction only accounts for a very small amount of the total heat loss and it is therefore often ignored.

When heat is transferred by means of a moving fluid (liquid or gas phase) it is called convection. Convective heat transfer from persons is a very important parameter to consider when dealing with personal exposure assessment. Apart from transferring heat from the person to the environment an ascending air current along the body is generated with a substantial ability to transport contaminated air from the lower part of the body to the breathing zone where it eventually leads to exposure of the person. Convective heat transfer is treated in more detail in Chapter 2.2.2.2.

Heat transfer by radiation takes place by means of electromagnetic waves that are generated by molecular vibrations from heated surfaces. Heat radiation is the name for part of the electromagnetic radiation spectrum extending from the visible wavelengths (0.4 - 0.8 μm) to the much longer radio waves (Kerslake, 1972). These waves travel away from the body with the speed of light leaving the surface cooler and, at the same time, heating surrounding surfaces with temperatures lower than the surface temperature of the person. Calculation of radiative heat transfer is discussed in Chapter 2.2.2.3.

Evaporation is the mode of heat transfer where vapour diffuses away from the surface of exposed liquid with the extraction of latent heat from the remaining liquid. Sweating is a very important thermoregulatory mechanism, for instance when persons are doing strenuous exercises or they are located in a hot climate evaporative heat transfer may be the dominating way of heat removal.

Evaporation through the skin surface may also take place by diffusion of water vapour even though no sweating occurs and the skin seems dry. Together with evaporation during respiration it is known as insensible evaporation (Clark and Edholm, 1985).

The total heat loss from the body may vary from about 100 W at sedentary activity level to more than 1000 W during athletic activities (Fanger, 1972).

Usually, the heat output from persons is calculated as a heat flux in W/m^2 using the surface area of the person. The body surface area, A_{Du}, may be described as a function of weight and height (DuBois and DuBois, 1916)

$$A_{Du} = 0.20236 \cdot W_e^{\,0.425} \cdot H^{\,0.725} \qquad (2.4)$$

where

A_{Du} = DuBois surface area (m^2)
W_e = Weight (kg)
H = Height (m)

The partition of heat loss by the different routes depends highly on the activity level, the kind of activity and the surrounding environment. In absence of strenuous exercises and visible sweating the relative partition of heat loss may be described as follows in Table 2.1.

Table 2.1. Partition of heat loss from persons by different modes (Clark and Edholm, 1985; Åstrand and Rodahl, 1986; Asmussen and Nielsen, 1989).

Sensible heat loss ~ 75 % Convection and radiation amounts for approximately one half of the sensible heat transfer each one.
Latent heat loss ~ 25 % The insensible water loss may range from approximately equal amounts from the respiration and the skin surface, to a dominating evaporative heat loss from the skin surface. When visible sweating occurs it may dominate the total heat loss.
Conduction etc. Heat transfer by conduction (usually less than 1 - 2 % of total) and by warming of food and air and liberation of CO_2 (less than 10 % of total) is normally ignored.

2.2.2.2. Convection

In the following chapter the convective heat transfer and flow will be discussed in more detail including a working relation for the overall convective heat transfer coefficient for a person.

Some important non-dimensional numbers will be mentioned which relate the heat transfer to the type of flow. Using these numbers it is possible to determine the kind of flow occurring around the person, i.e. laminar or turbulent flow, free or forced convective flow, etc.

The physiological aspects are discussed and the dimensionless numbers are applied on a simple cylinder model of a person.

Free convection

The convective heat transfer may be expressed as

$$C = h_c\left(t_s - t_a\right) \tag{2.5}$$

where

C = Rate of convective heat transfer (W/m^2)
h_c = Convective heat transfer coefficient (W/m^2°C)
t_s = Skin temperature (or surface temperature of clothing) (°C)
t_a = Ambient temperature (°C)

Even though the convection seems to be proportional to the temperature difference in the above formula it happens to be non-linear because the coefficient, h_c, depends on the temperature difference itself. Apart from the temperature difference, h_c also depends on the type of flow. This dependence may be expressed by means of non-dimensional numbers.

The variables describing a certain physical problem (in this case the flow around a person) may be numerous. By application of dimensional analysis these dependent variables are combined in a few non-dimensional groups.

The convective heat transfer coefficient is part of the Nusselt number which may be thought of as a dimensionless group incorporating this quantity in dimensionless form

$$Nu = \frac{h_c L}{k} \tag{2.6}$$

where

Nu = Nusselt number (n.d.)
L = Characteristic length (m)
k = Thermal conductivity of the surrounding fluid (W/m°C)

In usual indoor environments where people are present the ambient air temperature will be lower than the temperature of the skin or the clothing. The air which is in close contact with the person will thus be heated by conduction.

Due to the buoyancy of the warm air it will ascent along the entire person creating a natural convection boundary layer.

The flow is termed as free convection if not disturbed by a dominating flow field in the surroundings.

The mathematical expression governing the free convection flow is the Grashof number, *Gr*. In the application of a person *Gr* may be written as (Clark and Toy, 1975a)

$$Gr = \frac{gH^3\left(T_s - T_a\right)}{\nu^2 T_a} \tag{2.7}$$

where

Gr = Grashof number (n.d.)
g = Gravitational acceleration (9.82 m/s^2)
H = Vertical height of the body (m)
ν = Kinematic viscosity (m^2/s)
T_s = Absolute temperature of the skin (K)
T_a = Absolute temperature of the ambient air (K)

The Grashof number is proportional to the ratio of the buoyancy to the viscous forces within the air flow. The size of *Gr* determines the characteristics of the flow (Clark and Edholm, 1985)

$Gr < 10^9$ Laminar flow

$Gr > 10^{10}$ Turbulent flow

As will be shown later, it is possible for the boundary layer flow to remain laminar over the entire height of the person, especially if the person is clothed.

Apart from *Gr* the free convection heat transfer is governed by the Prandtl number

$$\mathrm{Pr} = \frac{c_p \mu}{k} = \frac{\nu}{\alpha} \tag{2.8}$$

where

Pr = Prandtl number (n.d.)
c_p = Specific heat of ambient air at constant pressure (J/kg°C)
μ = Dynamic viscosity (kg/m s)
k = Thermal conductivity (W/m°C)
ν = Kinematic viscosity (m^2/s)
α = Thermal diffusivity (m^2/s)

The Prandtl number is a physical property of the fluid itself related to the relative rates of transport of momentum and energy by the elements of the fluid. The kinematic viscosity, ν, determines the way in which momentum is transferred across a velocity gradient, and the thermal diffusivity, α, determines the way in which heat is transferred across a temperature gradient, thus Pr connects the momentum transfer with the heat transfer.

It can be shown by using dimensional analysis that during free convection the three dimensionless groups mentioned earlier are related by the expression (Holman, 1989)

$$Nu_{free} \propto \mathrm{Pr}^{m}\, Gr^{n} \tag{2.9}$$

In the usual range of applications Pr is approximately constant, i.e.

$$Nu_{free} = a \cdot Gr^{n} \tag{2.10}$$

Here, a and n may be determined empirically by means of measurements on persons or by using an approximation where the person is simulated by a heated cylinder which is not too slender.

Forced convection

If a person is exposed to a velocity field where the speed is considerable the flow may change into forced convection. In case of forced convection the convective heat transfer coefficient does not depend on a temperature difference between the skin and the environment. The flow depends on the Reynolds number, Re, which is proportional to the ratio of fluid inertial forces to viscous forces.

$$\mathrm{Re} = \frac{UD}{\nu} \tag{2.11}$$

where

Re = Reynolds number (n.d.)
U = Free stream velocity (m/s)
D = Characteristic length (m)
ν = Kinematic viscosity (m^2/s)

The size of *Re* determines whether the flow is laminar or turbulent (Schlichting, 1979; Clark and Edholm, 1985)

Re < $2 \cdot 10^5$ Laminar flow

Re > $2 \cdot 10^5$ Turbulent flow

Here, the characteristic length, *D*, in *Re* is taken as the diameter of a cylinder with the same height and the same surface area as a person.

The convective heat transfer coefficient incorporated in *Nu* may be determined as (Holman, 1989)

$$Nu_{forced} \propto \mathrm{Pr}^m \, \mathrm{Re}^n \tag{2.12}$$

and as *Pr* is approximately constant

$$Nu_{forced} = a \cdot \mathrm{Re}^n \tag{2.13}$$

for smooth cylinders in normal air environments. If the characteristic length in *Nu* and *Re* is termed *L*, we have

$$\frac{h_c L}{k} = a \frac{U^n L^n}{\nu^n} \tag{2.14}$$

and thus

$$h_c = \frac{akL^{n-1}}{\nu^n} U^n \cong b \cdot U^n \tag{2.15}$$

where b may vary in general but will be constant for a fixed L and a fixed environment. A number of different working relations for h_c exist (see e.g. ASHRAE, 1993), for instance

$$h_c = 4.0 \qquad 0 \text{ m/s} < U < 0.15 \text{ m/s} \tag{2.16}$$

$$h_c = 14.8 \cdot U^{0.69} \qquad 0.15 \text{ m/s} < U < 1.5 \text{ m/s} \tag{2.17}$$

which are valid for a standing person in moving air.

The h_c above is the overall convective heat transfer coefficient. The local coefficient may vary both with respect to the height and also around the circumference of the body. For instance, Clark and Toy (1975b) measured the local convective heat transfer coefficient around the head, see Figure 2.2.

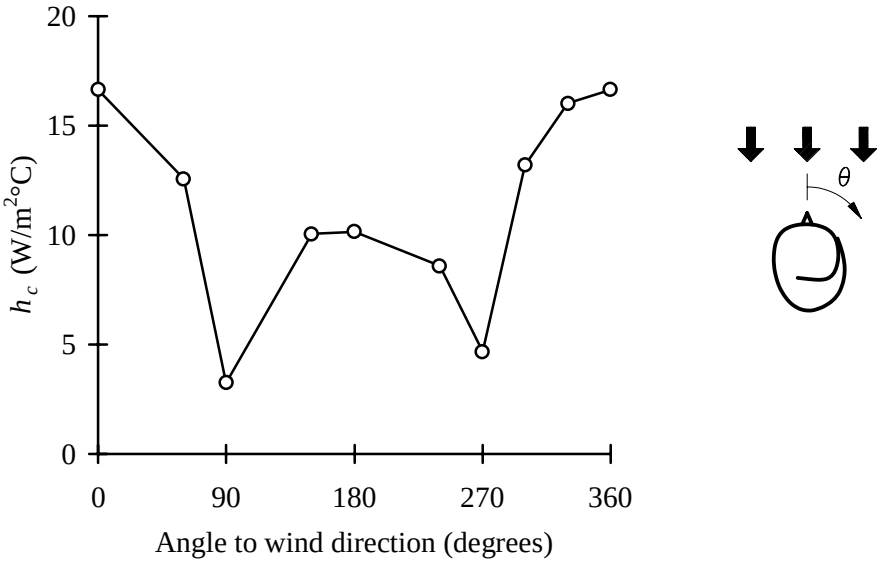

Figure 2.2. Variation of the local convective heat transfer coefficient h_c (W/m^2°C) from the head with the angle, θ, to the flow in an air stream of 0.8 m/s. Reproduced from Clark and Toy, 1975b.

The above dependence of the angle shows a very close agreement with the flow around a cylinder (Holman, 1989).

The local convective heat transfer coefficient may vary highly in vertical direction in case of free convection due to the development of the boundary layer thickness. For instance, Murakami et al. (1995) found a local h_c - variation between 2 W/m^2°C (upper part) and 7 W/m^2°C (at the feet) for a computer simulated person standing in a stagnant flow, see also Appendix C.

Mixed free and forced convection

The temperature difference between the surface of a person and the surroundings creates a buoyancy that may highly affect the free stream locally around a person. This fact means that a relatively high velocity level is required to establish a state of forced convection. In many cases mixed free and forced convection will occur when a person is located in a certain velocity field. In this case the flow will depend on both *Gr* and *Re* that may be combined into another non-dimensional group, the Archimedes number

$$Ar = \frac{Gr}{\mathrm{Re}^2} = \frac{gH\left(T_s - T_a\right)}{U^2 T_a} \tag{2.18}$$

The Archimedes number, *Ar*, expresses the relative influence of buoyancy forces versus the inertial forces within the fluid. Using *Ar*, it is possible to determine the type of flow (Clark and Cox, 1973) as shown in Table 2.2.

Table 2.2. Flow characteristics described as a function of the non-dimensional Archimedes number (Clark and Cox, 1973).

Ar (n.d.)	**Type of flow**
0-0.06	Forced convection
0.06 - 16	Mixed flow
> 16	Free convection

Some physiological aspects

In many cases it is possible to simulate the body heat loss by using a uniformly heated model, for instance, a cylinder where the heat loss continues to rise with increasing air speed. However, the thermoregulatory mechanisms of the human body can alter the heat loss by changing the surface temperature. This may be done by varying the blood supply to the skin, and also by changing the latent heat loss (sweating and water diffusion through the skin).

Clark and Edholm (1985) showed some local heat loss measurements on a person where the heat loss reached a maximum value and then began to decrease, even though the wind speed was increased.

Another physiological parameter that may act differently on a human being than on a heated model is the effect of movements. When a person walks or runs only the head and the trunk move in a linear or unidirectional fashion. The upper arms and thighs perform a “pendulum” motion and the forearms and lower legs have a whiplash movement (Clark and Edholm, 1985).

This “pendulum” movements produce a different air flow pattern from the one found assuming a uniform translation during movements. Clark and Edholm (1985) suggest that the convective heat transfer coefficient for the swinging parts should be increased by a factor of approximately 2 compared with uniform translation.

Cylinder model of person

To give an example on the usage of the above-mentioned dimensionless numbers, a cylinder model of a person is applied in the following. This also gives an idea of the characteristics of the flow around the person including the influence of different insulation values of the clothing.

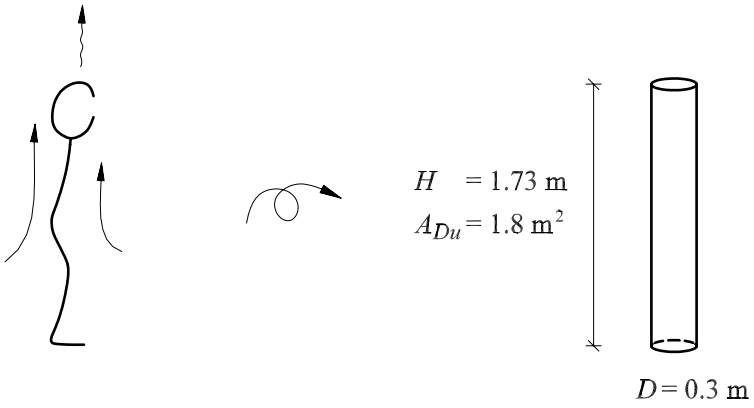

Figure 2.3. Cylinder model of an average sized person.

In Figure 2.3. the cylinder model of an average sized person is shown. The height is 1.73 m and the weight is 70 kg corresponding to a surface area of 1.8 m^2 (ASHRAE, 1993). The person is modelled by a cylinder with a height of 1.73 m and a diameter of 0.3 m.

The Reynolds number may be found if the cylinder diameter is taken as the characteristic length and the temperature of the ambient air is 20°C.

$$\mathrm{Re} = \frac{UD}{\nu} = \frac{U \cdot 0.3}{15.11 \cdot 10^{-6}} \cong 2 \cdot 10^4 \cdot U \tag{2.19}$$

For $Re = 2 \cdot 10^5$ the flow around the person (cylinder) is turbulent which in this case corresponds to a free stream velocity of 10 m/s, i.e. well above velocities obtained in usual indoor environments.

If the surroundings are quiescent we may determine the kind of flow in the natural convection boundary layer along the person by means of the Grashof number. This is done for three different cases corresponding to different thermal insulation values of the clothes.

For a naked person (I_{cl} = 0 clo) the skin temperature is taken as 33.7 °C which is the "neutral value" obtained when the body maintains its thermal equilibrium with the environment with minimum regulatory effect (ASHRAE, 1993). Using this

skin temperature it is possible to calculate the surface temperature of the clothing, t_{cl}, for a certain insulation value of the clothes, I_{cl}, see Appendix A. For typically indoor summer clothes (I_{cl} = 0.5 clo), t_{cl} = 29.8°C, and for a typically indoor winter clothes (I_{cl} = 1.0), t_{cl} = 26.0°C. If the ambient air temperature is kept at 20°C the following relationship between the local Grashof number and the vertical distance is found for the three cases, see Figure 2.4.

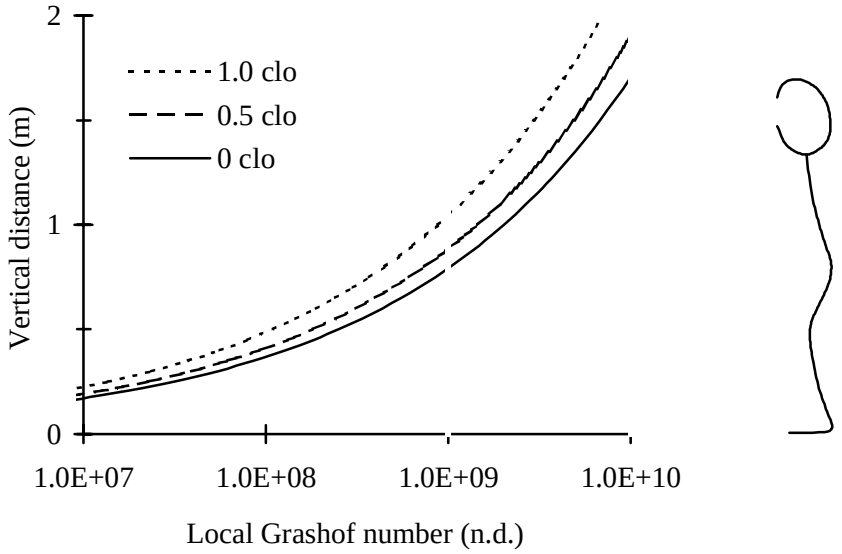

Figure 2.4. Vertical variation of the local Grashof number, *Gr*, for a person in surroundings of 20°C when the person is naked (0 clo), wearing summer clothes (0.5 clo) and wearing winter clothes (1.0 clo). When $Gr < 10^9$ the flow is laminar, and when $Gr > 10^{10}$ the flow is turbulent which is indicated by the two vertical lines.

In Table 2.3. the Archimedes number, *Ar*, is used to estimate the velocity level of a uniform free stream around a person necessary to achieve a certain type of flow. The results in Table 2.3. are based on a calculation of the free stream velocity, *U*, for a person with a height of 1.73 m standing in surroundings of 20°C. When $Ar < 0.06$ the flow is forced convection and when $Ar > 16$ the flow around the person is free convection.

The velocity levels obtained for the free convection case correspond well with measurements and observations by Brohus and Nielsen (1994a) and Hyldgaard (1994).

Table 2.3. Uniform free stream velocity, *U*, necessary to obtain free convection and forced convection around a person, respectively, for three insulation values of the clothing. When the velocity level is found between the two flow types mentioned in the table, the flow is termed mixed free and forced convection.

Uniform free stream velocity around a person, *U*		
Clothing insulation (clo)	Type of convective flow	
	Free (m/s)	Forced (m/s)
0	0.22	3.64
0.5	0.19	3.08
1.0	0.15	2.40

2.2.2.3. Radiation

Radiative heat loss from persons may be found by using an application of the Stefan-Boltzmann equation for radiative heat transfer.

The surface area of naked persons should be turned into an effective radiation area, i.e. the area of the person actually exposed to the radiation. This area should also consider the effect of clothing.

$$A_{eff} = f_{eff}\, f_{cl}\, A_{Du} \tag{2.20}$$

where

A_{eff} = Effective radiation area (m^2)
A_{Du} = DuBois area (naked surface area of the person) (m^2)
f_{eff} = Effective radiation area factor (n.d.)
f_{cl} = Clothing area factor (n.d.)

Fanger (1972) found the effective radiation area factor, f_{eff}, to be 0.696 for sedentary body position and 0.725 for a standing person. The clothing area factor, f_{cl}, can be found by (McCullough et al., 1989)

$$f_{cl} = \frac{A_{cl}}{A_{Du}} = 1 + 0.3 I_{cl} \tag{2.21}$$

where

A_{cl} = Clothed surface area (m^2)
I_{cl} = Clothing insulation (clo)

The radiative heat loss may then be expressed as

$$\Phi_r = A_{eff}\, \varepsilon \sigma \left[T_s^{\,4} - \overline{T}_r^{\,4} \right] \tag{2.22}$$

where

Φ_r = Radiative heat loss (W)
ε = Average emissivity of clothing and body area (n.d.)
σ = Stefan-Boltzmann constant ($5.669 \cdot 10^{-8}$ W/m^2K^4)
T_s = Absolute skin temperature (K)
$\overline{T}_r$ = Absolute mean radiant temperature (K)

The emittance, ε, for human skin is close to 1.0, and since most types of clothing have emittances of 0.95 it is suggested to use the mean value of 0.97 (Fanger, 1972).

The mean radiant temperature is the uniform temperature of an imaginary enclosure (black surroundings), in which radiant heat transfer from the human body equals the radiant heat transfer in the actual non-uniform enclosure (ASHRAE, 1993).

Most building materials have high emittance, therefore, it is usually assumed that the surrounding surfaces act as black bodies, i.e.

$$\overline{T}_r^{\,4} = T_1^{\,4} F_{P-1} + T_2^{\,4} F_{P-2} + \ldots + T_N^{\,4} F_{P-N} \tag{2.23}$$

where

$\overline{T}_r$ = Absolute mean radiant temperature (K)
T_N = Absolute surface temperature of surface N (K)

$F_{P\text{-}N}$ = Angle factor between a person and surface N (n.d.)

If the mutual temperature differences of the surfaces are relatively small the above equation may be simplified to a linear form (ASHRAE, 1993)

$$\bar{t}_r = t_1 F_{P-1} + t_2 F_{P-2} + \ldots + t_N F_{P-N} \tag{2.24}$$

where the temperature unit is °C in this expression. The above formula assumes that reflections between the surfaces can be disregarded. If this is not the case the radiosity of the surfaces should be used in calculating $\overline{T}_r$ (Holman, 1989), which will complicate the calculation extensively.

Radiative heat loss from persons may also be expressed in a linearized form using the radiative heat transfer coefficient in the same manner as the convective heat transfer coefficient (ASHRAE, 1993)

$$R = f_{cl} h_r \left(t_{cl} - \bar{t}_r \right) \tag{2.25}$$

where

R = Radiative heat transfer (W/m^2 outer surface of clothed body)
h_r = Linear radiative heat transfer coefficient (W/m^2°C)
t_{cl} = Mean temperature of outer surface of the clothed body (°C)
$\bar{t}_r$ = Mean radiant temperature (°C)

and

$$h_r = 4\varepsilon\sigma f_{eff} \left[273.15 + \frac{t_{cl} + \bar{t}_r}{2} \right]^3 \tag{2.26}$$

Magnitude of the radiative heat transfer coefficient

As for the convective heat transfer coefficient in the preceding chapter, the radiative heat transfer coefficient is calculated for an environment of 20°C to give an idea of the order of magnitude for three different levels of clothing insulation, see Table 2.4.

Table 2.4. Example of the linear radiative heat transfer coefficient for a standing person in surroundings with a mean radiant temperature of 20°C for three different cases corresponding to a naked person (0 clo), typically summer clothes (0.5 clo), and typically winter clothes (1.0 clo). ε = 0.97 and f_{eff} = 0.725. The calculation of t_{cl} is described in Appendix A.

Radiative heat transfer coefficient		
Clothing insulation (clo)	t_{cl} (°C)	h_r (W/m^2°C)
0	33.7	4.3
0.5	29.8	4.2
1.0	26.0	4.1

2.2.3. Respiration

In Chapter 1 it was mentioned that the route for personal exposure examined in the present work is exposure via the respiration. Therefore, a short introduction to the respiratory system will be given in the subsequent chapter, including a formula used for the calculation of the pulmonary ventilation which is necessary for the assessment of the dose, see Chapter 1.

The living cells in the human body use oxygen for its metabolism, and as a result of this process carbon dioxide is produced. Two transport systems are used to carry the O_2 and the CO_2 between the cells and the environment surrounding the person: a circulatory system supplies the blood and a respiratory system supplies air to the lungs. Thus, the main function of the respiratory system is to provide oxygen to the cells of the body and to remove excess carbon dioxide (Turiel, 1985).

The pulmonary airways consist of three different parts, see Figure 2.5. First, the upper airways, extending from the nares and the lips to the larynx. Here, the air is warmed and moistened. Secondly, the conducting airways where the air is distributed in the lungs in a branched-tube network starting at the trachea and extending to include the terminal bronchioles. Third, the respiratory zone that begins with the respiratory bronchioles and ends with the alveoli (little air sacs). Here, the gas exchange takes place (Ultman, 1988).

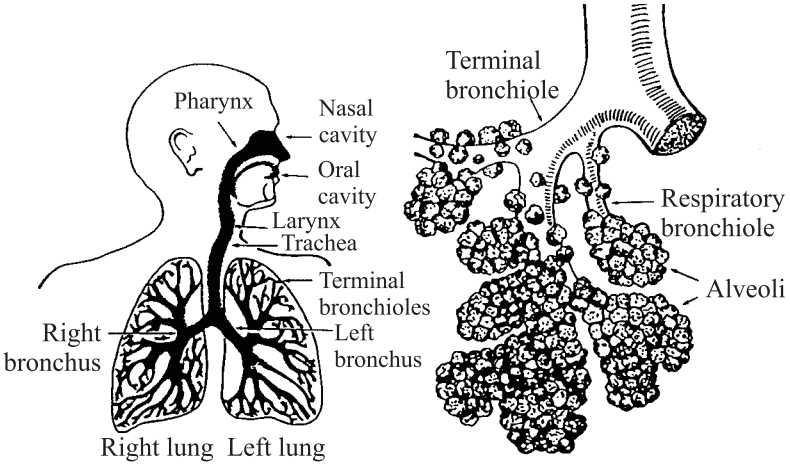

Figure 2.5. Major anatomical features of the human respiratory system. *Reference*: Turiel, 1985.

The state of the air in the lungs is 37°C and 100% rh at barometric pressure, while the exhaled air in usual surroundings is approximately 34°C and 100% rh (see also Appendix A).

The pulmonary ventilation is defined as the volume of air which is *exhaled* per minute. By definition the pulmonary ventilation equals the frequency of respiration multiplied by the mean expired volume (Åstrand and Rodahl, 1986)

$$\dot{V}_{res} = f_{res} \cdot \overline{V}_T \tag{2.27}$$

where

$\dot{V}_{res}$ = Pulmonary ventilation (litre/min)
f_{res} = Frequency of respiration (min^{-1})
$\overline{V}_T$ = Mean expired tidal volume (litre)

At rest the frequency of respiration is 10 - 20 min^{-1} and increasing depending on the activity level of the person. For well trained athletes 60 min^{-1} is not unusual. The pulmonary ventilation at rest is about 6 litre/min increasing according to the activity level up to 200 litre/min in the extreme case (Åstrand and Rodahl, 1986).

In Table 2.5. examples of typical levels of the three above mentioned parameters are shown for different activity levels.

Table 2.5. Examples on tidal volume, frequency of respiration and pulmonary ventilation for different activity levels (Asmussen and Nielsen, 1989).

Activity level	Tidal volume (litre)	Frequency (min^{-1})	Pulmonary ventilation (litre/min)
Rest	0.5	12	6
Moderate work	~ 2.5	12	30
Maximal work	~ 3.0	30 - 40	90 - 120

According to ASHRAE (1993) the pulmonary ventilation may be expressed as a function of the activity level as follows

$$\dot{m}_{res} = K_{res} \cdot M \tag{2.28}$$

where

$\dot{m}_{res}$ = Pulmonary ventilation rate (kg/s)
K_{res} = Constant ($2.58 \cdot 10^{-6}$ kg m^2/J)
M = Rate of metabolic heat production (activity level) (W/m^2)

If it is assumed that the temperature of the expired air is 34°C, $\dot{m}_{res}$ in kg/s may be converted into $\dot{V}_{res}$ in litre/min, i.e.

$$\dot{V}_{res} = K_{res}' \cdot M = 0.1348 \cdot M \tag{2.29}$$

where

$\dot{V}_{res}$ = Pulmonary ventilation (litre/min)
K_{res}' = Constant (0.1348 litre m^2 / W min)
M = Rate of metabolic heat production (activity level) (W/m^2)

2.2.4. Description of the Breathing Thermal Manikin

2.2.4.1. Introduction

An extensive number of different physical models of human beings have been used in research for various purposes. Table 2.6. gives an overview of the topic.

Table 2.6. Overview of characteristics and purpose for different physical models of a human being.

Physical models of human beings
Features: - Geometry (anatomically correct, small-scale, cylinder, cuboid, sphere, etc.) - Posture (standing, seated, lying, movements) - Heating (none, surface temperature, heat flux, etc.) - Respiration (none, exhaust from point, artificial lung, etc.) - Etc.
Purpose: - Thermal insulation of clothing - Heat transfer coefficients - Flow characteristics around the body - Thermal comfort - Personal exposure - Source of heat, contamination and momentum - Interaction between persons - Etc.

The main interest in the present work is physical models of humans used for determination of personal exposure. The models used for this purpose may roughly be divided in three different categories:

1. Heated cylinders (e.g. Nickel et al., 1990; Holmberg et al., 1990; Stymne et al., 1991; Mattsson and Sandberg, 1994; Krühne and Fitzner, 1994).

2. Unheated, anatomically correct, small-scale models (e.g. Fletcher and Johnson, 1988; Flynn and Shelton, 1990; George et al., 1990; Flynn and George, 1991; Kim and Flynn, 1991a, 1991b, 1992).

3. Heated, anatomically correct, full-scale models with respiration (e.g. Clark and Cox, 1973; Säteri, 1992a, 1992b; Brohus and Nielsen, 1994a; 1995; 1996b; Rodes et al., 1995; Bjørn and Nielsen, 1996a; b).

The physical models of a human being used in the present work belong to the third category, i.e. the Breathing Thermal Manikin shown in Figure 2.7.

2.2.4.2. Construction of manikin

The Breathing Thermal Manikin (BTM) is developed at the Thermal Insulation Laboratory, Technical University of Denmark. The BTM is shaped as a 1.7 m high average sized woman, developed from a nearly anatomically correct female display manikin consisting of a 4 mm fibreglass-armed polyester shell. The shell is wound with nickel wire of 0.3 mm in diameter at a maximum spacing of 2 mm, see Figure 2.6. The wire is used sequentially both for the heating of the manikin and for measuring and controlling the skin temperature. Outside the wiring a protective shield is placed with a thickness less than 1 mm.

The manikin is divided in 16 parts, and it is supplied with joints in shoulders, hips and knees. This enables it to stand, sit and to move, e.g. on a bicycle (with the energy of movements supplied from outside). The different surface areas of the individual parts can be found in Appendix B.

Figure 2.6. The Breathing Thermal Manikin under construction at the Technical University of Denmark. Here, the resistance wire used for heating, measuring and controlling the skin temperature and the heat output is mounted on the head.

The BTM is controlled to obtain a skin temperature and a heat output corresponding to people in thermal comfort. Fanger (1972) found a relationship between the skin temperature and the total heat output necessary to achieve thermal comfort. However, due to the fact that the manikin is not able to evaporate moisture the sensible heat loss is used in stead of the total heat loss. Therefore, the following relationship between the skin temperature, t_s, and the sensible heat output, Q_t, is derived and used for the control (Tanabe et al., 1994). The full derivation is found in Appendix A.

$$t_s = 36.4 - 0.054 \cdot Q_t \tag{2.30}$$

Each of the 16 parts of the body is equipped with individual systems for heating and control. The control circuit is designed as a proportional control system with a set-point of 36.4 °C and a load error of 0.054 m^2°C/W. The load error will react as a thermal resistance equal to the resistance between the skin and the deep body.

The skin temperature is measured in the range of 18°C - 37°C with a resolution of 0.1°C and a maximum heat loss of 140 W/m^2. The BTM is calibrated in the laboratory by the author to an uncertainty of ± 0.2°C.

Figure 2.7. Breathing Thermal Manikin used to measure the personal exposure. The manikin is separated in 16 individual parts of the body, each with the same surface temperature and heat output as people in thermal comfort. The manikin has an artificial lung to simulate breathing. Height = 1.7 m, A_{Du} = 1.5 m^2, I_{cl} = 0.8 clo.

The control and the function of the manikin are verified by measuring the convective heat transfer coefficient among other things, see Appendix C.

The BTM is wearing tight-fitting clothes with an insulation value, I_{cl}, of 0.8 clo. This value corresponds well to typical indoor clothing insulation which is usually found in the interval between 0.5 clo and 1.0 clo. In Appendix D measurements of the clothing insulation are reported.

Tight-fitting clothes are chosen instead of loose-fitting clothes where the local surface temperatures, heat transfer and thus the flow field may change significantly due to large variations in the location of insulating enclosures of stagnant air. The choice of tight-fitting clothes results in more consistent and reproducible measurements.

Respiration is simulated by means of an artificial lung which is able to provide the breathing either through the mouth or through the nose. It is possible to adjust both the frequency of respiration (number of breaths per minute) in the range of 3 - 30 min^{-1} and the pulmonary ventilation (litre per minute) in the range of 5 - 18 litre/min.

In this work 10 min^{-1} is chosen as the frequency of respiration and 10 litre/min as the pulmonary ventilation. The respiration is performed through the mouth.

2.2.5. Personal exposure assessment using the BTM

Due to the fact that the Breathing Thermal Manikin is equipped with both an artificial lung and the possibility to breathe either through the mouth or the nose, it is relatively easy to determine the personal exposure by analysing a sample of substance which is actually inhaled, according to the definition of personal exposure in Chapter 1.

In the present work only gaseous contaminants are considered. The transport of contaminant is modelled by means of tracer gas which is assumed to simulate the behaviour of a gaseous contaminant source satisfactory.

Nitrous oxide (N_2O) is used as tracer gas. However, the gas has a density approximately 1.5 times higher than atmospheric air, which is found to influence the dispersion pattern substantially, especially in case of quiescent surroundings.

To eliminate that problem the tracer gas is mixed with the lighter helium (He) to obtain a mixture which is density neutral compared with the density of the surrounding air.

The tracer gas concentration is measured by means of photoacoustic spectroscopy (PAS). Here, a gas property is used, namely that the gas molecules can absorb certain frequencies of infrared light, gain energy and vibrate more vigorously. The exited molecules thus transform their extra energy to other molecules by collision which causes increased molecular speed which finally results in a raised temperature of the gas.

When PAS is used a gas sample is collected in a measurement chamber. The chamber is irradiated with pulsed (chopped) light. The gas absorbs light proportional to its concentration and converts it into heat, quickly afterwards the gas cools again. The chopped light causes temperature fluctuations that generates pressure waves. Finally, the pressure waves are detected by a microphone.

In the present measurements a Brüel & Kjær 1302 Multi-gas Monitor is used together with a Brüel & Kjær 1303 Multipoint Sampler and Doser. The concentration is measured by sampling with a frequency of approximately one sample per minute. The equipment is calibrated to an uncertainty of ± 2%, including cross calibration and water interference calibration.

2.3. Computer Simulated Person

2.3.1. Introduction

This Chapter 2.3. will present a numerical tool for personal exposure assessment, namely the Computer Simulated Person. Three different models are proposed ranging from a heated cuboid to a model including “legs” and “head”.

First, the mathematical equations governing the fluid flow and the contaminant transport processes are mentioned together with a description of the numerical solution procedure and the treatment of selected boundary conditions.

Then the three different versions of the Computer Simulated Person (CSP) are introduced and, finally, the procedure for personal exposure assessment using the CSP is discussed.

2.3.2. Computational Fluid Dynamics

2.3.2.1. Governing equations

The aim of Computational Fluid Dynamics (CFD) is to provide a numerical solution of the mathematical equations governing fluid flow and related physical processes. The description of fluid dynamics will often include the topics of heat transfer, mass transfer and very often also turbulence modelling etc.

The set of equations actually involved and the appearance of the specific terms in the equations depend on the case of interest due to different assumptions and possible simplifications. For instance, it makes a difference whether the flow is isothermal or not, compressible or incompressible, etc.

In this work only steady-state problems will be considered. The flow is assumed to be three-dimensional, incompressible, non-isothermal and turbulent (or laminar). To account for the dispersion of contaminant and thus personal exposure an equation for the transport of contaminant (mass) must be included. This leads to the following set of governing equations.

Continuity equation

One of the basic laws in fluid motion, conservation of mass, is derived by means of a mass balance for a control volume in the fluid where the incoming mass flow equals the outgoing mass flow (incompressible fluid), in cartesian tensor notation the continuity equation is

$$\frac{\partial\left(\rho u_i\right)}{\partial x_i} = 0 \tag{2.31}$$

where

ρ = Density of the fluid (kg/m^3)
u_i = Mean velocity component corresponding to the *i* direction (m/s)
x_i = Co-ordinate direction *i* (m)

Navier-Stokes equations

The Navier-Stokes equations, which are also termed the momentum equations, are expressing Newton's second law of motion for the fluid, i.e. the transport and conservation of momentum. The equations are derived by applying Newton's second law on a fluid element influenced by surface forces (shear stresses and pressure) and volume forces (buoyancy)

$$\frac{\partial\left(\rho u_i u_j\right)}{\partial x_j} = \frac{\partial}{\partial x_j}\left(\mu_l\left(\frac{\partial u_i}{\partial x_j} + \frac{\partial u_j}{\partial x_i}\right) - \rho\overline{u_i' u_j'}\right) - \frac{\partial p}{\partial x_i} + B_i + S_u \qquad (2.32)$$

where

p = Pressure (N/m^2 or Pa)
μ_l = Laminar dynamic viscosity (kg/m s)
u_i' = Fluctuating velocity component in the *i* direction (m/s)
B_i = Volume force in the *i* direction (N/m^3)
S_u = Source term (N/m^3)

The term on the left side, the convection term, expresses the net supply of momentum from the surroundings. First term on the right side, the diffusion term, expresses the influence from the shear forces. Second term is the pressure gradient term which is due to the normal forces and, finally, the buoyancy term which accounts for the volume forces acting on the fluid and the source term which is frequently used to implement the boundary conditions.

In the diffusion term the quantity $-\rho\overline{u_i' u_j'}$ is called the Reynolds stresses (or additional stresses) and they result from taking the instantaneous equations into mean equations (Rodi, 1980). The physical meaning of the Reynolds stresses is the effect of the turbulent transport of fluid across the main flow direction, which influences the flow in the same way as increased shear stress.

The various turbulence models are making assumptions for the Reynolds stresses for the closure of the mean equation. In the present work the eddy viscosity concept is used. Here, the turbulent stresses are assumed to be proportional to the gradient of the mean velocity and the turbulence is assumed to be isotropic (Rodi, 1980), i.e.

$$-\rho\overline{u_i' u_j'} = \mu_t\left(\frac{\partial u_i}{\partial x_j} + \frac{\partial u_j}{\partial x_i}\right) - \frac{2}{3}\rho k\delta_{ij} \tag{2.33}$$

where

μ_t = Turbulent viscosity (eddy viscosity) (kg/m s)
k = Turbulent kinetic energy (J/kg)
δ_{ij} = Kronecker delta (equals 1 for $i = j$ and equals 0 for $i \neq j$)

In that way an effective viscosity, μ_{eff}, can be defined as the sum of the laminar and the turbulent viscosity

$$\mu_{eff} = \mu_l + \mu_t \tag{2.34}$$

It is important to acknowledge the differences between the laminar and the turbulent viscosity. While the laminar dynamic viscosity, μ_l, is a constant for a specific fluid, the turbulent viscosity, μ_t, depends on the flow, and it may vary highly throughout the flow domain. μ_t is found by means of a turbulence model.

The last term in the expression of the Reynolds stresses must be included to be consistent with the subsequent definition of the turbulent kinetic energy, k. The term expresses the normal stresses, i.e. when $i = j$, in which case the first term on the right side is zero according to the continuity equation. These normal stresses act like pressure forces and, therefore, they are sometimes included in the pressure gradient term as an "effective" pressure $p + 2/3\ k$ (Rodi, 1980). This last term, however, is often small for what reason it is frequently ignored in the numerical scheme.

The buoyancy term, B_i, may be described as follows, using the Boussinesq approximation (Arpaci and Larsen, 1984)

$$B_i = -\rho\beta g_i\left(t - t_{ref}\right) \tag{2.35}$$

where

β = Coefficient of cubic expansion (1/K)
g_i = Gravitational acceleration in the i direction (m/s^2)
t = Temperature of the fluid (°C)
t_{ref} = Reference temperature (°C)

Inserting the above expressions for the Reynolds stresses and for the buoyancy term in the Navier-Stokes equations results in

$$\frac{\partial\left(\rho u_i u_j\right)}{\partial x_j} = \frac{\partial}{\partial x_j}\left(\mu_{eff}\left(\frac{\partial u_i}{\partial x_j} + \frac{\partial u_j}{\partial x_i}\right)\right) - \frac{\partial p}{\partial x_i} - \rho\beta g_i\left(t - t_{ref}\right) + S_u \tag{2.36}$$

Energy equation

To obtain a description of the temperature distribution throughout the non-isothermal flow domain the energy equation is used. This equation is derived from the basic law of conservation of energy, i.e. the first law of thermodynamics applied on a fluid element assuming that the fluid is acting as a perfect gas

$$\frac{\partial\left(\rho c_p u_j t\right)}{\partial x_j} = \frac{\partial}{\partial x_j}\left(\lambda_{eff}\,\frac{\partial t}{\partial x_j}\right) + S_t \tag{2.37}$$

where

ρ = Density of the fluid (kg/m^3)
c_p = Specific heat at constant pressure (J/kg°C)
t = Mean temperature of the fluid (°C)
λ_{eff} = Effective conductivity (W/m°C)
S_t = Source term (W/m^3)

The source term, S_t, includes eventual heat sources and sinks. The effective conductivity, λ_{eff}, is expressed as

$$\lambda_{eff} = \lambda_l + \lambda_t \tag{2.38}$$

where

λ_l = Laminar thermal conductivity (W/m°C)
λ_t = Turbulent conductivity (W/m°C)

The laminar thermal conductivity, λ_l, is a fluid property that is constant throughout the domain, whereas the turbulent conductivity, λ_t, depends on the local flow field in the same way as μ_t. λ_t is usually found by means of the turbulent Prandtl number, σ_t, in an analogy between the transfer of energy and momentum

$$\sigma_t = \frac{\nu_t}{\alpha_t} = \frac{c_p \mu_t}{\lambda_t} \tag{2.39}$$

where

σ_t = Turbulent Prandtl number (n.d.)
ν_t = Turbulent kinetic viscosity (m^2/s)
α_t = Turbulent thermal diffusivity (m^2/s)

The turbulent kinetic viscosity, ν_t, of the fluid conveys information about the rate of which momentum may diffuse through the fluid because of turbulent motion (stresses). The turbulent thermal diffusivity, α_t, explains the same thing in regard to the diffusion of heat, i.e. thermal energy, in the fluid. The turbulent Prandtl number is thus the connecting link between the velocity field and the temperature field. It is usually considered to be constant and close to unity, in this work it will be $\sigma_t = 0.9$.

Concentration equation

As mentioned previously an additional equation is required to calculate the dispersion and transport of a gaseous contaminant. This equation, the concentration equation, is based on mass conservation

$$\frac{\partial\left(u_j c\right)}{\partial x_j} = \frac{\partial}{\partial x_j}\left(D_{eff} \frac{\partial c}{\partial x_j} \right) + S_c \tag{2.40}$$

where

c = Concentration of contaminant (kg of species / kg of air)
D_{eff} = Effective diffusivity (m^2/s)
S_c = Source term (kg of species / kg of air · s)

The concentration, c, may easily be converted into the unit of mg/m^3 or ppm where it is convenient. The effective diffusivity, D_{eff}, is defined as

$$D_{eff} = D_l + D_t \tag{2.41}$$

where

D_l = Mass molecular diffusivity (m^2/s)
D_t = Turbulent diffusivity (m^2/s)

The turbulent diffusivity is found by means of a turbulent Schmidt number for concentration, σ_c, analogue to the turbulent Prandtl number for the energy equation

$$\sigma_c = \frac{\nu_t}{D_t} = 0.9 \tag{2.42}$$

Turbulence model

In order to describe the turbulent viscosity (eddy viscosity), μ_t, the following relation is used (Rodi, 1980)

$$\mu_t = \rho c_\mu \frac{k^2}{\varepsilon} \tag{2.43}$$

where

μ_t = Turbulent viscosity (kg/m s)
ρ = Density of the fluid (kg/m^3)
c_μ = Constant (= 0.09) (n.d.)
k = Turbulent kinetic energy (J/kg)
ε = Rate of dissipation of turbulent kinetic energy (J/kg s)

The turbulent kinetic energy, k, and the rate of dissipation of turbulent kinetic energy, ε, are defined as (Abbott and Basco, 1989)

$$k \equiv \frac{1}{2}\overline{u_i' u_i'} \tag{2.44}$$

$$\varepsilon \equiv -2\nu \overline{s_{ij} s_{ij}} \tag{2.45}$$

where s_{ij} is the strain rate of the fluctuating flow (s^{-1})

$$s_{ij} \equiv \frac{1}{2}\left(\frac{\partial u_i'}{\partial x_j} + \frac{\partial u_j'}{\partial x_i} \right) \tag{2.46}$$

and u_i' is the fluctuating component of the instantaneous velocity in the i direction (m/s).

The above expression for μ_t is derived on the basis of dimensional analysis and considerations of the velocity and length scales in the flow, assuming that there is a constant rate of energy transfer from the largest energy containing eddies to the dissipative small structures of the flow. Two additional partial differential equations are required for k and ε to close the set of equations, see Appendix E.

General form of equations

It is possible to write the equations in a more general form facilitating the discretisation and the solution. If the dependent variable is denoted ϕ, a diffusion coefficient is denoted Γ_ϕ, and a source term S_ϕ the following form of the differential equations can be written which is more comprehensible for the discretisation

$$\frac{\partial\left(\rho u_j \phi\right)}{\partial x_j} = \frac{\partial}{\partial x_j}\left(\Gamma_\phi \frac{\partial \phi}{\partial x_j}\right) + S_\phi \qquad (2.47)$$

with different meanings of ϕ, Γ_ϕ and S_ϕ according to the respective equations. The left term is the convection term, the first term on the right side is the diffusion term and the last term is the source term.

2.3.2.2. Numerical solution of equations

Discretisation technique

Using the Finite Volume Method the calculation domain is divided into a finite number of control volumes and grid points, so that there is one volume surrounding each grid point.

The differential equations are integrated over each control volume and piecewise profiles expressing the variation between the grid points are used to evaluate the required integrals (Brohus, 1992; Nielsen, 1994).

The hybrid scheme, i.e. a combination of central difference and upwind difference, is used in the evaluation of the convection terms (Patankar, 1980).

The source term, S_ϕ, is most often dependent on the variable ϕ. This dependence is described in a linear form even though it may be non-linear.

Pressure is deduced indirectly from the continuity equation by using the SIMPLE algorithm, for instance described by Patankar (1980).

After the discretisation a set of linear algebraic equations is obtained which can be solved using standard solution techniques, e.g. the TriDiagonal-Matrix Algorithm.

Non-linearities

Non-linearities are handled by iteration starting by guessing or estimating the variables at all grid points. From these values and the boundary conditions the coefficients in the discretized equations are calculated. Each of the coupled transport equations is solved separately in linearized form. In that way new values of the concerned variable are obtained which can be used to calculate the coefficients of the following equations and so on, until the convergence of the equations.

In the iterative solution of the algebraic equations, employed for handling the non-linearity, it is most often necessary to slow down the changes of a dependent variable from iteration to iteration to avoid divergence. This process is called underrelaxation, and it is a very useful device for non-linear problems (Patankar, 1980).

2.3.2.3. Boundary conditions

Due to the elliptic nature of the governing equations boundary conditions (BC) are required along all boundaries of the solution domain.

In the present CFD calculations several BC´s are used, for instance inlet opening, return opening, symmetry plane, wall functions for the description of friction and heat transfer etc. The last two will be explained in more detail in the subsequent.

The description is made in accordance with the formulas applied by Flovent (1994) to be consistent with the software used for the calculations.

Friction at the walls

When the fluid, i.e. the air in a ventilated room, is passing a wall the velocity in the boundary layer is decreasing from "free stream" velocity level to zero velocity on the surface, the so called no slip condition. This process causes a surface friction which highly affects the flow field, especially close to the surface. In order to provide a satisfactory numerical description of this phenomenon it is necessary to use a high number of grid points (control volumes) close to the walls.

Another approach that is used in this work is to employ wall functions in order to evaluate surface friction between the wall surface and the near-wall grid node. This approach will save a great number of grid points in the proximity of surfaces and, therefore, decrease the demand of computer power and CPU time considerably.

Standard wall functions separate the boundary layer in two regimes, a viscous sub-layer and a fully turbulent region. The wall functions are based on measurements and calculations on a steady, turbulent channel flow (Arpaci and Larsen, 1984). This implies that the boundary layer along surfaces in the CFD simulations is assumed to act as the boundary layer obtained in the case of a channel flow.

Two non-dimensional quantities are used in the description of the wall functions, namely a velocity, u^+, and a length, y^+ defined as (analogue to the velocities v^+ and w^+ and the length x^+ and z^+)

$$u^+ = \frac{u}{u_\tau} \tag{2.48}$$

and

$$y^+ = \frac{\rho y u_\tau}{\mu} \tag{2.49}$$

$$u_\tau = \sqrt{\frac{\tau_w}{\rho}} \tag{2.50}$$

where

u^+ = Dimensionless velocity (n.d.)
u = Velocity in x direction (transversely to the y direction) (m/s)
u_τ = Friction velocity (m/s)
τ_w = Wall shear stress (N/m^2)
y = Co-ordinate in y direction (m)
y^+ = Dimensionless length (n.d.)
ρ = Density of fluid (kg/m^3)
μ = Laminar dynamic viscosity (kg/m s)

The non-dimensional distance from the wall, y^+, can also be viewed as a local Reynolds number, which clearly appears from the definition above.

For the laminar regime, i.e. the viscous sub-layer, we get for $y^+ \leq 11.5$ (Flovent, 1994)

$$u^+ = y^+ \qquad \text{(viscous sub-layer, laminar regime)} \qquad (2.51)$$

and for the fully developed turbulent regime, for $y^+ > 11.5$, we get the logarithmic law-of-the-wall

$$u^+ = \frac{1}{0.435}\ln\left(9y^+\right) \qquad \text{(turbulent region)} \qquad (2.52)$$

In the numerical solution procedure the wall shear stress, τ_w, is deduced from the above formulas by means of the calculated values of the velocity, u, in the first grid node at the distance, y, from the wall surface. This is straightforward in the laminar case, while in the turbulent region it involves iteration. The wall shear stress is then applied as a negative source of momentum in the Navier-Stokes equations for the near-wall cell. In that way the no slip condition and the effect of friction are included in the CFD calculations.

Heat transfer at the walls

Two different boundary conditions are used to model heat transfer at the walls in the CFD calculations.

The most simple and also the most exact and grid independent heat transfer BC is a direct prescription of the heat flux at the surface, e.g. in W/m^2. This procedure should be applied whenever possible.

Often, however, the applied BC regarding heat transfer at the walls is the surface temperature, t_w. This raises a demand for the calculation of a local convective heat transfer coefficient to express the heat flow between the wall and the first grid node, i.e.

$$Q_c = h_c\left(t_p - t_w\right) \tag{2.53}$$

where

Q_c = Local convective heat transfer (W/m^2)
h_c = Local convective heat transfer coefficient (W/m^2°C)
t_p = Air temperature at the first grid node (°C)
t_w = Surface temperature at the wall (°C)

The heat transfer is determined by means of the non-dimensional Stanton number, *St*, which is an expression of the ratio of energy flux to momentum flux in the fluid

$$St = \frac{Nu}{\mathrm{Re}\,\mathrm{Pr}} = \frac{h_c}{\rho c_p u} \tag{2.54}$$

where

St = Stanton number (n.d.)
Nu = Nusselt number (n.d.)
Re = Reynolds number (n.d.)
Pr = Prandtl number (n.d.)

If the Stanton number is known Q_c may be found as

$$Q_c = \rho c_p u\left(t_p - t_w\right)St \tag{2.55}$$

As for the description of the wall friction the boundary layer is divided in two regions. For the laminar flow, $y^+ \leq 11.5$, we obviously have

$$St = \frac{1}{\mathrm{Re}\,\mathrm{Pr}} \qquad \text{(viscous sub-layer, laminar region)} \qquad (2.56)$$

i.e.

$$Q_c = \frac{\lambda_l}{y}\left(t_p - t_w\right) \qquad \text{(viscous sub-layer, laminar region)} \qquad (2.57)$$

where λ_l is the laminar thermal conductivity of the flow.

In case of turbulent flow, where $y^+ > 11.5$, St is found in an analogy between heat and momentum transfer. Assuming that the turbulent diffusivities are order of magnitudes larger than the molecular diffusivities, and that the turbulent Prandtl number is approximately equal to one the Reynolds analogy is obtained (Arpaci and Larsen, 1984)

$$St = s \qquad (2.58)$$

where

$$s = \frac{\tau_w}{\rho u^2} \qquad (2.59)$$

However, to include a possible variation of the Prandtl number the Prandtl-Taylor correction is applied in a generalised form, including the sub-layer resistance function by Jayatilleke (1969), (Patankar and Spalding, 1970)

$$St = \frac{s}{\sigma_t\left(1 + P_j\sqrt{s}\right)} \qquad \text{(turbulent region)} \qquad (2.60)$$

and

$$P_j = 9\left(\frac{\sigma_l}{\sigma_t} - 1\right)\left(\frac{\sigma_t}{\sigma_l}\right)^{1/4} \tag{2.61}$$

where

P_j = Jayatilleke´s sub-layer resistance function (n.d.)
σ_l = Laminar Prandtl number (n.d.)
σ_t = Turbulent Prandtl number (n.d.)

As mentioned in the previous paragraph σ_t = 0.9 is used. The laminar Prandtl number, σ_l, is close to 0.71 for room air at usual indoor conditions, i.e.

$$St = \frac{s}{0.9\left(1 - 2\sqrt{s}\right)} \qquad \text{(room air, turbulent region)} \tag{2.62}$$

which is the relation used in the present CFD calculations for the turbulent region.

Consequently, when the heat transfer BC is the wall temperature and the flow is turbulent *St* may be found by means of u, τ_w (hence s) and t_p. Q_c is calculated from the Stanton number and then applied as a heat source in the energy equation for the affected near-wall cell.

Even though the boundary layer is separated in two regions, the solution depends on the choice of grid layout, both regarding the heat transfer BC where the surface temperature is prescribed and also regarding the surface friction BC. This topic is discussed in more detail in Chapter 2.3.3.2.

2.3.2.4. Software

The equations and the numerical scheme mentioned above are implemented in the commercial software product FLOVENT from Flomerics Ltd. This software has been used to perform the CFD calculations presented here.

FLOVENT is a special-purpose CFD program which has been developed in collaboration between Flomerics Ltd. and BSRIA (The Building Services Research and Information Association, Berkshire, UK) , especially focusing on the topics of heating, ventilating and air-conditioning for buildings. The special-

purpose features, however, do not affect the generality of the governing equations and the discretisation scheme, etc.

The code is closed but the author of this work has compared it with other commercial products and also with an almost similar and open code. In all cases a close correspondence is found indicating that the function of the program is reliable and consistent with the theory.

2.3.3. Description of Computer Simulated Person

2.3.3.1. Introduction

During the last few years a growing number of Computer Simulated Persons (CSP) have been proposed with the purpose of determining the personal exposure and different thermal comfort indices for various indoor environments.

Most of the models are “heated” and they are made in a three-dimensional, rectangular geometry simulating the entire person.

Some two-dimensional models have been used, for instance Dunnett (1994) proposed a not-heated elliptical cylinder to simulate a standing person, and Niwa et al. (1996) applied a heated box representing a seated person. Davidson and Nielsen (1995) simulated the air flow in facial regions and nasal cavity by means of two-dimensional, isothermal simulations with a detailed model of the human head.

In three-dimensional, rectangular geometry Heinsohn (1991) used a not-heated cuboid (parallelepiped) to model the exposure of a standing person. Tjelflaat and Knott (1996) proposed a not-heated cuboid suspended from the floor to calculate thermal comfort indices, particularly in large enclosures.

A number of references have used a three-dimensional, heated cuboid in rectangular geometry to model either a seated person (Iwamoto, 1996) or a standing person (e.g. Bluyssen and Lemaire, 1992; Gan et al., 1993; Gan, 1994; Brohus and Nielsen, 1995, 1996a; Awbi, 1996).

Murakami et al. (1995, 1996) and Kato et al. (1996) developed the computational thermal manikin in a generalised curvilinear geometry (boundary fitted co-ordinates) and used a low-Reynolds-number k-ε turbulence model for the calculations.

2.3.3.2. Geometry and boundary conditions of models

Purpose

The purpose of the models proposed in the following is to create a tool for assessing the personal exposure by means of CFD. It has been the aim to propose models which are both able to re-create the characteristic flow phenomena observed close to a person, and at the same time they should be kept at a level of complexity that allows use in practical engineering purposes. Another purpose is to investigate whether inclusion of "legs" and "head" in the models is important.

Geometry

The three models shown in Figure 2.8. correspond to an average sized woman where the clothing has an insulation value of 0.8 clo. The reasons for this choice are to make the models useful in general and also to facilitate comparisons with the Breathing Thermal Manikin, see Chapter 2.2.

The BTM has a naked surface area, A_{Du}, of 1.47 m^2. This surface area is increased according to the clothing insulation. According to the formula by McCullough et al. (1985)

$$f_{cl} = 1 + 0.3 I_{cl} = 1 + 0.3 \cdot 0.8 = 1.24 \qquad (2.63)$$

the surface area should be increased by 24 %.

The applied clothing ensemble of the BTM, however, is tight-fitting why the increase in surface area is estimated to be only 10 %, which in fact correspond well to an alternative expression of f_{cl} for $I_{cl} > 0.5$ clo (Awbi, 1991), i.e.

$$A_{cl} = 1.1 \cdot A_{Du} = 1.1 \cdot 1.47 = 1.62 \text{ m}^2 \quad (2.64)$$

The height of the models corresponds to the height of the BTM, i.e. 1.7 m. The aspect ratio of the width and the depth for the models are kept approximately constant and equal to two, as applied in Dunnett (1994). “Legs” and “head” also correspond approximately to the geometry of the Breathing Thermal Manikin applied in a simplified rectangular geometry.

Three different models are proposed. They are made in a rectangular geometry, ranging from a heated cuboid to a model including “legs” and “head”. The outline is shown in Figure 2.8. and the geometry is summarised in Table 2.7.

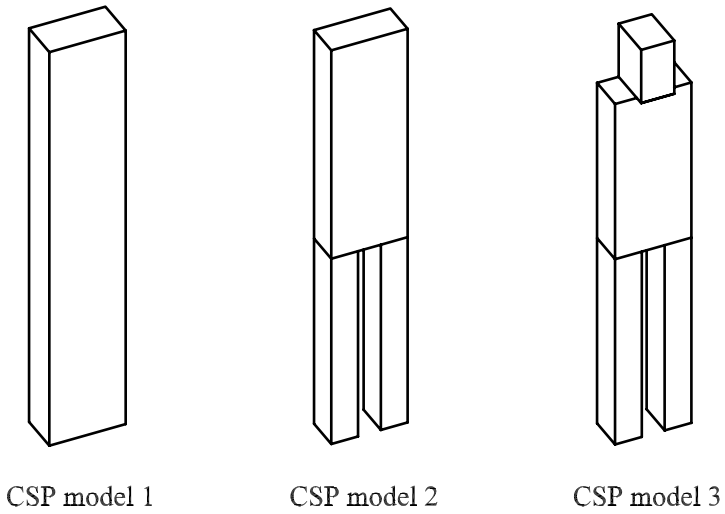

Figure 2.8. Outline of the three Computer Simulated Persons made in a rectangular geometry simulating an average sized woman.

The heat transfer boundary condition is chosen as a convection heat flux of 25 W/m^2, which corresponds to an activity level of a person standing relaxed, i.e. approximately 1 met. By choosing a heat flux BC in stead of a surface temperature it makes the heat transfer from the models independent of the grid layout in the numerical solution.

Table 2.7. Geometry of the three Computer Simulated Persons (CSP).

PART	**CSP model 1**	**CSP model 2**	**CSP model 3**
Torso	1.7 x 0.3 x 0.16216	0.9 x 0.3 x 0.13803	0.67 x 0.3 x 0.14429
Leg	-	0.8 x 0.105 x 0.13803	0.8 x 0.105 x 0.14429
Head	-	-	0.23 x 0.13 x 0.18
Length x width x depth in m. Convective heat flux: 25 W/m^2 (activity level ~ 1 met). Surface area: 1.62 m^2 The surface area is the "exposed area", i.e. the part of the surface in contact with the surrounding air (this implies that the area in contact with the floor is not included).			

Grid layout

Even though the heat transfer regarding the CSP is independent of the grid layout, the convective boundary layer flow will be affected when wall functions are applied and thus the transport of contaminants and the personal exposure may be influenced. Therefore, the location of the first grid node is important and it is examined in more detail in the following.

To investigate the influence of the grid layout a simple test case is examined. The surface temperature of the CSP is prescribed as BC and the simulated heat output is used as an indicator of the suitability of the grid.

A two-dimensional calculation of a person standing in a uniform free stream of 0.3 m/s is used as the test case. Four different grids are tested, corresponding to a distance from the surface of the CSP to the first grid node of 0.25 cm, 0.5 cm, 1.0 cm and 2.5 cm, see Figure 2.10.

In Figure 2.9. the relative error of the convective heat transfer is plotted versus the distance to the first grid node.
As shown in Figure 2.9. a grid node distance of 0.5 cm from the surface of the CSP results in the smallest relative error. This corresponds to a location of the first grid line adjacent to the surface at a distance of 1 cm. This distance is applied in all simulations. An example of the grid layout around the head of CSP model 3 is shown in Figure 2.10.

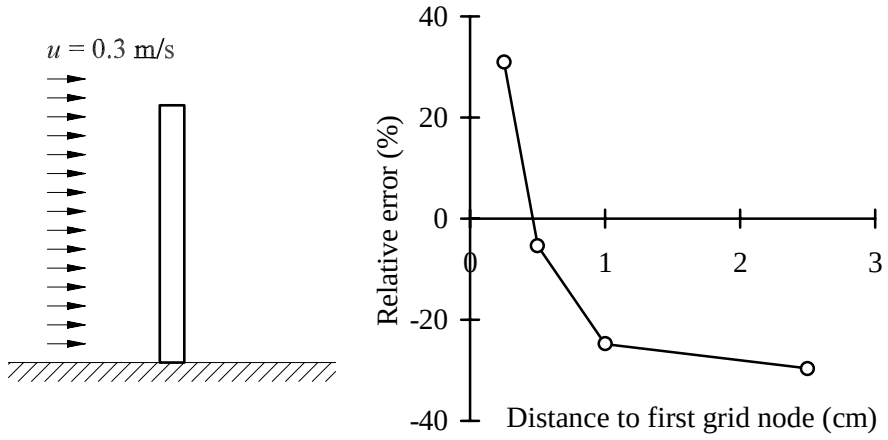

Figure 2.9. Relative error of the convective heat transfer (in %) versus distance to the first grid node (in cm) for a two-dimensional test case where the surface temperature is prescribed and wall functions applied. Person: height 1.7 m and depth 0.15 m . The relative error is found by comparing the simulated results with an analytical solution.

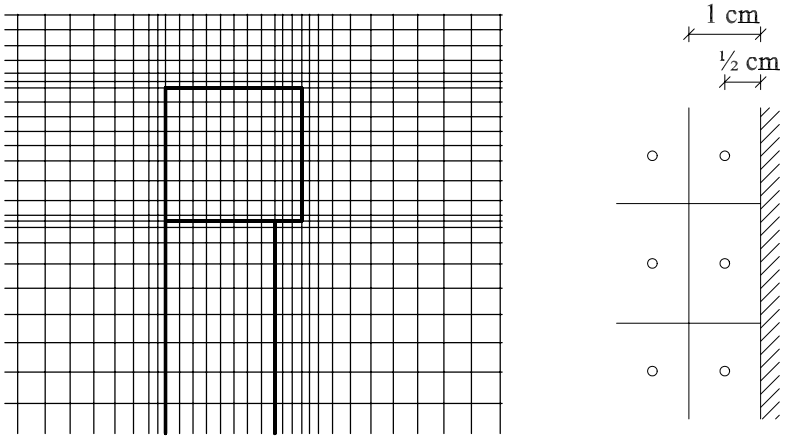

Figure 2.10. Close-up of the grid layout around the head of the CSP model 3. The first grid line is located at a distance of 1 cm, corresponding to a grid node distance of 0.5 cm from the surface.

Another way of evaluating the grid is to calculate the non-dimensional distance, y^+, that determines whether the flow is classified laminar or turbulent in the boundary layer when the wall functions are applied (see Chapter 2.3.2.3. for further explanation of the parameters)

$$y^+ = \frac{y_p u_\tau}{\nu} = \frac{y_p \sqrt{\frac{\tau_w}{\rho}}}{\nu} \tag{2.65}$$

According to Patankar and Spalding (1970) the wall shear stress in the turbulent region, τ_w, can be expressed as

$$\tau_w = c_\mu^{\frac{1}{2}} \rho k_p \tag{2.66}$$

where

τ_w = Wall shear stress (N/m^2 or Pa)
c_μ = Constant (= 0.09) (n.d.)
ρ = Density of the fluid (kg/m^3)
k_p = Turbulent kinetic energy at first grid node adjacent to surface (J/kg)

In the laminar region, however, equation (2.51) gives $y^+ = u^+$

Thus, u_τ in equation (2.65) may be expressed in general as

$$u_\tau = \sqrt{MAX\left[\frac{\nu |u_p|}{y_p}, c_\mu^{1/2} k_p\right]} \tag{2.67}$$

As mentioned above y_p = 0.005 m is fixed, c_μ, ρ and μ are also constants for the specific simulations, therefore, only k_p is required in order to calculate y^+. This has been done for the CFD simulations presented in the subsequent chapters.

In all cases $2 < y^+ < 30$ for the CSP´s with mean values ranging from 5 to 19. Typical values are found around $y^+ = 6$. This shows that the boundary layer flow around the Computer Simulated Persons is included under both the laminar and the turbulent regimes, but mainly under the laminar regime, where $y^+ \leq 11.5$.

An other important consideration regarding the location of the grid is that the second grid node adjacent to the surface should be found in the turbulent region to comply with the assumptions of the k-ε turbulence model. Another point to consider, regarding the size of y^+, is that the determination of u^+ is poorest around $y^+ = 11.5$ where the two regions meet. The size of y^+ mentioned above indicates that the choice of y_p in the present simulations is reasonable.

2.3.4. Personal exposure assessment using the CSP

Personal exposure is defined as the concentration of contaminant in the inhaled air according to Chapter 1. The three Computer Simulated Persons presented above, however, do not simulate respiration directly. Therefore, the concentration of inhaled contaminant must be determined in another way.

The inhaled contamination obviously comes from the contaminated air in the breathing zone close to the mouth and the nose. To examine from what distance or volume the air is inhaled, a simplified approach is used where the nose (or mouth) is treated as an exhaust opening with a total area of 1.3 cm^2 corresponding to the two nostrils of the Breathing Thermal Manikin, see Figure 2.11.

The capture velocity generated by the “exhaust opening”, which is necessary to capture the contaminant, may correspond approximately to the maximum velocity in the convection boundary layer along the body in breathing zone height, i.e. around 0.25 m/s (Homma and Yakiyama, 1988).

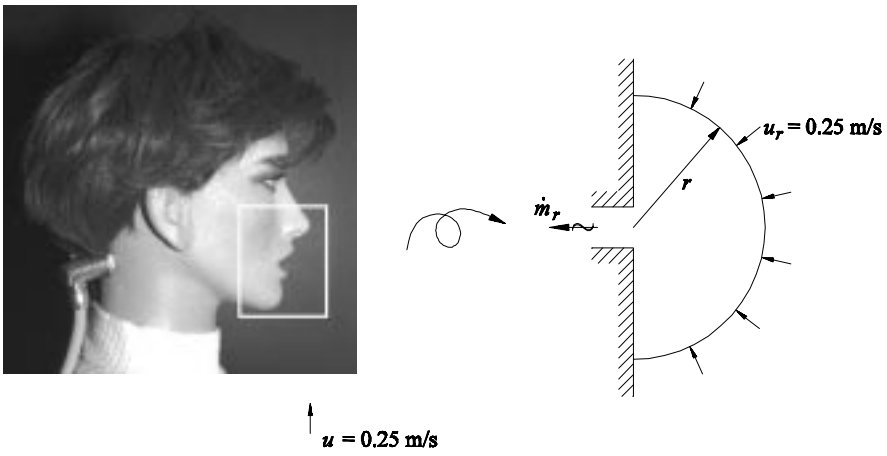

Figure 2.11. Simplified model of the inhalation from a person to estimate from what volume the air is drawn. The area of the "exhaust opening" is 1.3 cm^2 and the necessary capture velocity is assumed to be 0.25 m/s.

The velocity, u_r, in the distance r of the opening may be found by assuming inhalation from a hemisphere

$$u_r = \frac{\dot{m}_r}{A_{Ex} + 2\pi r^2} \tag{2.68}$$

where

u_r = Velocity in the distance r (m/s)
$\dot{m}_r$ = Exhaust air flow (m^3/s)
A_{Ex} = Exhaust opening (nostril area) (m^2)
r = Distance from the opening (radius in a hemisphere) (m)

Still, $\dot{m}_r$ needs to be determined in order to find r and thus the volume of the hemisphere from where the inhaled air is assumed to come.

According to Table 2.5. the pulmonary ventilation for a person at moderate work is 30 l/min. The inhalation, however, does not take place continuously but approximately 12 times per minute, intermittently. If the inhalation takes place half the time, $\dot{m}_r$ = 60 l/min is obtained. For u_r = 0.25 m/s and A_{Ex} = 1.3 cm^2, r = 2.5 cm. This corresponds to a hemisphere volume of approximately 30 cm^3.

For an activity level corresponding to rest r = 1 cm, and the hemisphere volume is approximately 2 cm^3, i.e. in both cases relatively small volumes and small distances from the nose/mouth are obtained.

The above analysis suggests that the personal exposure for the CSP´s may be simulated as the mean concentration of a volume between 2 cm^3 and 30 cm^3 adjacent to the surface in breathing zone height, i.e. 1.5 m above the floor for a standing average sized woman and for the BTM.

In the CFD simulations two different concentrations regarding the personal exposure have been determined, namely the concentration in the cell closest to the breathing zone (~ 10 cm^3) and the mean concentration of a volume around the breathing zone including more cells (~ 30 cm^3).

Comparing the two concentrations reveals a relatively strong dependence on the concentration gradient close to the breathing zone, the higher gradient the greater is the deviation between the two concentrations, as may be expected. Ratios between the concentration in the “volume” and the nearest cell are found in the range of 0.5 to 5. This stresses the importance of the topic and the possible influence on the personal exposure assessment. Most of the results, however, show approximately equal concentration levels.

In the following chapters the personal exposure calculated by means of CFD corresponds to the contaminant concentration in the nearest cell along the Computer Simulated Person at a height of 1.5 m.

2.4. Trained Sensory Panel

2.4.1. Introduction

The aim of modelling the personal exposure is to assess what people actually inhale when they are located in a certain environment where contaminant sources prevail. Therefore, it seems obvious to use people as measuring instruments if possible and affordable.

People may be applied as an instrument in the determination of the contaminant concentration in two different ways, directly and indirectly.

Indirectly, by wearing a passive or an active sampling device, i.e. personal monitors located close to the breathing zone. Continuously or integrated this device may collect different kinds of gasses, particles, etc. In order to interpret the results it is necessary to know the relationship between the concentration measured by the sampler and what is actually inhaled. This is usually assumed to be the same, even though some investigations have reported deviations (e.g. Martinelli et al., 1983; Rodes et al., 1991; 1995). As mentioned in Chapter 1 the deviations depend on the concentration gradients in the breathing zone, among other things, which will be discussed in greater detail in the subsequent chapters.

Directly, personal exposure may be determined by locating a sampling device inside or very close to the mouth or the nose, for instance in shape of a tube connected to a pump and a gas analyser. This approach has been applied by Mundt (1994).

Another method is biological monitoring where biological markers are used to indicate exposure. The markers may be blood, urine, sputum or exhaled air (Sexton and Ryan, 1988). For instance, exhaled air was filled on a bottle and analysed to assess the personal exposure by Pleil and Lindstrom (1995). However, some difficulties arise when biological monitoring is used due to the fact that it is the dose rather than the exposure that is determined, and assumptions regarding respiration frequency, depth of inspiration, etc. may be necessary in order to assess the personal exposure where this approach is used.

A third way of determining personal exposure is by means of a Trained Sensory Panel (TSP). This is especially convenient when transient phenomena are studied

which occur when people are entering a room causing disturbances while they are inhaling room air and judging the air quality (Brohus et al., 1996).

A TSP is applied in this work to assess the personal exposure and the perceived air quality. The topic is further discussed in the following, including the assessment of perceived air quality and definitions of the sensory units olf and decipol.

2.4.2. Assessment of perceived air quality

Humans perceive the air as a combined response of the olfactory sense and the general chemical sense. The olfactory sense is situated in the nasal cavity and is sensitive to several hundred thousand odorants in the air. The general chemical sense is located all over the mucous membranes in the eyes and in the nose, and it is sensitive to a similarly large number of irritants in the air (ECA, 1992). These senses determine whether the air feels fresh and pleasant or stale and stuffy, whether the air irritates or not, and whether the air can be judged acceptable or unacceptable.

Perceived air quality is defined as the immediate impression of the indoor air quality experienced by the people entering a space (Fanger, 1988). Perceived air quality can also be expressed as the percentage of dissatisfied, *PD*, i.e. those persons who perceive the air to be unacceptable just after entering the space.

Sensory units

In order to quantify air pollution and air pollution sources as perceived by humans Fanger (1988) defined the two sensory units, the olf and the decipol.

One olf is the emission rate of air pollution (bioeffluents) from a standard person (sedentary activity level of 1 met , average skin area of 1.8 m^2, hygienic standard of 0.7 bath/day and changing underwear every day). Other pollution sources are then expressed as person equivalents, i.e. the number of standard persons (olfs) required to make the air as annoying, thus causing the same dissatisfaction, as the actual pollution source.

When more sensory pollution sources are present at the same time the total sensory pollution load can as a first approximation be determined by simple addition of the sensory load of the single sources (Bluyssen and Fanger, 1991; Wargocki et al., 1996).

Bluyssen and Fanger (1991), however, emphasise that further research may show that air qualities caused by mixtures of some materials may be perceived stronger or weaker than predicted by simple addition. Knudsen et al. (1994) found that the sensory emission rates for three frequently used materials vary with the pollution concentration, but they also found that the mixture of the three materials causes a percentage of dissatisfied approximately equal to the average of the individual materials.

Figure 2.12. shows the percentage of dissatisfied, *PD*, as a function of the ventilation rate per olf (standard person).

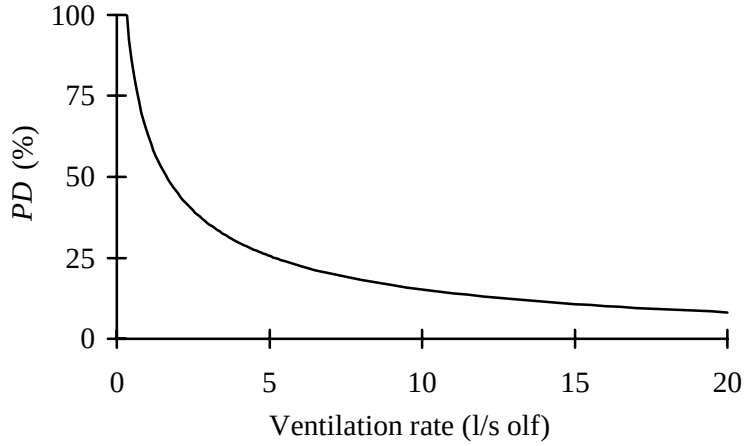

Figure 2.12. Dissatisfaction caused by one standard person (one olf) when ventilated by unpolluted outdoor air at different ventilation rates, *q*. Based on equations (2.69) and (2.70) by Fanger (1988).

$$PD = 395 \cdot \exp\left(-1.38 q^{0.25}\right) \quad \text{for } q \geq 0.32 \text{ l/s·olf} \tag{2.69}$$

$$PD = 100\% \text{ for } q < 0.32 \text{ l/s·olf} \tag{2.70}$$

The perceived air quality is measured in the unit decipol

1 decipol = 0.1 olf/(l/s) (2.71)

One decipol is the pollution caused by one standard person (olf) ventilated by 10 l/s of unpolluted air.

Figure 2.13. shows the relation between the air quality expressed in percentage of dissatisfied, *PD*, and expressed in decipol derived from the relations mentioned in Figure 2.12.

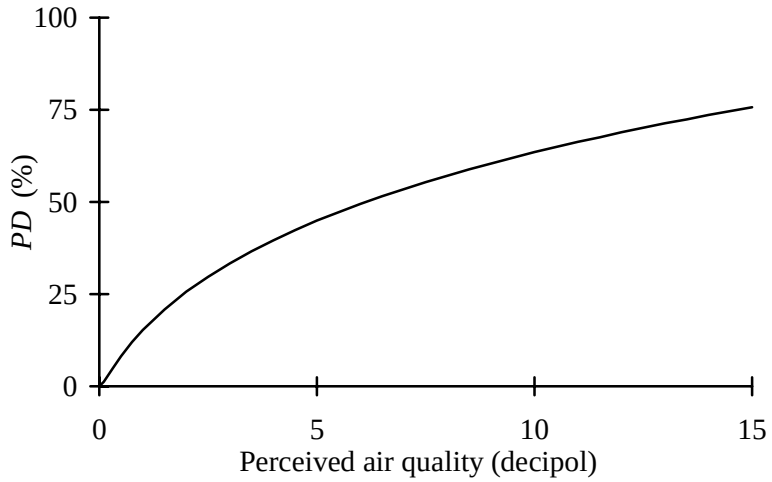

Figure 2.13. Relation between percentage of dissatisfied, *PD* (%), and the perceived air quality (decipol). Based on equations (2.72) and (2.73) by Fanger (1988).

$$PD = 395 \cdot \exp\left(-3.25 c^{-0.25}\right) \quad \text{for} \quad c \le 31.3 \text{ decipol} \tag{2.72}$$

PD = 100 % for $c > 31.3$ decipol (2.73)

or

$$c = 112 \cdot \left(\ln(PD) - 5.98\right)^{-4} \tag{2.74}$$

If it is assumed that the sensory sources are additive the total effect may be expressed, taking the ventilation effectiveness into account, as

$$c_e = c_{out} + \frac{10^{-2}}{q_{out}}\left(G_{eq} + \frac{G_1}{\varepsilon_{e,1}} + \frac{G_2}{\varepsilon_{e,2}} + \cdots + \frac{G_n}{\varepsilon_{e,n}} \right) \tag{2.75}$$

where

c_e = Personal exposure *or* perceived air quality (decipol)
c_{out} = Perceived air quality of outdoor air (decipol)
q_{out} = Ventilation rate of unpolluted outdoor air (m^3/s)
G_{eq} = Source strength of ventilation equipment (olf)
G_n = Pollution source strength regarding source no. *n* (olf)
$\varepsilon_{e,n}$ = Personal exposure index regarding source no. *n* (n.d.)

The addition of sensory sources should not be confused with the addition of sensory effects on people. Percentage of dissatisfied, intensity of odour or sensory irritation are not proportional to the concentration, consequently, they are not additive (Wargocki et al., 1996).

Sensory panel

In order to determine the perceived air quality a sensory panel is used. The panel may be untrained (naïve) or trained.

An untrained panel comprises a group of persons unrelated to the space to be examined. The panel members are asked to judge whether the air quality is acceptable or not, imaging s/he be exposed to such air quality every day. Thus the percentage of dissatisfied provides the perceived air quality (ECA, 1992). The necessary number of panel members depends on the required statistical confidence but it will typically be in the range of 20 - 50 people (Pejtersen and Mayer, 1993).

In this work a Trained Sensory Panel (TSP) is applied. A TSP comprises a group of persons trained to judge the air quality in comparison with references with known levels of perceived air quality. A panel of minimum six persons is recommended (ECA, 1992). Here, a panel of 14 persons (eleven male and three female) is selected from a larger group of naïve subjects on the basis of an entrance test.

The panel is trained to assess the air quality directly in the sensory unit decipol in comparison with five 2-propanone references ranging from 1 to 20 decipol, see Figure 2.14.

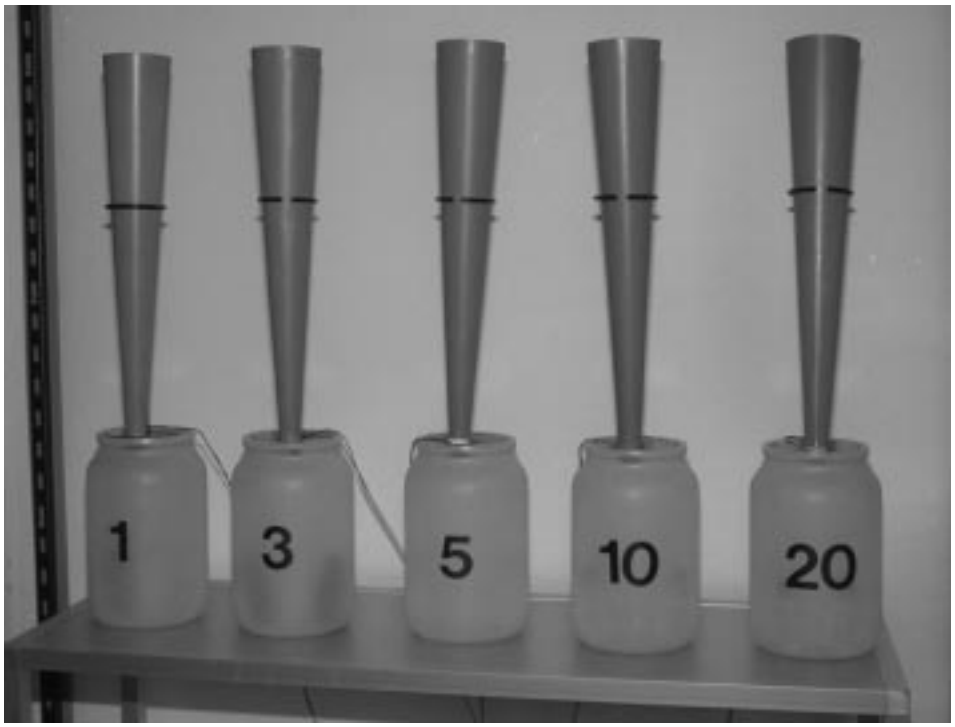

Figure 2.14. Five known 2-propanone references (milestones) of 1, 3, 5, 10 and 20 decipol used by the Trained Sensory Panel for judging the perceived air quality. The references consist of a 3-litre glass jar with a ventilated diffuser (~ 0.9 l/s). Inside the jar the 2-propanone is generated by passive evaporation from pure liquid 2-propanone in 30 ml bottles. According to Bluyssen and Fanger (1991) the references can be calibrated using the relation: decipol = 0.84 + 0.22·ppm.

During the training the panel members are exposed to unknown 2-propranone concentrations which should be compared with the known references in order to determine the perceived air quality.

The subjects are allowed to go back and forth between the unknown and the known concentrations as many times they require, but they should always take at least two inhalations of fresh air between each judgement to avoid adaptation. After the voting they are told the correct answer.

The training of the panel is started with a larger initial training period and then followed by approximately half an hour of training before each experimental session, corresponding to two unknown 2-propanone concentrations.

In order to evaluate the performance of the panel and to be able to calibrate the TSP, 8 different 2-propanone concentrations unknown to the panel are judged by every member on every experimental session without any feedback. It is thus assumed that if a panel member has judged the 8 2-propanone concentrations satisfying s/he will also be able to perform satisfying during the actual experiment.

It has been observed (e.g. Pejtersen and Mayer, 1993; Knudsen et al., 1994) that some subjects may have a systematic error when assessing the 2-propanone concentrations. The subjects tend to vote too high on concentrations below five decipol and too low on concentrations above five decipol. To eliminate this systematic error, the relation between voted and expected perceived air quality is modelled by means of a power function (Pejtersen and Mayer, 1993)

Figure 2.15. Members of a Trained Sensory Panel assessing the air quality in comparison with five levels of a known reference.

$$\text{Voted perceived air quality} = A \cdot (\text{Expected perceived air quality})^{B} \qquad (2.76)$$

The coefficients A and B are estimated by non-linear least-squares regression. A and B are determined for every single subject on account of all assessments during the entire experimental period according to the recommendations of Knudsen (1994). The specific coefficients for the single subjects are then used to calibrate the assessments by

$$\text{Calibrated perceived air quality} = (1/A \text{ voted perceived air quality})^{1/B} \qquad (2.77)$$

2.4.3. Personal exposure assessment using the TSP

A TSP can be used in personal exposure assessment in different ways. It can of cause be applied in the assessment of perceived air quality. This may de done

both in full scale, and also in small-scale using a diffuser like the ones shown in Figure 2.15. (Knudsen et al., 1993). Assumptions regarding full scale versus small scale air flow pattern and contaminant distribution have to be made, for instance, it can be necessary to apply fully mixed conditions in small scale and then translate the results to full scale by using the personal exposure index, ε_e, or by other means (Jensen and Nielsen, 1995).

The TSP may also be used to determine the concentration of a certain reference gas in comparison with "milestones" of known levels, for instance the 2-propanone. In case of 2-propanone the level assessed in the decipol unit may easily be converted to the ppm unit using the following relation (Bluyssen and Fanger, 1991)

$$c_{dp} = 0.84 + 0.22 \cdot c_{ppm} \tag{2.78}$$

where

c_{dp} = Perceived air quality using 2-propanone as reference (decipol)
c_{ppm} = Concentration of 2-propanone (ppm)

In this way it is possible to use 2-propanone as a tracer gas that may simulate the behaviour of contaminant sources in a ventilated room etc. The perceived air quality assessed by the sensory panel, c_{dp}, may then be converted into the personal exposure, c_e, which in this case equals c_{ppm}. One great advantage of this approach is the fact that it is also possible to measure the concentration of the reference gas chemically. Consequently, in the case of a ventilated room where 2-propanone is used as tracer gas the exhaust concentration, c_R, may be determined chemically and the personal exposure may be assessed by real persons and, finally, the personal exposure index, ε_e, can be determined. In that way it is possible to include the effect of transient behaviour of real people, which may be relevant, especially in assessment of short-term exposure and determination of the perceived air quality (Brohus et al., 1996).

A very important limitation of the approach is the adaptation. On account of the adaptation only the first impression of the air quality is valid, i.e. when a member of the trained panel enters a polluted room only the first inhalation can be used in the assessment. This method is limited to (very) short-term exposure measurements.

Chapter 3

Displacement ventilation

3.1. Introduction

The tools for personal exposure assessment described in Chapter 2 will now be applied on the two major room ventilation principles, the displacement principle and the mixing principle in Chapter 3 and Chapter 4, respectively.

This will be done in order to examine some of the characteristics regarding personal exposure for the two ventilation principles, and to develop knowledge and models that may facilitate the assessment. This will also highlight the deviations between the actual exposure and the assessment by means of the widely used compartmental approach, where the room air is assumed to be completely mixed.

Chapter 3 and Chapter 4 may serve as an illustration on the usage of the tools introduced in Chapter 2, i.e. the Breathing Thermal Manikin, the Computer Simulated Person, and the Trained Sensory Panel. The tools will be discussed and evaluated by means of comparisons with each other together with results from the literature.

The present Chapter 3 will start by summarising the characteristics of displacement ventilation. Then full-scale measurements and CFD simulations on personal exposure will be presented including the proposal of a simple exposure model that may be applied in the practical design of displacement ventilation systems. To generate the contamination warm and cold point contaminant sources are applied together with a planar source in the shape of the floor in the displacement ventilated room.

3.2. Characteristics of displacement ventilation

In the following some of the important characteristics of displacement ventilation will be mentioned and discussed in order to give an overview of the ventilation principle, and to clarify some concepts and ideas applied in the presented measurements and simulations presented.

According to Mundt (1996) displacement ventilation has been used in buildings to extract excess heat and contaminants since the antique and the middle age. From the 1950s displacement ventilation experienced a renaissance in industrial applications, and from the 1980s the principle became popular in comfort ventilation, especially in the Scandinavian countries.

The reason for the growing interest in the displacement principle is a possibility of obtaining a relatively high ventilation effectiveness and temperature effectiveness, and thus the possibility both to supply fresh air to the occupants and to remove contaminants and excess heat in an energy efficient and cost effective way. However, there are some limitations that should be acknowledged in order to perform a proper choice of ventilation principle and a successful design of the system.

Thermally controlled ventilation

Using displacement ventilation subcooled air is supplied in the lower part of the occupied zone of the ventilated room. The air is supplied with a low momentum (velocity) and a low turbulence level. Due to the gravity force affecting the dense air it spreads out radially along the entire floor in an almost horizontal layer with only very limited entrainment of the surrounding room air.

If the room is large (long) the flow will gradually be dissolved and entrained into the heat sources. If the room is small multiple reflections occur at the walls (Etheridge and Sandberg, 1996), see Figure 3.1. By repeated reflections the lower part of the room is filled with air, while part of the gravity current is entrained into the plumes of the heat sources or in the boundary layer flow along the walls which are often warmer than the surrounding air in the lower part of a typical displacement ventilated room.

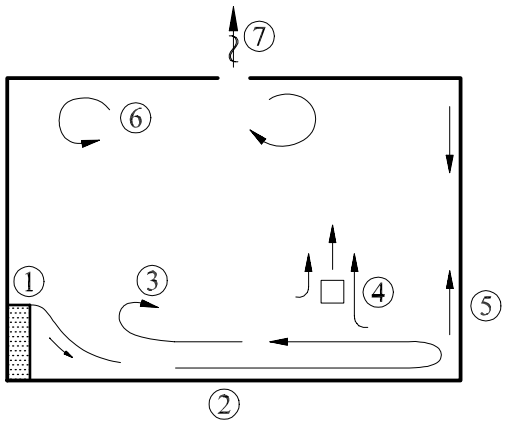

Figure 3.1. Air distribution in a typical displacement ventilated room. The subcooled air is supplied in the occupied zone (1), it spreads radially along the floor (2), it is reflected at the walls (3), and part of the current is entrained into heat sources (4) and warm walls (5). In the upper part of the room a recirculation zone is generated (6), and the air is extracted through exhaust openings located close to the ceiling (7).

In that way a stratified flow is obtained which is almost unidirectional in the lower part of the room. This kind of flow is thermally controlled and it is governed by the buoyancy forces in the fluid (e.g. expressed by the Archimedes number, *Ar*).

Even though the "old" air is displaced upwards, it must not be confused with piston flow (or plug flow) where the flow is controlled mainly by inertial forces (i.e. $Ar \sim 0$). Displacement ventilation is significantly influenced by the internal heat sources of the room and it is therefore also called source ventilation, especially in German literature (Fitzner, 1996).

The heat from the internal heat sources raises to the ceiling which in this way is heated together with the upper part of the room. Part of this heat is redistributed to the floor and the lower part of the room by means of radiative heat transfer. It results in a temperature distribution with a significantly vertical gradient. This temperature gradient facilitates removal of exhaust air at ceiling level several degrees above the temperature in the occupied zone. This allows an efficient use of energy, but it may also give rise to thermal discomfort if the temperature

differences are too large. Therefore, the vertical temperature gradient is an important design parameter to consider (Nielsen, 1993).

Stratification

The flow is unidirectional until the height where the net air flow rate of plumes generated by the heat sources equals the supply air flow rate. Above this height, i.e. the stratification height y_{st}, a recirculation zone is generated.

If the contaminant sources also are heat sources the displacement ventilation system can have a high ventilation effectiveness. In this case the stratified flow implies that the room is separated in a lower, cleaner part and an upper, more contaminated part. The two zones are separated at the stratification height, y_{st}, by an interfacial layer with a typical thickness of approximately 0.5 m (Etheridge and Sandberg, 1996), see Figure 3.2.

The concentration distribution is one of the important differences between displacement ventilation and conventional mixing ventilation regarding the air quality. In displacement ventilated rooms the air quality in the occupied zone is comparable with the supply air quality, while in mixing ventilation it is comparable with the exhaust air quality.

If the convection current from the contaminant source, in a room with several heat sources, is not the warmest, the contaminant may settle in a layer where the concentration locally exceeds the exhaust concentration (Skistad, 1994), see Figure 3.2. This phenomenon may influence the air quality, especially if a certain concentration peak is located in the lower part of the occupied zone.

It is found that the stratification of the flow is quite stable, even if people are moving around in a displacement ventilated room. Especially the thermal stratification is stable (also in case of relatively violent movements in the ventilated room), while the concentration distribution is slightly more affected, but even if the room air is temporarily mixed, the stratification is quickly re-established (Brohus and Nielsen, 1994a).

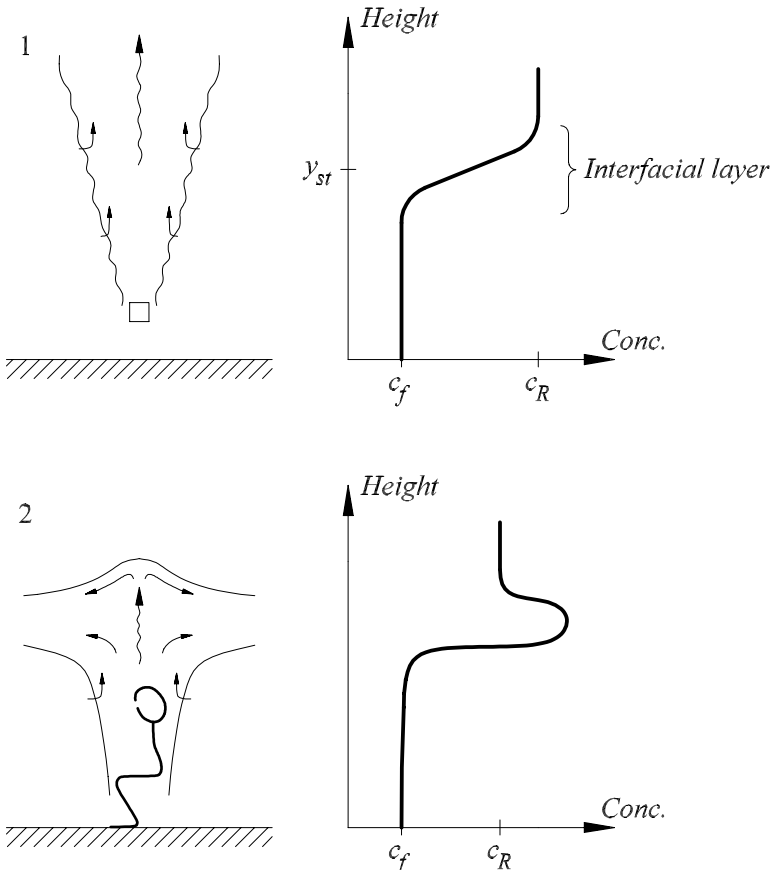

Figure 3.2. Concentration distribution in a displacement ventilated room. Typical distribution where the contaminant source also is the warmest convective current (1), and where it is not the warmest convective current (2). The concentration level in the lower part of the room close to the floor, c_f, depends on cold downdraught, disturbances in the room, etc.

Limitations

As mentioned previously, the supply air must be colder than the room air, therefore, there should always be some excess heat to be removed, at least for the major part of the year. If there is a temporary heating demand it can be handled by a radiator installation in the ventilated room, etc.

The contaminant sources should also be heat sources or lighter than the ambient air to obtain the concentration stratification. At the same time the exhaust opening must be located close to the ceiling.

In order to avoid thermal discomfort it is important to be aware of the adjacent zone close to the inlet device where the velocity is high and the temperature is low, as well as the vertical room air temperature gradient.

Personal exposure considerations

When dealing with personal exposure, displacement ventilation seems to be an obvious way to obtain a very high personal exposure index, ε_e, in the case of warm contaminant sources and a stratification height located above the breathing zone.

However, what happens when the stratification height is located below the breathing zone height? This is an important question due to the fact that the stratification height is determined primarily by the supply air flow rate in a given set-up of heat and contaminant sources. Therefore, if it is possible to reduce the necessary stratification height, the flow rate and consequently the energy consumption will be reduced accordingly.

Another relevant question regarding personal exposure is the influence of thermally passive contaminant sources, e.g. a point source located close to a person or a planar source in the shape of the entire floor, etc.

Furthermore, how is the perceived air quality in a ventilated room affected when the displacement principle is applied? Here, the transient behaviour is considerable whereas most recommendations and measurements assume steady-state conditions.

The above-mentioned questions will, among other things, be examined by means of the following measurements and simulations.

3.3. Measurements using a BTM

In this chapter personal exposure measurements comprising a Breathing Thermal Manikin in a displacement ventilated room are presented. First, the experimental set-up will be outlined, then the topic “exposure in proportion to the stratification height” will be examined and, finally, the effect of a passive point source will be investigated.

3.3.1. Experimental set-up

The personal exposure measurements presented in this chapter are performed by means of the Breathing Thermal Manikin (BTM) which is discussed in detail in Chapter 2.2. The measurements are performed in the full-scale displacement ventilated room shown in Figure 3.3. and Figure 3.4.

The room in Figure 3.3. consists of an outer steel framework to which the floor, ceiling and the walls are attached. Two of the walls consist of double glazed windows in order to facilitate smoke visualisation, the other walls are made of 20 mm Douglas wood laminates. The floor and the ceiling are insulated with 10 mm polystyrene and 50 mm glass wool, respectively. The entire test room is contained inside a conditioned laboratory building, see Figure 3.5.

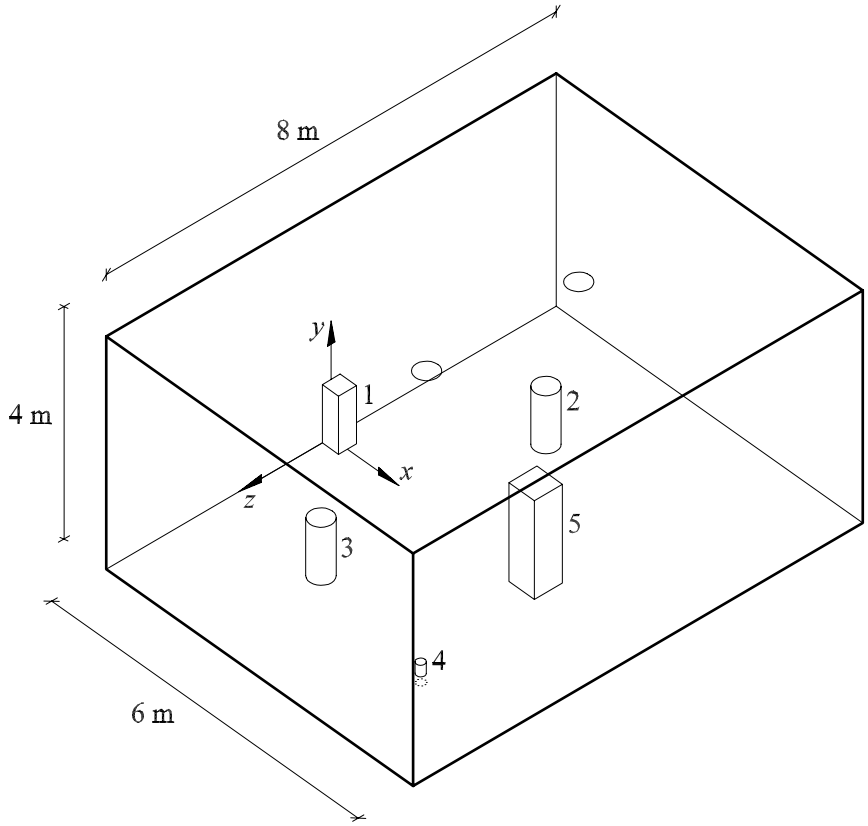

Figure 3.3. Displacement ventilated full-scale test room. The subcooled air is supplied by a low-velocity inlet device (1) and it is exhausted through two return openings in the ceiling. The heat load is generated by two person simulators (2,3), a point heat source (4) and the Breathing Thermal Manikin (5), represented by a box in the figure.

In Figure 3.4. the displacement ventilated room is shown in a two-dimensional plot where the locations of the different heat sources also are included.

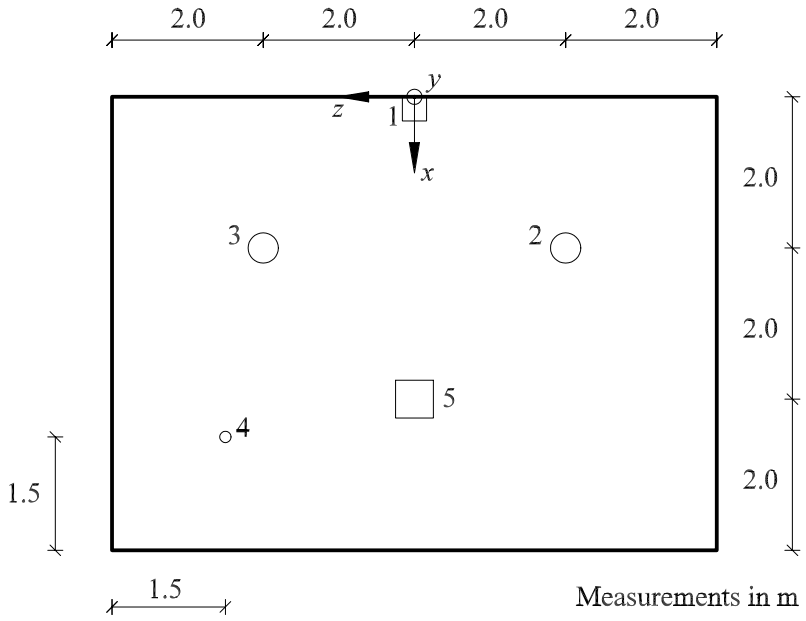

Figure 3.4. Displacement ventilated full-scale test room. The subcooled air is supplied by a low-velocity inlet device (1) and it is exhausted through two return openings in the ceiling. The heat load is generated by two person simulators (2,3), a point heat source (4) and the Breathing Thermal Manikin (5), represented by a box in the figure.

Figure 3.5. Photo of the full-scale test room with a floor area of 48 m^2 and a height of 4 m in the present set-up. On the photo the double glazing in one of the walls is seen, applied to facilitate smoke visualisation.

Three different heat sources are used: a point heat source consisting of heated coils mounted on an iron base surrounded by a 0.2 m high tube, ø 0.15 m; a person simulator in the shape of a 1 m high black-painted closed cylinder, ø 0.4 m, heated by four light bulbs (see Figure 3.6.); and finally, the BTM acts as a heat source.

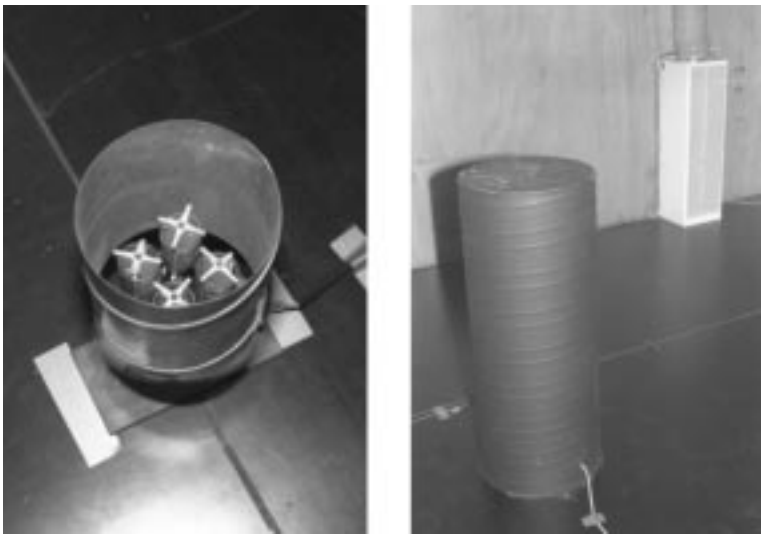

Figure 3.6. Photos of the point heat source (left) and the person simulator (right). The inlet device is seen in the upper right corner.

Two kinds of contaminant sources are examined, a passive source and a non-passive source. The non-passive source is simulated by nitrous oxide (N_2O) injected through an upward pointing tube, ø 0.01 m. The tube is located above a heat source at an elevation of 2 m. The passive contaminant source is simulated by a neutral density mixture of nitrous oxide and helium (He) injected through a porous foam rubber ball, ø 0.1 m, see Figure 3.7.

The tracer gas concentration is measured by photoacoustic spectroscopy (uncertainty ± 2%). The temperatures are measured by thermocouples, type k (uncertainty ± 0.2°C). The velocities are measured by temperature-compensated hot sphere anemometers (uncertainty ± 0.02 m/s).

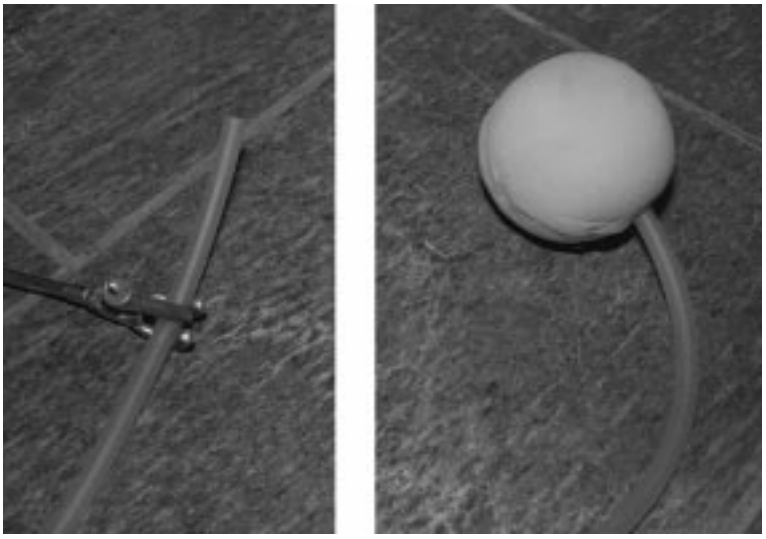

Figure 3.7. Photos of the two contaminant sources applied in the measurements. Both are used for tracer gas injection. Left: upward pointing tube, ø 0.01 m, located above a heat source (non-passive source). Right: porous foam rubber ball, ø 0.1 m (passive source). N_2O is used as tracer gas in both cases, and for the passive source it is mixed with He to obtain a neutral density mixture compared with the room air.

3.3.2. Exposure in proportion to stratification height

The measurements presented in Chapter 3.3.2. are made in collaboration with Christensen and Stevnhoved (1993). The steady-state exposure measurements are carried out with respiration through the mouth. In the present measurements no significant differences between respiration through the mouth and respiration through the nose are found.

Three different cases are examined corresponding to different stratification heights. In Table 3.1. the key parameters are summarised, and in Figure 3.8. and Figure 3.9. the vertical temperature distribution and the velocity profile are shown, respectively.

Table 3.1. Specification of the three cases examined in the full-scale measurements. q is the supply air flow rate, n is the air change rate, Φ is the heat load, t_0 is the supply air temperature, t_R is the return air temperature and y_{st} is the stratification height (found by means of the measurements).

Case	**Parameters**					
	q (m^3/h)	n (h^{-1})	Φ (W)	t_0 (°C)	t_R (°C)	y_{st} (m)
A	145	0.8	771	14.7	24.4	1.00
B	290	1.5	376	17.6	22.6	1.35
C	395	2.1	781	15.8	23.4	2.25

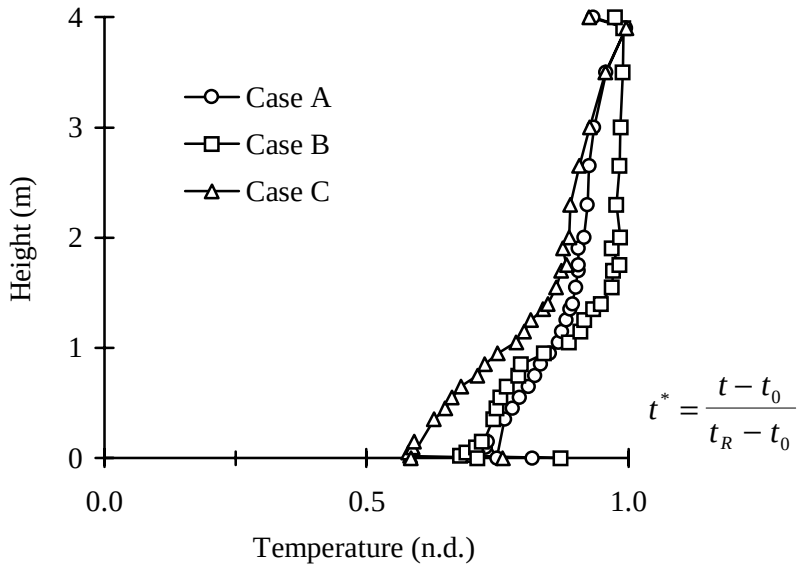

Figure 3.8. Dimensionless vertical temperature distribution in the displacement ventilated room in Case A, B and C. The measurements are performed at $(x,y) = (4,-1)$, i.e. 1 m beside the BTM, see Figure 3.4. The temperatures are made dimensionless by subtracting the supply air temperature and dividing by the difference between the return and the supply air temperature, i.e. $t^* = (t - t_0)/(t_R - t_0)$.

The temperature profiles seen in Figure 3.8. are typical for a displacement ventilated room, both regarding the surface temperatures and the vertical air temperature distribution. The outline of the curves with a relatively high gradient in the lower part of the room and a smaller (or almost no) vertical gradient in the upper part is also quite typical, even though differences may occur depending on the type and the intensity of the heat sources, among other things, (Nielsen, 1996; Mundt, 1996).

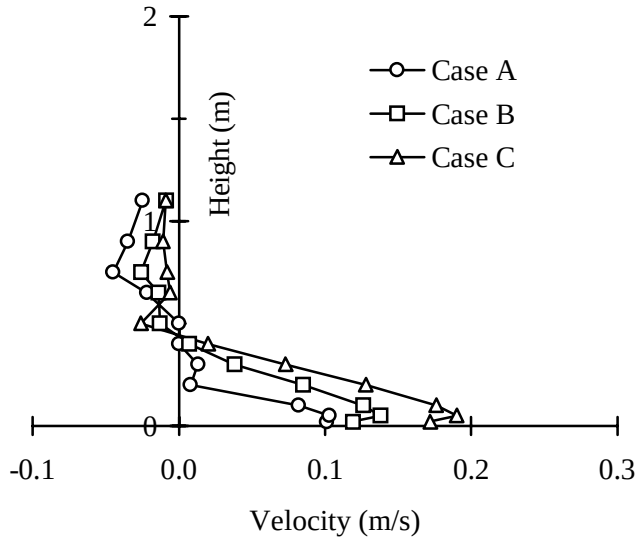

Figure 3.9. Vertical velocity profiles in the displacement ventilated room in Case A, B and C. The measurements are performed at (x,z) = (4,0) which corresponds to the location of the BTM. During the velocity measurements, the manikin is temporarily moved, for which reason the velocities represent the undisturbed velocity field at the location of the BTM.

Like the temperature distribution the velocity profiles are typical for a displacement ventilated room with high velocities close to the floor, and above the primary flow a secondary return flow in the opposite direction with a significantly lower level.

Both the temperature and the velocity levels correspond well to thermal comfort conditions for a typical activity level in usual indoor environments.

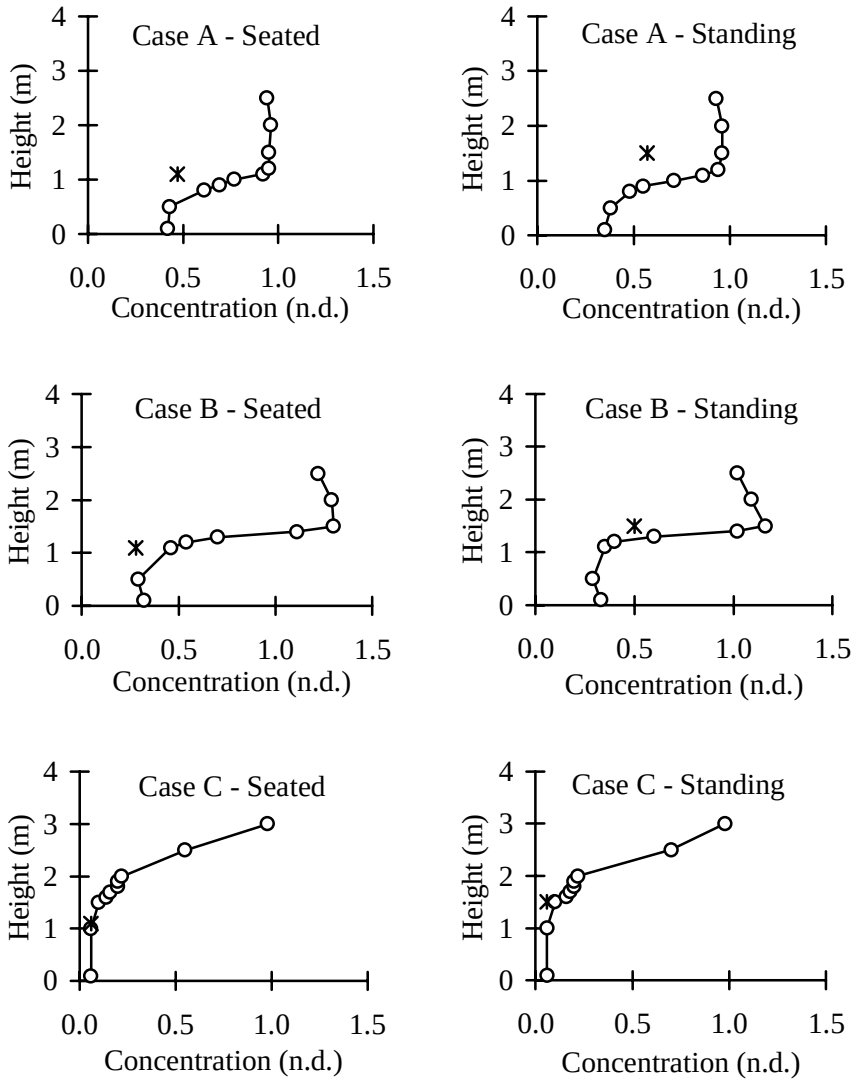

Figure 3.10. Dimensionless exposure (✱) and vertical concentration distribution (O) measured for the three stratification heights 1.00 m (Case A), 1.35 m (Case B) and 2.25 m (Case C) for the seated (left) and standing (right) BTM. The measurements are performed at $(x,z) = (3,-1)$. The exposure is measured at y_e = 1.1 m for the seated manikin and at y_e = 1.5 m for the standing manikin. In Case A and B the tracer gas is supplied above the heat source (3) in Figure 3.3. In Case C the tracer gas is supplied above the heat source (4) in Figure 3.3.

Table 3.2. Results from personal exposure measurements in a displacement ventilated room using a Breathing Thermal Manikin. c_e^* is the dimensionless personal exposure, ε_{oc} is the ventilation effectiveness in the occupied zone, and ε_e is the personal exposure index. The results correspond to the concentration distributions shown in Figure 3.10. and the specifications in Table 3.1.

Case	**BTM** position	c_e^* (n.d.)	ε_{oc} (n.d.)	ε_e (n.d.)
A	Seated	0.47	1.44	2.13
	Standing	0.57	1.54	1.75
B	Seated	0.28	1.65	3.57
	Standing	0.50	1.84	2.00
C	Seated	0.06	12.41	16.67
	Standing	0.06	12.08	16.67

In Figure 3.10. the exposure of a seated and a standing person in the shape of the BTM is shown at the three stratification heights, y_{st}, 1.00 m, 1.35 m and 2.25 m. The dimensionless exposure, c_e^*, the ventilation effectiveness in the occupied zone, ε_{oc}, and the personal exposure index, ε_e, for the three cases are summarised in Table 3.2. In all three cases the manikin (approximately 75 W), the two person simulators (2 x 100 W), and the point heat source (100 W or 500 W) constitute the heat load in the room.

Due to the uninsulated walls there is a slight heat transfer between the room and the surrounding laboratory. The difference between the mean room air temperature and the mean surface temperature is less than 0.5°C. Nevertheless, due to the temperature gradient there will be a heat gain in the lower part and a heat loss in the upper part. At the walls this causes a slight upward convective flow at the lower surfaces and a slight downward convective flow at the upper surfaces. The net effect is presumably of no significant importance in this context, a conclusion that is confirmed also by smoke tests.

One effect, however, that is clearly seen on the concentration profiles is the relatively high concentration in the lower part of the room, which is considerably higher than zero. This may have been caused by transport of contaminant from the upper part of the room to the lower part by downward convection currents in some parts of the room. This phenomenon may easily be found in practice too, e.g. in case of cold downdraught from windows, etc. Therefore, it is relevant to take this into account when the personal exposure is assessed, which is possible by using the present measurements.

As seen in Figure 3.10. the effect of entrainment and transport of room air from the lower and cleaner zone to the breathing zone is distinct, which is also pointed out by Holmberg et al. (1990), Stymne et al. (1991) and Etheridge and Sandberg (1996) among others. This means that the concentration of inhaled contaminant is smaller than the corresponding concentration at the same height at a "neutral" place in the room. In this case the entrainment provides a better indoor air quality in the displacement ventilated room than in a room with mixing ventilation.

The figure shows also that the ventilation effectiveness in the occupied zone is higher than in the case of mixing ventilation, where ε_{oc} approaches 1 in the ideal case. As expected, the effectiveness increases with increasing stratification height. In all cases the personal exposure index, ε_e, exceeds ε_{oc}, indicating that the quality of the inhaled air exceeds the mean indoor air quality in the occupied zone.

3.3.3. Personal exposure model for a displacement ventilated room

The exposure depends, among other things, on the concentration in the lower zone of the room. At the same stratification height this concentration may vary from case to case depending on the inlet device, the air temperature differences, the heat and contaminant source configuration, room surface temperatures, etc. To be able to take the concentration in the lower zone into account a new quantity is defined: the effectiveness of entrainment in the human boundary layer, designated η_e

$$\eta_e = \frac{c_P - c_e}{c_P - c_f} \tag{3.1}$$

where c_f is the concentration at the floor that typically corresponds to the concentration in the lower, cleaner zone of the displacement ventilated room, see Figure 3.11.

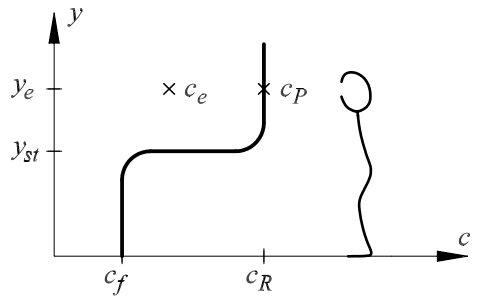

Figure 3.11. Virtual concentration distribution in a displacement ventilated room. y_e is the breathing zone height and y_{st} is the stratification height. c_e is located in between c_P and c_f due to the effect of entrainment in the human boundary layer.

The effectiveness of entrainment in the human boundary layer, η_e, expresses the ability to supply (fresh) air from the floor area to the breathing zone. It expresses the utilised fraction (c_P - c_e) of the possible concentration difference (c_P - c_f).

When η_e = 1, all the inhaled air comes from the lower zone and c_e equals the concentration at the floor, c_f. When η_e = 0 the exposure equals the concentration c_P at the breathing zone height, i.e. no particular effect because of the convective transport in the human boundary layer, see Figure 3.12.

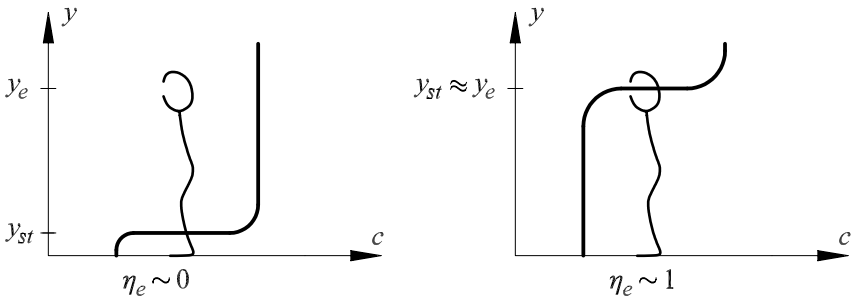

Figure 3.12. Effectiveness of entrainment in the human boundary layer, η_e. When the stratification height, y_{st}, decreases, the effectiveness decreases. When the stratification increases to the breathing zone height, y_e, the effectiveness of entrainment in the human boundary layer approaches 1.

In the case of complete mixing as well as in displacement ventilation with a stratification height located above the breathing zone, η_e is not defined. In these cases c_e equals the homogeneous concentration in the room or the concentration in the lower zone, respectively. This implies that $\eta_e \equiv 1$ for $c_P = c_f$.

One advantage of using η_e is the independence of the concentration in the lower zone that may vary in different cases. This enables and improves the comparison of results from different test rooms and different experimental set-ups.

From the results in Figure 3.10., η_e is calculated for Case A - Seated (0.91), Case A - Standing (0.66) and Case B - Standing (0.78), where the quantity is defined. It illustrates the extent to which the inhaled air is supplied from the lower and cleaner zone. In Case A - Seated, almost all air comes from the lower zone, while in Case A - Standing, only somewhat more than half of the air arises from the lower zone. The reason why η_e is lower in the Case A - Standing is the fact that the breathing zone is located at a higher level. This implies that more contaminated air is entrained in the boundary layer before it reaches the breathing zone where it is inhaled.

If c_e is expressed by means of the new quantity, we get the following equation

$$c_e = c_P - \eta_e \left(c_P - c_f \right) \tag{3.2}$$

i.e. the concentration of inhaled contaminant is expressed as a function of the concentration at the breathing zone height unaffected by a present person (c_P), the concentration at the floor, and the effectiveness of entrainment in the human boundary layer. If η_e is known, equation (3.2) can be used to estimate the personal exposure in a displacement ventilated room.

In the expression for η_e, the stratification height must be considered due to the significant influence of this parameter. If we furthermore want to incorporate the height of the breathing zone, y_e, the dimensionless height y_{st}/y_e may be used. This quantity attains the value from 0 to 1 when the stratification height increases from the floor to the breathing zone height, which is the range of interest in this context. Consequently, if the effectiveness of entrainment in the human boundary layer is expressed as a function of y_{st}/y_e, we may expect that η_e ranges from 0 to 1 when y_{st}/y_e increases from 0 to 1 (see Figure 3.12.).

The effectiveness of entrainment in the human boundary layer versus y_{st}/y_e is plotted in Figure 3.13..

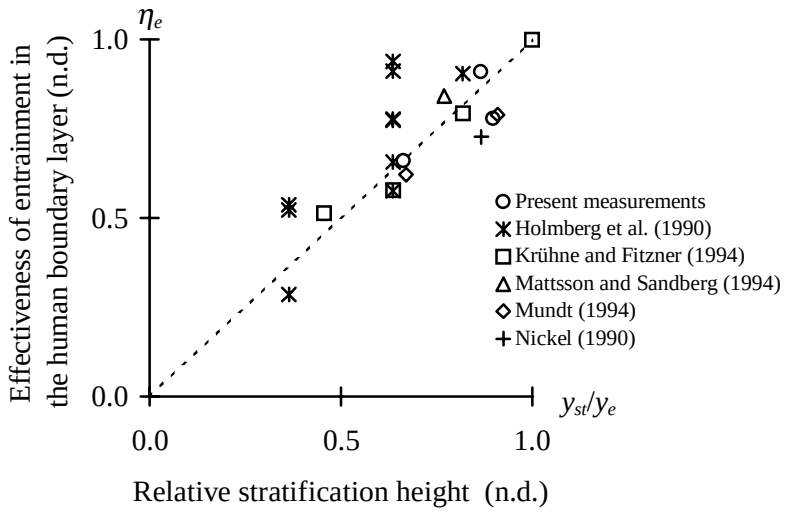

Figure 3.13. Effectiveness of entrainment in the human boundary layer, η_e, as a function of the dimensionless height, y_{st}/y_e, that may also be considered as a relative stratification height. The dotted line shows the approximate relation mentioned in equation (3.3)

The results shown in Figure 3.13. come from η_e calculated from the measurements presented in Figure 3.10. and corresponding results from different references. Here, the effectiveness and the dimensionless height are calculated on the basis of the various full-scale measurements performed in displacement ventilated rooms. Holmberg et al. (1990) have made measurements with tracer gas and paraffin oil particles (< 2 µm) in a room with heated cylinders as well as persons. The measurements were performed at different stratification heights for the persons sitting perfectly still and for seated persons with natural movements. Krühne and Fitzner (1994) performed measurements at different stratification heights with a heated cylinder. Mattsson and Sandberg (1994) performed measurements with a heated cylinder continuously moved back-and-forth as well as standing still. Here, the results from the "standing still" situation are used. Mundt (1994) has made measurements in a displacement ventilated room with a

person sitting and a person walking around, respectively. Nickel (1990) performed measurements with a heated cylinder.

Although different "models" of a person are used in different experimental set-ups, the quantity η_e and the relation y_{st}/y_e seem to establish a way of expressing the various results more generally.

If we make a linear equation fit on the plot in Figure 3.13. to obtain the coefficients of the equation $\eta_e = A + B(y_{st}/y_e)$, we find that $A = 0.22$ and $B = 0.73$ with a coefficient of determination $R^2 = 0.58$. This reveals that A is close to zero and that B is close to one. With a power equation fit, the following relation $\eta_e = C(y_{st}/y_e)^D$ is obtained. Here the coefficients $C = 0.95$ and $D = 0.75$ are found with $R^2 = 0.62$.

These results suggest an almost linear relationship between η_e and y_{st}/y_e with a starting point close to origo and with the effectiveness of entrainment in the human boundary layer approaching 1 when the relative height approaches 1.

For practical engineering purposes and without considerable loss of accuracy, one may use the simple relation

$$\eta_e = \frac{y_{st}}{y_e} \tag{3.3}$$

By inserting the above expression in equation (3.2) we obtain a model for the personal exposure in a displacement ventilated room.

This exposure model may also be obtained in another way by means of a zonal model approach. If it is assumed that the concentration of inhaled contaminant is a mixture of the concentration in the lower, cleaner part of the displacement ventilated room and the upper, more contaminated part, we may get the following expression if the two parts of the room are assumed to contribute with an amount proportional to the height occupied by the person, i.e.

$$c_e = \frac{y_{st} c_f + \left(y_e - y_{st}\right) c_P}{y_e} \tag{3.4}$$

Hence,

$$c_e = c_P - \left(\frac{y_{st}}{y_e} \right) \left(c_P - c_f \right) \tag{3.5}$$

Comparing equations (3.2) and (3.5) reveals that η_e is expressed as y_{st}/y_e which in fact is the approximate relation (3.3) found empirically from Figure 3.13.

Further analysis of the human boundary layer may show a non-linear dependence of η_e on y_{st}/y_e and relations where more parameters are considered may be found, but still the above expression may serve as a reasonable approximation for practical engineering use in the case of an exposed subject in a displacement ventilated room.

One limitation of the model is the effect of persons' movements. Since the basic results arise mainly from cases where a "still" model of a person is used, the equation (3.5) is not valid when the person is making violent movements or when the person is walking fast through the ventilated room. This topic is discussed in greater detail below.

Another limitation may be the influence of an obstacle in front of the person. If the boundary layer is disturbed or partially destroyed, the effect of entrainment and transport is obviously reduced.

If, for instance, a person is sitting (or standing) very close to the edge of a table, the thermal boundary layer is locally interrupted and the convective transport of air from below the table is significantly limited. The effect of this limitation depends to a great extent on the horizontal distance between the person and the obstacle. If the distance between the table and the person exceeds the boundary layer thickness, there will presumably be no reduction in the entrainment and transport in the human boundary layer. According to Homma and Yakiyama (1988), the thickness of the thermal boundary layer in front of the chest of a standing person is 0.07 - 0.15 m. Although the boundary layer thickness in a seated position is greater, the order of magnitude suggests that even relatively small gaps between the person and the table will enable convective mass transfer to take place.

When the two-zonal approach is applied together with the above personal exposure model it is possible to find theoretical expressions for the different ventilation effectiveness in a displacement ventilated room, when the stratification height, y_{st}, the return concentration, c_R, and the concentration in the lower part of the room, c_f, are known.

Table 3.3. Expressions of the different ventilation effectiveness as a function of the stratification height, y_{st}, etc. $\bar{\varepsilon}$ is the mean ventilation effectiveness, ε_{oc} is the ventilation effectiveness in the occupied zone, ε_P is the local ventilation index, and ε_e is the personal exposure index. c_R is the return concentration, and c_f is the concentration in the lower part of the room, y_{oc} is the height of the occupied zone, usually up to 1.8 m, and H is the room height.

Ventilation effectiveness	Definition	Location relative to stratification height	Expression in case of displacement ventilation
$\bar{\varepsilon}$	$c_R / \bar{c}$	-	$\dfrac{H}{H + y_{st}\left(c_f / c_R - 1\right)}$
ε_{oc}	c_R / c_{oc}	$y_{oc} \le y_{st}$	c_R / c_f
		$y_{oc} > y_{st}$	$\dfrac{y_{oc}}{y_{oc} + y_{st}\left(c_f / c_R - 1\right)}$
ε_P	c_R / c_P	$y_P \le y_{st}$	c_R / c_f
		$y_P > y_{st}$	$c_R / c_R \quad (= 1)$
ε_e	c_R / c_e	$y_e \le y_{st}$	c_R / c_f
		$y_e > y_{st}$	$\dfrac{y_e}{y_e + y_{st}\left(c_f / c_R - 1\right)}$

As seen from Table 3.3. all effectiveness apart from $\bar{\varepsilon}$ behaves in two different ways depending on the location relative to the stratification height.

In Figure 3.14. a plot of ε_e and ε_{oc} versus stratification height is seen in case of a displacement ventilated room where $c_f = 0.3\ c_R$.

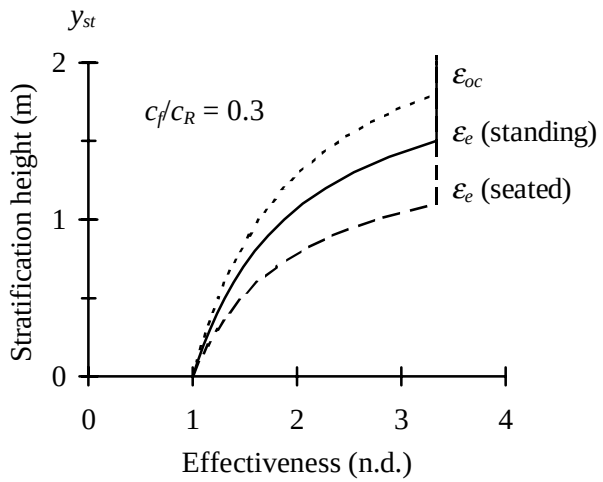

Figure 3.14. Ventilation effectiveness in the occupied zone (y_{oc} = 1.8 m), ε_{oc}, and personal exposure index, ε_e, for a standing person (y_e = 1.5 m) and a seated person (y_e = 1.1 m). c_f/c_R = 0.3, i.e. the concentration in the lower, cleaner part of the room amounts to 30% of the concentration in the upper, more contaminated part. The curves are based on the formulas shown in Table 3.3.

Figure 3.14. clearly shows the theoretical growth of effectiveness for increasing stratification height. It is found that ε_e (seated) ≥ ε_e (standing) ≥ ε_{oc}, ranging from 1.00 to 3.33, where y_e and y_{oc} are both exceeded by the stratification height. If y_{st} is further increased ε_e and ε_{oc} remain constant as indicated in the figure.

The shape of the curves depends on the ratio between the concentration levels in the lower part and the upper part of the room, c_f/c_R. In theory and in laboratory measurements c_f may equal zero, but in practice the concentration in the lower part of the room may easily deviate from zero due to cold downdraught, movements in the room, use of cooled ceilings, etc. Figure 3.15. shows the effect of the ratio c_f/c_R on the personal exposure index, ε_e, for a standing person.

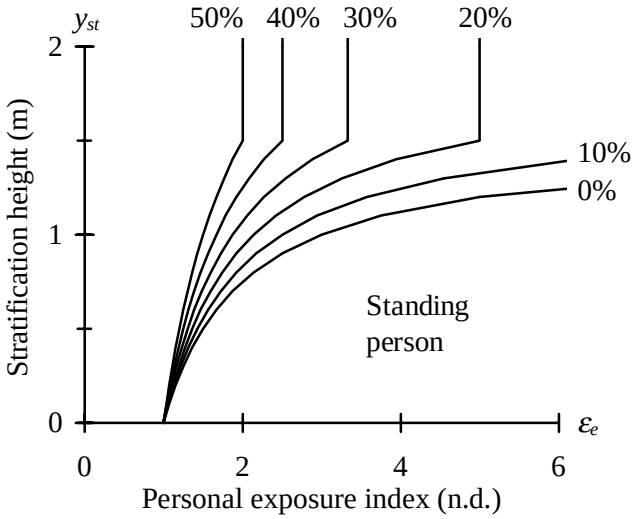

Figure 3.15. Personal exposure index, ε_e, for a standing person (y_e = 1.5 m) as a function of the stratification height, y_{st}, for different levels of the ratio between the concentration in the lower and the upper part of a displacement ventilated room, c_f/c_R, ranging from 0% to 50%. The curves are based on the formula in Table 3.3.

Figure 3.15. shows the significance of the concentration level in the lower part of the room, and stresses that it is important to reduce the possible factors that may facilitate and increase mixing of the stratified air in this part of the room.

If the personal exposure model is used to design a displacement ventilation system one has to know or to estimate c_f. This may be done by means of measurements or computer simulations or by means of assumptions based on experience. The assumptions may be based on knowledge of the geometry and the boundaries of the room together with the contaminant sources and the activities performed by the occupants. c_f will presumably be found in the range of 0 - 0.5 c_R.

The effect of movements on personal exposure

The measurements shown in Figure 3.13. mainly represent cases where the model of a person is sedentary or standing still. This fact raises the question as to the effect of movement on personal exposure.

One extreme is a sedentary person or a person standing still. Here, equation (3.5) provides a reasonable model for personal exposure in a displacement ventilated room. The second extreme is the case of a person walking quickly through a ventilated room. Here, the concentration of inhaled contaminant, c_e, obviously approaches the neutral concentration in the breathing zone height, c_P, due to the considerable horizontal velocity generated around the breathing zone. This case corresponds to $\eta_e = 0$. The actual case may be found somewhere between the two situations, depending on several parameters, for example the type of work, activity level, etc.

This point is supported by measurements of Holmberg et al. (1990), where η_e changed from 0.94 to 0.66 when the persons present changed from motionless to natural motion in a seated position.

Measurements of Mattsson and Sandberg (1994) with a moving heated cylinder may serve as another illustration. From these measurements the effectiveness η_e is calculated and shown in Figure 3.16. for three different velocities of the heated cylinder continuously moved back-and-forth in a displacement ventilated room. Even though Figure 3.16. is an example involving only one heated cylinder in "systematic motions" at one stratification height, it clearly illustrates that the effectiveness, η_e decreases when the movements increase as mentioned above.

Measurements and smoke tests with the Breathing Thermal Manikin located in a wind channel confirm that the thermal boundary layer is considerably affected at uniform velocities above 0.05 - 0.10 m/s (Brohus and Nielsen, 1994b; Hyldgaard, 1994).

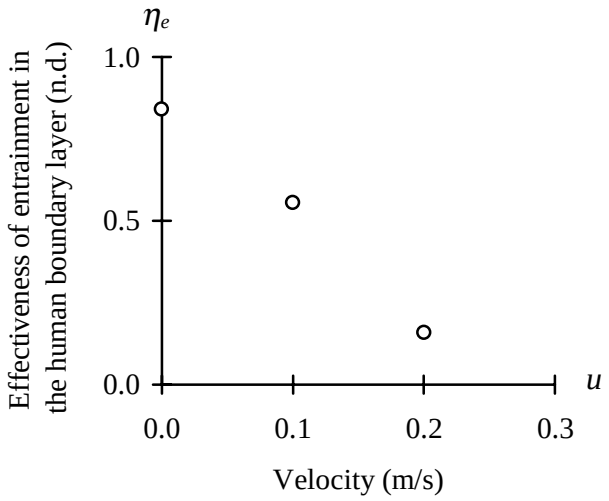

Figure 3.16. η_e as a function of the velocity relative to a moving cylinder. Measurements from Mattsson and Sandberg (1994) with a heated cylinder continuously moved back-and-forth in a displacement ventilated room.

Although the measurements, mentioned previously from Holmberg et al. (1990), show a decrease in η_e, there is still a significant effect of entrainment in the human boundary layer during "natural motion" in a seated position. This point is supported by Mundt (1994) who reports measurements where the concentration is found close to the nose of a person walking around in a displacement ventilated room. Here, the exposure is significantly below the corresponding concentration in the surroundings.

An improvement of the personal exposure model suggested above may be obtained by including the relative velocity, u, or the movements of the exposed person, e.g.

$$\eta_e = f\left(\frac{y_{st}}{y_e}, u\right) \tag{3.6}$$

General model

The two-zonal approach, which is quite convenient in case of displacement ventilation, may be expanded to a multi-zonal approach that may presumably be used in general. Here, the personal exposure, c_e, may be thought of as a combination of a number of vertical concentrations along the height of the human body, e.g.

$$c_e = \sum_{i=1}^{n} w_i c_i \tag{3.7}$$

where

c_e = Personal exposure (ppm)
c_i = Concentration at location i (ppm)
w_i = Weight function for location i (n.d.)

The weights w_i may be based on geometry (height or area covered by c_i) or it may be more sophisticated and consider a number of significant parameters, for instance

$$w_i = f\left(geometry, activity, u_i, t_i, Ar_i \ldots\right) \tag{3.8}$$

The simple model proposed in equation (3.5) may also be expressed in terms of weights where the two concentrations are weighted according to their relative heights, i.e.

$$c_e = w_f c_f + w_P c_P \tag{3.9}$$

where

$$w_f = \eta_e = \frac{y_{st}}{y_e} \qquad \text{and} \qquad w_P = 1 - \eta_e = \frac{y_e - y_{st}}{y_e} \tag{3.10}$$

which is valid for $y_e \geq y_{st}$.

3.3.4. Exposure in proportion to location of a passive point contaminant source

The above conclusions assume that the contaminant sources are also heat sources, generating the characteristic two-zone concentration distribution in the displacement ventilated room.

If the contaminant sources are passive, e.g. from building materials and other “cold” sources, the concentration distribution may be changed radically, and thus affect the personal exposure.

A passive point contaminant source is defined as a pollutant source without any significant initial momentum or buoyancy, i.e. the pollution is supplied with a very low velocity at room air temperature and at room air density.

In Figure 3.17. the exposure of the standing BTM is found in the case of a "high" and a "low" location of a passive point contaminant source. Figure 3.17. shows the effect of the two different concentration distributions corresponding to the different point source locations. In the case of high location of the source, c_e^* is 1.17 (Case 1) which must be considered rather low compared with the concentration peak in the height of the breathing zone. However, in the case of low location of the source, the dimensionless exposure amounts to 1.74 (Case 2) while the concentration at the height of the breathing zone approaches 1.

This reveals the advantage and the disadvantage of entrainment and transport in the human boundary layer. In Case 1 the boundary layer transports fresh air to the breathing zone and only a slight influence from the high local concentration in the breathing zone height is seen. In Case 2 the boundary layer obviously transports contaminated air to the breathing zone even though no particularly high concentration is found at the breathing zone height at a distance of 0.9 m.

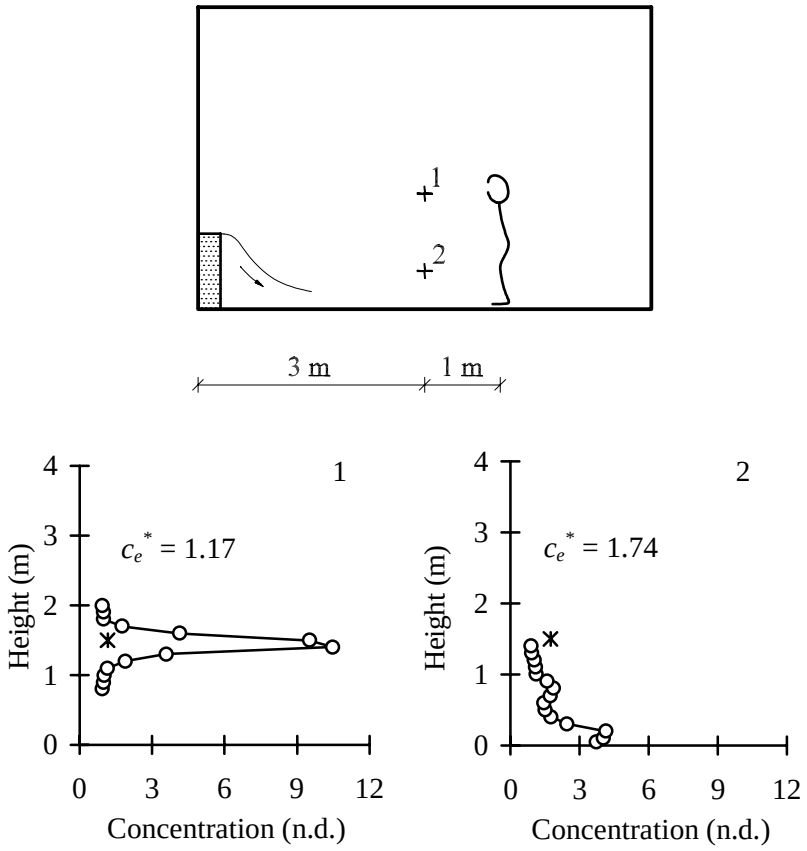

Figure 3.17. Dimensionless personal exposure (**∗**) at vertical concentration distribution (O) corresponding to a high (Case 1) and a low (Case 2) location of a point contaminant source in the displacement ventilated room. The concentration profile is measured 0.9 m from the BTM and 0.1 m from the source. The measurements are performed under conditions corresponding to Case B (see Table 3.1.). Neutral density tracer gas N_2O mixed with He is supplied through a porous foam rubber ball.

Personal exposure as a function of the point source height and the point source location is further examined in Figure 3.18. Two different cases are investigated. Case 1: the standing BTM facing the inlet device. Case 2: the standing BTM reversed as shown in the figure.

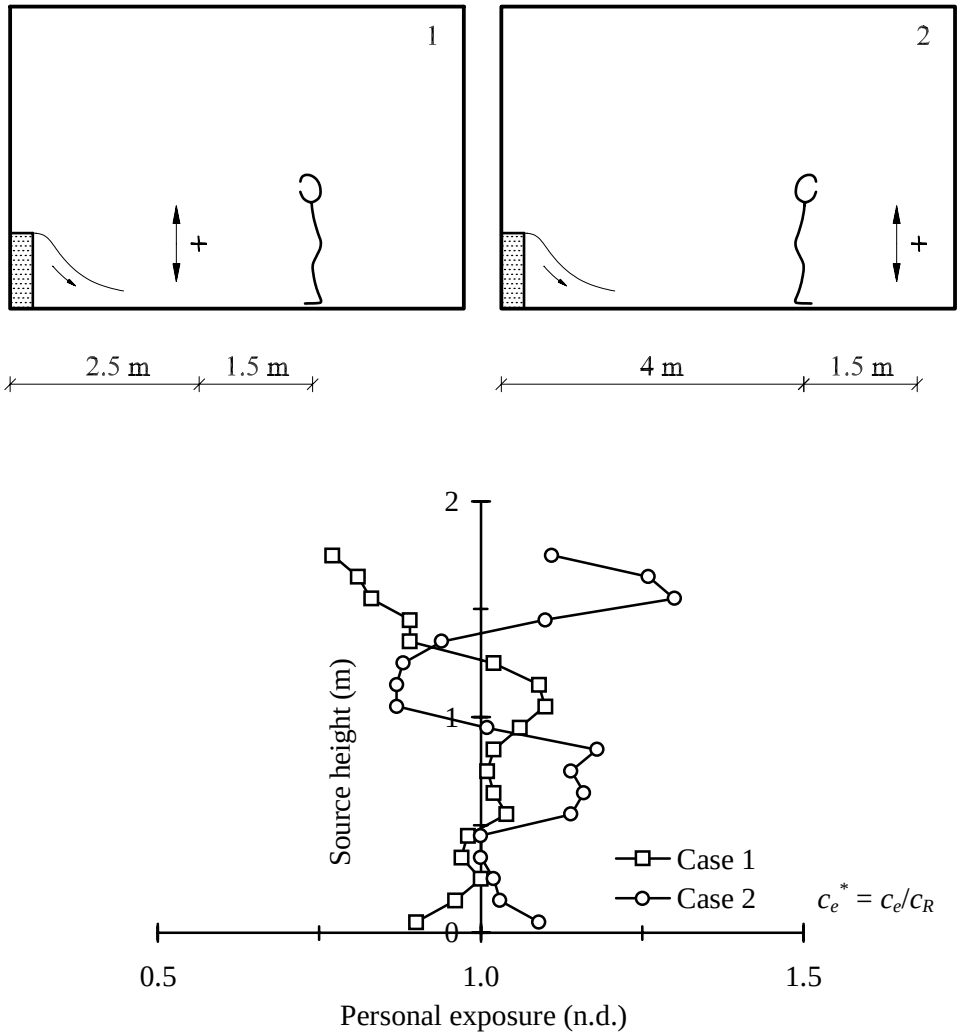

Figure 3.18. Dimensionless personal exposure, c_e^*, as a function of point contaminant source height in the displacement ventilated room. The horizontal distance between the source and the BTM is 1.5 m. Case 1: BTM facing inlet device (□). Case 2: BTM reversed (o). The measurements are performed under conditions corresponding to Case B (see Table 3.1.). Neutral density tracer gas N_2O mixed with He is supplied through a porous foam rubber ball.

Figure 3.18. shows how the exposure clearly varies with the elevation of the point source in the room. Both improved as well as deteriorated indoor air quality compared with the case of complete mixing is found. A distinct dependence on the flow field stresses the importance of convective mass transfer when pollutant dispersion is addressed (Brohus and Nielsen, 1994a). In Case 2 where the BTM, still facing the source located 1.5 m away, is turned around the exposure is almost opposite to Case 1, as if mirrored in the ordinate axis of Figure 3.18. In the one case the horizontal convective flow removes or dilutes the contamination, either giving rise to improved conditions ($c_e^* < 1$) or somewhat "mixed" conditions ($c_e^* \sim 1$) in the lower zone. In the other case the horizontal convective flow transports the contamination directly against the manikin where a fraction is entrained in the boundary layer giving rise to enhanced exposure ($c_e^* > 1$). Actually, this result may to some extent be expected when the stratified flow is considered with a main flow at the floor, reverse flow above, etc.

In Figure 3.19. a similar experimental set-up is used but now the BTM is seated. The results in Figure 3.19. show a generally lower exposure level in Case 2 but, otherwise, the same tendencies are found as regards Figure 3.18.

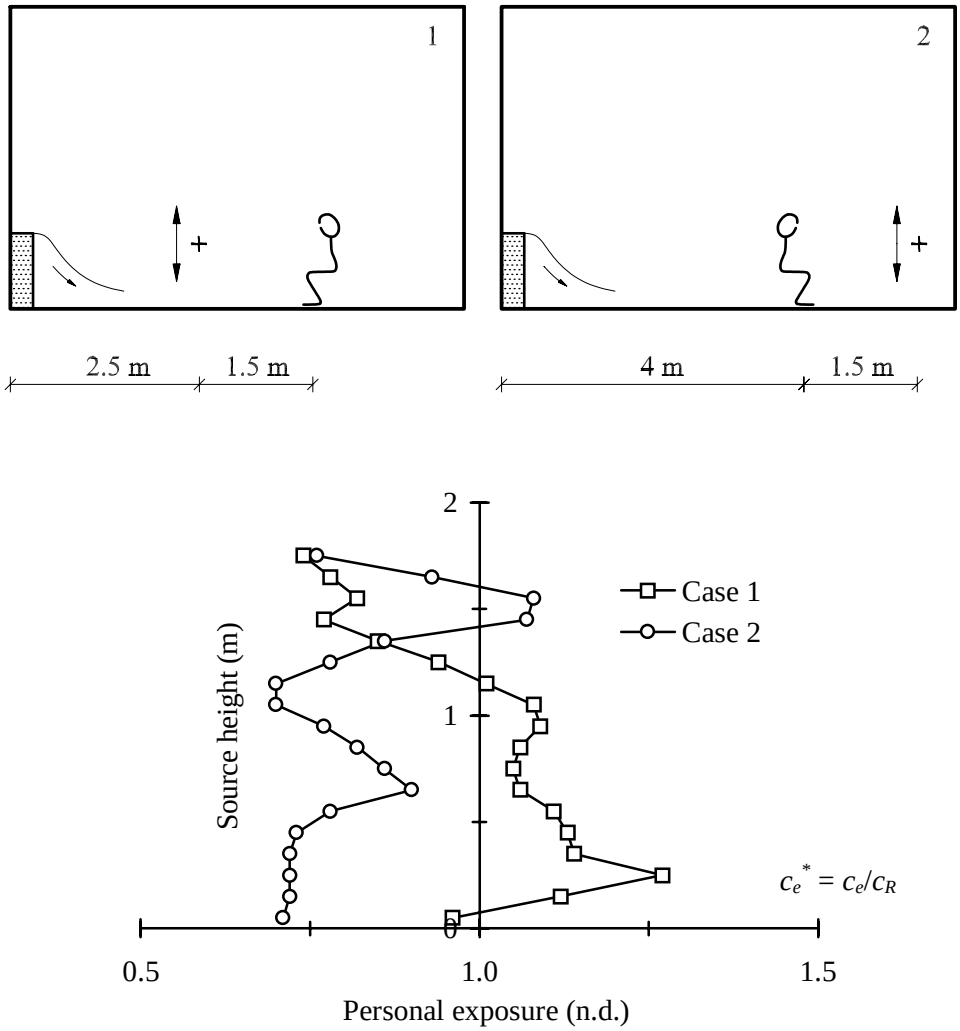

Figure 3.19. BTM seated, otherwise the conditions are the same as mentioned in Figure 3.18.

To illustrate the route of the contaminant in the boundary layer measurements are performed on the contaminant concentration at the chest and the contaminant concentration at the back in proportion to the point source height, see Figure 3.20. The conditions are otherwise the same as in Figure 3.18., Case 2.

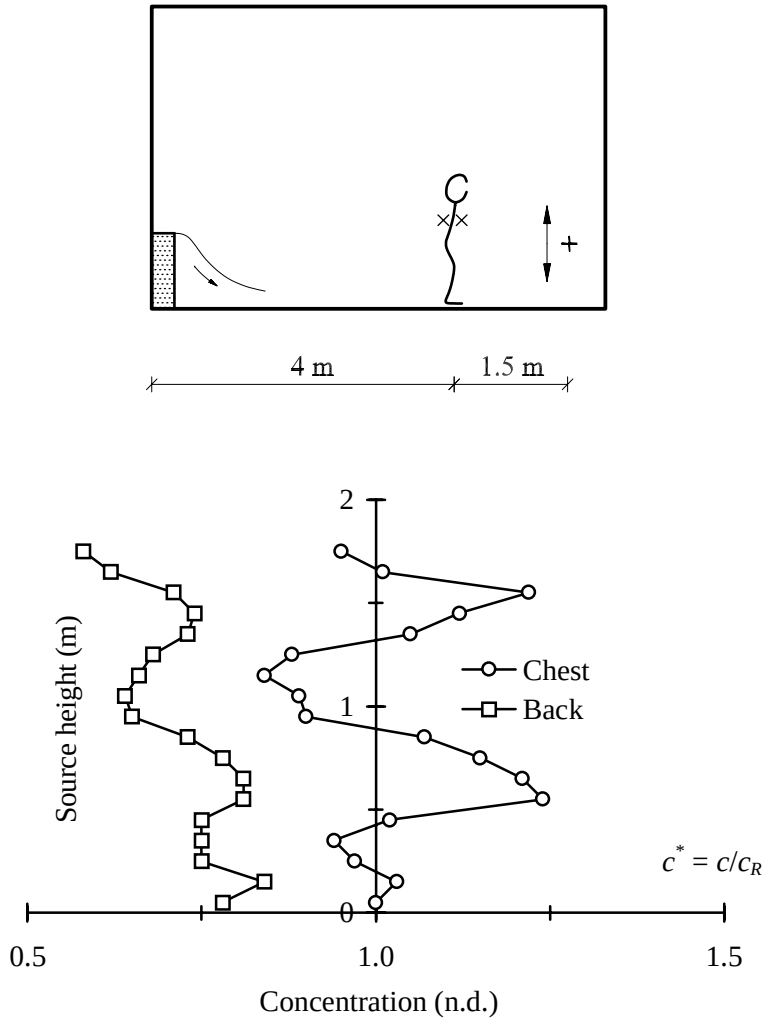

Figure 3.20. Dimensionless concentrations measured at the chest (o) and at the back (□) at a distance of 0.3 m from a virtual point between the ears of the BTM. The concentrations are found as a function of the vertical location of the point contaminant source. The conditions are otherwise the same as in Figure 3.18., Case 2.

The concentration at the two points in Figure 3.20. are measured at the same height in the room. If the Breathing Thermal Manikin was not present they would be approximately the same, while in the actual case there is a significant difference. What makes the difference is the presence of a person and the entrainment and transport of the contaminant as well as the fresh air in the boundary layer.

If the concentration at the chest is compared with the personal exposure in Figure 3.18., Case 2, a very good correspondence is seen. This is due to the fact that the main part of the inhaled air comes from the boundary layer in front of the person, anyhow, in the case of an almost motionless person, unaffected by obstacles in a room, where the velocities from the air distribution system are sufficiently low to avoid draught and to ensure thermal comfort.

The measurements show a significant influence of the person's orientation relative to the flow field and relative to the passive point contaminant source. If the BTM is turned around to face the inlet, the exposure may presumably be reduced by 25% in the present case.

If a contaminant source (passive as well as non-passive) is located close to a person, e.g. in the occupant's hands or on the desk top, very high exposures may be obtained. In this case personal exposure depends to a large extent on local flow phenomena around the person and the source (Brohus and Nielsen, 1995). In Figure 3.21. the personal exposure to a point contaminant source located close to the BTM is examined for standing position and seated position, respectively.

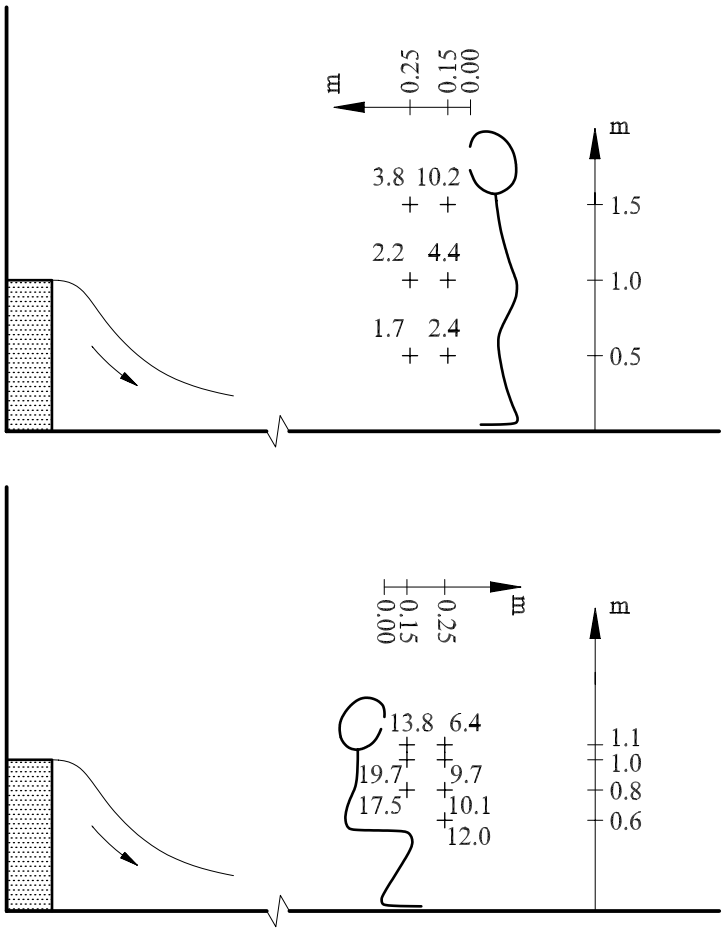

Figure 3.21. Dimensionless personal exposure, c_e^*, for different locations of a passive point contaminant source located close to the standing BTM (top) and the seated BTM (bottom). The measurements are performed under conditions corresponding to Case B (see Table 3.1.). Neutral density tracer gas N_2O mixed with He is supplied through a porous foam rubber ball. The horizontal distances shown in the figure correspond to the distance from the front edge of the mouth to the centre of the source.

Figure 3.21. clearly illustrates the effect of entrainment in the human convective boundary layer and stresses the importance of taking it into consideration when significant local gradients in the concentration field prevail. For instance, where the BTM is seated we see that for the point source located just in front of the

head, at a horizontal distance of 0.25 m the dimensionless concentration is 6.4. When the source is lowered by approximately half a metre, the exposure is actually doubled due to entrainment along the legs and the trunk.

Personal exposure index in displacement ventilated rooms

In the figures shown above, all concentrations are made dimensionless by dividing by the return concentration, c_R. Consequently, the personal exposure index, ε_e, is easily obtained as the inverse of the dimensionless exposure.

If the room air is fully mixed, both the dimensionless personal exposure, c_e^*, and the personal exposure index, ε_e, equal 1. When the exposure decreases due to improved indoor air quality, ε_e exceeds 1. This is the typical case in displacement ventilated rooms, see Figure 3.22.

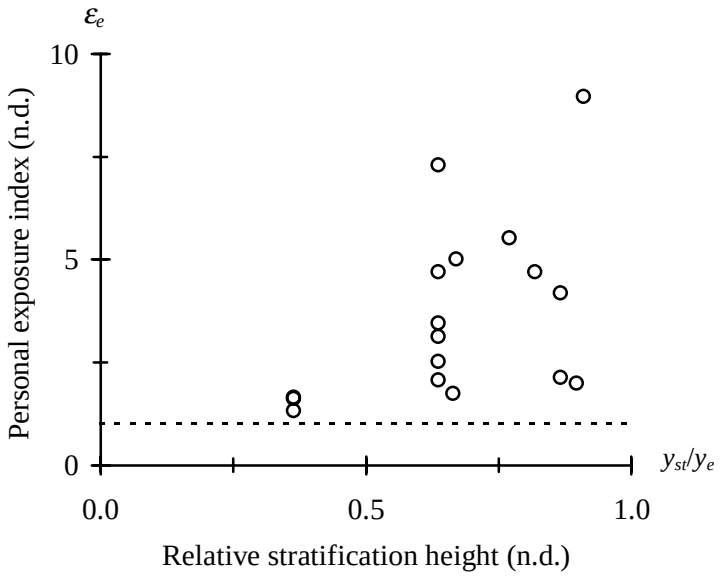

Figure 3.22. Personal exposure index, ε_e, as a function of the dimensionless height y_{st}/y_e (relative stratification height). The results correspond to those shown in Figure 3.12. The personal exposure index in case of complete mixing is indicated by the dotted line, i.e. $\varepsilon_e = 1$.

In Figure 3.22., ε_e is plotted as a function of y_{st}/y_e for the measurements corresponding to Figure 3.13. The dotted line indicates complete mixing. The results show how the displacement principle improves the air quality compared with dilution ventilation. In practice, the results will appear less significant due to persons' movements and other disturbances in a displacement ventilated room as discussed previously.

One of the advantages of using ε_e, compared to for example the ventilation effectiveness in the occupied zone, is the fact that the personal exposure index relates to what is actually experienced by a person and not just a kind of "mean" air quality. If ε_e is known, we may, as a first step, treat the ventilated room as fully mixed. The personal exposure index is then used to convert the "fully mixed exposure" into "actual exposure" when the mean concentration is divided by ε_e (Brohus and Nielsen, 1996c).

3.4. Measurements using a TSP

The results shown in the preceding chapter are all chemical measurements performed at steady-state conditions. Consequently, the results apply mainly for mid-term and long-term exposure assessments. Perceived air quality, however, is defined as the immediate impression of the indoor air quality experienced by the people entering a room (Fanger, 1988). In that case it is crucial to consider the transient phenomena which occur when people are entering a room causing disturbances, while they are inhaling room air and judging the air quality.

In this chapter results will be presented which are highly transient. Here, the air quality in a displacement ventilated room will be determined by a Trained Sensory Panel (TSP) together with chemical measurements. This implies that the personal exposure in the present measurements is found directly by asking humans.

One of the objectives of the measurements is to examine whether the improved air quality in displacement ventilated rooms found by long-term chemical measurements, can be confirmed in the short-term case applying the concept of perceived air quality. Some measurements on the entrainment and transport of fresh air in the human convective boundary layer will also be presented and discussed.

3.4.1. Experimental set-up

Facilities

The measurements are performed in a test room of stainless steel with a floor area of 9 m^2 and a height of 2.5 m, see Figure 3.23. Subcooled air is supplied through a perforated floor and exhausted through four openings in the ceiling. The supply air temperature is controlled to keep the air temperature in the breathing zone height close to 22°C during the experiments. Five light bulbs of 100 W located 0.1 m above the floor constitute the heat sources.

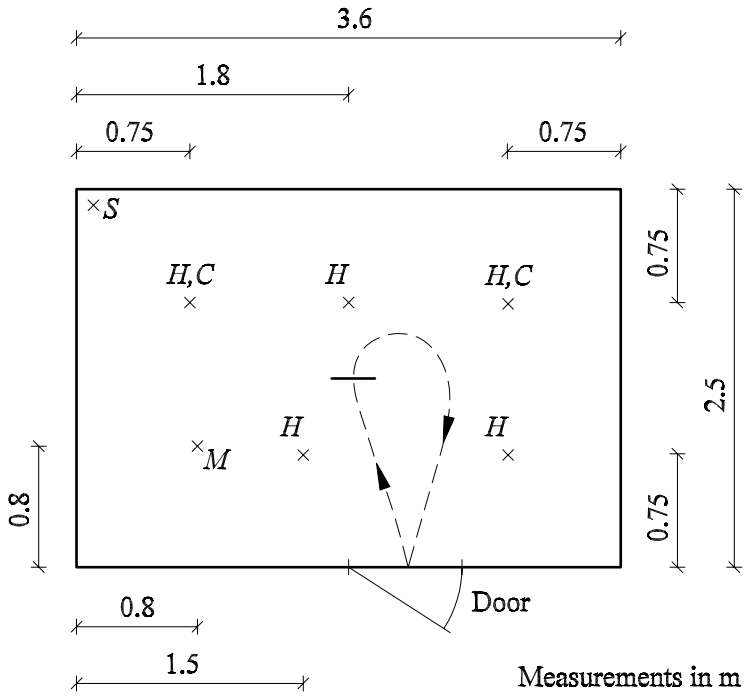

Figure 3.23. Location of heat sources (*H*) and contaminant sources (*C*) in the displacement ventilated full-scale test room. Measurement location for the vertical concentration and temperature profiles (*M*). A large stop watch is located at (*S*). The route of the subjects is shown by the dotted line. The bold line on the route shows where the subjects do the assessment. The room height is 2.5 m.

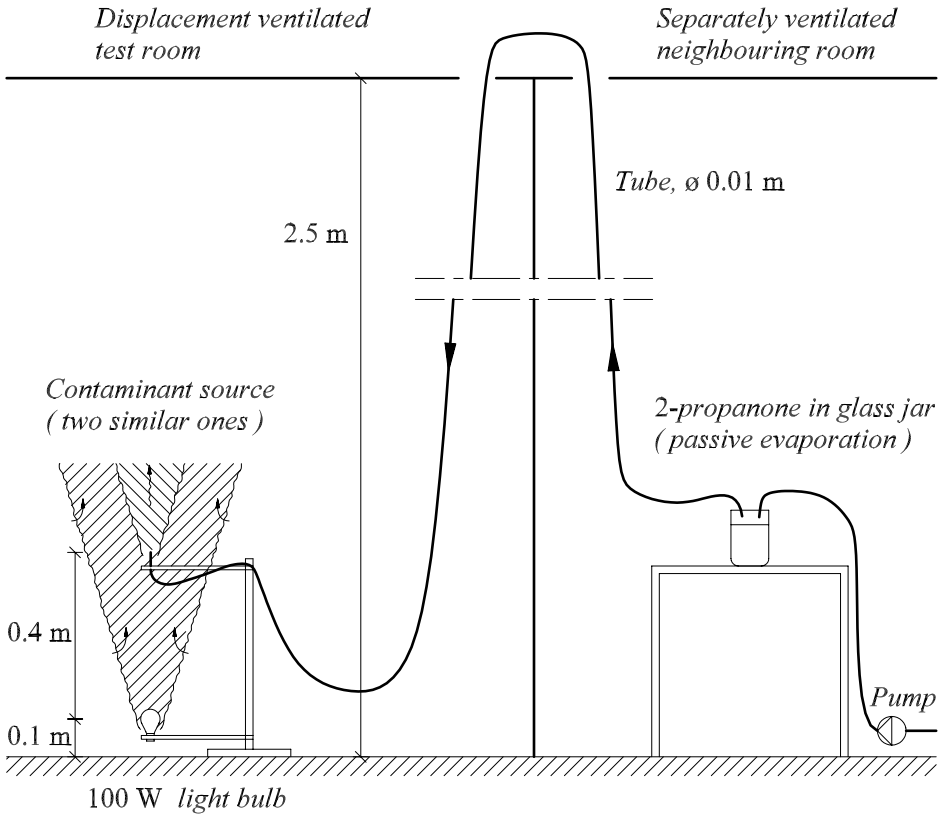

Figure 3.24. Sensory and chemical contaminant source used in the present measurements. The source consists of 2-propanone generated by passive evaporation from liquid phase in a 3 litre glass jar. The gaseous contaminant is transported from the glass jar to the test room by means of a pump and a tube, ø 0.01 m. The 2-propanone is delivered by the tube with an initial upward velocity. Then it is contained and transported to the upper part of the test room in the plume of ascending air formed by a hot light bulb (100 W) located below the tubes, see photos in Figure 3.25. Two identical sources are used in the experiments, both supplied from the same glass jar by means of a T-junction. The location (*C*) is shown in Figure 3.23.

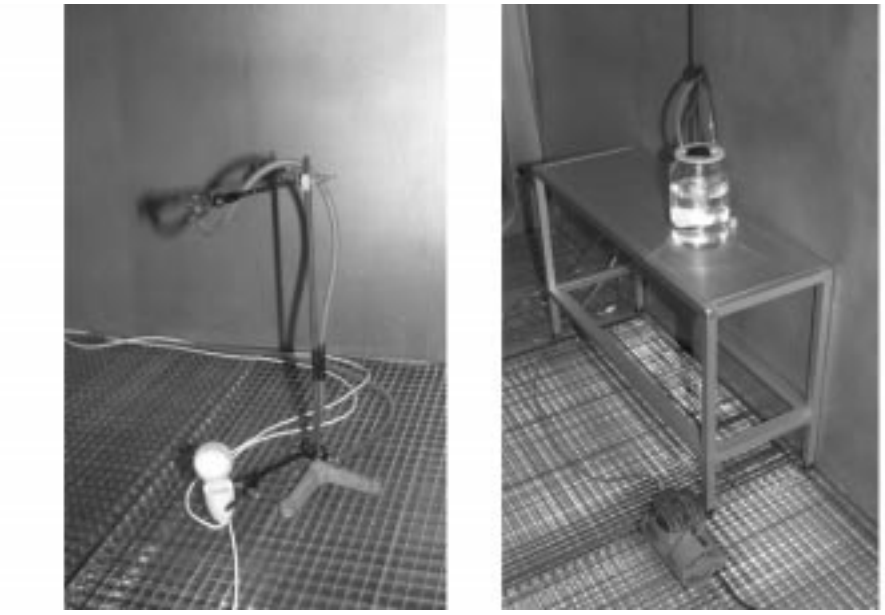

Figure 3.25. Photo of the Sensory and chemical contaminant source used in the present measurements (see Figure 3.24.). Left: 2-propanone delivered above a hot light bulb. Right: Passive evaporation of liquid 2-propanone.

Sensory panel

A panel of 12 judges is trained to assess perceived air quality directly in the sensory unit, decipol. The panel is trained to assess the air quality in comparison with five known 2-propanone references ranging from 1 to 20 decipol. The assessments are calibrated according to the description in Chapter 2.4.2. The contaminant concentration is also measured chemically by means of a gas analyser (in ppm 2-propanone) and converted to perceived air quality (in decipol) as explained in Chapter 2.4.3.

Test cases

Three test cases are examined in the study, see Table 3.4. The cases correspond to different concentration distributions generated by changing the air flow rate and the heat load, while the supply of contamination is kept approximately constant.

Table 3.4. Specification of the three test cases. q is the supply air flow rate, n is the air change rate, Φ is the heat load, t_0 is the supply air temperature, and t_R is the return air temperature. The heat load is generated by five 100 W light bulbs in Case 1 and Case 2. In Case 3 only the light bulbs below the two contaminant sources are switched-on.

Case	**Parameters**					
	No. of subjects	q (m^3/h)	n (h^{-1})	Φ (W)	t_0 (°C)	t_R (°C)
1	12	263	12	500	17.4	23.1
2	11	473	21	500	18.7	22.3
3	12	572	25	200	20.2	22.5

The heat load and the air flow rate are chosen to obtain different concentration distributions, corresponding to stratification heights below as well as above the breathing zone height. The average height of the panel is 1.79 m, corresponding to a breathing zone height of approximately 1.6 m.

Procedure

The experiment is performed over three days, one case a day, where the subjects of the panel assess the perceived air quality one by one. There is an interval of approximately 15 minutes between each assessment to ensure that the flow field and the contaminant distribution are re-established. The subjects are told to walk in a usual, calm speed and to follow a certain predetermined route in the room indicated in Figure 3.23. When they pass a certain location in the middle of the room they do the assessment and walk out of the room again. The door to the test room is operated by another person to ensure minimum disturbance of the flow field before entering the room.

The vertical profile of 2-propanone in the room is measured chemically both during the assessments as well as over a longer period with the same set-up but without the panel (see Figure 3.27.)

3.4.2. Perceived air quality in a displacement ventilated room

The vertical temperature distribution in the displacement ventilated room for the three test cases is shown in Figure 3.26. The temperature profiles are recorded during the assessments.

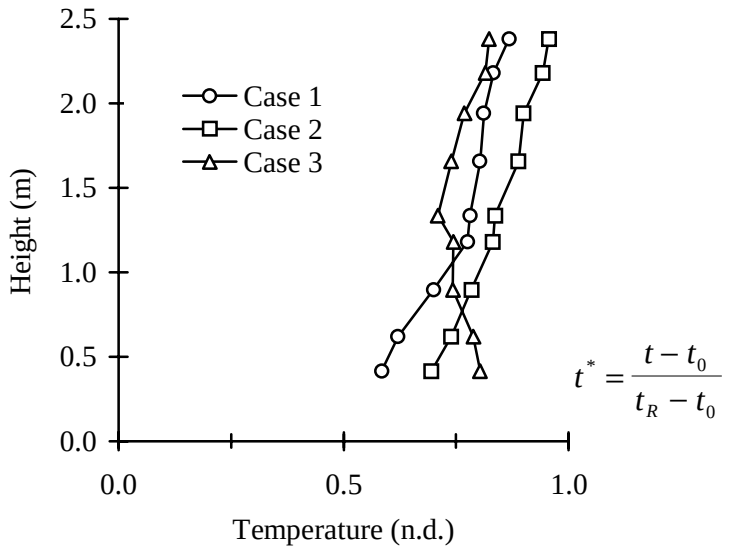

Figure 3.26. Dimensionless vertical temperature distribution in the displacement ventilated test room in Case 1, 2 and 3 during the assessments. The supply temperature, t_0, and the return temperature, t_R, for the three cases are summarised in Table 3.4. The measurement location (*M*) is shown in Figure 3.23.

As seen in Figure 3.26. the temperature distribution in Case 1 looks like the ones found in Figure 3.7. with a relatively high gradient in the lower part of the room and almost no gradient in the upper part. In Case 2 the gradient is reduced, and in Case 3 with a low heat supply and a very high air change rate the gradient is almost disappeared, which is also expected.

Figure 3.27. shows the vertical contaminant concentration in the three test cases mentioned in Table 3.4. The concentration profiles are expected to be representative for the whole room except in the close vicinity of the contaminant sources and in the air current just above, i.e. no significant, horizontal concentration gradient is expected to prevail in the displacement ventilated room (Nielsen, 1993).

In Figure 3.28. the concentration distribution for the three cases is summarised in a dimensionless plot.

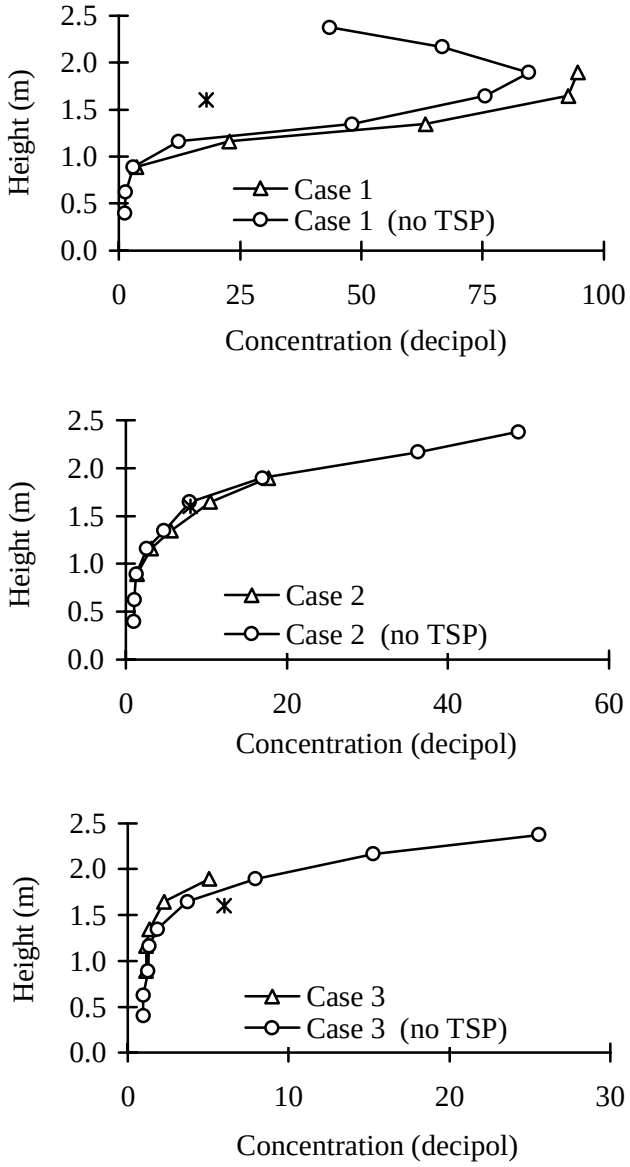

Figure 3.27. Vertical concentration profiles measured chemically for Case 1, 2 and 3 during the periods of assessment (TSP present, Δ), and during a longer period of approximately 12 hours (no TSP, O). The perceived air quality assessed by the TSP is also shown for the approximate breathing zone height of 1.6 m (✱). The measurement location (*M*) is shown in Figure 3.23.

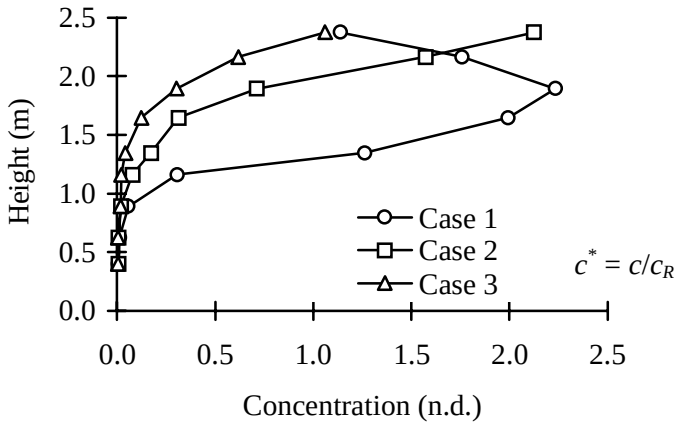

Figure 3.28. Dimensionless vertical concentration profiles in Case 1, Case 2 and Case 3. The results correspond to measurements without the TSP, performed over a longer period of approximately 12 hours. The concentrations are made dimensionless by dividing by the return concentration, $c^* = c/c_R$.

The significant concentration peaks in Case 1 and Case 2 are found to exceed the exhaust concentration by a factor of approximately two. The reason may be that the contaminated convection currents are not the warmest as indicated in Figure 3.2.

Table 3.5. shows the results of the assessments of the Trained Sensory Panel and the exhaust air quality in sensory units as well as in chemical units.

The concentration measurements show a highly stratified flow with a very low concentration at the floor level increasing strongly with the height. A significant separation of the cleaner, lower part of the room and the upper, more contaminated part is found. The stratification height is seen to range from a level below the breathing zone height (Case 1, Figure 3.27.) to a level above the breathing zone height (Case 3, Figure 3.27.).

Table 3.5. Upper part, sensory units: Perceived air quality assessed by the TSP, and exhaust air concentrations measured chemically and then converted to perceived air quality. Lower part, chemical units: Personal exposure, c_e, determined by the TSP in sensory units and then converted to ppm 2-propanone, exhaust air concentration, c_R, and the personal exposure index, ε_e.

Sensory units			
Case	Perceived air quality (decipol)	Exhaust air quality (decipol)	
1	18	47	
2	8	23	
3	6	29	
Chemical units			
Case	c_e (ppm)	c_R (ppm)	ε_e (n.d.)
1	79	209	2.6
2	33	103	3.1
3	24	128	5.3

A good correspondence is seen if the measurements without the TSP in the room are compared with the measurements where the subjects visited the room one by one. This indicates that the flow has been stable during the experiments and that the subjects have been exposed to almost the same indoor environment in the test room.

This is a typical example of concentration distributions in a displacement ventilated room. If the room had been ventilated after the mixing principle, the concentrations would be uniform and equal to the exhaust concentrations mentioned in Table 3.5. in the ideal case. This reveals a high ventilation effectiveness in the occupied zone with a local concentration significantly below the exhaust concentration.

An important objective of the present experiment was to see if the high ventilation effectiveness measured chemically also applied when humans are asked directly about how they perceive the air quality. The measurements show that the perceived air quality in the displacement ventilated room is substantially better than in case of mixing ventilation (see Table 3.5.). The concentration measured in decipol is assessed to be 3 - 5 times lower than in case of mixing ventilation. For instance, in Case 3 the TSP assesses the air quality to be 6 decipol when the

concentration in the exhaust air is 29 decipol. This difference exceeds the usual ventilation effectiveness found in displacement ventilated rooms (ECA, 1992).

If the personal exposure, c_e, is compared with the concentration measured at a "neutral" point at breathing zone height, c_P, in Figure 3.27., it is found that $c_e \approx c_P$ in Case 2 and Case 3, while c_e is significantly lower than c_P. in Case 1.

This indicates that the assumptions in Chapter 3.3.3. on exposure during movements through a concentration field are reasonable, but it also indicates that deviations may occur. The reason for the deviation in Case 1 requires further investigation, but it may be caused by a damming up along the torso of cleaner air from the lower part of the room, or it may be due to local differences in contaminant concentrations, which is especially important in situations like Case 1 where significant concentration peaks occur in breathing zone height.

In this experiment the disturbances of the flow field in the test room are minimised. Apart from the subjects of the TSP and the door operation no disturbances took place. In a real room there will be frequent disturbances from occupants, openings of doors, cold downdraught from windows, etc. At the same time the efficiency of the ventilation system will presumably be lower than in this case, where the clean air is supplied through the entire perforated floor and the air change rates are very high. The combined effect of these parameters will be a lower personal exposure index and thereby a worse perceived air quality in practice.

Despite the inevitable differences between laboratory measurements and the conditions in a ventilated room in practice the results are promising. This indicates that the improved indoor air quality found in displacement ventilated rooms using chemical long-term measurements may be confirmed by asking humans directly (Brohus et al., 1996).

3.4.3. Effect of entrainment in the human boundary layer

The Trained Sensory Panel has also been used to examine if it is possible to show an effect of entrainment and transport of cleaner air in the human convective boundary layer in stratified surroundings by asking humans directly. This task is quite difficult due to the transient phenomena involved using humans in contrary to the steady-state measurements performed by means of the Breathing Thermal Manikin.

Procedure

The subjects of the TSP are told to walk in a usual, calm speed and to follow a predetermined route in the test room. When they arrive to a location in the middle of the room they have been told to stop, stand still, and wait for 15 seconds while holding the breath (looking at the stop watch shown in Figure 3.29.), and then do the assessment and walk out of the room again. The subjects exhale before they enter the room. Otherwise, the procedure is like the previous one described in Chapter 3.4.2.

This experiment is carried out in combination with the previous one in a randomised way due to requirements of the statistical tests that are performed. This implies that the subjects of the panel will do two different assessments for each of the three cases in random order.

Results

The three cases mentioned in Table 3.4. are examined together with a measurement performed without contamination. In Table 3.6. the results are summarised.

Table 3.6. Mean values of calibrated judgements made by the TSP in the case of assessments by means of the immediate impression, and after holding the breath for approximately 15 seconds. Location of subjects while judging and the overall temperature and contaminant distributions are similar for the two different approaches.

Case	**Immediate impression** (decipol)	**After holding the breath** (decipol)
1	18.2	16.7
2	8.1	5.3
3	6.0	4.4
No contamination	3.4	2.4

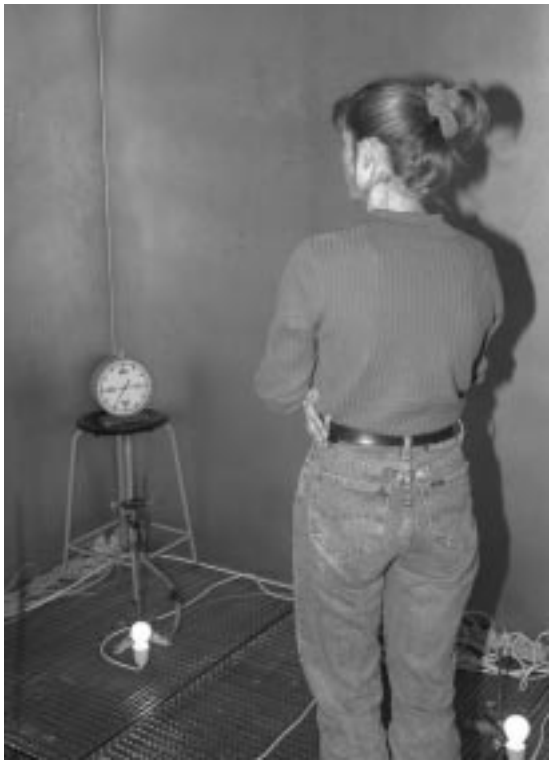

Figure 3.29. Member of the TSP standing still in the middle of the displacement ventilated test room. She is holding her breath for approximately 15 seconds before doing the assessment. In a corner of the room a large stop watch is located, see Figure 3.23. In the bottom of the photo some of the heat sources can be seen.

As seen in Table 3.6., the mean values of the perceived air quality "after holding the breath" are all smaller than for the "immediate impression". This indicates a possible tendency of a lower personal exposure, i.e. a better indoor air quality due to the ascending air current along the body. However, the mean values do not differ much and a statistical test has been performed to check the hypothesis: C*oncentration assessed after holding the breath is significantly lower than the concentration assessed by the immediate impression*.

A paired t-test has been made assuming random sampling and blocking with pairs in persons. In Table 3.7. the result of the test is summarised. Further details are found in Appendix F.

Table 3.7. Results of a statistical test of the hypothesis: Concentration assessed after holding the breath is significantly lower than the concentration assessed by the immediate impression. Measurements are performed by a TSP in the displacement ventilated test room described in Chapter 3.4.1.

Test of hypothesis	
Case	Significant at level
1	40%
2	5%
3	25%
No contamination	1%

The levels of significance indicate that only in Case 2 there is a significant effect (5% level) of the convective boundary layer flow along the persons, while the differences in Case 1 and Case 3 are insignificant. Furthermore, in case of an uncontaminated test room the hypothesis holds the best, which is quite unexpected.

This seems to show that the subjects dislike to hold the breath and, therefore, tend to vote too low (i.e. for a better air quality) when they were allowed to inhale again. This point is supported by the fact that most members of the TSP do the assessment after only 10 - 15 seconds, in stead of precisely 15 seconds.

Another possible reason for the insignificant results is the highly transient phenomena involved, compared with the short time allowed for the convective boundary layer to build up. When a subject is entering the room and walking to the middle before standing still, a lot of disturbances and vortices are created. While the disturbances are reduced by dispersion and dissipation, the boundary layer has to build up in about 10 seconds. If the velocity of the ascending air current is assumed to be of the order of 0.2 m/s, this time period corresponds to the approximate transport time of air from the floor area to the breathing zone. However, this does not include time to re-establish the boundary layer or to overcome eventual vortices or small movements made by the standing person.

In conclusion it must be stated that the time span, during which the subjects are able to hold their breath, is too short to show any significant effect of ascending air currents along the body. At the same time there seems to be a strong confounding effect of the restricted respiration where the panel tends to vote too low when allowed to inhale again.

3.5. Simulations using a CSP

This chapter presents results from CFD-simulations on personal exposure in a displacement ventilated room. The computer simulations are performed with both warm and cold sources, including a simulation of the floor as a contaminant source giving rise to exposure of the Computer Simulated Person (CSP) applied in the calculations. The main results are compared with corresponding full-scale measurements.

3.5.1. Geometry and boundary conditions

Three different cases are simulated corresponding to Case A, B and C in the full-scale measurements of Chapter 3.3. The flow field is assumed to be symmetric for which reason only one half of the room is simulated in order to save a large number of grid points, computer memory and CPU-time, accordingly.

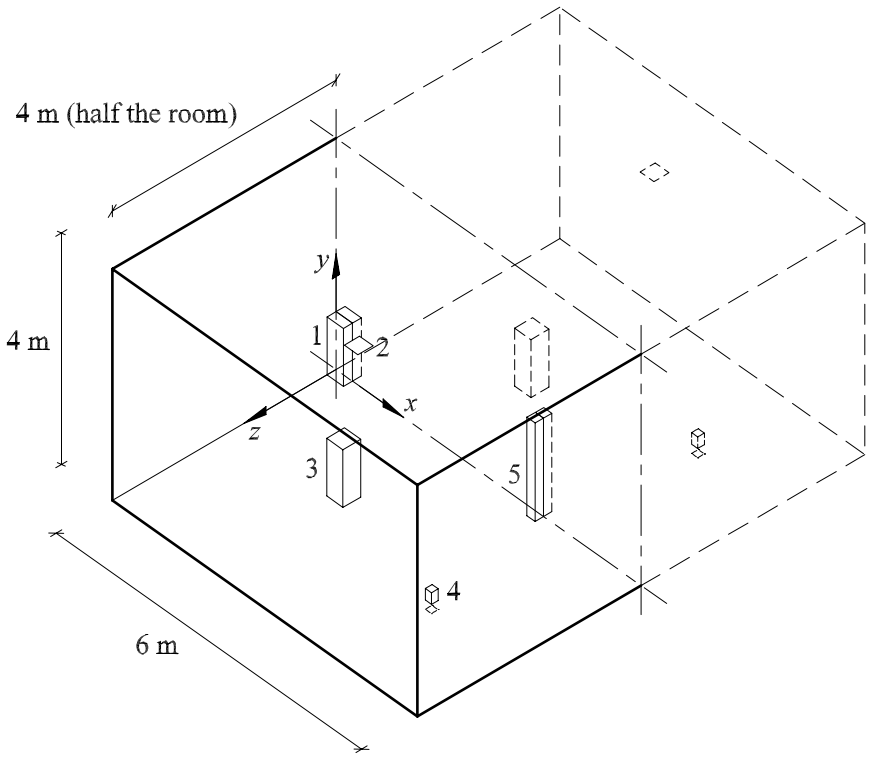

Figure 3.30. Geometry of the CFD simulated displacement ventilated room. Only one half of the symmetric room is simulated, shown in Figure 3.3. The subcooled air is supplied through the inlet device (1) and exhausted through return openings in the ceiling (2). The heat load is generated by person simulators (3), a point heat source (4), and the Computer Simulated Person model 1 (5), see Chapter 2.3.3.

The experimental set-up is not symmetrical regarding the point heat source, but in the simulations this heat source is assumed to consist of two symmetrically located heat sources, each emitting half the power of the single one. This assumption will be further discussed later.

Due to requirements of the computer software all circular geometry is converted into rectangular geometry as seen in Figure 3.30.

Radiation heat transfer is considered indirectly by prescribing the surface temperatures of floor, ceiling, and walls using results from the full-scale measurements summarised in Table 3.8.

Table 3.8. Boundary conditions used in the CFD simulations. q is the supply air flow rate and t_0 is the supply air temperature. The temperatures of the different surfaces are also mentioned. Wall functions are used to calculate the heat transfer between the room air and the surfaces (see Chapter 2.3.2.3.).

Parameter	Location	Case A	Case B	Case C
q_0 (m^3/h)	Supply	145	290	395
t_0 (°C)	Supply	14.67	17.63	15.80
t_{Floor}	y = 0 m	22.63	21.94	21.57
$t_{Ceiling}$	y = 4 m	23.70	22.44	23.01
t_{Front}	x = 6 m	23.22	22.49	22.71
t_{Back}	x = 0 m	22.87	22.21	22.30
t_{Side}	z = 4 m	22.17	22.42	22.64

The implementation of the heat sources is mentioned in Table 3.9. Only the convective part of the total heat output should be considered.

Table 3.9. Implementation of the person simulator and the point heat source in the CFD simulations of the displacement ventilated room.

Type (Case)	Total heat output (W)	Convective heat output (W)	Implementation in the CFD simulations as
Person simulator (A,B,C)	100	50	Obstacle with prescribed surface heat flux
Point heat source (A,C)	250	225	Transparent volume source
Point heat source (B)	50	45	Transparent volume source

Apart from the two heat sources the Computer Simulated Person (CSP) will also act as a heat source in the shape of an obstacle with a prescribed surface heat flux of 25 W/m^2. The CSP is discussed in detail in Chapter 2.3.3. In the present simulations only CSP model 1 is applied.

The grid used in the numerical calculations of the three cases consists of 82,764 cells distributed with 66, 33 and 38 cells in the *x, y,* and *z* direction, respectively.

3.5.2. Simulation of the flow field

Here, the flow field in the three cases will be shown by means of vector plots and comparisons between measurements and simulations regarding velocity and temperature profiles in the vicinity of the person.

Figure 3.31., 3.32. and 3.33. show vector plots from three different planes for Case A, B and C.

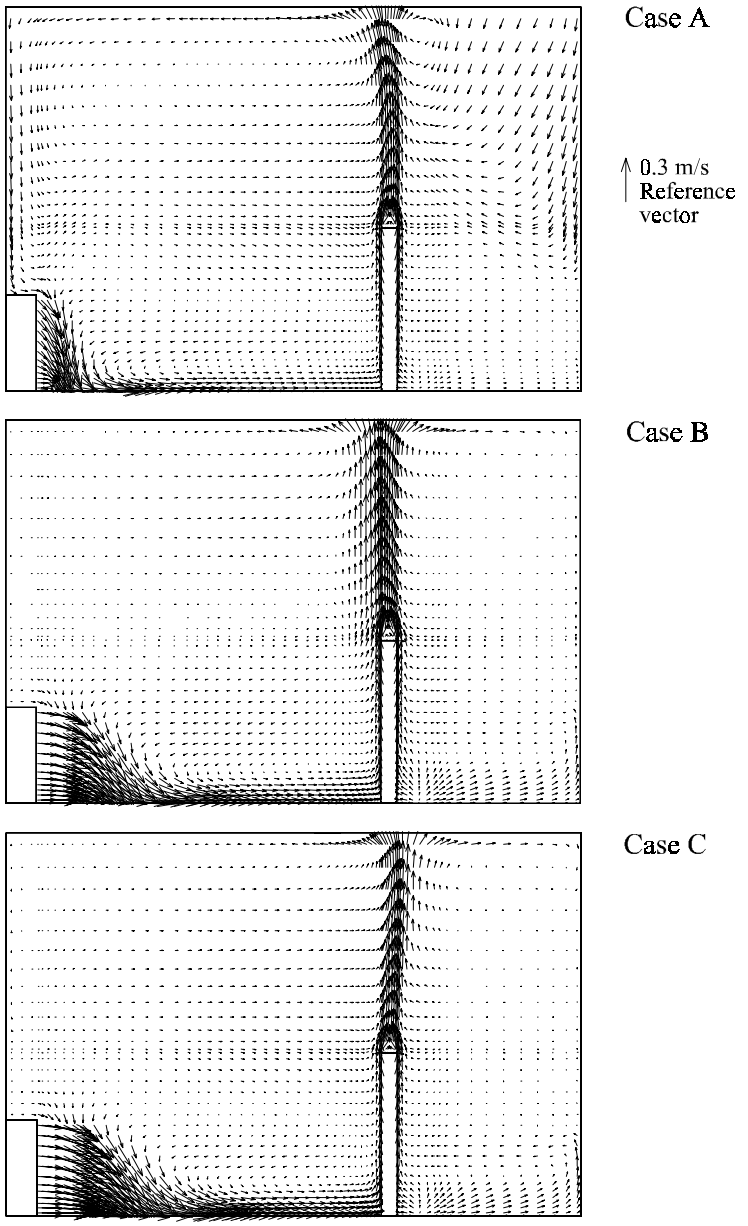

Figure 3.31. Vector plot from the displacement ventilated room Case A, B and C. Plane: z = 0 m (vertical symmetry plane).

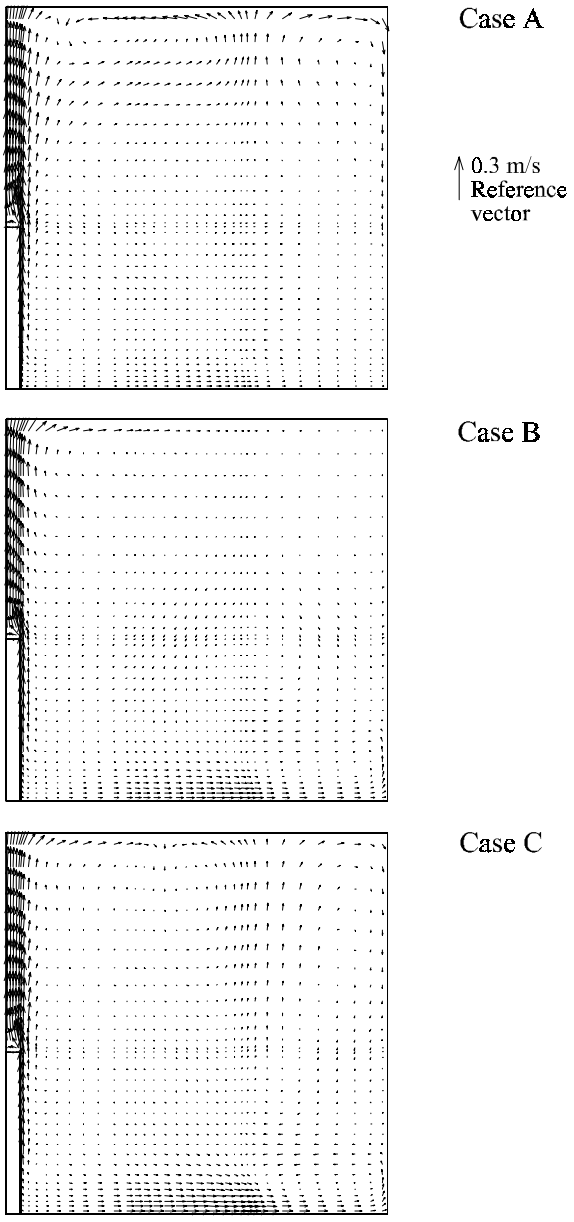

Figure 3.32. Vector plot from the displacement ventilated room Case A, B and C. Plane: x = 4 m (vertical section through CSP).

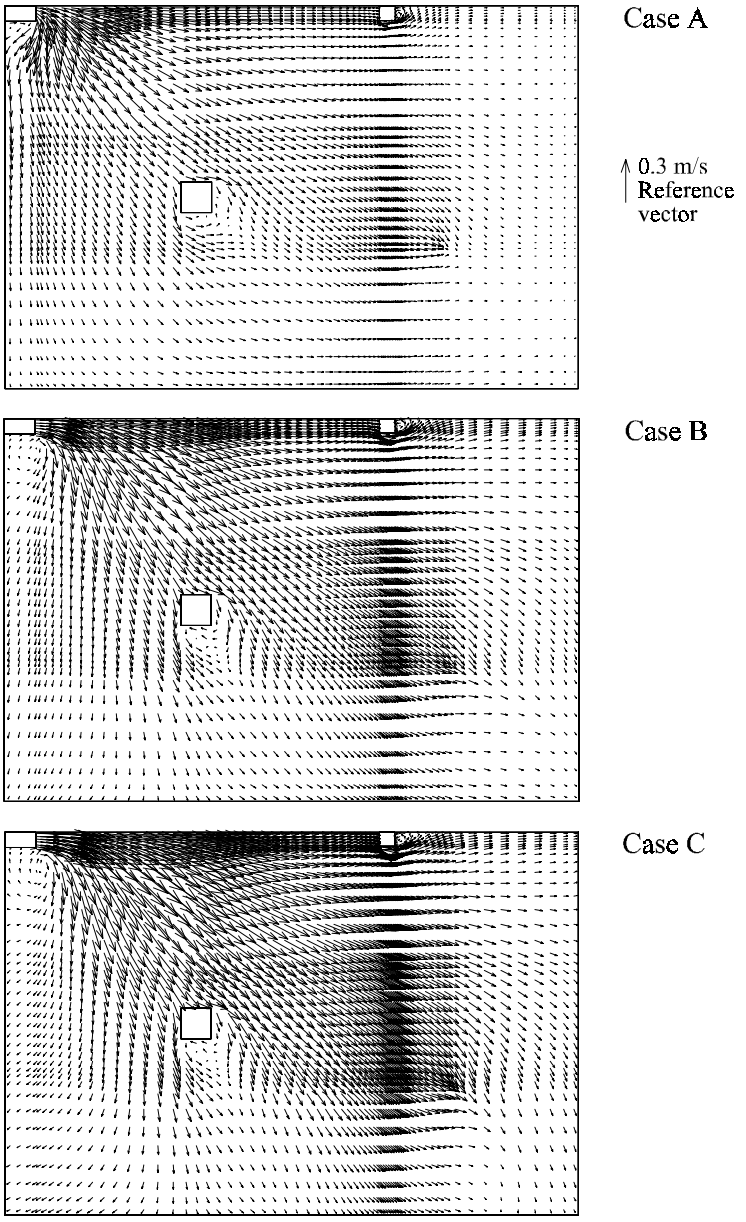

Figure 3.33. Vector plot from the displacement ventilated room Case A, B and C. Plane: y = 0.1 m (horizontal plane 0.1 m above the floor).

Figure 3.31. shows a vector plot from the vertical symmetry plane, z = 0 m. In this plane it is possible to see many of the characteristics of a displacement ventilated room, especially close to the inlet device and the CSP. The flow around the CSP clearly shows the convective flow causing entrainment and transport along a person in all three cases. In the adjacent zone of the inlet device the flow field is influenced by the air flow rate and the temperature difference between the supply air and the room air, i.e. the Archimedes number.

In the major part of the room the flow direction is horizontal as expected for a stratified flow domain. Only close to sources of momentum, like the inlet device and the heat sources (CSP, walls, etc.), significant non-horizontal movements prevail. In the upper right corner of the Case A vector plot downward movements are created by the point heat source which is not visible in this plane, see Figure 3.31.

Figure 3.32. shows a vertical section through the CSP, x = 4 m. Close to the CSP the ascending air current is seen again continuing to the ceiling where it is deflected. On top of the CSP a small recirculation zone is formed due to the rectangular geometry causing an edge which is sharper than the one found on real persons. However, in the case of displacement ventilation where the upward air movement along the body is assumed to be the main route of contamination it is not likely that this recirculation zone will affect the personal exposure significantly.

The differences in the overall flow pattern in Figure 3.32. are due to the different boundary conditions regarding air flow rate, heat load and surface temperatures. Especially the point heat source seems to affect the flow field considerably in the upper part of the room.

Figure 3.33. consists of three vector plots of the flow field in a horizontal plane 0.1 m above the floor, y = 0.1 m. As in Figure 3.31. the flow field close to the inlet device is highly affected by the Archimedes number. As expected, the subcooled air is seen to spread radially along the entire floor. Behind the person a small wake is created due to the relatively high velocities close to the floor. This wake region can also be seen in Figure 3.31. and it seems to continue up to a height of approximately 0.2 m where it is gradually diminished.

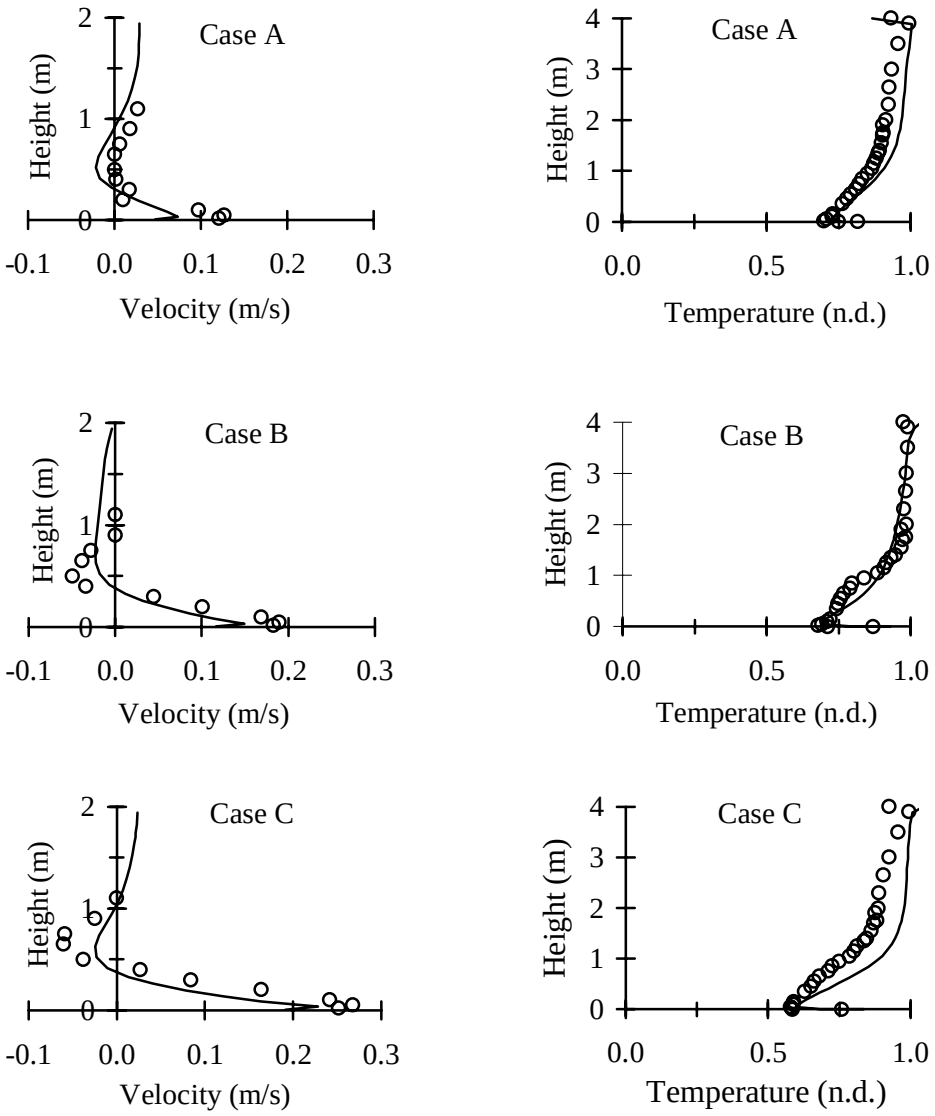

Figure 3.34. Velocity profiles (left) and dimensionless temperature profiles (right) for the CFD simulations (line) and full-scale measurements (o) for Case A, B and C for the displacement ventilated room. The location of the vertical velocity profile is $(x,z) = (3,0)$ and the vertical temperature profile is $(x,z) = (4,1)$. The temperature profiles are shown in a dimensionless plot, $t^* = (t - t_0)/(t_R - t_0)$, where t_0 is the supply air temperature and t_R is the return air temperature.

The simulated velocity profiles and temperature profiles for locations close the person are compared with results from the full-scale measurements in Figure 3.34. A reasonable agreement is found even though the simulation seems to underestimate the velocities slightly and the shape of the temperature profiles deviates somewhat in Case B and Case C. Comparisons between simulations and measurements will be discussed in the following chapter where the concentration distribution also is included.

3.5.3. Simulation of personal exposure

Simulations on personal exposure have been made using a non-passive (warm) contaminant source as well as two kinds of passive (cold) contaminant sources in the shape of a point contaminant source and the entire floor. In all cases the personal exposure of the Computer Simulated Person (CSP) corresponds to the contaminant concentration in the nearest cell along the computational model in a height of 1.5 m as explained in Chapter 2.3.4.

Non-passive point contaminant source

The concentration distribution in the present CFD simulations is generated by means of a contaminant source simulated as a transparent volume source (0.1 m x 0.1m x 0.1 m) located above the point heat source in a height of 2 m above the floor. The combination of the point heat source generating an ascending plume of warm air and the contaminant source located above causes a transport of the contamination to the upper part of the room, which is also the aim of this non-passive source.

The dimensionless concentration distribution is shown for Case A in Figure 3.35. The discrete results are converted into isopleths using a computer programme incorporating Kriging for the interpolations (Surfer, 1991; Davis, 1986).

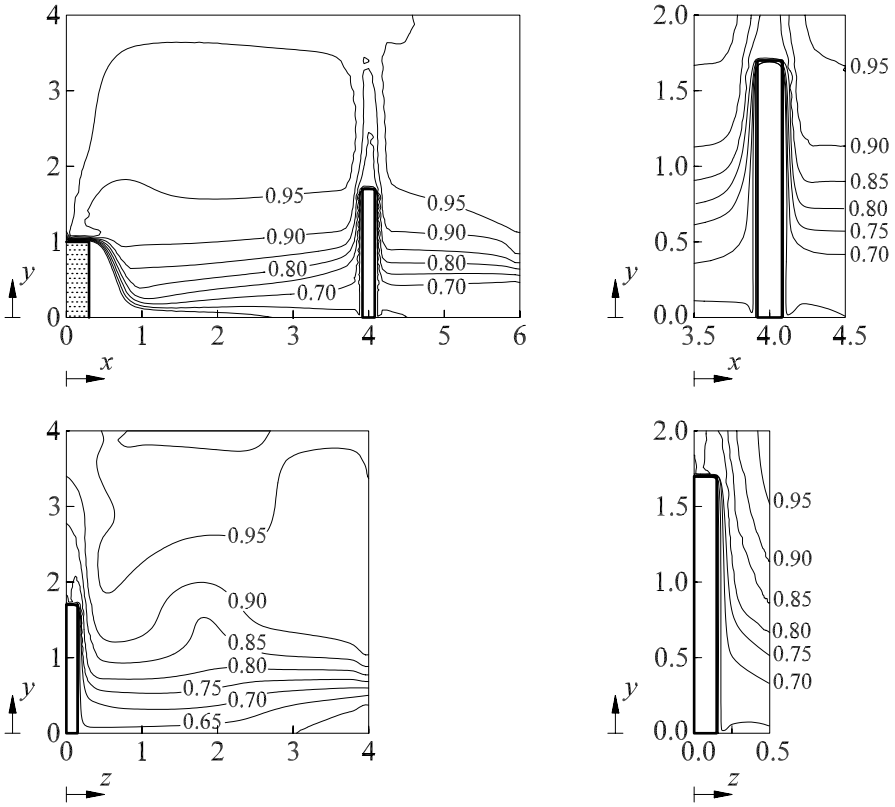

Figure 3.35. Dimensionless contaminant concentration distribution in the displacement ventilated room, Case A. Top: Vertical symmetry plane, z = 0 m. Bottom: Vertical section through person, x = 4 m. The two right figures are enlargements of the concentration field close to the CSP.

Figure 3.35. shows the concentration field in the ventilated room for two different vertical planes combined with an enlargement of the field close to the CSP. The concentrations are made non-dimensional by dividing by the return concentration, i.e. $c^* = c/c_R$, which implies that the dimensionless return concentration equals 1.

The results indicate a stratified flow with horizontal, almost parallel, isoconcentration curves increasing in level for increasing height above the floor. The clean air is supplied by the inlet device in the lower part of the room and subtracted again at ceiling height. In the plane x = 4 m we see the same local

effect of the point heat source on the concentration distribution, as the one found in the corresponding vector plot (Figure 3.32.).

Close to the CSP the concentration field is significantly modified due to the convective transport in the boundary layer. The cleaner air in the lower part of the displacement ventilated room is entrained and transported to the breathing zone. This is in fact one of the important reasons for applying the displacement principle in room ventilation. This phenomenon causes a high ventilation effectiveness locally around the person and thus a high personal exposure index, ε_e, which was also found in the case of full-scale measurements.

The corresponding results for Case B and Case C do not show any important differences from Figure 3.35. for which reason they are not included as isoconcentration plots.

In Figure 3.36. the personal exposure, c_e^*, and the vertical concentration distribution in the vicinity of the person are shown for the simulations and the measurements. The concentration profiles for the simulations clearly indicate a stratified flow, but comparison with measurements shows some significant deviations in the lower part of the room. Obviously, the simulations have not been able to re-create the considerable "step" in the concentration profiles found in the measurements. This subject will be discussed in more detail in the end of this chapter.

Even though the CFD calculated concentration distribution reveals some deviations compared with measurements, the personal exposure shows the same tendencies of a significantly lower concentration of inhaled contaminant than the corresponding concentration in the surroundings at a "neutral" point.

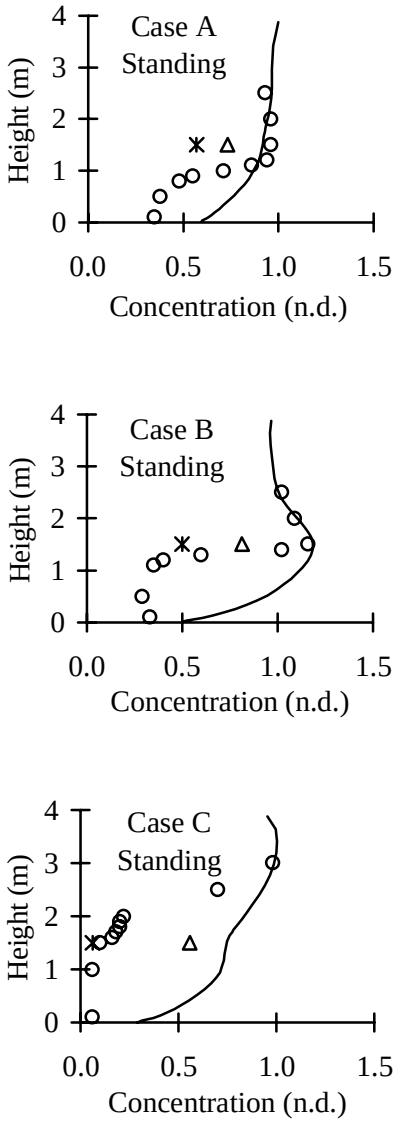

Figure 3.36. Vertical dimensionless concentration distribution in the displacement ventilated room for Case A, B and C at (x,z) = (3,1) for simulations (line) and measurements (o). The personal exposure of a standing person is shown for the simulations (CSP, Δ) and for the measurements (BTM, ∗). The breathing zone height is 1.5 m in both cases.

Passive point contaminant source

Two different kinds of passive sources are applied, a passive point source located close to the CSP and the floor as a passive emitting source.

The passive point source that is located close to the CSP, is the same source as mentioned previously. The contaminant is emitted without any initial buoyancy or momentum, i.e. the only contaminant transport is due to diffusion and convection caused by the general flow field in the room and the local flow field close to the CSP.

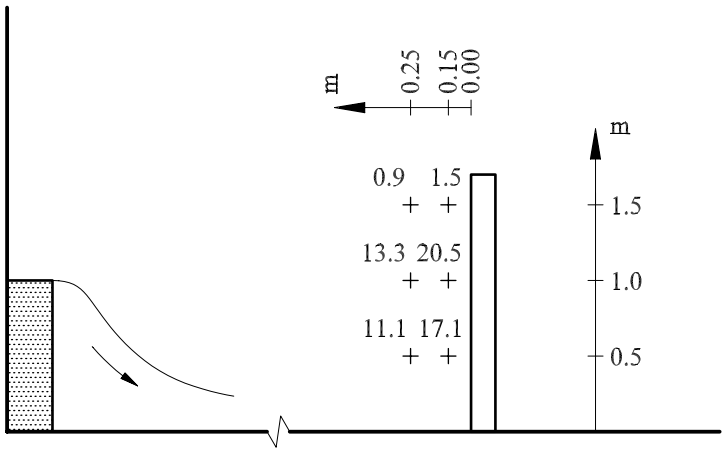

Figure 3.37. Personal exposure to a passive contaminant source located close to the CSP in the displacement ventilated room. The + marks show the different locations of the contaminant sources, and the corresponding number is the dimensionless personal exposure. The simulations are performed for each of the source locations one by one.

Figure 3.37. stresses the importance of the contaminant source location relative to the person. For instance, it is seen that a source location close to the breathing zone, just in front of the “mouth”, may not necessarily cause the highest exposure. Due to the convective air current along the torso the CSP is found to be more protected against exposure here, than for lower locations of the source. This phenomenon is also found for the measurements on the seated Breathing Thermal Manikin in Figure 3.21.

Planar contaminant source

In the previous examples of exposure to contaminant sources only point sources have been applied. For a typical indoor environment planar sources can also be very important to consider, e.g. walls and floor that may exert a considerably chemical and sensory pollution load on the room (ECA, 1992; Maroni et al., 1995).

A planar contaminant source in shape of the floor is applied in the results shown in Figure 3.38. The floor in this CFD simulation has a constant emission rate. This may be a good approximation for certain types of contaminant sources, while other types are dependent on velocity, temperature, back pressure, etc. and thus require more sophisticated emission models.

The isoconcentration curves in Figure 3.38. show how the clean, subcooled air from the inlet device is gradually more and more polluted during the flow throughout the floor. At the walls, x = 6 m and z = 4 m, the flow is deflected and a secondary opposing flow occurs above the primary flow. The vertical concentration profile close to the person is shown in Figure 3.39.

This scenery causes a complex local concentration distribution around the CSP, resulting in a dimensionless personal exposure of approximately 1, i.e. the same exposure level as if the room air was completely mixed.

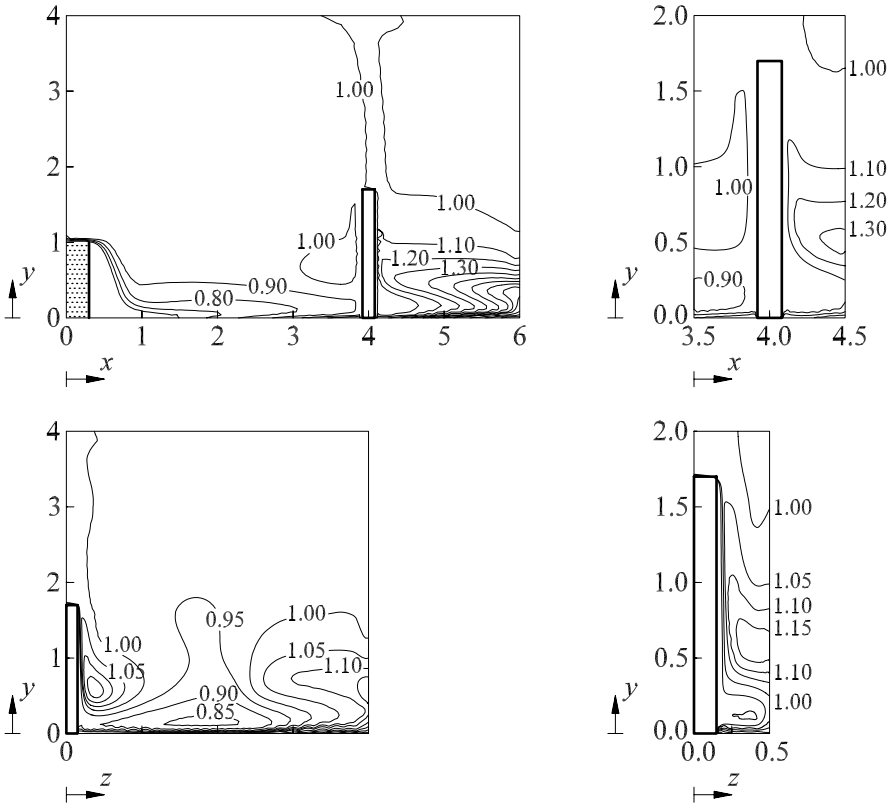

Figure 3.38. Dimensionless contaminant concentration distribution in the displacement ventilated room in case of the floor acting as a planar contaminant source with a constant emission rate. The flow field corresponds to Case A, see Table 3.8. Top: Vertical symmetry plane, z = 0 m. Bottom: Vertical section through person, x = 4 m. The two right figures are enlargements of the concentration field close to the CSP.

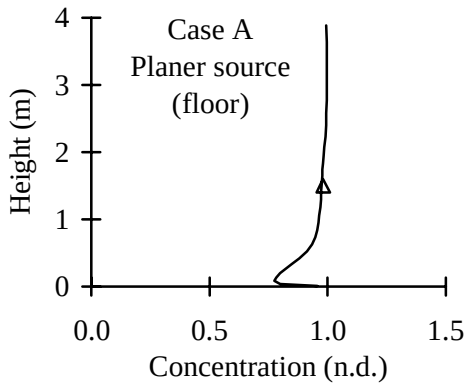

Figure 3.39. Vertical dimensionless concentration distribution at (x,z) = (3,1) in the displacement ventilated room in case of the floor acting as a planar contaminant source with constant emission. The flow field corresponds to Case A, see Table 3.8. The dimensionless personal exposure of the CSP is also shown (Δ).

Comparison between measurements and simulations

If the results from measurements and simulations are compared regarding the concentration distribution, significant deviations are found in the lower part of the room. As mentioned previously the simulations have not been able to re-create the considerable vertical step change in the concentration distribution. There are a number of possible reasons for the deviations, some of those will be outlined in the following.

The flow field is determined almost exclusively by the boundary conditions in the CFD calculations. If the boundary conditions are not properly applied deviations will inevitably occur. In the present simulations the surface temperatures of walls, floor and ceiling are prescribed as a single value for each surface. During the measurements there may be a temperature gradient throughout the single surfaces which is not implemented. This will to some extent affect the convective flow along the walls and thus it may influence the exchange of contamination between the upper and the lower part of the room.

In Chapter 2.3.3.2. the grid dependence of wall functions applied in the CFD simulations was discussed. Here, the wall functions are applied to account for surface friction and heat transfer along the surfaces where the temperature is

prescribed. The grid layout may also exert an influence on the representation of heat and contaminant sources as well as on the general flow field. For instance, if the grid is too coarse in the "step region" the simulations may fail to catch this important property of displacement ventilation.

The turbulence in the flow is represented by turbulent exchange parameters like the turbulent viscosity. The turbulent viscosity is found by means of the k-ε model as described in Chapter 2.3.2.1. In strongly temperature-stratified surroundings, the turbulence may be significantly influenced by the temperature gradient. Depending on the sign of the vertical temperature gradient the local turbulence may be damped or amplified. This phenomenon can be implemented in the turbulence model by the inclusion of a so-called buoyancy term, G_k, in the transport equation for turbulent kinetic energy, k, see Appendix E.

$$G_k = -\beta g_i \frac{\mu_t}{\sigma_k} \frac{\partial t}{\partial x_i} \tag{3.11}$$

where

G_k = Buoyancy term (J/m^3 s)
β = Expansivity (1/K)
g_i = Gravitational acceleration (m/s^2)
μ_t = Turbulent viscosity (kg/m s)
σ_k = Turbulent Prandtl number (n.d.)
t = Temperature (°C)
x_i = Distance in i direction (m)

The G_k term may also be included in the transport equation for the rate of dissipation of turbulent kinetic energy, ε. In both cases it should be included as an additional source term. The buoyancy term has not been applied in the present simulations, but it may be a possibility to obtain better numerical solutions.

Another reason for the deviations between the measurements and the simulations is the symmetry assumptions. In the measurements there is only one point heat source, see Figure 3.3., but in the simulations this source is assumed to consist of two symmetrical sources, each with only half the power as the single source. Due to the location of the contaminant source above this heat source in the non-passive case, the symmetry assumption may have a certain influence on the concentration distribution.

3.6. Conclusion

In this chapter personal exposure to contaminant sources in a displacement ventilated room is examined.

The topic is investigated by means of the three tools for exposure assessment introduced in Chapter 2, i.e. the Breathing Thermal Manikin, the Trained Sensory Panel and the Computer Simulated Person. The different tools are models of a person or real persons applied in order to include the local effect of the person when the exposure is estimated in surroundings with considerable concentration gradients.

The contaminant distribution is generated by point sources and also by a planar contaminant source in the case of CFD simulations including the Computer Simulated Person. Warm (non-passive) sources are applied to generate the characteristic two-zonal concentration distribution with a separation in a cleaner, lower zone and an upper, more contaminated zone in the displacement ventilated room. Cold (passive) point contaminant sources are, among other things, applied in order to investigate the influence of contaminant sources located close to persons.

Both chemical and sensory measurements and simulations are performed, mainly at steady-state conditions but also by transient behaviour in the shape of the Trained Sensory Panel assessing the perceived air quality.

It is found that the stratified flow and the considerable concentration gradients in a displacement ventilated room necessitate an improvement of the widely used compartmental approach.

The flow in the human boundary layer is able, to a great extent, to entrain air from below the breathing zone, thus improving the quality of the inhaled air in case of warm contaminant sources.

Persons´ movements cause the air quality to decrease due to the disturbance of the human boundary layer which promotes the high air quality transporting fresh air to the breathing zone.

A personal exposure model is proposed. The model takes the concentration gradient and the influence of the human thermal boundary layer into account. The model is easy-to-use and suitable for the design of displacement ventilation systems in practice.

Entrainment of air in the human boundary layer is usually an advantage, but the results show also the possible disadvantage when passive contaminant sources are present. In this case the convective current around the person may transport contaminated air to the breathing zone, giving rise to increased exposure.

A new quantity is defined: the effectiveness of entrainment in the human boundary layer, η_e, which expresses the ability to supply (fresh) air from the floor area to the breathing zone.

Chapter 4

Mixing ventilation

4.1. Introduction

In this chapter mixing ventilation will be examined as an application for personal exposure assessment, using some of the tools introduced in Chapter 2.

Mixing ventilation may cover a large number of ventilation systems and an even larger number of different devices used to supply and extract the air. Usually, the air is supplied outside the occupied zone with a high momentum in order to create a well-mixed flow field without any concentration gradients or temperature gradients in the ideal case. The supply air may be isothermal as well as non-isothermal and used for both heating and cooling and, of course, also for the removal of contamination and supply of fresh air.

When the mixing principle is used the contamination in a ventilated room is diluted to a sufficiently low level contrary to the displacement principle, where the contamination is displaced upwards while clean air is supplied directly to the occupied zone.

The assumption of completely mixed room air without concentration gradients is widely used in the design of ventilation systems. Using this approach the personal exposure may easily be found by means of a simple mass balance if the source strength and the air flow rate are known. In a large number of cases, however, the assumption will fail and erroneous exposures may be obtained. Rodes et al. (1991) and Brohus and Nielsen (1995) among others report errors in exposure assessment exceeding one order of magnitude.

In this chapter the topic will be highlighted, and different examples will demonstrate the importance of taking the local influence of a person into account when personal exposure is assessed in surroundings where concentration gradients prevail.

The flow field around persons in mixing ventilated rooms depends highly on the specific system design and also on the location of the person in the room, movements of the person, local obstacles, heat sources, etc. The flow may range from almost quiescent air over strongly turbulent flow to an almost uniform velocity field locally around the person, see Figure 4.1.

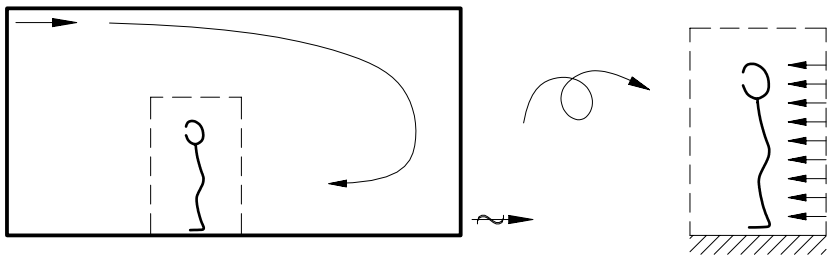

Figure 4.1. The flow field in a mixing ventilated room may locally act as a unidirectional flow field.

Measurements and computer simulations are performed on a person exposed to contaminant sources in a unidirectional flow field created by means of a wind channel. The results are presented and discussed in Chapter 4.2.

Chapter 4.3. presents a CFD simulation on the whole flow field in a mixing ventilated room and examines the personal exposure as a function of source locations as well as the flow direction relative to the person.

4.2. Unidirectional flow field

As mentioned previously this chapter presents measurements and simulations on a person located in a unidirectional flow field. The unidirectional flow field is assumed to be part of the total flow field in a mixing ventilated room, as indicated in Figure 4.1., but it may as well apply for industrial applications, for instance a worker located in a spray hood or close to a local exhaust ventilation device.

4.2.1. Experimental set-up

In order to create a unidirectional flow field a wind channel is built as shown in Figure 4.2.

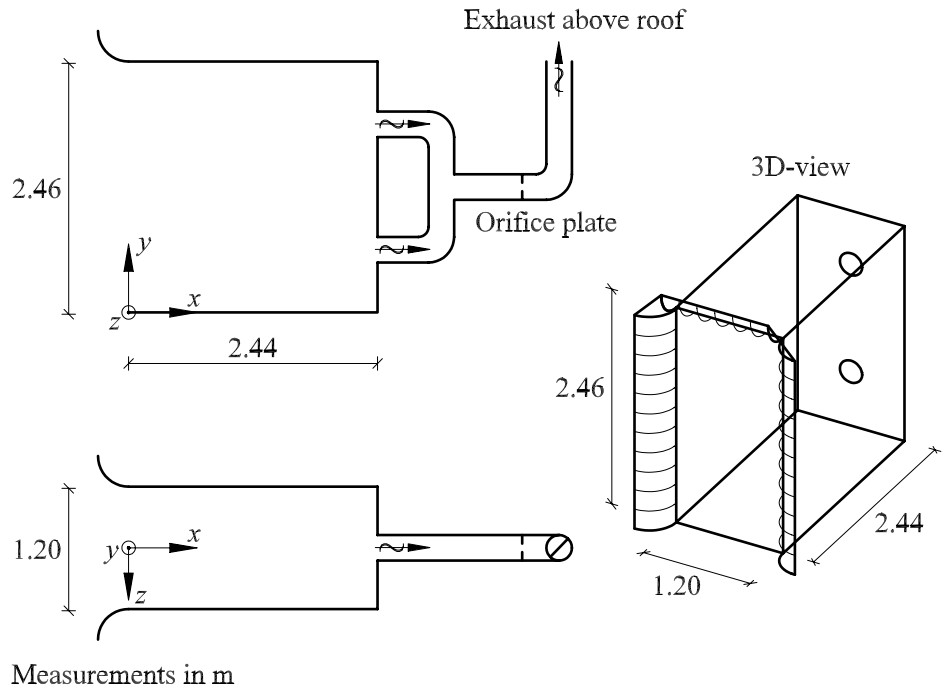

Figure 4.2. Geometry of wind channel used in the full-scale measurements on the BTM standing in a unidirectional flow field. The flow field is generated by extracting air through two exhaust openings, each ø 0.25 m.

The wind channel is made of chipboard and equipped with a rounded inlet opening to reduce turbulence generation at the edges, see Figure 4.3. The wind channel is located inside a laboratory building where the surrounding quiescent air is conditioned.

The uniform velocity field is created by extracting air through two exhaust openings in the one end. The amount of air is adjusted to obtain uniform velocity levels in the wind channel ranging from 0.05 m/s to 0.45 m/s.

Personal exposure is determined by means of the Breathing Thermal Manikin (BTM), which is described in Chapter 2.2. A passive point contaminant source is simulated by tracer gas injected through a porous foam rubber ball, ø 0.1 m. The tracer gas is a neutral density mixture of nitrous oxide and helium.

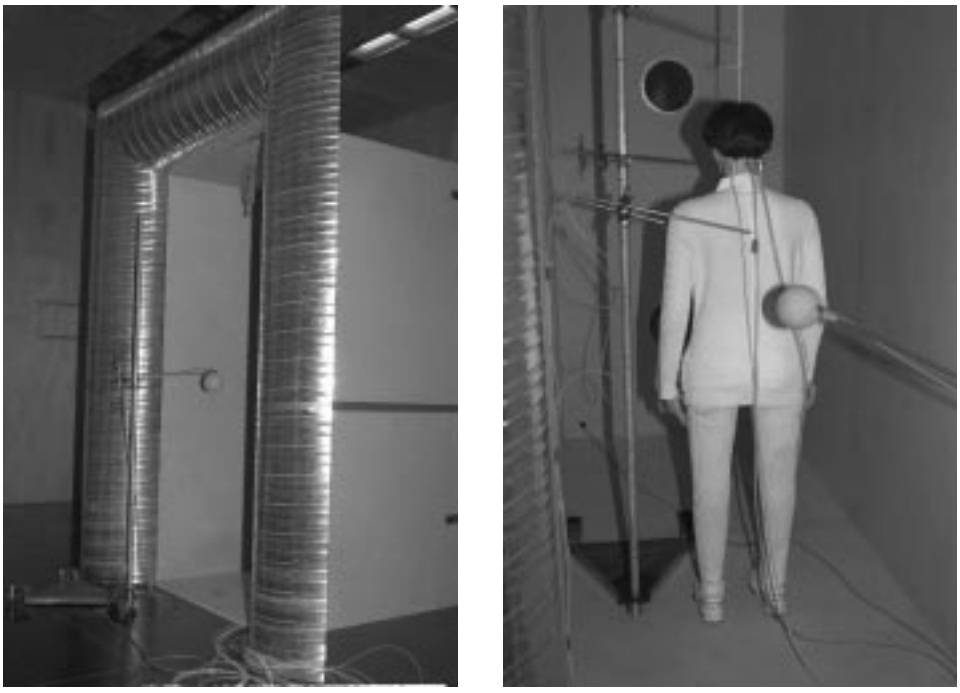

Figure 4.3. Left: Photo of the wind channel equipped with a rounded inlet opening to reduce turbulence generation at the edges. Right: The BTM standing in the wind channel. The point contaminant source is seen in the foreground, and the two exhaust openings can be found in the background.

4.2.2. Measurements using a BTM

In the following a number of cases are presented where the BTM is exposed to contamination from a passive point source in the uniform flow field in order to investigate the influence of velocity level, contaminant source location and the effect of a person's position relative to the flow field.

Figure 4.4. shows the dimensionless personal exposure of the BTM in two different positions relative to the flow field and the contaminant source as a function of vertical source location.

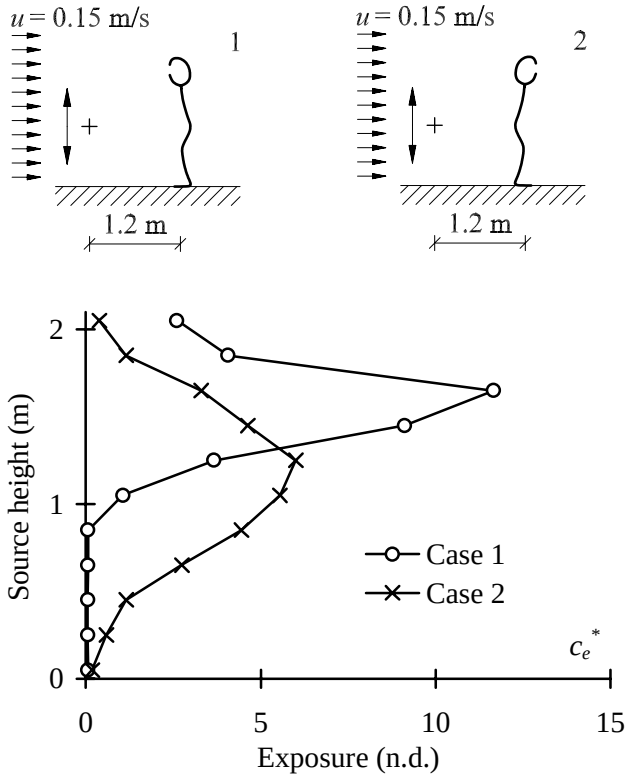

Figure 4.4. Dimensionless personal exposure of the BTM standing in a unidirectional flow field at a velocity level of 0.15 m/s. Case 1: BTM facing wind direction. Case 2: BTM facing opposite direction. The horizontal distance between the centre of the BTM, $(x,z) = (1.2,0)$, and the centre of the passive point contaminant source, $(x,z) = (0,0)$, is 1.2 m. The vertical location of the contaminant source is ranging from 0.05 m to 2.05 m.

The results are presented in dimensionless form regarding the personal exposure to make them more general and independent of the specific source strength chosen for the experiments. Another advantage of showing the results dimensionless is the ability to compare with completely mixed conditions, where c_e^* equals one. However, if the dimensionless exposure is used for physiological purposes, for instance as input in a dose-response relationship, the concentration of a specific gas must be converted to ppm or other relevant units. When the source strength, S, and the air flow rate, q, are known this may easily be done by

$$c_e = c_e^* c_R = \frac{c_e^* S}{q} \tag{4.1}$$

As expected, the measurements in Figure 4.4. show a substantial influence of the source location and they also show a significant influence of the position of the manikin.

In Case 1 no exposure takes place when the source is below 1 m. When the source is raised above 1 m the level increases to a maximum value around the breathing zone height, after which it decreases again. The maximum personal exposure is found to exceed the return concentration more than 10 times.

Case 2 shows a different pattern. Exposure occurs for almost every source location, and the location for maximum exposure is found at a lower level. Here, we see a distinct influence of the flow in the wake of a person standing in a uniform velocity field, a topic that will be examined in greater detail in the subsequent.

Figures 4.5., 4.6. and 4.7. present a more systematic investigation of the personal exposure as a function of velocity level and vertical location of the contaminant source in three different set-ups, all highly influenced by the wake generated in front of the BTM standing in a unidirectional flow field.

Each of the three figures shows results of exposure measurements at four velocity levels (0.05 m/s, 0.15 m/s, 0.30 m/s, 0.45 m/s) and five vertical source locations (0.50 m, 0.75 m, 1.00 m, 1.25 m, 1.50 m), i.e. 20 data points. The results are converted into isopleths by using a computer programme incorporating Kriging for the interpolation (Surfer, 1991; Davis, 1986).

The results are presented both in the ppm unit assuming a specific contaminant source strength as well as non-dimensional. In that way it is possible to comment on the exposure levels compared to complete mixing in a general way, and also to comment on the physiological effect on people where it is the absolute exposure level which counts.

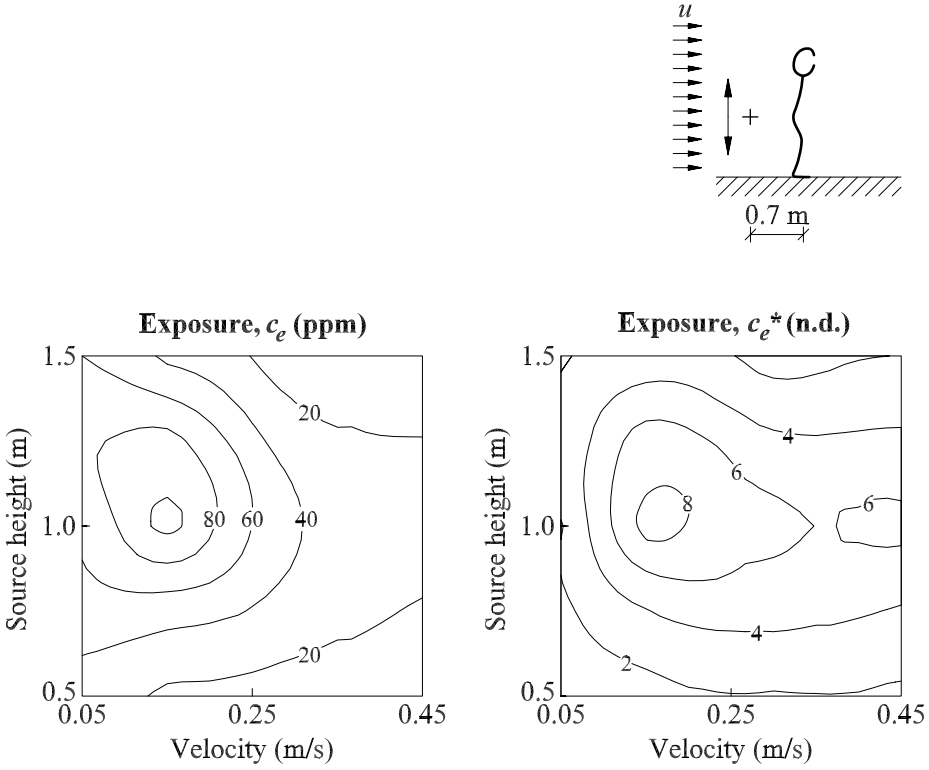

Figure 4.5. Personal exposure of the BTM standing in a uniform velocity field as a function of velocity level (0.05 m/s - 0.45 m/s) and vertical contaminant source height above the floor (0.5 m - 1.5 m). The horizontal distance between the centre of the BTM, $(x,z) = (0.7,0)$, and the centre of the source, $(x,z) = (0,0)$, is 0.7 m. The left plot is isopleths of personal exposure in ppm for a contaminant source strength of $S = 5 \cdot 10^{-6}$ m^3/s. The right plot is isopleths of the corresponding dimensionless personal exposure.

The contours in Figure 4.5. confirm the tendency found in Figure 4.4., Case 2, with the highest exposure level for the contaminant source located approximately

1 m above the floor. On the dimensionless plot (right side) an almost unchanged exposure level is found for increasing velocity levels, resulting in decreasing absolute levels (left side) due to the constant source strength.

It can also be seen that the exposure increases significantly when the uniform velocity is changed from 0.05 m/s to 0.15 m/s. This may be explained by an increased disturbance of the natural convection boundary layer around the BTM, which in this case seems to protect against exposure at low velocities.

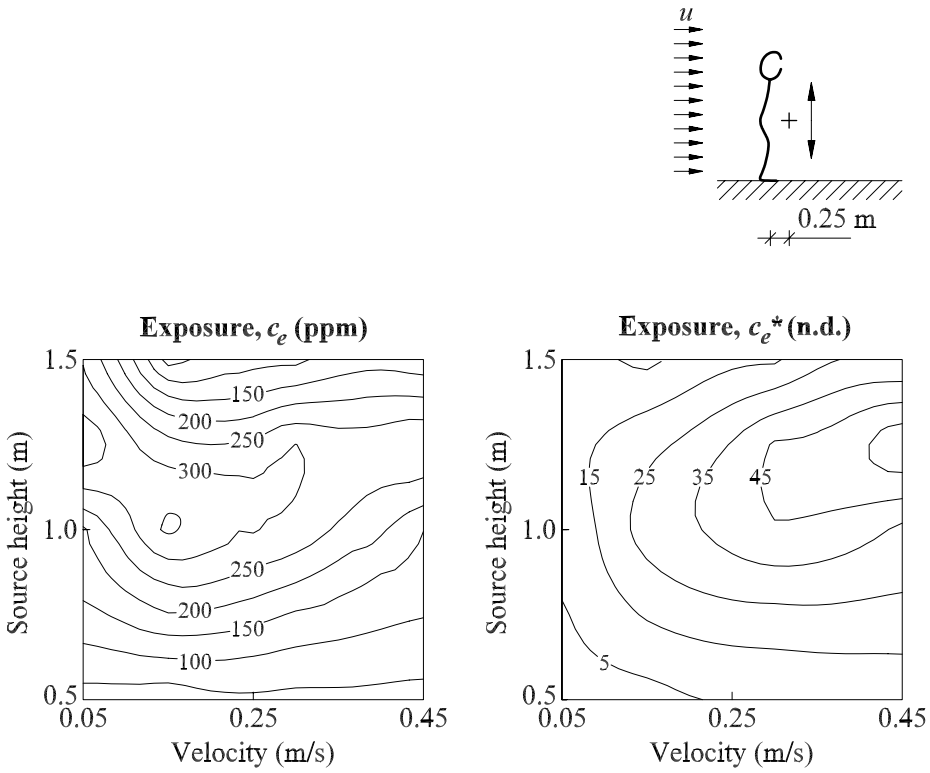

Figure 4.6. Personal exposure of the BTM standing in a uniform velocity field as a function of velocity level (0.05 m/s - 0.45 m/s) and vertical contaminant source height above the floor (0.5 m - 1.5 m). The horizontal distance between the centre of the BTM, $(x,z) = (0.7,0)$, and the centre of the source, $(x,z) = (0.95,0)$, is 0.25 m. The left plot is isopleths of personal exposure in ppm for a contaminant source strength of $S = 5 \cdot 10^{-6}$ m^3/s. The right plot is isopleths of the corresponding dimensionless personal exposure.

The set-up in Figures 4.6. and 4.7. are typical examples of locations of hand-held contaminant sources located close to the person, for instance in relation to a working process. It may take place in industrial applications like a spray hood or close to local exhaust ventilation devices, or it may be a person located in a ventilated office where the recirculating flow locally generates the field. Here, the contaminant source could be an ashtray or some kind of office equipment, etc.

If the exposure levels in Figure 4.5. and Figure 4.6. are compared, a remarkable increase is found when the source is located downstream the person. The reason for the significant increase must be found in the wake generated in front of the person. The wake consists of a mixture of turbulent diffusion and vortices with a considerable ability to entrain contaminant from a certain horizontal distance. This contamination is transported to the boundary layer and the breathing zone where it causes exposure (George et al., 1990; Brohus and Nielsen, 1994b; 1995). This is also verified by using smoke visualisation during the experimental work.

The dimensionless exposure in Figure 4.6. indicates a maximum level found for a source location between 1.00 m and 1.25 m above the floor. Furthermore, it is seen that the dimensionless exposure increases for increasing velocity levels, resulting in almost unchanged exposure levels in ppm, i.e. no improvement of the air quality for increased air flow rates.

A dimensional exposure, c_e^*, around 50 results in a personal exposure index ε_e = 0.02, which is extremely low and reveals that this source location relative to the person and the flow field may be rather critical. Unfortunately, this is in fact the case in a number of industrial applications, where the location actually was chosen in order to remove the contaminants efficiently (Kim and Flynn, 1991b; Ljungqvist and Reinmüller, 1993).

Treating the ventilated enclosure as fully mixed will result in $c_e^* = 1$ for all source locations and velocity levels. This may be compared with a measured personal exposure $c_e^* > 50$ in this case.

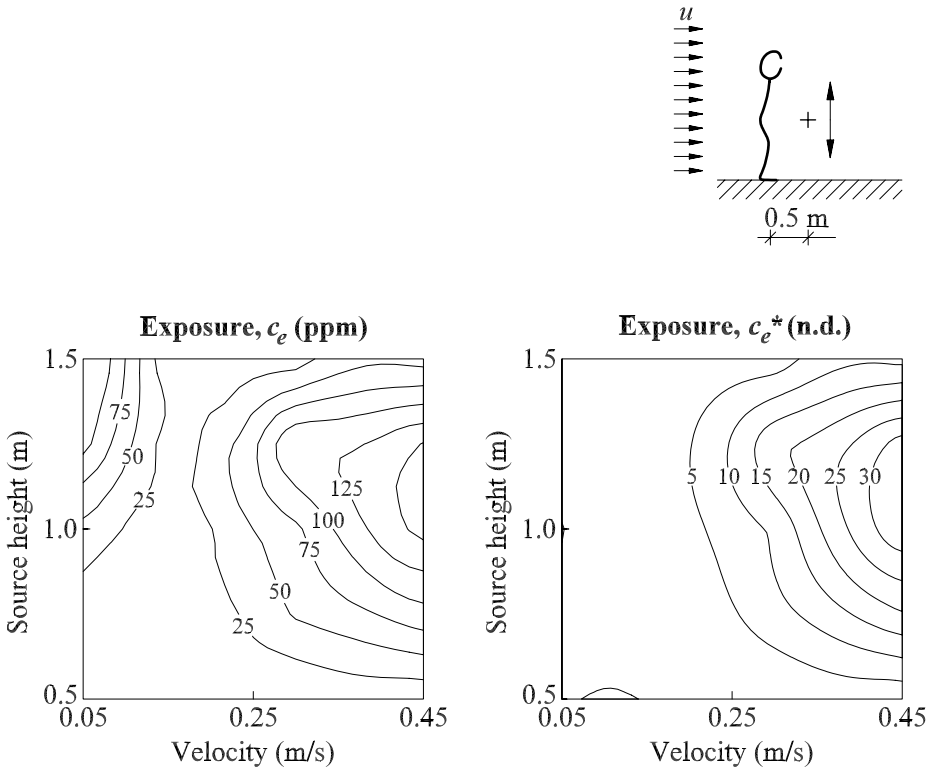

Figure 4.7. Personal exposure of the BTM standing in a uniform velocity field as a function of velocity level (0.05 m/s - 0.45 m/s) and vertical contaminant source height above the floor (0.5 m - 1.5 m). The horizontal distance between the centre of the BTM, $(x,z) = (0.7,0)$, and the centre of the source, $(x,z) = (1.2,0)$, is 0.5 m. The left plot is isopleths of personal exposure in ppm for a contaminant source strength of $S = 5 \cdot 10^{-6}$ m^3/s. The right plot is isopleths of the corresponding dimensionless personal exposure.

The horizontal distance between the contaminant source and the BTM is increased from 0.25 m to 0.5 m in Figure 4.7. This results in a reduction of the exposure level with a factor of approximately two in general, and locally even more, but still significantly higher than the one in Figure 4.5.

If the left plot (in ppm units) is examined there seem to be two different mechanisms causing high exposure levels. At a low velocity and a high source location the contamination may be dispersed by diffusion and entrained in the human convective boundary layer, where it is transported to the breathing zone

and causes exposure. When the velocity is increased the natural boundary layer is disturbed and the primary mechanism of contaminant dispersion may be entrainment due to vortices and turbulent diffusion in the wake generated in front of the BTM.

The momentum supplied by the unidirectional flow field around the person is the driving force on the vortices. Increased momentum may increase both the strength of the vortices and the turbulent diffusion. This topic is discussed in more detail in Chapter 4.2.3. where the corresponding CFD simulations are presented.

The effect of BTM heating

One of the important features of the Breathing Thermal Manikin is the heated surface. This was shown to be a very important factor to consider in the case of personal exposure assessment in a displacement ventilated room. In the following some measurements on the effect of a heated surface in a uniform flow field are presented.

Figure 4.8. shows only a small and insignificant effect of heating at 0.15 m/s for the BTM facing the flow field and the contaminant source.

In Figure 4.9., however, concentration measurements performed at the back (in the wake region) indicate a stronger influence of surface heating. Presumably this effect will be even more significant at velocity levels below 0.15 m/s.

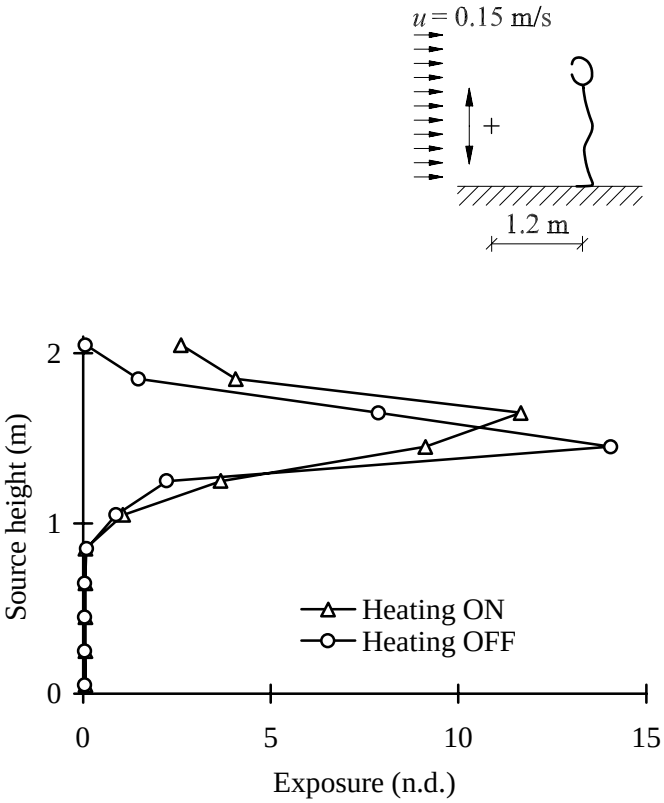

Figure 4.8. Dimensionless personal exposure of the BTM standing in unidirectional flow field at a velocity level of 0.15 m/s with the surface heating turned on (Δ) and off (o). Otherwise, same set-up as in Case 1 in Figure 4.4.

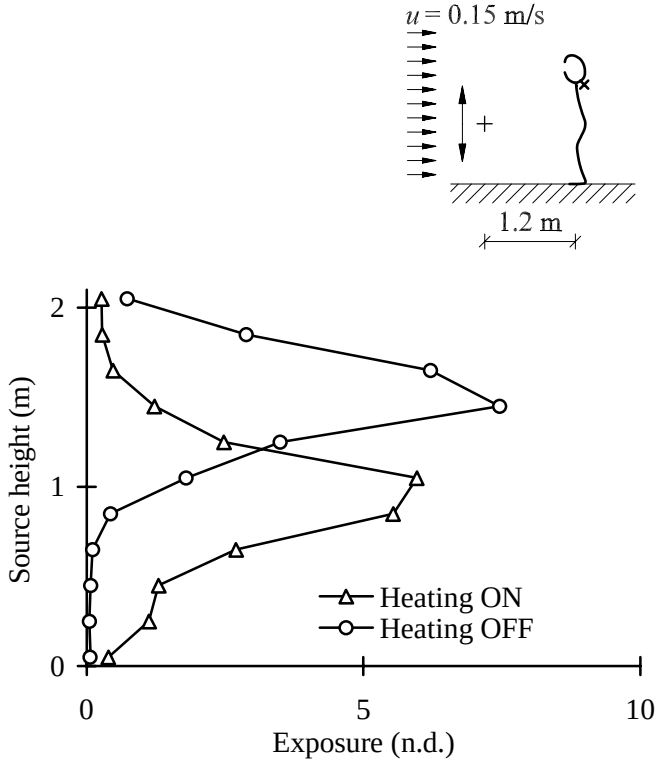

Figure 4.9. Dimensionless concentration measured at the back of the BTM located in a unidirectional flow field at a velocity level of 0.15 m/s. The results are shown for the heating turned on (Δ) and off (o). Otherwise, same set-up as in Case 1 in Figure 4.4.

In Figure 4.10. the exposure is found for a fixed source location and four different velocity levels ranging from 0.05 m/s to 0.45 m/s. The measurements are performed with the surface heating turned on and off.

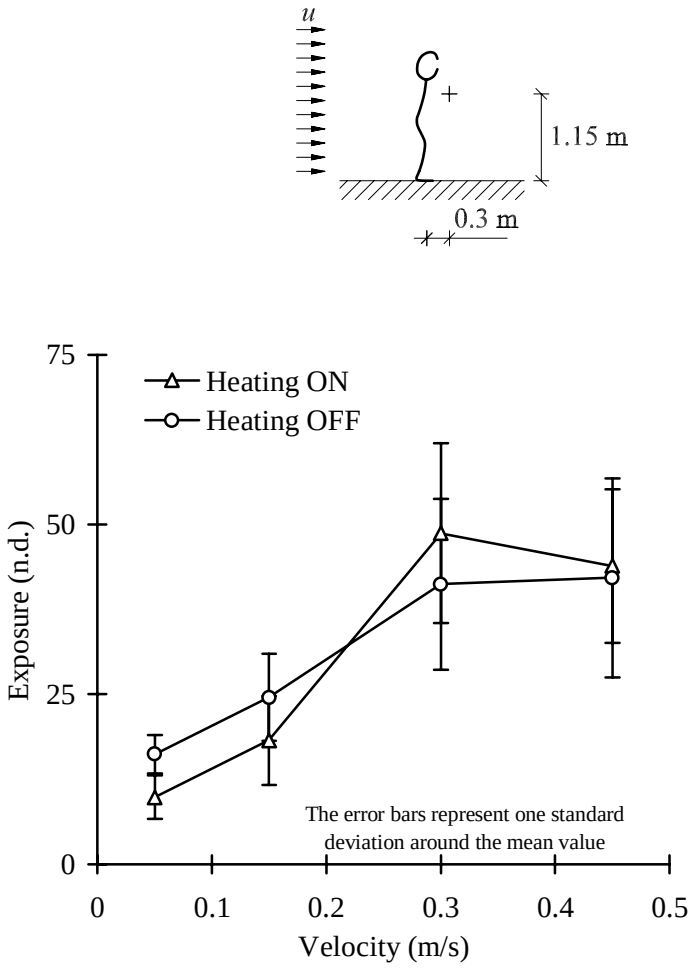

Figure 4.10. Dimensionless personal exposure of the BTM standing in a unidirectional flow field at four different velocity levels (0.05 m/s, 0.15 m/s, 0.30 m/s, 0.45 m/s) in case of the surface heating turned on (Δ) and off (o). The location of the BTM is (x,z) = (0.7,0) and the fixed point contaminant source (x,y,z) = (1.0,1.15,0).

The two curves and the corresponding standard deviations for the measuring points shown in Figure 4.10. indicate a possible effect of heating at the low velocity, and an insignificant effect of heating at the higher velocities, which was also to be expected (Brohus and Nielsen, 1994a; Hyldgaard, 1994).

Dimensionless numbers

Some of the dimensionless numbers mentioned in Chapter 2.2.2. are calculated for the present measurements and shown in Table 4.1

Table 4.1. Dimensionless numbers characterising the flow around the BTM standing in a unidirectional flow field in the wind channel shown in Figure 4.2. *Re* is the Reynolds number, *Gr* is the Grashof number and *Ar* is the Archimedes number. Expressions for the numbers are found in Chapter 2.2.2.

Uniform velocity level	**Dimensionless numbers**		
u (m/s)	Re (n.d.)	$Gr \cdot 10^9$ (n.d.)	Ar (n.d.)
0.05	1000	4.0	124.4
0.15	3000	3.9	13.6
0.30	6000	3.5	3.0
0.45	9000	3.5	1.3

If the size of the three dimensionless numbers is compared with the levels stated in Chapter 2.2.2., it can be concluded that the flow around the Breathing Thermal Manikin is laminar at each of the four velocity levels ($Re < 2 \cdot 10^5$). The convective flow in the boundary layer is found to be in the transition region between the laminar and the turbulent regime ($10^9 < Gr < 10^{10}$).

The Archimedes number shows a considerable variation. At the lowest velocity level the flow may clearly be characterised as free convection ($Ar > 16$), whereas the three other levels place the flow in the "mixed flow" category, i.e. in between the forced and free convection type ($0.06 < Ar < 16$).

4.2.3. CFD Simulation

The above-mentioned full-scale measurements on a person exposed to a point contaminant source in a unidirectional flow field will now be examined by means of Computational Fluid Dynamics. Furthermore, a planar contaminant source in the shape of the floor will be included as an other important kind of indoor pollution source.

An other purpose of the simulations is to compare the measurements and the simulations as well as the three different Computer Simulated Persons (CSP) defined in Chapter 2.3.

Finally, in Chapter 4.2.5. the results of computer simulations and the experiments are compared with models found in the literature on personal exposure in a uniform free stream.

Geometry and boundary conditions

The geometry applied in the computer simulations corresponds to the geometry of the full-scale wind channel shown in Figure 4.2. Some modifications have been made due to software requirements on a rectangular grid, i.e. the circular exhaust openings and the spherical contaminant source are converted into a rectangular geometry.

Only one half of the symmetric room is included in the simulations as seen in Figure 4.11., except from one case where the CSP model 1 is turning the side to the flow direction.

The flow field is generated by extracting air through the two exhaust openings. The walls are all treated adiabatically and surface friction is included by means of wall functions, see Chapter 2.3.2.3. Approximately 100,000 cells are used in the numerical grid. More details are mentioned in Table 4.2..

Table 4.2. Number of cells applied in the CFD simulations on a Computer Simulated Person standing in a wind channel.

CSP model	**Simulated flow domain**	**Cells in direction**			**Total**
		x	*y*	*z*	
1	Entire	69	48	33	109,296
1	Half	70	48	17	57,120
2	Half	69	52	20	71,760
3	Half	71	57	22	89,034

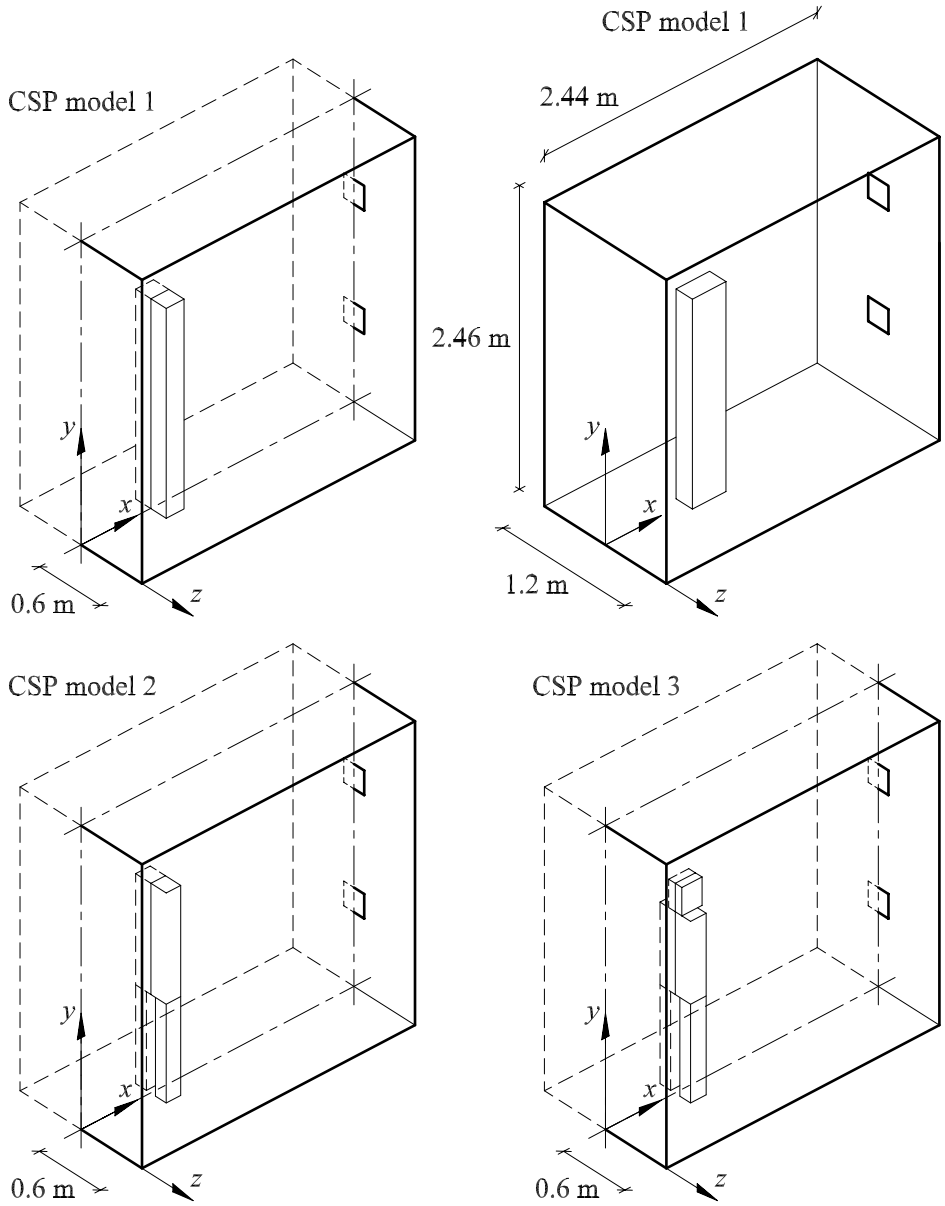

Figure 4.11. CFD simulation of the wind channel. Geometry and co-ordinate system correspond to Figure 4.2. Centre of the CSP is located at (x,z) = (0.7,0). An exception is shown in the upper right corner where CSP model 1 is turning the side to the flow field, located in (x,z) = (0.75,0.1).

Simulation of the flow field

In the five figures 4.12. to 4.16. the flow field in the wind channel will be shown for the two different velocity levels 0.05 m/s and 0.3 m/s. Each of the figures shows the three different CSP models together in order to compare the differences in the local flow field. Figure 4.17. shows the flow field around CSP model 1 turning the side to the flow field.

Figures 4.12. and 4.13. show the flow field in the vertical symmetry plane (z = 0 m) for the two velocity levels. Here, a considerable effect of both the velocity level and the three different models of a person is seen. In Figure 4.12. at 0.05 m/s the convective boundary layer plays a significant role in the vertical air movement along the body, even at the upstream side of the different CSP. A combination of convective boundary layer flow and transport by the vortices seen in Figure 4.15. are the two major driving transport mechanisms of air from the area in front of the person to the breathing zone.

In Figure 4.13. at 0.3 m/s the vortices generated downstream the person seems to have a more dominating role, which is also indicated by the flow close to the CSP in Figure 4.14., where the boundary layer beside the models is almost washed away at the higher velocity level.

The vortices seem to be able to entrain air from a horizontal distance up to approximately 0.5 m from the person, which corresponds well to the full-scale tracer gas measurements and smoke visualisations in the wind channel.

If the plume above the person in the displacement ventilation case (Figure 3.31.) is compared with the plume in Figure 4.12., the plume axis is moved from the centre of the CSP to a location just in front of the CSP. At a velocity level of 0.3 m/s no plume is found, see Figure 4.13., in stead a kind of “down wash” flow is seen in front of the head in a certain horizontal distance.

When the three different CFD models of a standing person are compared, a remarkable strong effect of the inclusion of “legs” in CSP model 2 and model 3 is found at both velocity levels. This may exert an important influence on the personal exposure, especially in case of a contaminant source located close to the floor. The topic will be further investigated in the subsequent chapter.

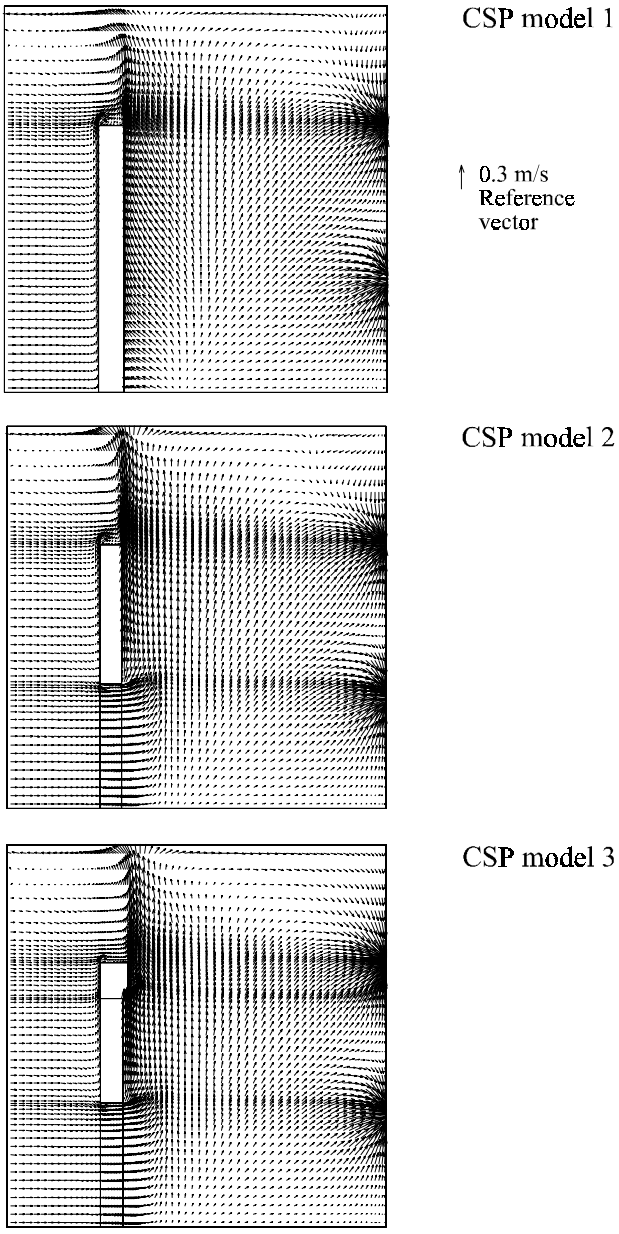

Figure 4.12. Vector plot from wind channel flow around the CSP. Velocity level 0.05 m/s. Plane: z = 0 m (vertical symmetry plane).

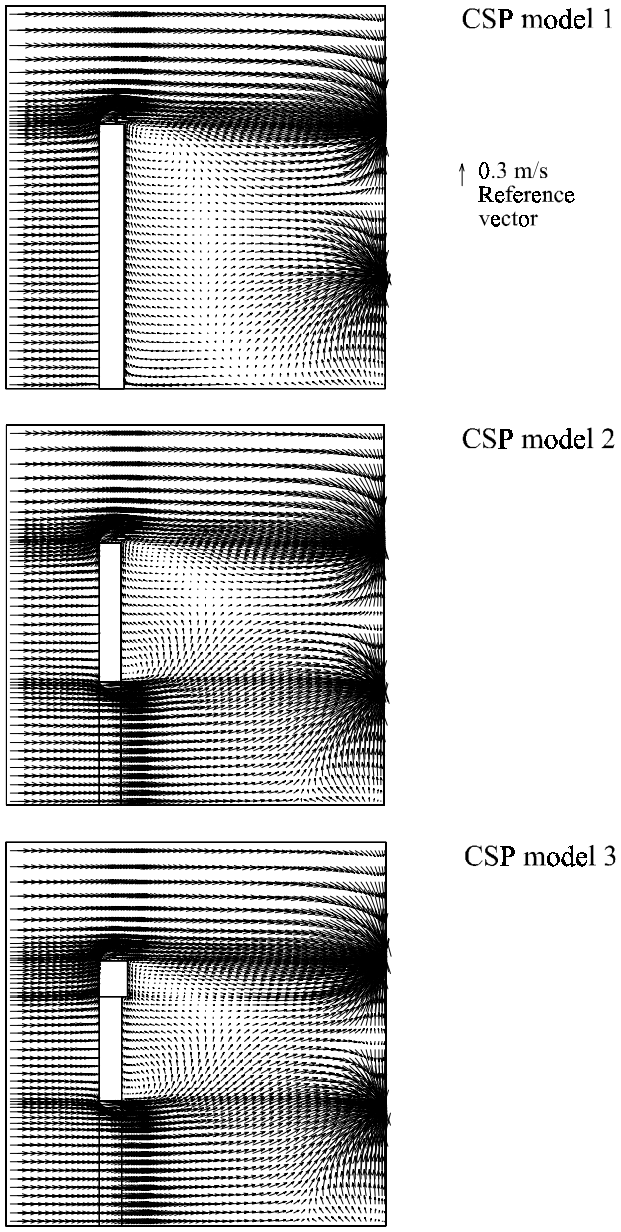

Figure 4.13. Vector plot from wind channel flow around the CSP. Velocity level 0.30 m/s. Plane: z = 0 m (vertical symmetry plane).

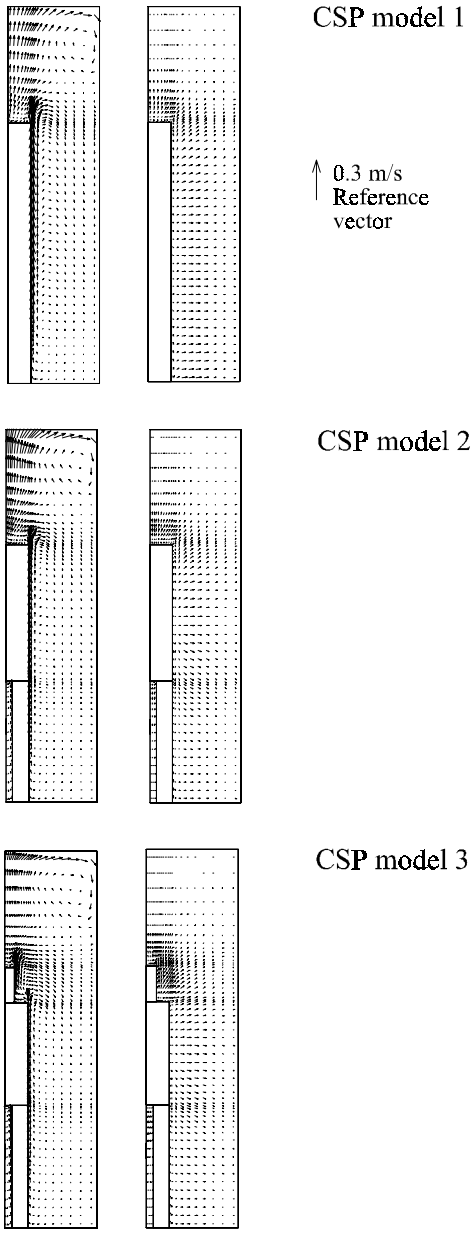

Figure 4.14. Vector plot from wind channel flow around the CSP. Plane: x = 0.7 m (vertical section through person). Left column: velocity level 0.05 m/s. Right column: velocity level 0.30 m/s.

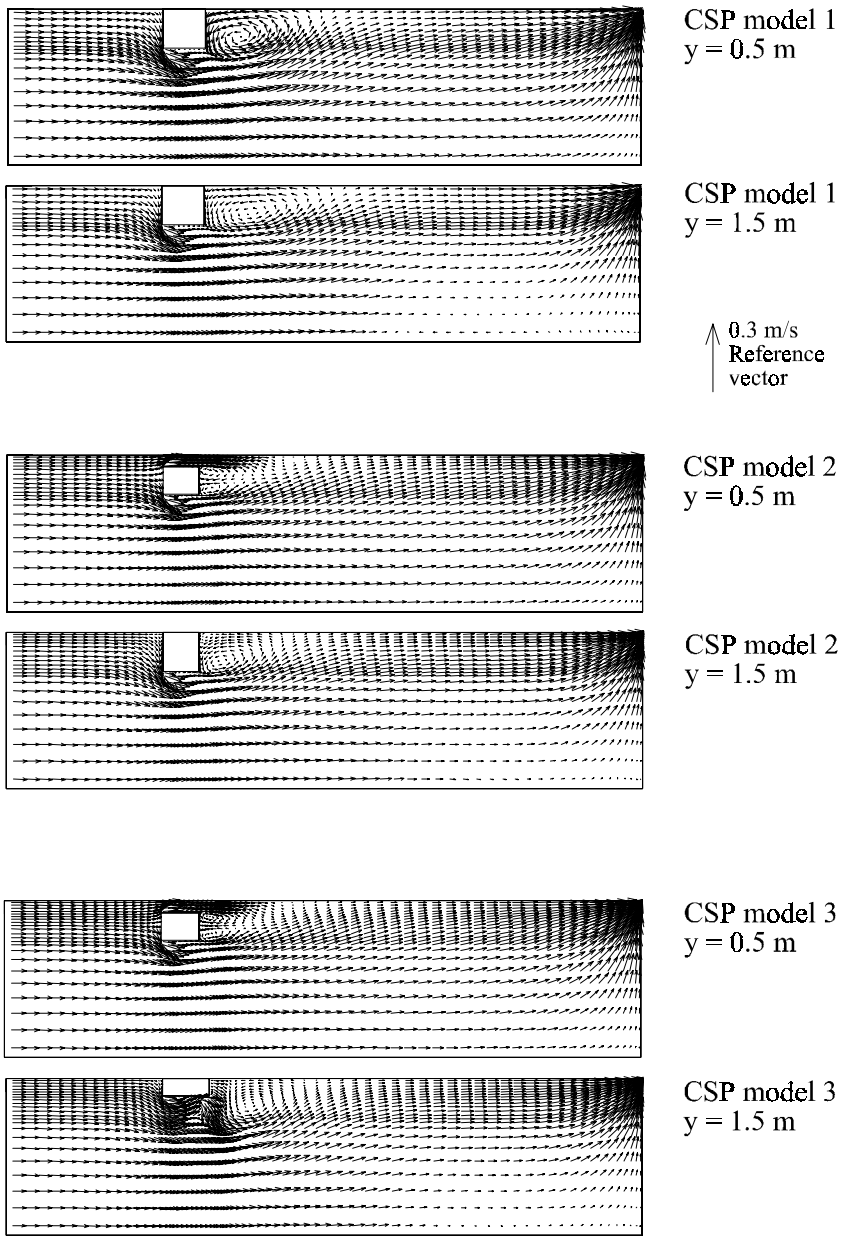

Figure 4.15. Vector plot from wind channel flow around the CSP. Velocity level 0.05 m/s. Planes: y = 0.5 m and y = 1.5 m (horizontal planes).

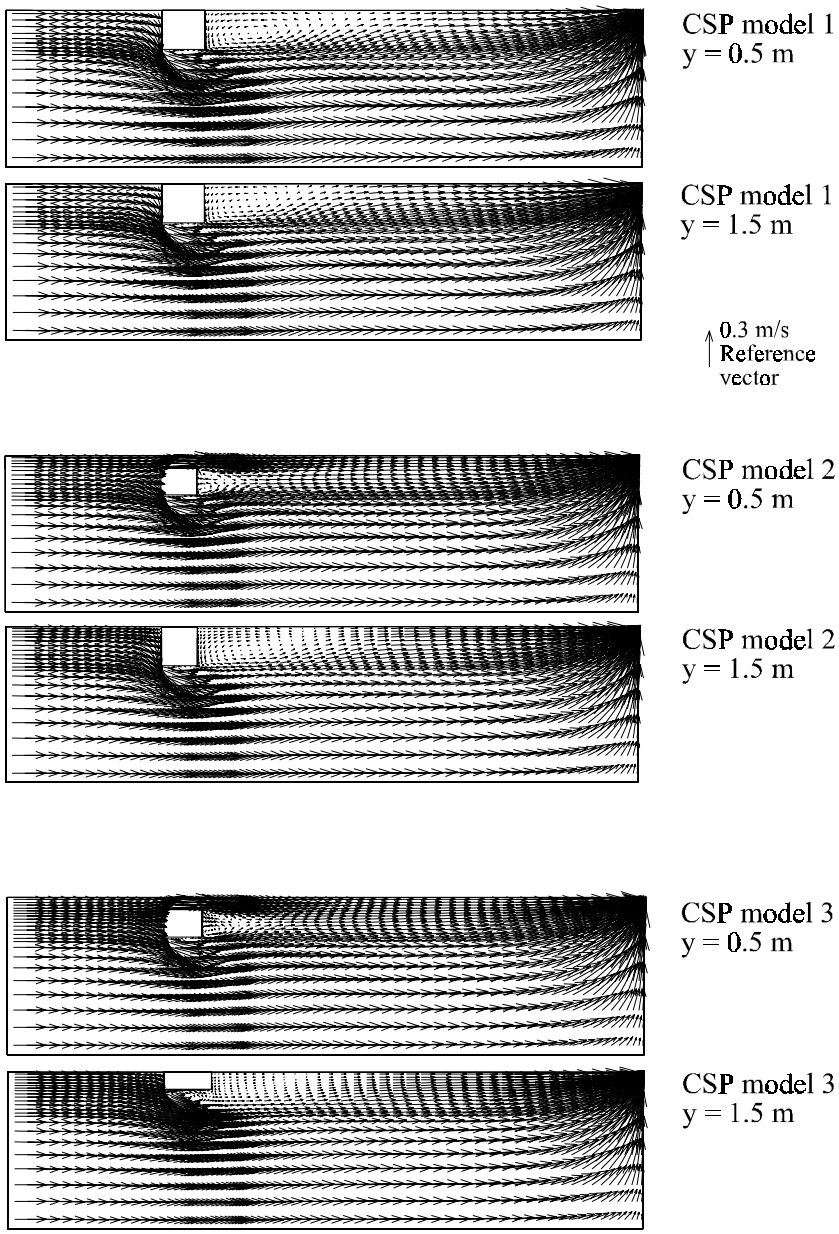

Figure 4.16. Vector plot from wind channel flow around the CSP. Velocity level 0.30 m/s. Planes: y = 0.5 m and y = 1.5 m (horizontal planes).

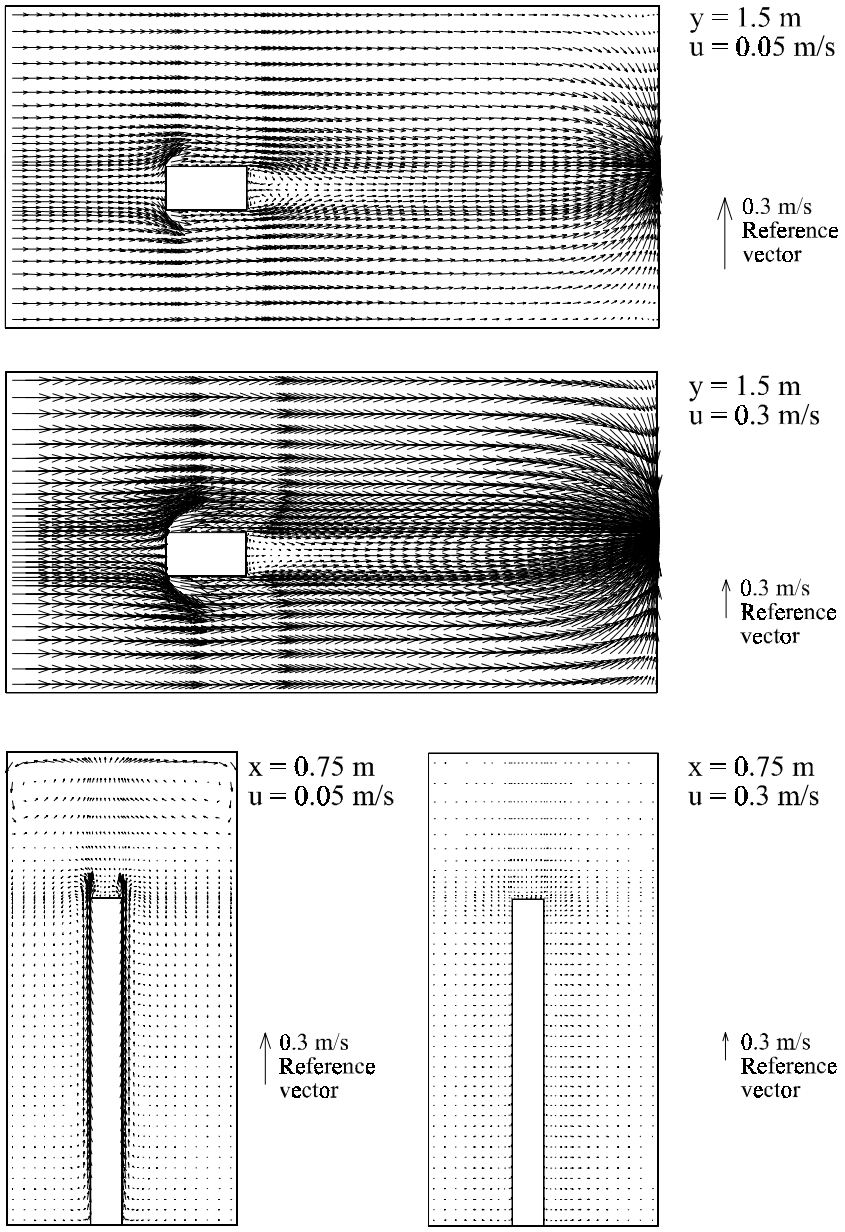

Figure 4.17. Vector plot from wind channel flow around the CSP model 1 turning the side to the flow field at the two velocity levels 0.05 m/s and 0.3 m/s.

Inclusion of “head” in CSP model 3 causes a slight deflection of the vertical flow around the chin, but no major changes of the local field compared with CSP model 2 are found. The simulations in Chapter 4.2.4. on personal exposure to contaminant sources will decide the effect of this possible improvement of the computer model of a person.

The purpose of the present simulations and the full-scale measurements in the preceding chapter is to examine the flow field around a person in a unidirectional flow field. Therefore, it is important to be aware of the influence of the boundaries on the local uniform flow field around the person, i.e. do the specific size and construction of the wind channel allow a uniform flow field or do they cause some restrictions in the flow field affecting the generality of the results?

If the vector plots in Figures 4.12. - 4.17. are examined, the geometry of the wind channel does not seem to influence the local flow field around the person in a way that may affect the personal exposure at the contaminant source locations applied in this work, which is also the conclusion of smoke visualisations performed during the experiments.

4.2.4. Simulation of personal exposure

This chapter will present results on personal exposure to a passive point contaminant source at different locations relative to the person in the unidirectional flow field, as well as exposure to a planar contaminant source in the shape of the floor of the wind channel.

Passive point contaminant source

First, some of the transport mechanisms mentioned in the preceding chapter will be illustrated by means of isoconcentration plots on different characteristic situations for two different velocity levels, see Figures 4.18. and 4.19.

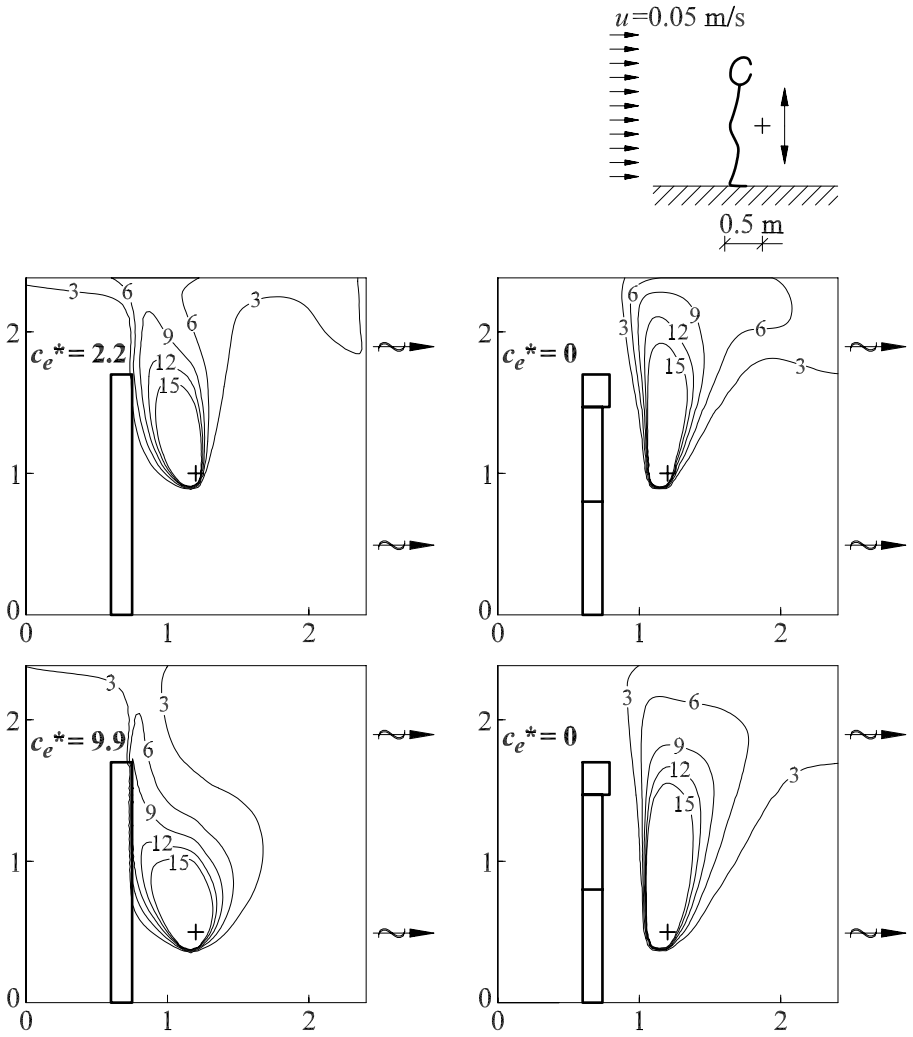

Figure 4.18. Dimensionless contaminant concentration distribution in the vertical symmetry plane (z = 0 m) of the unidirectional flow field created in the wind channel. Velocity level 0.05 m/s. CSP location (x,z) = (0.7,0). Top, left: CSP model 1, source location (x,y,z) = (1.2,1.0,0). Top, right: CSP model 3, source location (x,y,z) = (1.2,1.0,0). Bottom, left: CSP model 1, source location (x,y,z) = (1.2,0.5,0). Bottom, right: CSP model 3, source location (x,y,z) = (1.2,0.5,0). The corresponding dimensionless personal exposure, c_e^*, is mentioned in the figure. The velocity field is shown in Figure 4.12.

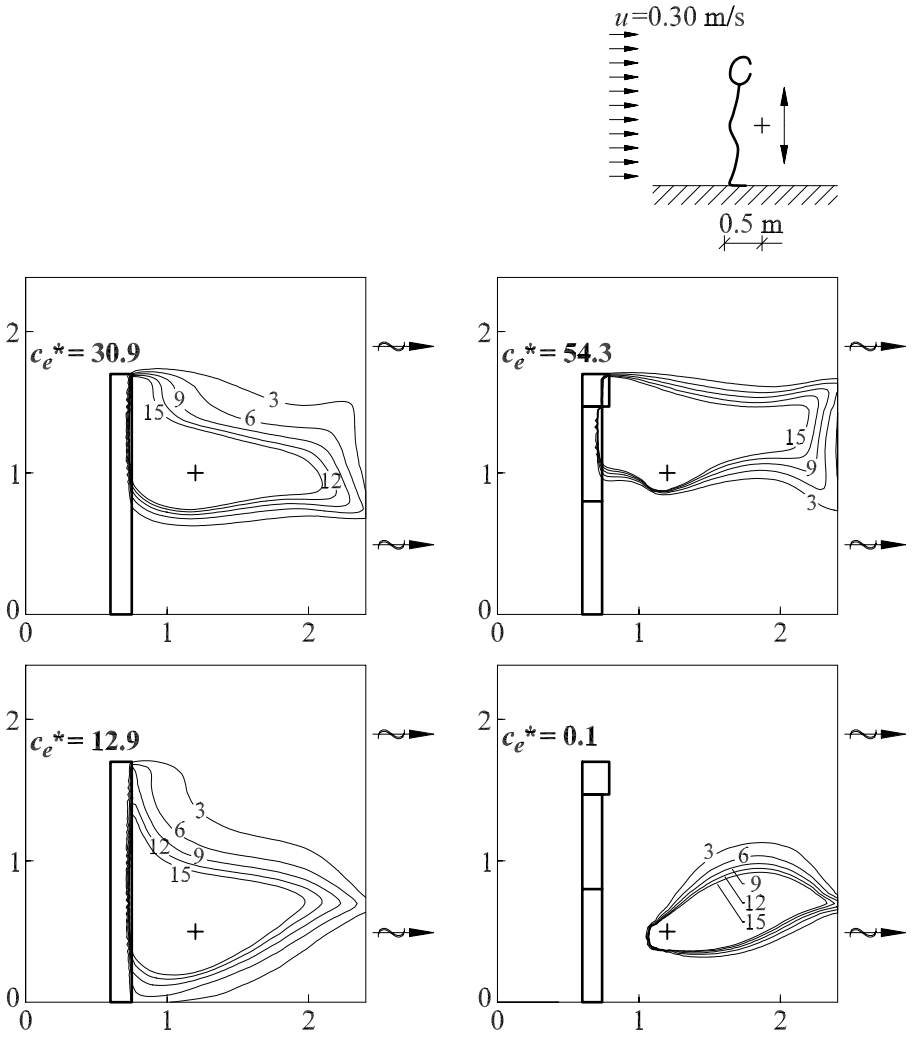

Figure 4.19. Dimensionless contaminant concentration distribution in the vertical symmetry plane (z = 0 m) of the unidirectional flow field created in the wind channel. Velocity level 0.30 m/s. CSP location (x,z) = (0.7,0). Top, left: CSP model 1, source location (x,y,z) = (1.2,1.0,0). Top, right: CSP model 3, source location (x,y,z) = (1.2,1.0,0). Bottom, left: CSP model 1, source location (x,y,z) = (1.2,0.5,0). Bottom, right: CSP model 3, source location (x,y,z) = (1.2,0.5,0). The corresponding dimensionless personal exposure, c_e^*, is mentioned in the figure. The velocity field is shown in Figure 4.13.

Figures 4.18. and 4.19. clearly illustrate many of the characteristics of the two different models of a person mentioned in Chapter 4.2.3., in this case by means of the concentration distribution. The significant influence of the velocity level as well as inclusion of legs is easily seen on the isoconcentration curves and also very clearly on the actual personal exposure levels.

The ability of the vortices in the wake region and the human convective boundary layer in combination to entrain and transport contamination from relative large distances to the breathing zone is considerable. This applies to both velocity levels and the two different models of the CSP shown in the two figures. If the exposure levels are compared with completely mixed conditions, i.e. $c_e^* = 1$, both improved ($c_e^* = 0$) and deteriorated ($c_e^* = 54.3$) air quality is found.

In the four figures 4.20. - 4.23. the dimensionless personal exposure is shown as a function of velocity level and the vertical contaminant source location. The results are shown for the three different versions of the Computer Simulated Person. The exposure measurements made by means of a Breathing Thermal Manikin are also included to facilitate the comparisons.

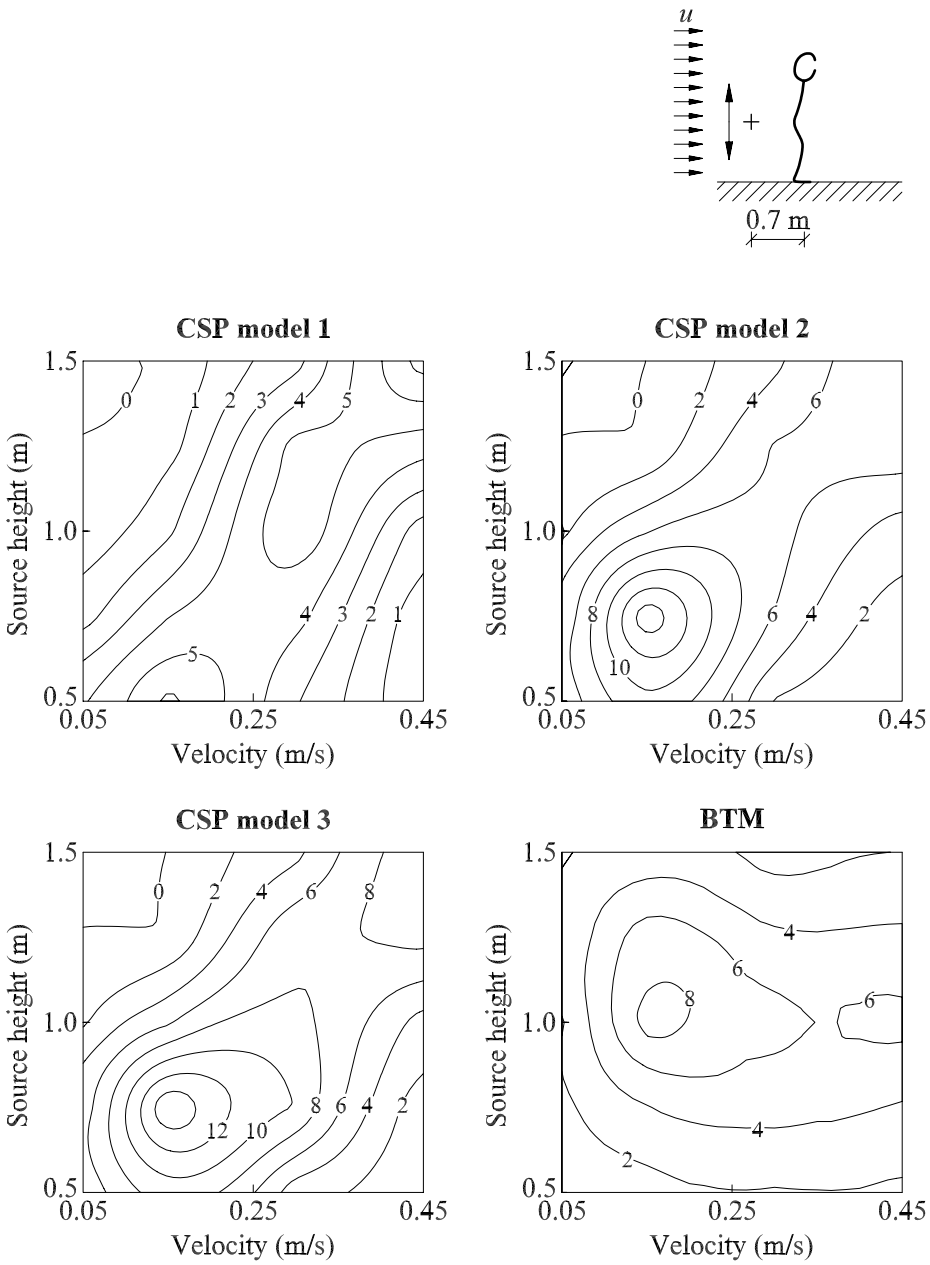

Figure 4.20. Dimensionless personal exposure, c_e^*, of a person standing in a uniform velocity field as a function of the velocity level and the vertical contaminant source height above the floor.

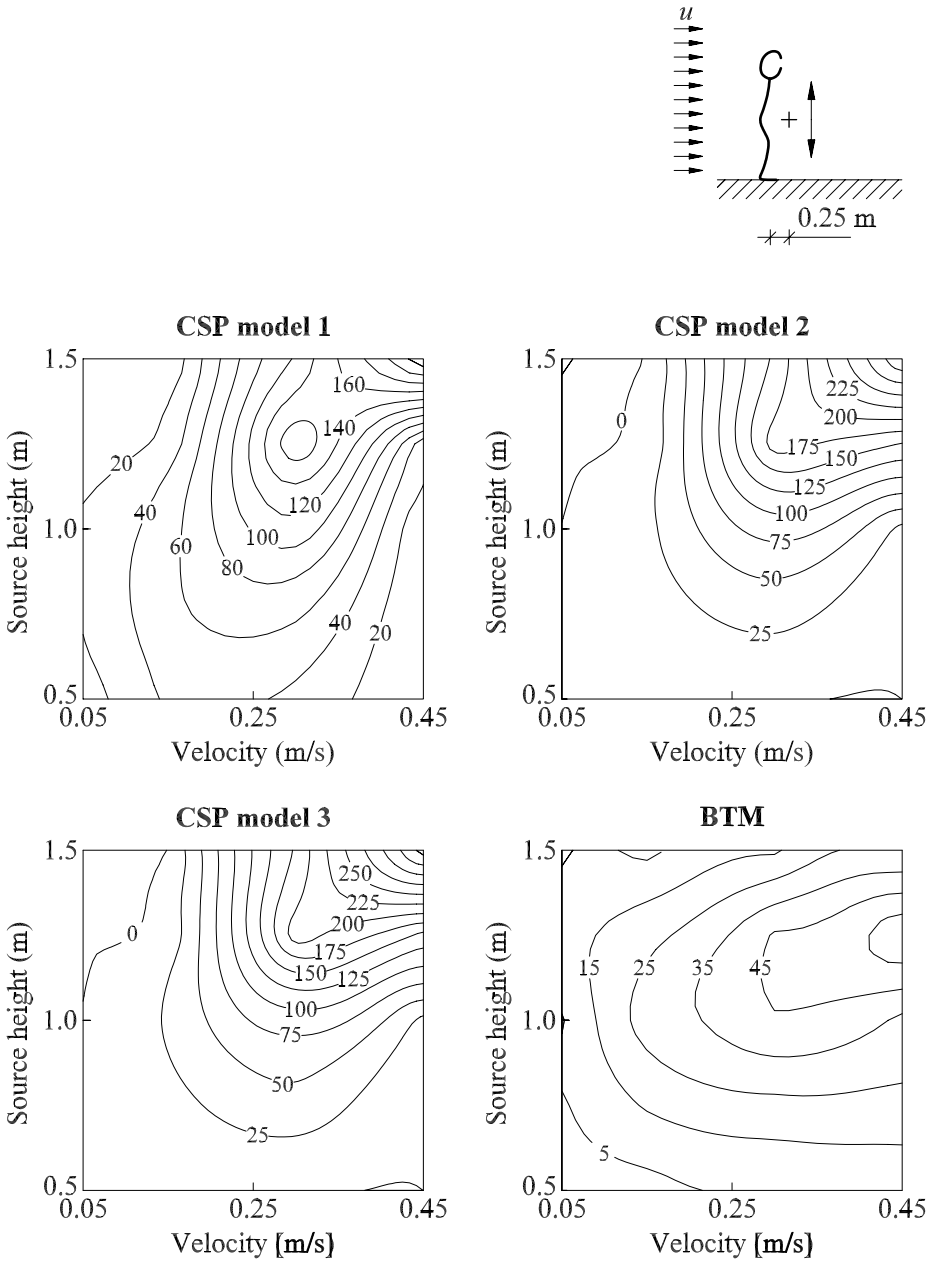

Figure 4.21. Dimensionless personal exposure, c_e^*, of a person standing in a uniform velocity field as a function of the velocity level and the vertical contaminant source height above the floor.

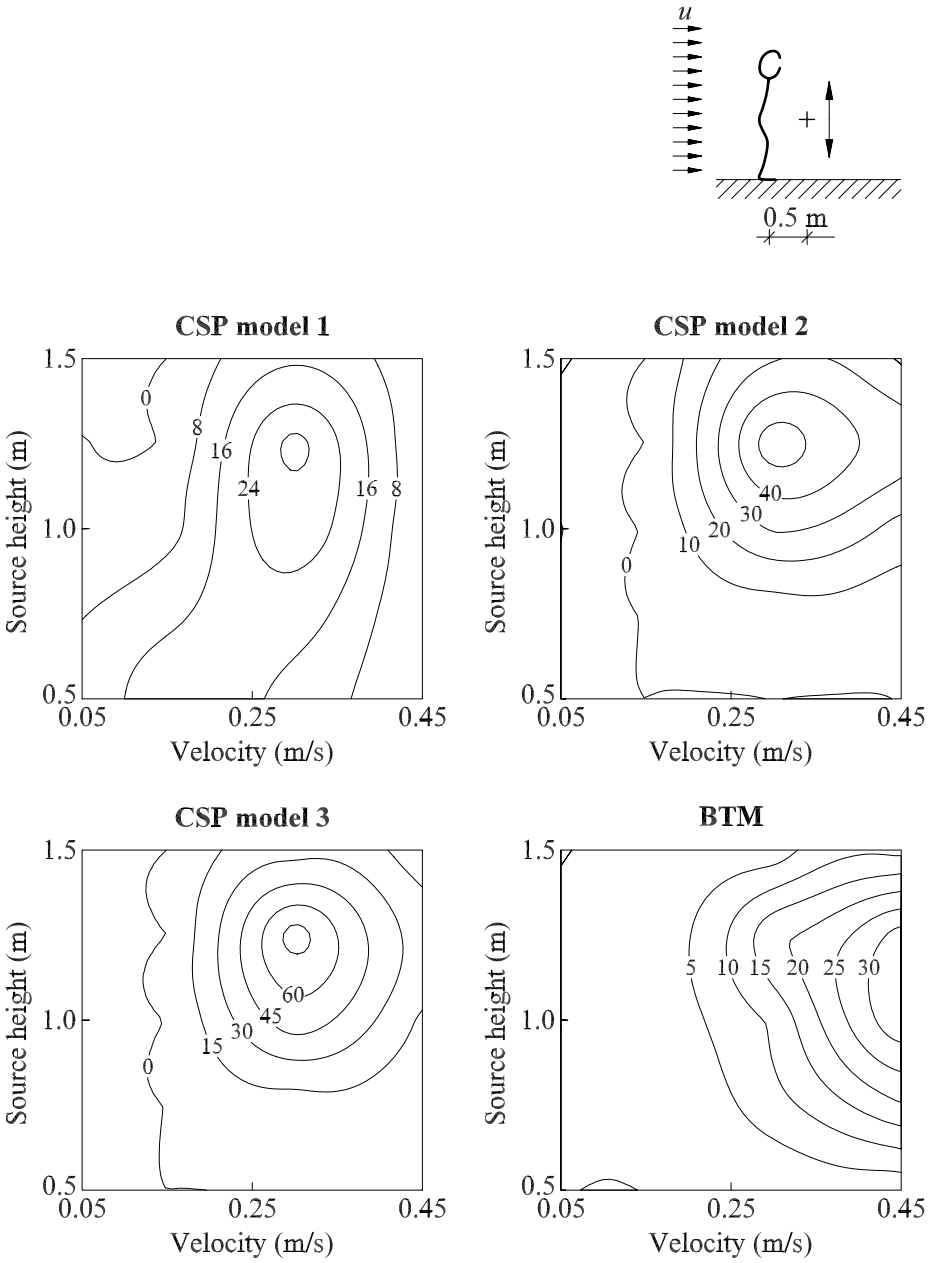

Figure 4.22. Dimensionless personal exposure, c_e^*, of a person standing in a uniform velocity field as a function of the velocity level and the vertical contaminant source height above the floor.

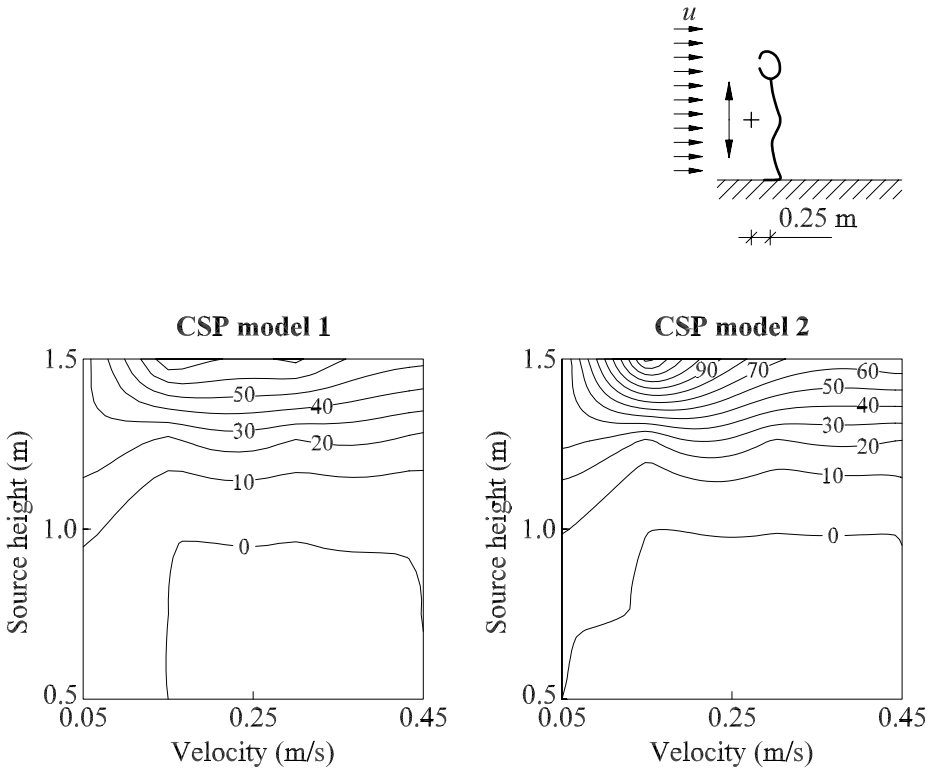

Figure 4.23. Dimensionless personal exposure, c_e^*, of a person standing in a uniform velocity field as a function of the velocity level and the vertical contaminant source height above the floor. In this case the person is facing the flow field opposite the location in Figures 4.20. - 4.22.

Figure 4.20. shows the exposure in the case of a passive point contaminant source located 0.7 m behind the person upstream in the unidirectional flow field. The results indicate a considerable influence of both velocity level, source location and also the kind of model used to simulate a person. The variation in the dimensionless exposure level is found to exceed one order of magnitude both in case of simulations and measurements.

When the exposure of the three CSP models is examined, a kind of diagonal is found in the plots where relatively high exposures occur, starting at a low velocity level and a low vertical source location, continuing to a high velocity level and a high vertical contaminant source location. In case of the low velocity level the convective ascending air current along the person is able to transport the

contamination from the lower part of the person to the breathing zone, whereas at the higher velocities the vortices in the wake region are able to entrain the contamination and transport it to the breathing zone.

When the source is located at a high level at low velocities the boundary layer flow will protect against exposure, and in case of a low source location at high velocities the contamination is "washed away", even though some exposure always occurs due to the dispersion of the contamination along the route from the source until the contaminant field reaches the person.

This particular effect is not found to influence the measurements where the BTM is applied, but the exposure levels are found to be of the same order of magnitude, slightly higher than the CSP model 1 and slightly lower than CSP model 2 and 3.

The inclusion of "legs" (CSP model 2 and 3) is seen to influence the results highly in this case, whereas the inclusion of "head" (CSP model 3) does not alter neither the overall flow pattern nor the outline of the exposure isopleths, but in general it seems to increase the exposure level slightly.

Figure 4.21. shows the exposure in the case of a passive point contaminant source located 0.25 m downstream in front of the person. This case shows some very high levels of exposure. For the measurements the dimensionless exposure, c_e^* , is found to exceed 50 and for the simulations levels above 200 are found.

The vertical source location for the maximum dimensionless exposure is found between 1.0 m and 1.5 m above the floor, i.e. a natural location for a hand-held contaminant source. Even at velocity levels required to be in a state of thermal comfort in typical office environments the exposure levels exceed the "completely mixed conditions" more than 10 times. This fact clearly stresses the importance of considering the local influence of a person located in surroundings where concentration gradients prevail.

In Figure 4.22. the horizontal distance between the person and the source of contamination is increased from 0.25 m to 0.5 m. Here, the level of exposure is reduced considerably compared with Figure 4.21., which is also expected. Still, however, high dimensionless personal exposure levels are found (exceeding 30 for the measurements and 60 for the simulations).

At a low velocity level a protective boundary layer is created in front of the person in the case of assessments by means of the BTM and CSP models 2 and 3. In this case $c_e^* = 0$ and no exposure takes place.

This particular effect is not caught by CSP model 1 where no "legs" are implemented. It indicates that the exposure is quite sensitive to the outline of the models, but it also indicates that even a small change from a standing position with the legs assembled to a standing position with the legs slightly spread may exert an important influence on the exposure in a unidirectional velocity field.

Figure 4.23. shows a simulation of the dimensionless personal exposure where the source is located 0.25 m in front of the person facing the velocity field. Only CSP model 1 and 2 are included. Here, the person is facing the velocity field contrary to the other cases.

For velocity levels above 0.05 m/s - 0.15 m/s the contamination is "washed away" around the person in the case of source locations below 1.0 m This corresponds well with the measurements presented in Figure 4.4. For source locations above 1.0 m the dimensionless exposure is almost constant for the different velocity levels.

It is remarkable that this location causes generally lower exposure levels than the ones found in Figure 4.21., where the person facing the contaminant source is turning the back to the flow direction. This is clearly caused by the vortices created in the wake region which can be seen, for instance, in Figure 4.15. (Kim and Flynn, 1991b; Brohus and Nielsen, 1995; 1996a).

To illustrate the influence of the direction of the flow field relative to a person holding a contaminant source, three different cases are shown in Figure 4.24.

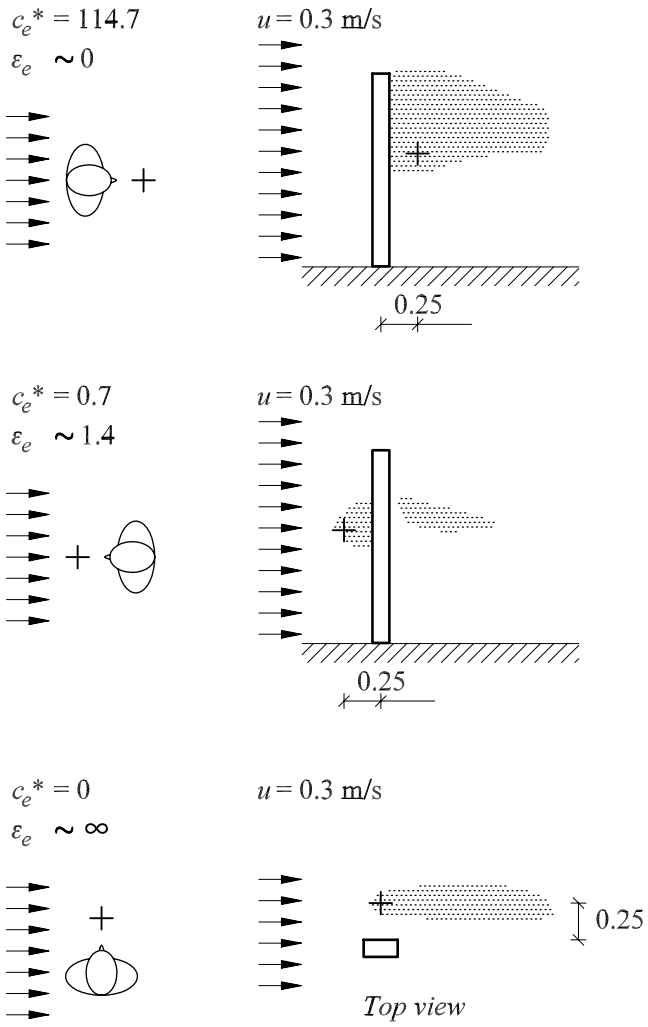

Figure 4.24. Personal exposure to a hand-held point contaminant source in a unidirectional velocity field of 0.3 m/s. In all cases the contaminant source is located 1 m above the floor and in a horizontal distance of 0.25 m in front of the CSP model 1. The hatched areas represent contaminant concentrations exceeding 10 times the exhaust concentration of the wind channel, i.e. $c^* \geq 10$. The dimensionless personal exposure, c_e^*, and the personal exposure index, ε_e, are mentioned in the figure for the three different locations relative to the flow field. The source strength and the air flow rate are the same for the three cases.

Figure 4.24. clearly shows that it may cause an erroneous exposure assessment if the personal exposure is calculated solely on the basis of a source strength and an air flow rate. It also suggests the possible benefit that may be obtained if the worker in a spray hood etc. is turning the side to the flow direction instead of the back, both regarding the health effect and also regarding the energy consumption necessary to ensure a sufficiently low exposure level.

Planar contaminant source

In the following a planar contaminant source will be applied in the shape of the floor of the wind channel. The planar source has a constant emission rate.

Figure 4.25. shows some characteristic examples of the concentration distribution generated in the wind channel where the entire floor is a contaminant source. This kind of source gives a good illustration of the persons ability to entrain and transport air and thus contaminant from the floor area to the breathing zone.

Again, the influence of the velocity level and the model layout is distinct. The exposure levels, however, are significantly lower than the previous ones obtained in the case of a point source located close to the person.

In Figure 4.26. the dimensionless personal exposure is shown as a function of the velocity level. The exposure of CSP model 2 and 3 is almost similar, and it decreases when the velocity level increases. CSP model 1 shows a peak in the dimensionless exposure level for 0.15 m/s. This is due to the “assembled legs” and the change from a local flow field dominated by free convection to a local flow field where vortices generated in the wake region play a more and more important role in the contaminant transport processes.

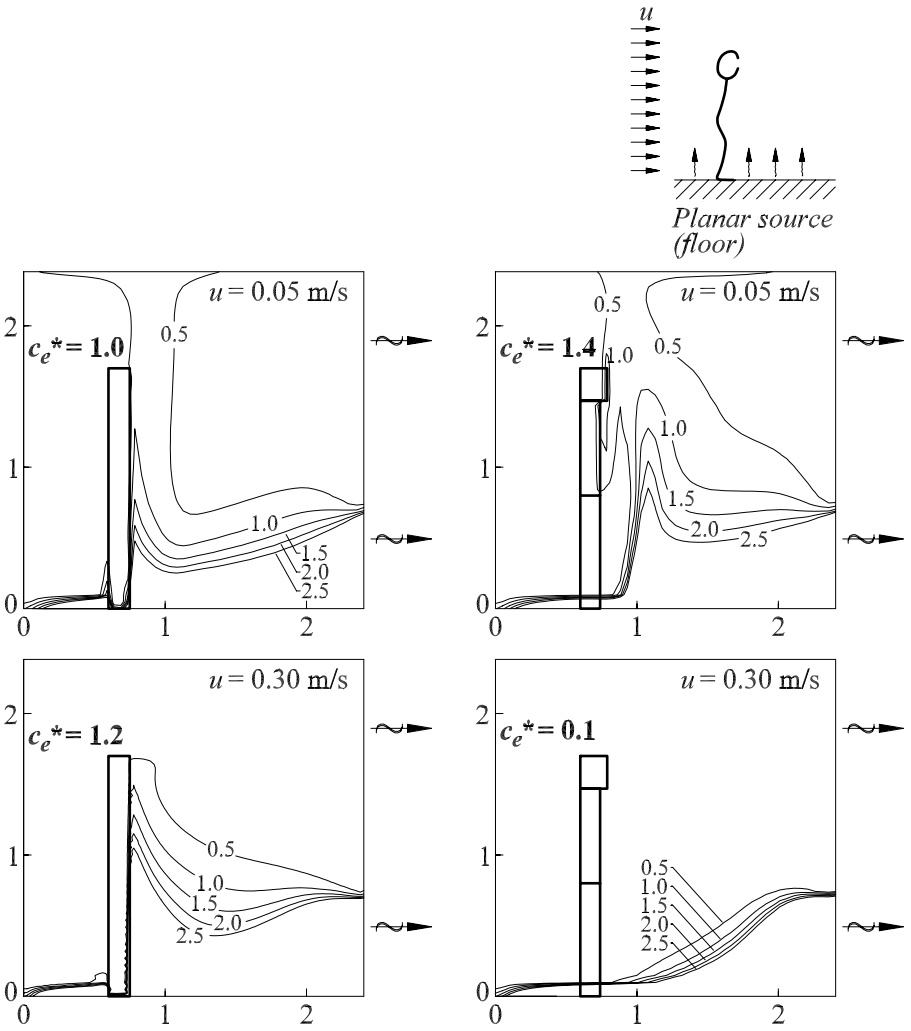

Figure 4.25. Dimensionless contaminant concentration distribution in the vertical symmetry plane (z = 0 m) of the unidirectional flow field created in the wind channel. The floor (y = 0 m) is a planar contaminant source with a constant emission rate. CSP location (x,z) = (0.7,0). Top, left: CSP model 1, velocity level 0.05 m/s. Top, right: CSP model 3, velocity level 0.05 m/s. Bottom, left: CSP model 1, velocity level 0.3 m/s. Bottom, right: CSP model 3, velocity level 0.3 m/s. The corresponding dimensionless personal exposure, c_e^*, is mentioned in the figure.

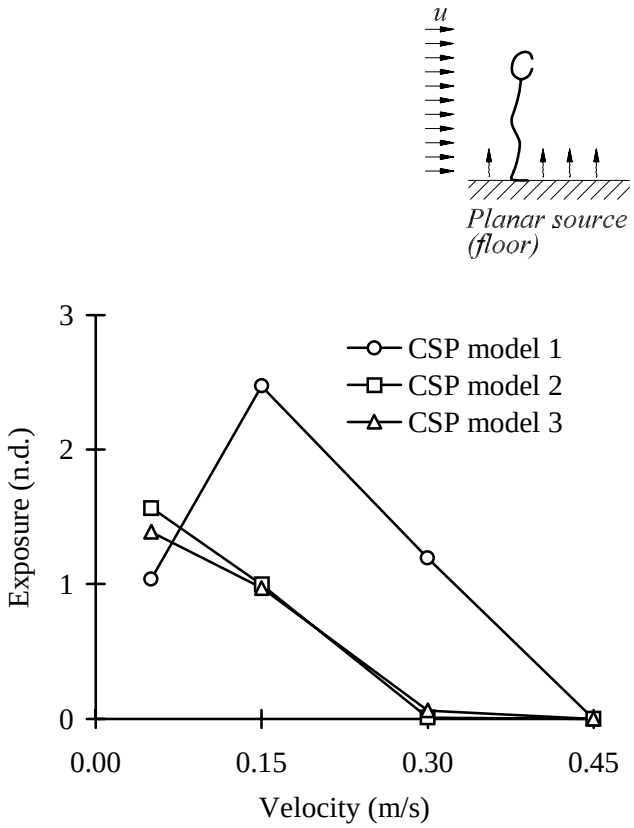

Figure 4.26. Dimensionless personal exposure to a planar contaminant source in the shape of the floor in the wind channel. The exposure is shown for the three different computational models of a person located at (x,z) = (0.7,0) and for four velocity levels 0.05 m/s, 0.15 m/s, 0.30 m/s and 0.45 m/s.

4.2.5. Comparison with exposure models

The results of measurements and computer simulations presented in Chapters 4.2.3. and 4.2.4. demonstrate that the personal exposure assessment in the case of a person exposed to a contaminant source in a unidirectional flow field may be rather complex. This fact indicates that there are a number of cases where it is necessary to apply measurements or computer simulations of the flow field and the contaminant field if detailed information on the personal exposure is required.

However, in the literature two different exposure models are found on a person standing in a uniform velocity field exposed to a contaminant source located downstream in front of the person. These models are not based on potential flow theory where the fluid is assumed to be inviscid, like the major part of the existing analytical models. This is very important in this case, where recirculation obviously plays a significant role. In the subsequent the two models will be described and compared with the results of the present work.

Description of exposure models

The two exposure models described in the following are proposed by George et al. (1990) and further developed by Kim and Flynn (1991a;b).

According to George et al. (1990) the flow around a person standing in a uniform flow field may be compared with the flow around a circular cylinder, see Figure 4.27. On that basis a simple conceptual model is developed.

It is assumed that a contaminant source is located close to the person in the recirculation region. The mechanism for contaminant removal from this zone is a mixture of turbulent diffusion and vortex shedding (George et al., 1990). The model assumes that the person is a two-dimensional circular cylinder, and that vortex shedding is the principal contaminant removal mechanism.

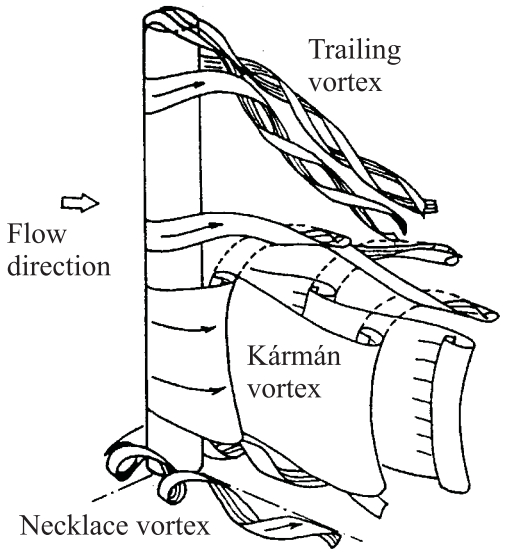

Figure 4.27. Visualisation of the flow around a person in a uniform flow field, modelled as a circular cylinder. In part of the wake a Kármán vortex street may be generated. *Reference*: Kawamura et al. (1984).

The average steady-state concentration within the recirculation zone is

$$c_{st} = \frac{S_{st}}{q_{st}} \tag{4.2}$$

where

c_{st} = Average steady-state concentration in recirculation zone (ppm)
S_{st} = Contaminant flow into the recirculation zone (m^3/s)
q_{st} = Air flow out of the recirculation zone (m^3/s)

In order to determine q_{st}, the frequency of vortex shedding, f, has to be known by means of the Strouhal number, S

$$S = \frac{fD}{u} \tag{4.3}$$

where

S = Strouhal number (n.d.)
f = Frequency of vortex shedding (s^{-1})
D = Diameter of object (m)
u = Free stream velocity (m/s)

The Strouhal number is a dimensionless group that may be thought of as a dimensionless frequency which is a function of the Reynolds number. For a two-dimensional circular cylinder $S \approx 0.21$ for $Re = 400 - 2 \cdot 10^5$ (Schlichting, 1979). The flow around a person in an office environment or a worker in the industry will almost always be below $Re = 2 \cdot 10^5$ (George et al., 1990), which is also demonstrated in Chapter 2.2.2.

The formation region for the vortices is assumed to equal the cylinder diameter, D, and the height of the region is equal to the cylinder height, H. If one-half of the volume is cleared every time a vortex is shed, the volume contained in one vortex, V, equals

$$V = \frac{\pi\left(\frac{D}{2}\right)^2 H}{2} \tag{4.4}$$

where

V = Volume cleared when a vortex is shed (m^3)
D = Diameter of cylinder (m)
H = Height of cylinder (m)

The frequency, f, determined by the Strouhal number corresponds only to one side of the cylinder, which gives the total air flow out of the recirculation zone caused by vortex shedding

$$q_{st} = 2fV \tag{4.5}$$

And, finally (George et al, 1990)

$$c_{st} = \frac{19 S_{st}}{\pi u H D} \tag{4.6}$$

where D is taken as the width of the chest measured just under the armpits.

Kim and Flynn (1991a) examined the three-dimensional flow around a manikin by means of flow visualisation and hot-film anemometry. They found that the region subject to vortex shedding ranged only from the chest to the hip, i.e. ~ $0.3 \cdot H$, and they found that the average area of one vortex appeared to be 0.7 times the area of the circle mentioned above. Furthermore, they measured a somewhat lower Strouhal number, $S = 0.19$.

If the modifications are implemented in the model the following revised version is obtained (Kim and Flynn, 1991b)

$$c_{st,revised} = \frac{50 S_{st}}{\pi u H D} \tag{4.7}$$

Measurements by Kim and Flynn (1991b), using a small-scale, unheated 1 m high manikin standing in a wind channel with a hand-held point contaminant source, showed that the original model by George et al. (1990) underestimated the average concentration in the recirculation region, c_{st}, and that the revised model overestimated the concentration. An empirical relation obtained by least square regression was found both for c_{st} and also for the personal exposure, c_e, i.e. (Kim and Flynn, 1991b)

$$c_{st,empirical} = \frac{10.96 S_{st}}{u H D} \tag{4.8}$$

$$c_{e,empirical} = \frac{8.62 S_{st}}{u H D} \tag{4.9}$$

Apart from the above model George et al. (1990) found an empirical expression for the personal exposure as a function of the straight line distance between the mouth and the point contaminant source, R. Here, the dimensionless exposure, c_e^*, is expressed as a function of the dimensionless distance R/D (George et al., 1990)

$$c_e^* = 695(0.135)^{R/D} \tag{4.10}$$

where

c_e^* = Dimensionless personal exposure (n.d.)
R = Straight line distance between mouth and contaminant source (m)
D = Diameter of object (width of chest) (m)

The empirical expression was found using the above-mentioned small-scale manikin located in a wind channel. The manikin was exposed to a point contaminant source simulated by tracer gas supplied through a ceramic sphere, ø 0.64 cm.

Comparison with models

If the empirical expression for the personal exposure to a hand-held point contaminant source in a uniform flow field is made dimensionless the following formula is obtained, where q is the air flow rate (m^3/s) of the wind channel

$$c_e^* = \frac{c_e}{c_R} = \frac{\frac{8.62 S_{st}}{uHD}}{\frac{S_{st}}{q}} = \frac{8.62q}{uHD} \tag{4.11}$$

The width of the chest for the BTM, the CSP models, and also the cylinder model of a person mentioned in Chapter 2.2.2. is the same: D = 0.3 m. Inserting the other parameters in equation (4.11) gives

$$c_e^* \approx 50 \tag{4.12}$$

when the exposure model by Kim and Flynn (1991b) is applied.

In order to make comparisons the small-scale manikin together with the contaminant source used by Kim and Flynn (1991a;b) and George et al. (1990) must be converted into full scale.

This results in a source location 1.15 m above the floor. To maintain Reynolds number equality the velocity levels are converted to 0.3 m/s - 0.9 m/s. Thus, the comparisons should be performed for results in this range.

For the BTM standing in the wind channel with the contaminant source located 0.3 m downstream at a height of 1.15 m above the floor, c_e^* is found to be 49 and 44 for the two velocity levels 0.30 m/s and 0.45 m/s, respectively (see Figure 4.10.). This corresponds well with the exposure found by means of the above model in equation (4.10).

Figure 4.28. shows comparisons between the model by George et al. (1990) mentioned in equation (4.10) and measurements using the BTM as well as simulations using CSP model 1 and model 3.

The exposure model mentioned in equation (4.10) and applied in Figure 4.28. is developed for velocity levels ranging from 0.2 m/s to 0.9 m/s when it is converted to full scale. Furthermore, it has been developed by means of an unheated manikin. The results are therefore expected to have the closest correspondence in the case of the high velocity level. Actually, a rather good correspondence between the model and the full-scale measurements using the BTM is found for a velocity level of 0.30 m/s.

For the low velocity level the model overestimates the personal exposure. This is presumably due to the important effect of the convective boundary layer at the low velocities which is not considered in this exposure model.

The simulations seem to overestimate the exposure at 0.30 m/s when the source is located close to the breathing zone.

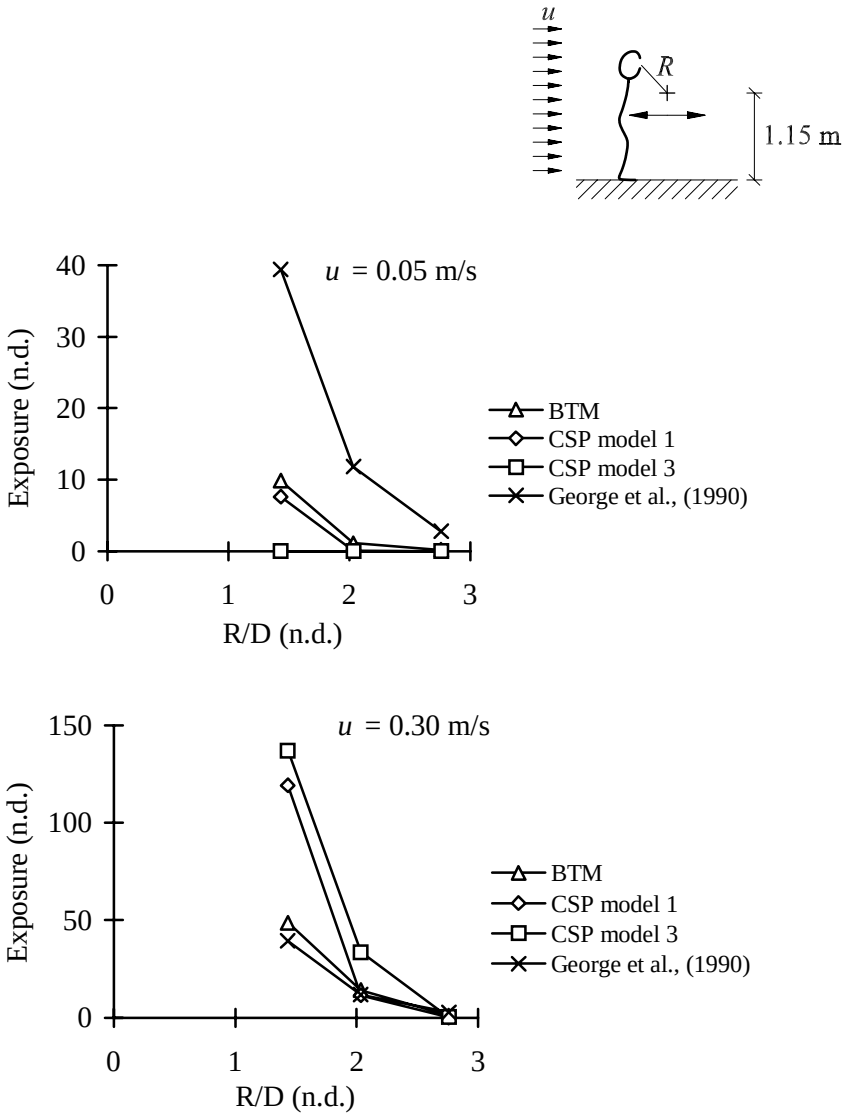

Figure 4.28. Dimensionless personal exposure, c_e^*, as a function of the dimensional straight line distance between the mouth and the point contaminant source, *R*/*D*. *R* is the distance (m) and *D* is the chest width (m). The person is located in the wind channel at (*x*,*z*) = (0.7,0). The source is located 1.15 m above the floor and at the horizontal distances of 0.30 m, 0.55 m and 0.80 m between the centre of the source and the centre of the person. Two different velocity levels 0.05 m/s (top) and 0.30 m/s (bottom) are applied.

Both of the above-mentioned exposure models are shown to correspond well with the present full-scale measurements when they are used in their range of application. However, for different source locations and lower velocities they should not be used. This is clearly seen in Figure 4.28. and is also illustrated from the fact that equation (4.9) leads to a statement of $c_e^* \approx 50$, i.e. no variation with respect to source location or velocity level which was found to be highly significant in the preceding chapters.

The range of application for the present measurements and simulations, together with some other limitations will be discussed in Chapter 5.

4.3. Mixing ventilated room

In the previous Chapter 4.2. personal exposure assessment in the case of mixing ventilation was examined by looking at a part of the flow field in a room. The local flow field was assumed to be unidirectional, see Figure 4.1., and a wind channel was applied in order to generate the flow. This chapter presents CFD simulations on personal exposure to contaminant sources located in a mixing ventilated room where the entire flow field in a mixing ventilated room is included.

4.3.1. Geometry and boundary conditions

It is chosen to perform the simulations on a well documented test case in order to facilitate comparisons between the present simulations and the measurements and simulations found in the literature. The test case is described by Nielsen (1990), and it has been used as part of the International Energy Agency, Annex 20 work.

The mixing ventilated room is shown in Figure 4.29. where the co-ordinate system is defined and the dimensions are mentioned.

Like the previous CFD simulations only one half of the symmetric room is simulated ($z \geq 0$ m). Three different cases are examined: an empty room and two different locations of the Computer Simulated Person (CSP) model 1 as shown in Figure 4.30.

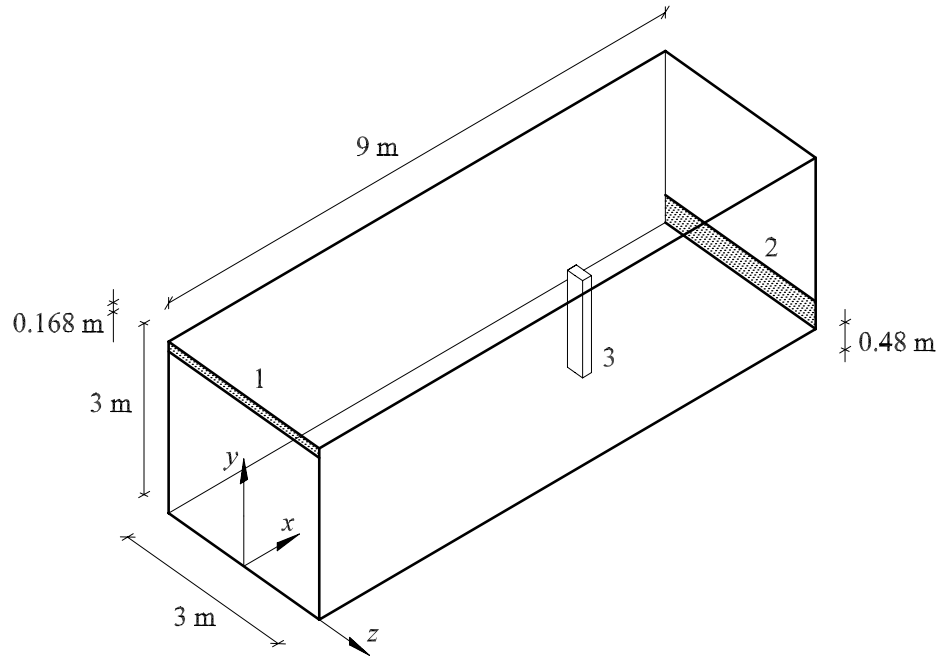

Figure 4.29. Geometry of the mixing ventilated room applied in the CFD simulation. The air is supplied by the inlet (1) located close to the ceiling, and the air is exhausted by the return opening (2) located close to the floor in the opposite end. The CSP model 1 (3) is located in the symmetry plane, $z = 0$ m.

The inlet conditions for the test case are prescribed according to Nielsen (1990), for instance, the inlet velocity is 0.455 m/s which correspond to an air change rate of 10 h^{-1}. The supply air temperature is 21°C. In Case 1 the flow is isothermal, and in Case 2 and Case 3 the only heat source is the CSP with a surface heat flux of 25 W/m^2. The walls are adiabatic and surface friction is included by means of wall functions (see Chapter 2.3.2.3.). The grid size is summarised in Table 4.3..

Table 4.3. Number of cells applied in simulation of the mixing ventilated room.

Case	Cells in direction			Total
	x	*y*	*z*	
1	63	35	18	39,690
2, 3	75	48	21	75,600

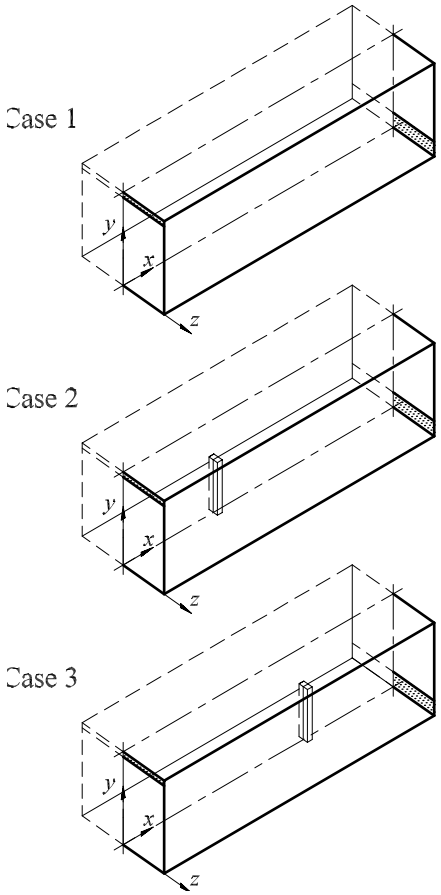

Figure 4.30. In the CFD simulations only one half of the symmetric room is simulated, $z \geq 0$ m. Three different cases are examined, Case 1: empty room, Case 2: CSP model 1 located at $(x,z) = (3,0)$, and Case 3: CSP model 1 located at $(x,z) = (6,0)$.

4.3.2. Simulation of the flow field

In Figures 4.31., 4.32. and 4.33. the flow field of the mixing ventilated room is shown by means of vector plots for the three different cases.

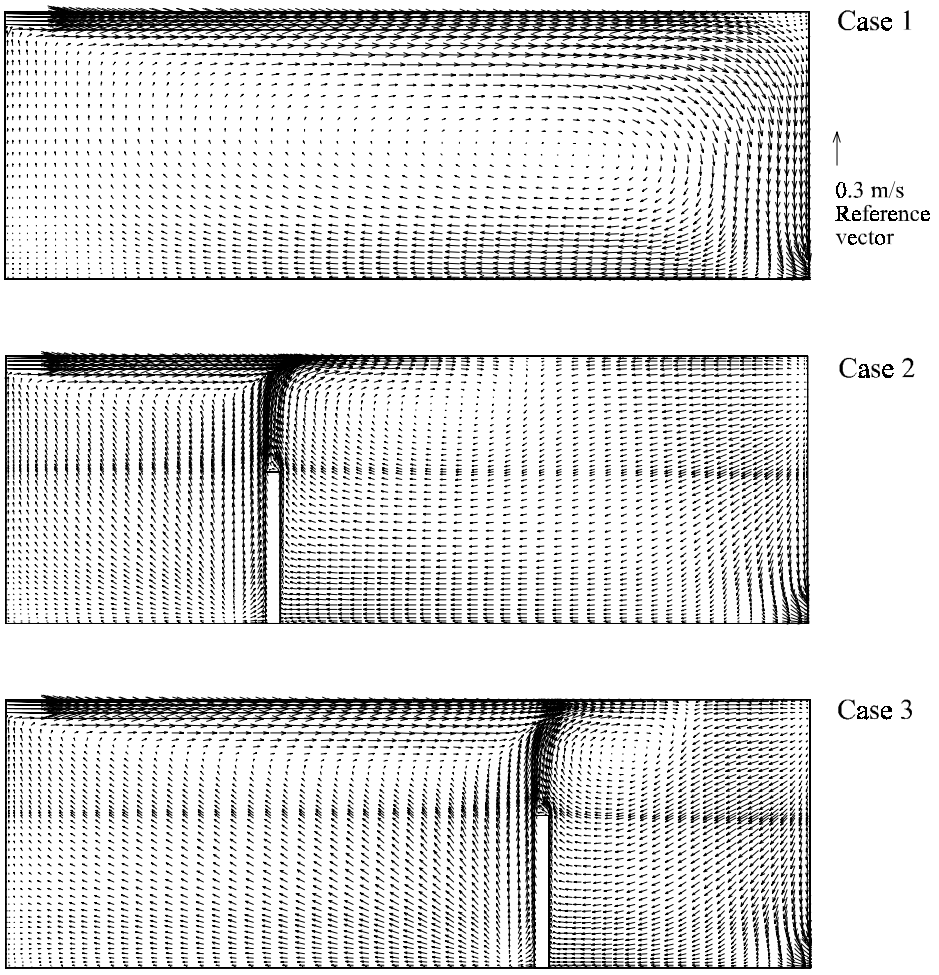

Figure 4.31. Vector plot from mixing ventilated room Case 1, 2 and 3. Plane z = 0 m (vertical symmetry plane). See also Figure 4.30.

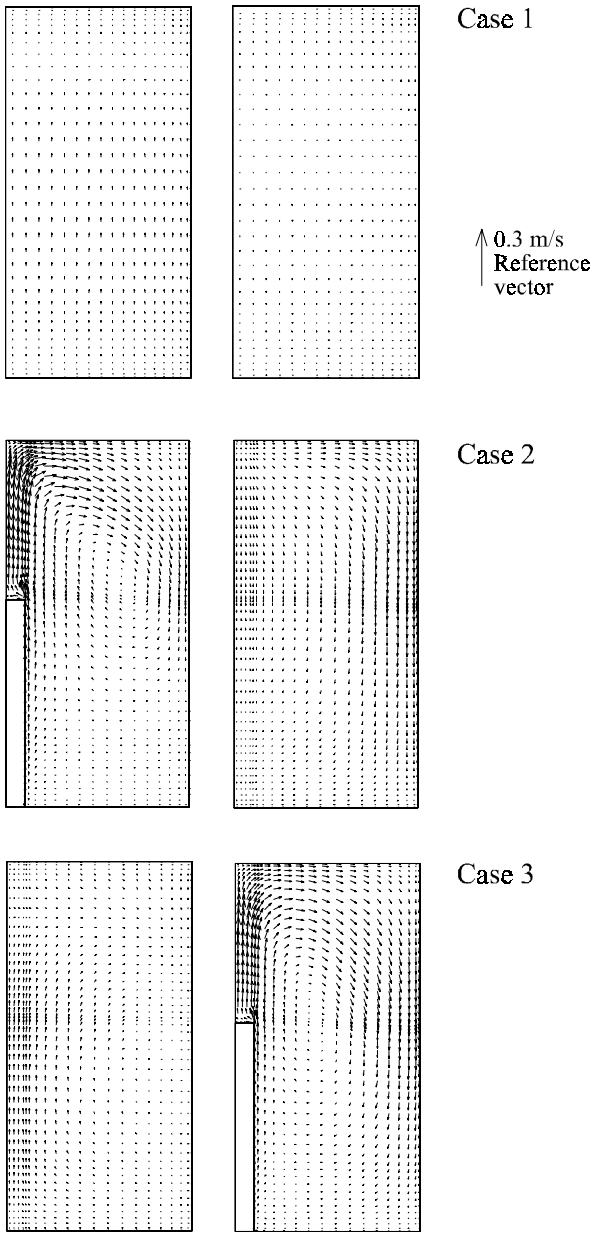

Figure 4.32. Vector plot from mixing ventilated room. Case 1, 2 and 3. Left column: Plane x = 3 m. Right column: Plane x = 6 m (vertical section through the two different locations of the CSP). See also Figure 4.30.

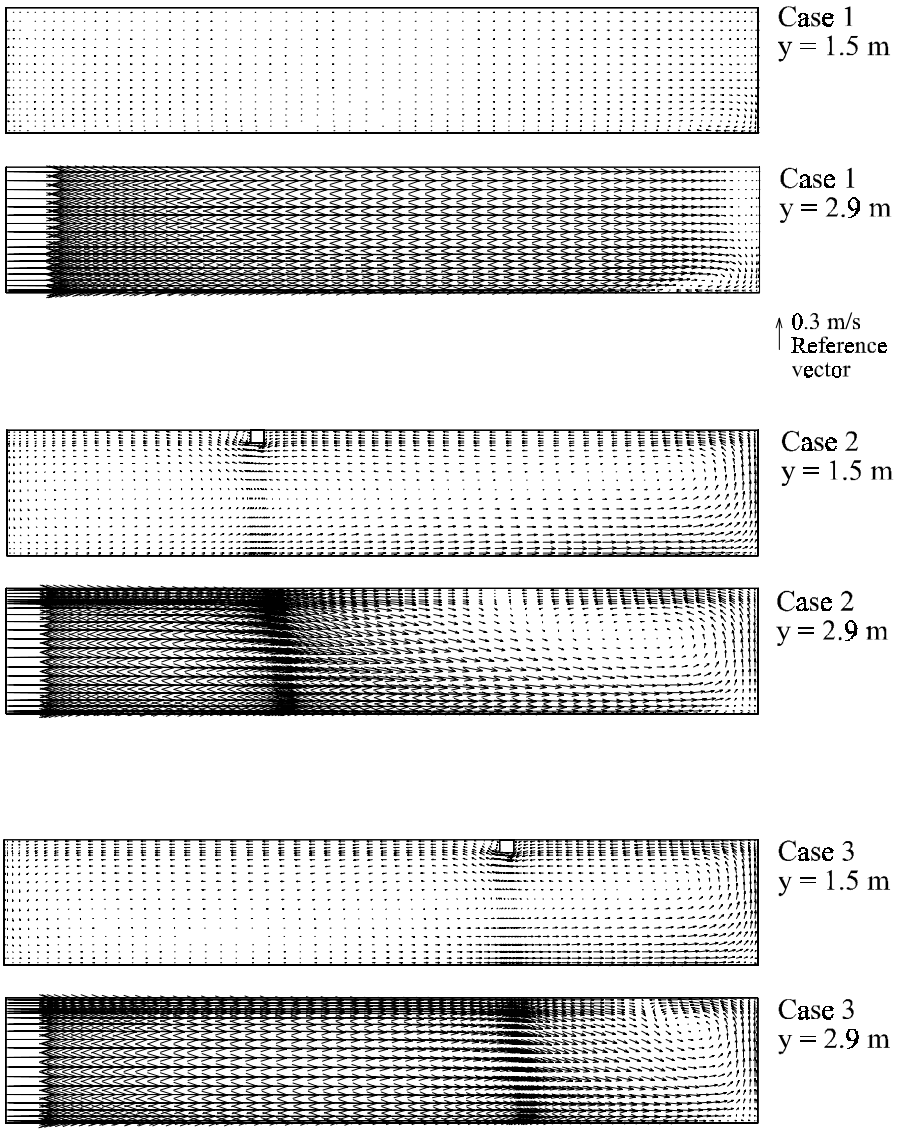

Figure 4.33. Vector plot from mixing ventilated room Case 1, 2 and 3. For each case the two horizontal planes are shown: y = 1.5 m (breathing zone height) and y = 2. 9 m (0.1 m below the ceiling). See also Figure 4.30.

The flow field in the empty mixing ventilated room (Case 1) shows a typical recirculating flow field. The flow is found to be unidirectional in the major part of the room, even though the direction changes sign from the upper part of the room to the lower part. The exhaust is seen to exert only a small and local influence on the general field, whereas the inlet is decisive in combination with the boundary conditions. If the three figures 4.31., 4.32. and 4.33. are observed with respect to the empty room an almost two-dimensional flow is seen and only in Figure 4.33. minor parts if the field are found to be three-dimensional.

When a person in the shape of a CSP is located in the room (Case 2 and Case 3) the flow field is significantly affected both in general and, especially, close to the person where the local Archimedes number is high. The plume above the person is distinct and only close to the ceiling it is possible for the supply air jet and the ceiling to entrain and deflect it, see Figure 4.31.

In Figure 4.32. which shows vertical sections through the different locations of the person a local recirculating flow is generated perpendicular to the main flow direction. A strong three-dimensional effect of the CSP is also clearly seen in Figure 4.33. close to the ceiling.

In the breathing zone height the velocity level is increased in Case 2 and Case 3 compared with the empty room. The explanation on the increased velocity level may be found in a combination of a redistribution of the momentum from the inlet device and also from a supply of momentum from the plume created by the heated CSP.

If the flow field close to the CSP is examined in both Case 2 and Case 3, it is found to approach the uniform flow field in the wind channel well, for instance, the important recirculating vortices in the wake region are clearly recreated in this case, see Figure 4.33. The velocity level obtained around the CSP in the mixing ventilated room is approximately 0.05 m/s.

Figures 4.34. and 4.35. show comparisons between measurements by Nielsen (1990) and the present simulations regarding a vertical velocity profile at two different locations in the ventilated room.

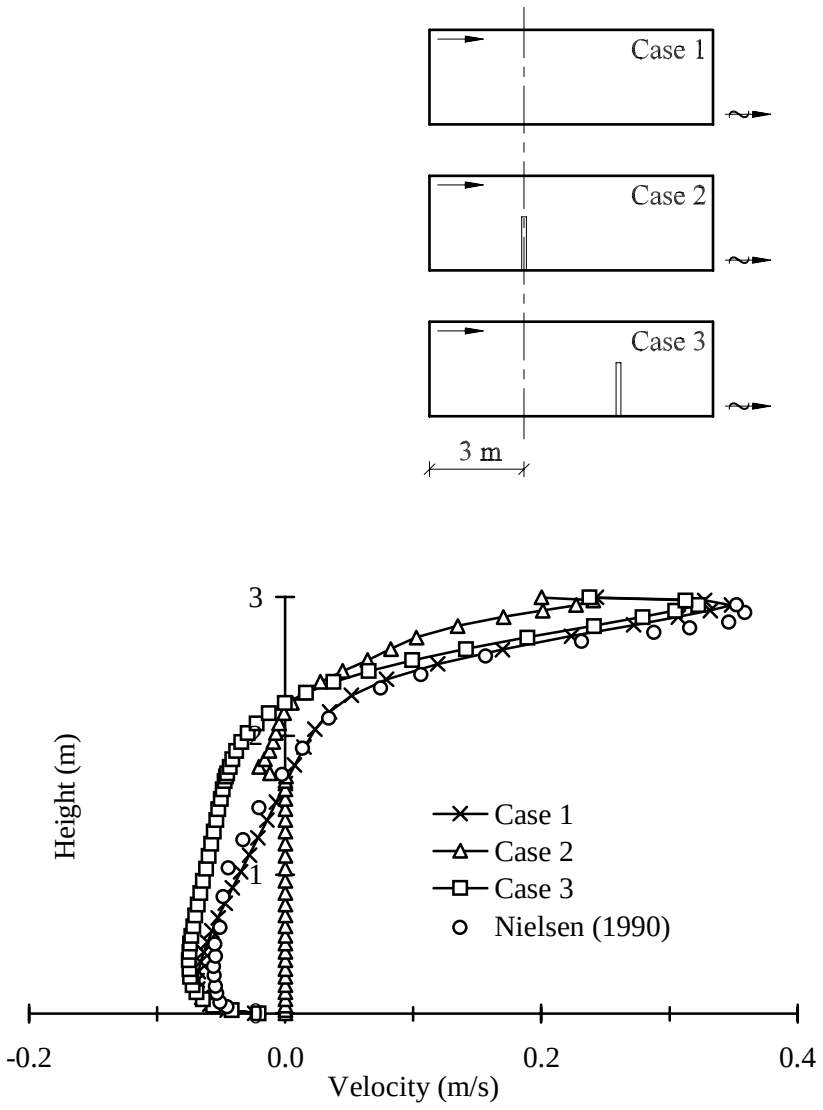

Figure 4.34. Vertical velocity profiles in the mixing ventilated room at (*x*,*z*) = (3,0) in Case 1, 2 and 3 compared with measurements from Nielsen (1990).

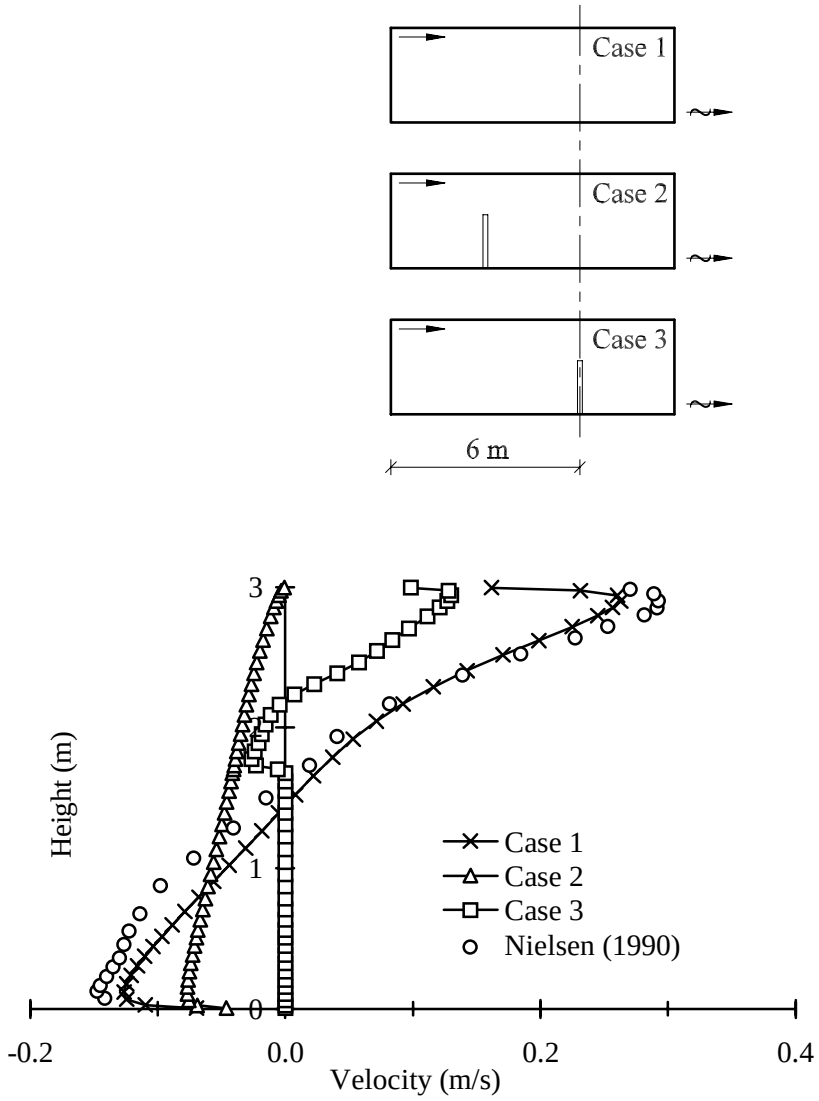

Figure 4.35. Vertical velocity profiles in the mixing ventilated room at (x,z) = (6,0) in Case 1, 2 and 3 compared with measurements from Nielsen (1990).

If the velocity profiles obtained at the simulation of the empty room (Case 1) are compared with the measurements a reasonable correspondence is found, both regarding the peak levels and the profile shape. As it was also seen on the vector

plots the velocity field is significantly influenced by the presence of the CSP. This fact results in a decreased maximum velocity close to the ceiling, especially pronounced in Figure 4.35. where the distance between the inlet opening and the profile location is high. A local increase in the velocity level in the occupied zone is found in Case 3, Figure 4.34.

4.3.3. Simulation of personal exposure

This chapter will present simulations of personal exposure to point sources at different locations in the mixing ventilated room as well as a planar source in the shape of the floor. The simulations are performed for the empty room and two different locations of the CSP.

Passive point contaminant source

The point source is the same one as applied in the case of displacement ventilation and of flow in the wind channel.

In order to examine how the contaminant source and the CSP interact with the general flow in the mixing ventilated room the source is located at a higher horizontal distance than in the previous simulations on the wind channel.

In Figure 4.36. and Figure 4.37. isoconcentration plots are shown for two different locations of the contaminant source relative to the person in Case 2 and Case 3, respectively.

If the room air is assumed to be completely mixed, the dimensionless contaminant concentration as well as the personal exposure will equal 1 in all cases shown in Figure 4.36. and Figure 4.37. This is due to the fact that the air flow rate and the source strength are the same in the different situations. However, the simulations clearly show the significant concentration gradients generated close to the contaminant sources and also close to the CSP in two of the plots.

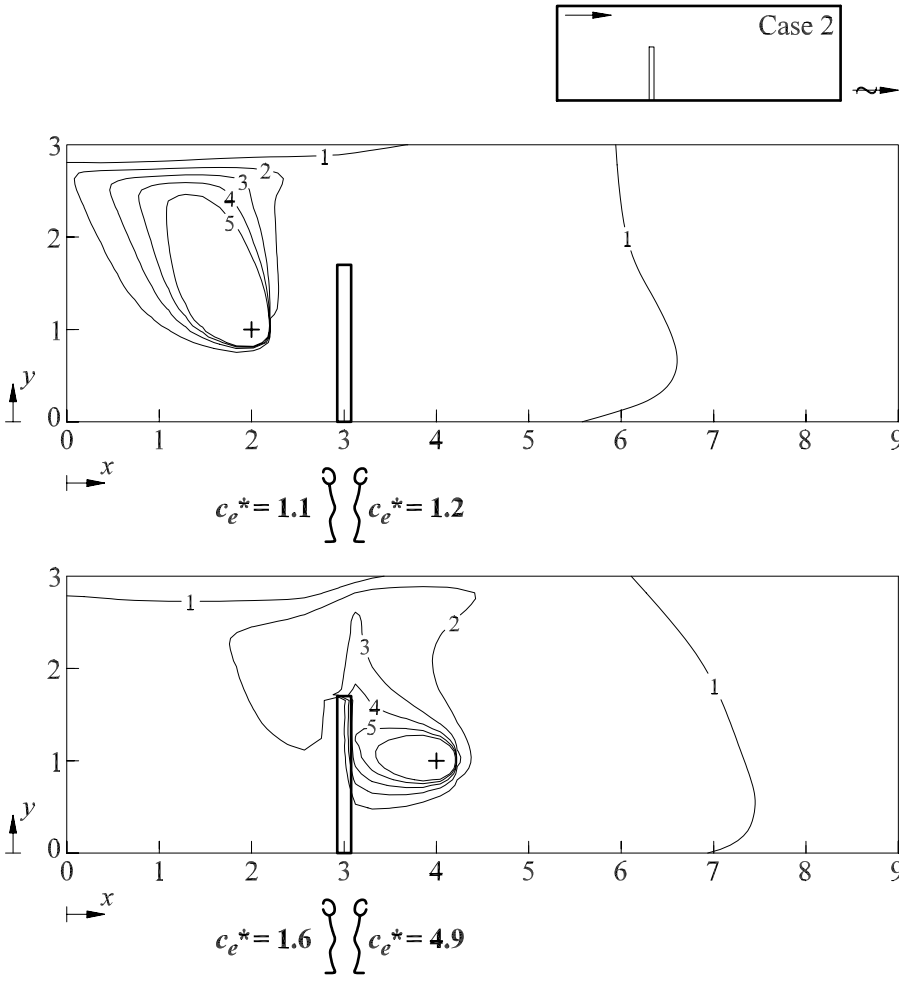

Figure 4.36. Dimensionless isoconcentration plot from the vertical symmetry plane (z = 0 m) for two different locations of the passive point contaminant source in the mixing ventilated room, Case 2. The CSP model 1 is located at (x,z) = (3,0). Top: Source location (x,y,z) = (2,1,0). Bottom: Source location (x,y,z) = (4,1,0). The dimensionless personal exposure, c_e^*, is mentioned in the figure for two different orientations of the person in each case. The concentrations are made dimensionless by dividing by the return concentration, i.e. $c^* = c/c_R$.

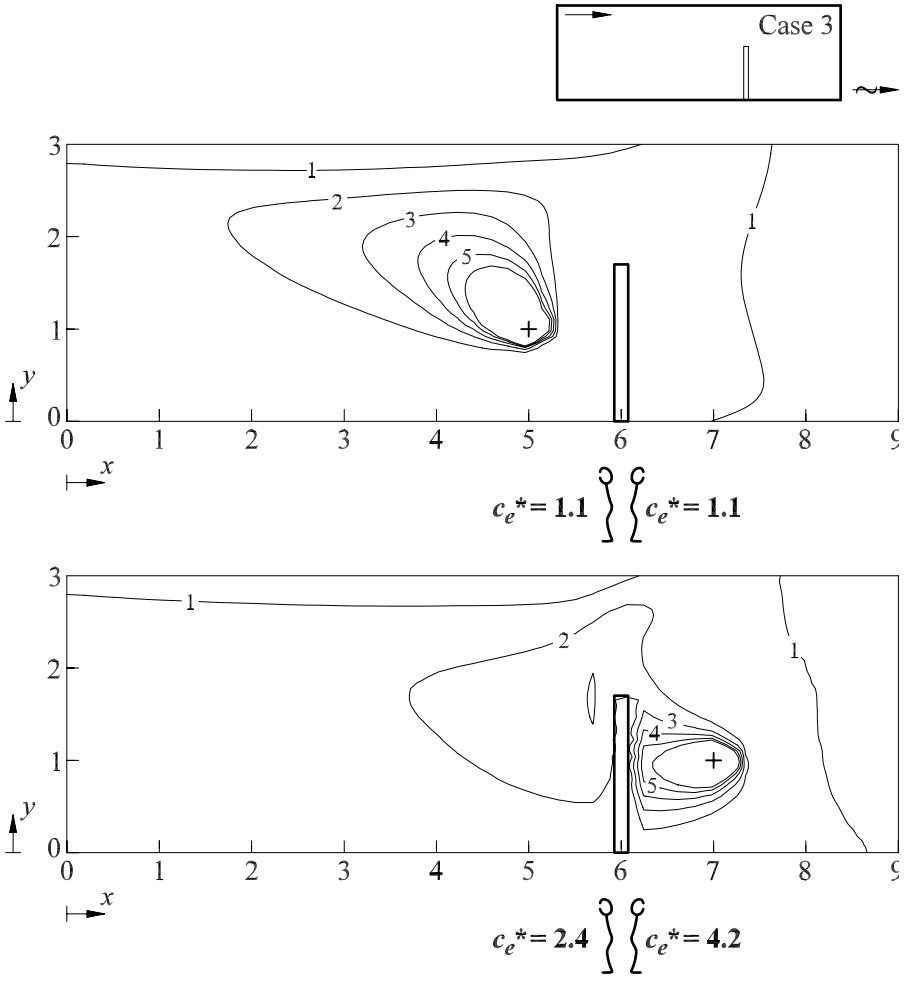

Figure 4.37. Dimensionless isoconcentration plot from the vertical symmetry plane (z = 0 m) for two different locations of the passive point contaminant source in the mixing ventilated room, Case 3. The CSP model 1 is located at (*x*,*z*) = (6,0). Top: Source location (*x*,*y*,*z*) = (5,1,0). Bottom: Source location (*x*,*y*,*z*) = (7,1,0). The dimensionless personal exposure, c_e^*, is mentioned in the figure for two different orientations of the person in each case. The concentrations are made dimensionless by dividing by the return concentration, i.e. $c^* = c/c_R$.

The concentration gradients result in a dimensionless exposure ranging form 1.1 to 4.9, highly dependent on source location and CSP location. Furthermore, different orientations of the CSP, for a fixed location, manage to change the exposure from 1.6 to 4.9 in Figure 4.36.

A dimensionless personal exposure of 4.9 is an exposure approximately five times as high as found in the exhaust air. This corresponds to a personal exposure index of ε_e = 0.2. Even higher exposure levels may be obtained if the source is located closer to the person as shown in Chapter 4.2.4.

The three figures 4.38., 4.39. and 4.40. show the personal exposure as a function of contaminant source location in the vertical symmetry plane (z = 0 m) of the mixing ventilated room in Case 1, 2 and 3, respectively.

The results in Figures 4.38., 4.39. and 4.40. show the exposure as a function of the location of the passive point contaminant source. For source locations in the occupied zone it is found that the dimensionless personal exposure often exceeds 2. Very high levels may be obtained when the source is found close to the person.

At a certain location of the person, the exposure level may be significantly affected if the person is turned around. In all cases the dimensionless exposure levels are found to exceed 1, i.e. $c_e^* \geq 1$, resulting in a personal exposure index $\varepsilon_e \leq 1$. This result is quite contrary to displacement ventilation where $\varepsilon_e \geq 1$, see Chapter 3.

The local influence of a person in a ventilated room with concentration gradients may be examined if the empty room in Figure 4.38. is compared with the simulations including a person as shown in Figures 4.39. and 4.40. Here, it is demonstrated that the personal exposure may deviate considerably from the concentration at the same location, but without the local impact of a person, i.e. $\varepsilon_P \neq \varepsilon_e$.

This obviously stresses the importance of including the local influence of a person when the exposure is assessed. It is not sufficient to know the local concentration level of an empty room, the local impact of the person is distinct and should be considered in the exposure assessment.

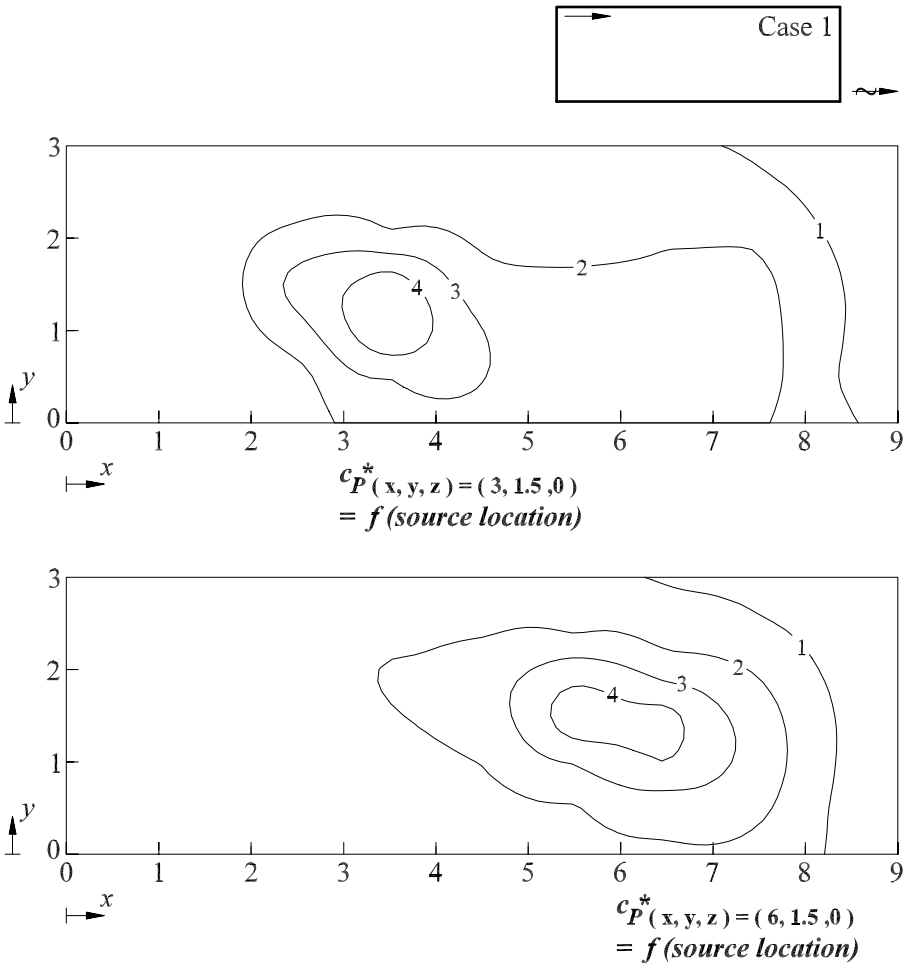

Figure 4.38. Dimensionless concentration at the breathing zone location, c_P^*, as a function of point contaminant source location in the empty vertical symmetry plane (z = 0 m) of the mixing ventilated room, Case 1. Top: Dimensionless concentration at (x,y,z) = (3,1.5,0). Bottom: Dimensionless concentration at (x,y,z) = (6,1.5,0). The concentrations are made dimensionless by dividing by the return concentration, i.e. $c_P^* = c_P/c_R$.

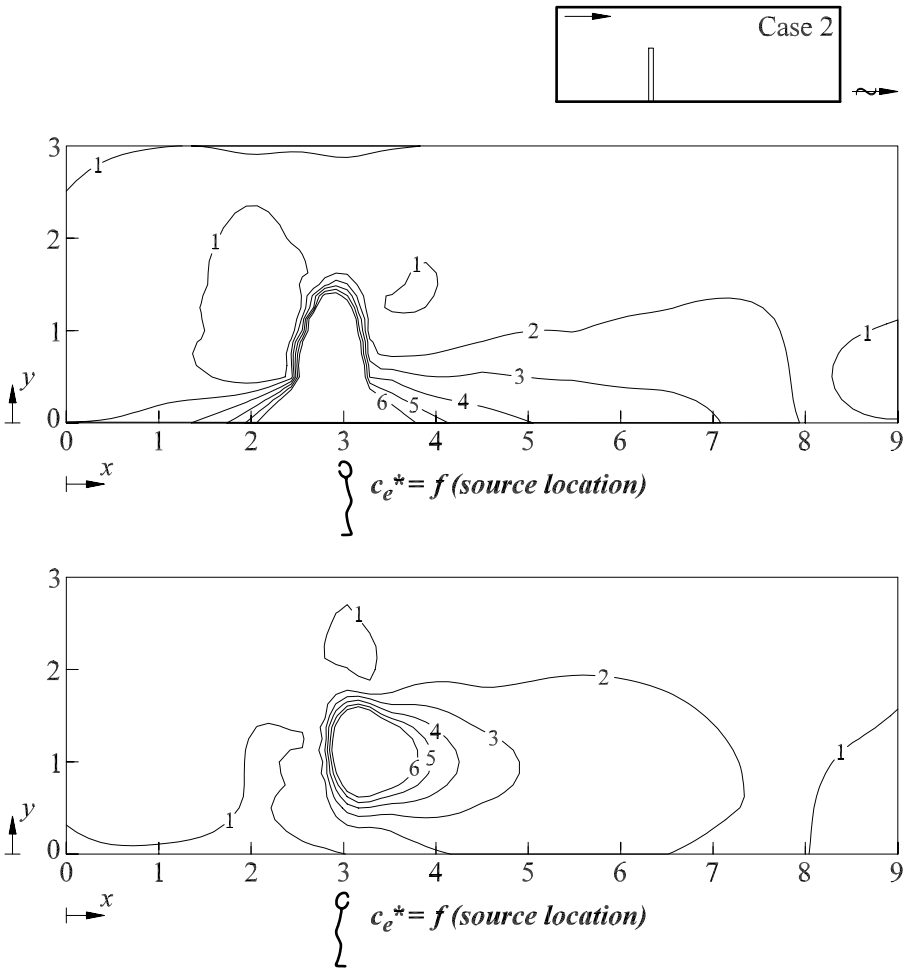

Figure 4.39. Dimensionless personal exposure, c_e^*, as a function of point contaminant source location in the vertical symmetry plane (z = 0 m) of the mixing ventilated room, Case 2. The results are shown for two different orientations of the CSP model 1, located at (x,z) = (3,0). The personal exposure is made dimensionless by dividing by the return concentration, i.e. $c_e^* = c_e/c_R$.

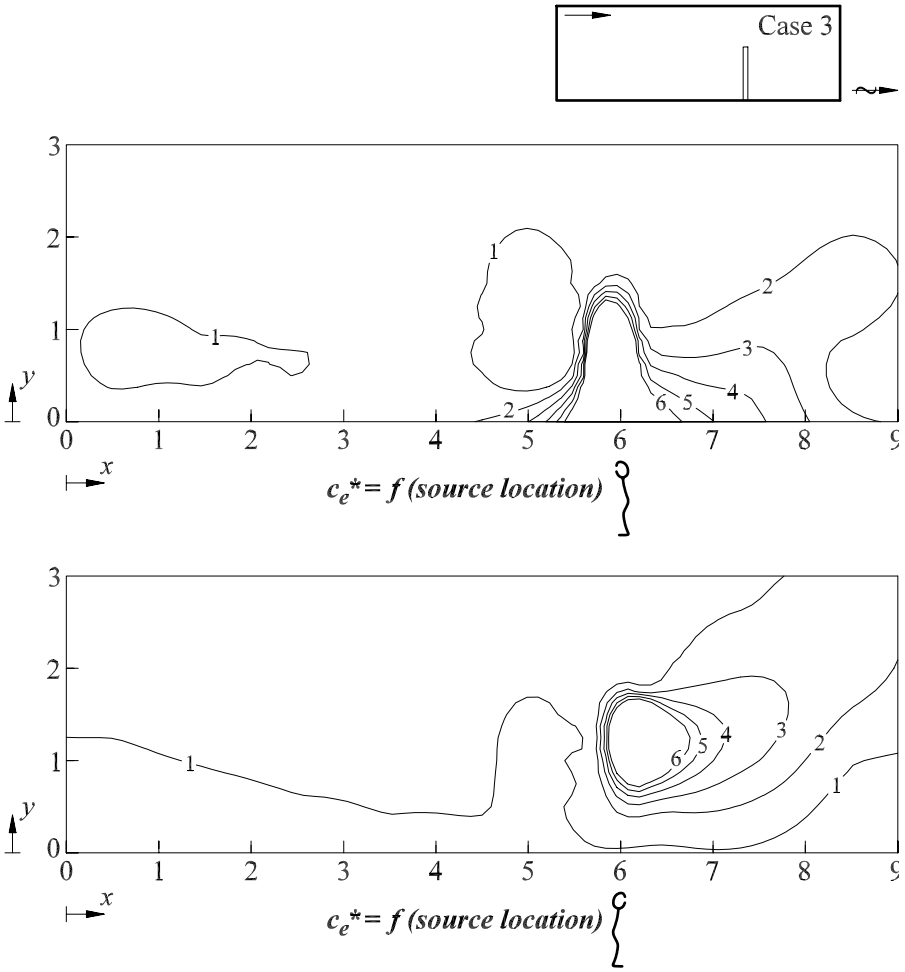

Figure 4.40. Dimensionless personal exposure, c_e^*, as a function of point contaminant source location in the vertical symmetry plane (z = 0 m) of the mixing ventilated room, Case 3. The results are shown for two different orientations of the CSP model 1, located at (x,z) = (6,0). The personal exposure is made dimensionless by dividing by the return concentration, i.e. $c_e^* = c_e/c_R$.

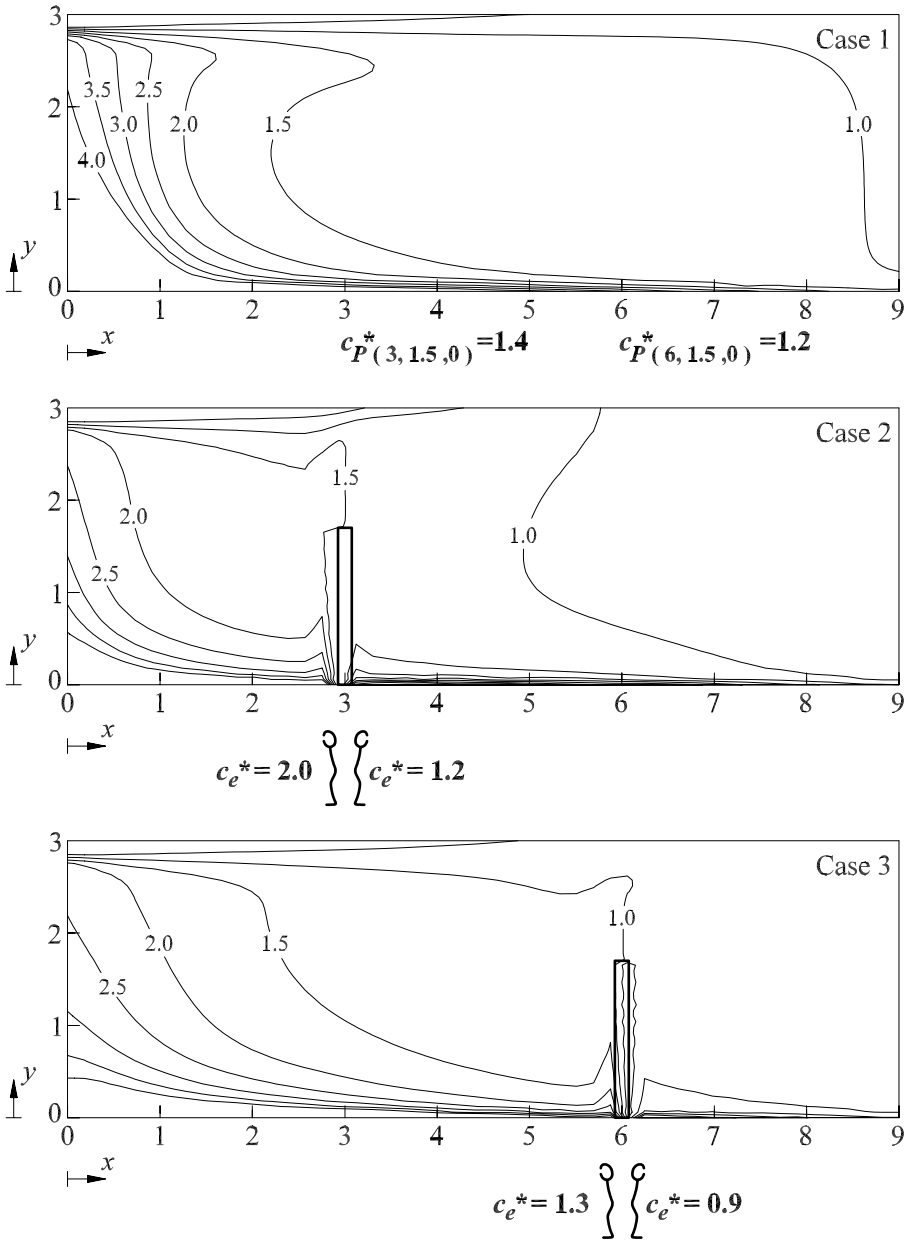

Figure 4.41. Dimensionless concentration in the vertical symmetry plane (z = 0 m). The floor is a planar source. The dimensionless personal exposure, c_e^* (c_P^* in Case 1) is mentioned for the different orientations of the CSP model 1.

Planar contaminant source

Figure 4.41. shows the concentration distribution in the mixing ventilated room in the case of a constantly emitting planar contaminant source in the shape of the floor.

The concentration distribution in Figure 4.41. for Case 1 is also simulated by Nielsen (1981) using a two-dimensional CFD calculation, and a very good agreement is found.

It is seen how the concentration level increases towards the lower left part of the room and how the CSP modifies the distribution for the two different locations.

When the exposure levels are compared an important influence of location and orientation of the person are found again. Furthermore, it is found that $c_P^* \neq c_e^*$. In Case 3 an example of a dimensionless exposure below 1 is found, i.e. improved air quality compared with “completely mixed conditions”.

4.4. Conclusion

In this chapter personal exposure to contaminant sources in a mixing ventilated room is examined.

The unidirectional flow field generated in a wind channel is assumed to represent the local flow field around a person in a mixing ventilated room.

Full-scale wind channel measurements using the Breathing Thermal Manikin (BTM) are performed as well as CFD simulations using the three different versions of the Computer Simulated Person (CSP). The CSP is also applied in a simulation including the whole flow field in a mixing ventilated room.

The contaminant distribution is generated by a passive contaminant source. For the computer simulations a planar source is also applied in the shape of the floor in the wind channel and in the mixing ventilated room.

It is found that the personal exposure to a contaminant source in a unidirectional flow field depends highly on the source location as well as the flow direction

relative to the person. The uniform velocity level is also a very important factor to consider.
The vortices generated in the wake in front of a person turning the back to the flow direction have a considerable ability to entrain contamination. The contamination is transported to the breathing zone where is causes exposure. The vortices are found to entrain contamination from a horizontal distance exceeding 0.5 m.

Personal exposure levels in the wind channel for a typical hand-held source are found to be more than 50 times higher than the exhaust concentration for the measurements, and even higher levels are obtained for the simulations. This means that the actual exposure in this case is 50 times higher than it would be if the exposure was assessed by an assumption of fully mixing. This effect is also seen in the computer simulations of the mixing ventilated room.

The measurements in the wind channel by means of the BTM are found to correspond well to results from the literature.

Personal exposure assessed by the CSP deviates somewhat from the exposure assessed by the BTM. However, the results are of the same order of magnitude and the CSP is capable of simulating all the important phenomena observed close to a person. Inclusion of “legs” in the CSP is found to affect the exposure considerably, especially when the contaminant source is located close to the floor.

Chapter 5

General discussion and conclusion

This chapter will summarise and discuss the results presented in the thesis regarding the tools for personal exposure assessment, the displacement ventilation case and the mixing ventilation case. Furthermore, some limitations are discussed and, finally, a number of future perspectives will be outlined.

Purpose

In Chapter 1 it is stated that many people spend more than 90% of their time in a more or less artificial indoor environment. This indoor environment is often subject to contaminant sources both in the case of residential buildings, offices and occupational buildings. This stresses the importance of a proper exposure assessment.

Usually, the exposure models treat the indoor environment as well-mixed compartments without concentration gradients. However, in practice gradients will prevail, for instance, close to the contaminant sources or in the case of displacement ventilation where the concentration gradients are utilised to improve the ventilation effectiveness.

When gradients prevail in a ventilated room the presence of a person may modify the concentration field locally due to the influence of e.g.:

- excess surface temperature
- obstacle to the flow field
- movements, etc.

The local influence on the flow field and concentration field may affect the personal exposure significantly. This raises the need for improved exposure models where concentration gradients and the influence of a person are considered.

Tools for personal exposure assessment

Three different tools for personal exposure assessment are presented in Chapter 2 together with the theoretical basis:

1. A Breathing Thermal Manikin which is a heated full-scale model of a woman equipped with an artificial lung to simulate respiration. Tracer gas is used to simulate contamination.

2. A Computer Simulated Person which is a numerical model of a person applied in Computational Fluid Dynamics where the flow field and the contaminant transport are simulated.

3. A Trained Sensory Panel which is a group of persons trained to judge the air quality in comparison with references with known levels of perceived air quality.

The three tools are all able to consider the local influence of persons in ventilated rooms where concentration gradients prevail.

The tools are applied on the two major room ventilation principles, namely the displacement principle and the mixing principle. This is done both in order to examine the tools on different test cases, but also to investigate how the exposure assessment is influenced when concentration gradients and the local effect of a person are considered.

The Breathing Thermal Manikin (BTM) and the Trained Sensory Panel (TSP) are most suitable for laboratory and field investigations where the main purpose is research and development of exposure models, etc. The Computer Simulated Person (CSP) may also be used for practical engineering purposes due to the relatively simple geometry.

The BTM is very suitable in steady-state (mid term and log term) exposure measurements where tracer gas is used to simulate contaminant dispersion. Due to the artificial lung the concentration of inhaled air is easily found.

If movements have to be considered they may be simulated by locating the BTM in a unidirectional flow of a wind channel, or it may be necessary to replace the BTM with a real person equipped with a sampling device.

The TSP may of course be applied to assess the perceived air quality, but it can also be used to assess the contaminant concentration of inhaled air where the relation between concentration and perceived air quality is known for a tracer gas. This is the case for the reference gas 2-propanone. However, the TSP is limited to (very) short-term exposure assessment in order to avoid adaptation. This implies, strictly speaking, that only the first inhalation of contaminated air may be assessed properly by the TSP.

If the CSP is applied for exposure assessment it is necessary to have a certain amount of experience in using Computational Fluid Dynamics in order to prescribe a proper set of boundary conditions etc. which are decisive for the result. Using the CSP it is possible to simulate transient behaviour, too, even though it is quite time-consuming and limited to a relatively short time span in practice.

One limitation of the three tools for personal exposure in this thesis is the fact that they are used only to assess personal exposure to gaseous contaminants or smaller particles acting like a gas. However, both the BTM and the CSP may be extended to assess exposure to for instance dust particles. It requires new measuring equipment to analyse the contents of the inhaled air and a modification of the concentration equation governing the contaminant transport, respectively.

Measurements made by using the BTM standing in the wind channel are found to correspond well with results from the literature.

The exposure assessed by means of the CSP deviates somewhat from the exposure assessed by the BTM. However, the results are of the same order of magnitude and the CSP is capable of simulating the important phenomena observed close to a person. Inclusion of “legs” in the CSP is found to affect the exposure considerably, especially for contaminant sources which are located close to the floor. Some possible improvements of the CSP are mentioned in the subsequent.

New quantities

Two new quantities are defined.

A new ventilation effectiveness: the personal exposure index, ε_e, see equation (1.4). The personal exposure index expresses the effectiveness actually experienced by a person in a ventilated room.

The other new quantity is: the effectiveness of entrainment in the human boundary layer, η_e, see equation (3.1). η_e expresses the ability to supply (fresh) air from the floor area to the breathing zone. It is mainly used in connection with displacement ventilation and applied in an exposure model for displacement ventilation.

Both of the new quantities result from considering the local impact of persons on the personal exposure. Results from full-scale measurements and computer simulations demonstrate their applicability in expressing the difference between the air quality actually experienced and the mean air quality in the occupied zone or in the breathing zone height at a “neutral” place.

Displacement ventilation

Personal exposure in rooms ventilated after the displacement principle is examined by means of full-scale measurements in two different test rooms and computer simulations of the flow in one of the rooms.

The contaminant distribution in the measurements is generated by point sources. Non-passive (warm) sources are applied to generate the characteristic two-zonal concentration distribution with a separation in a cleaner, lower zone and an upper, more contaminated zone in the displacement ventilated room. Upward pointing tubes located above heat sources supply the contamination (N_2O or 2-propanone). A passive (cold) source is applied in order to investigate the influence of contaminant sources located close to persons. This contaminant source comprises a neutral density mixture of N_2O and He supplied through a porous foam rubber ball. In the CFD simulations a planar source is applied in the shape of a constantly emitting floor, apart from the above-mentioned sources.

It is found that the stratified flow and the considerable concentration gradients in a displacement ventilated room necessitate an improvement of the widely used compartmental approach, where the room air is assumed to be fully mixed.

The flow in the human boundary layer is able, to a great extent, to entrain air from below the breathing zone, thus improving the quality of the inhaled air in case of non-passive contaminant sources.

The air quality experienced by the occupants in the displacement ventilated room is significantly improved compared with mixing ventilation. The improved air quality is both found by means of steady-state chemical measurements and sensory measurements where the TSP judges the perceived air quality.

Movements cause the air quality to decrease due to the disturbance of the human boundary layer which promotes the high air quality.

A personal exposure model for displacement ventilated rooms is proposed. The model takes the concentration gradient and the influence of the human thermal boundary layer into account. It is based on the present full-scale measurements together with measurements from various references. The model is easy-to-use and suitable for the design of displacement ventilation systems in practice. It is limited to cases where the characteristic two-zonal flow prevail, and to cases without considerable movements of the persons.

Entrainment of air in the human boundary layer is usually an advantage but the results show also the possible disadvantage when passive contaminant sources are present. In this case the convective current around the person may transport contaminated air to the breathing zone, giving rise to increased exposure. Poor system performance is found in the case of a passive contaminant released in the lower part of the room close to the occupant.

Mixing ventilation

Exposure assessment in a mixing ventilated room is examined by means of measurements and simulations of the unidirectional flow around a person standing in a wind channel as well as by simulations of the entire flow field in a mixing ventilated room.

The unidirectional flow field generated in the wind channel is assumed to represent the local flow field around a person in a mixing ventilated room.

Here, the contaminant distribution is generated by a passive point contaminant source. For the computer simulations a planar source is also applied in the shape of the floor in the wind channel and in the mixing ventilated room.

The personal exposure to a contaminant source in the unidirectional flow field is found to depend highly on both the source location and the flow direction relative to the person. The uniform velocity level is also found to be an important factor to consider.

Vortices generated in the wake in front of a person turning the back to the flow direction have a considerable ability to entrain contamination. The contamination is transported to the breathing zone where is causes exposure. The vortices are found to entrain contamination from a horizontal distance exceeding 0.5 m.

Personal exposure measured by means of the BTM standing in the wind channel with a typical hand-held source is found to be more than 50 times higher than the exhaust concentration, and even higher levels are obtained for the corresponding computer simulations. This effect is also seen in the computer simulations of the mixing ventilated room.

The findings clearly stress the need of an improved exposure assessment in cases where the contaminant source is located in the vicinity of persons.

The computer simulations of the mixing ventilated room reveal that the concentration of inhaled contaminant may easily be twice as high as the return concentration, even though the contaminant source is located at some distance from the person depending on the flow direction relative to the person and the contaminant source.

The simulations show also that it is not sufficient to know the local concentration level of an empty room, the local impact of a person is distinct and should be considered in the exposure assessment.

Limitations

Apart from the limitations that are already mentioned a number of other things may be useful to acknowledge.

Only the personal exposure to gaseous contaminants by means of respiration is considered in the thesis. Exposure to larger particles, dust, fibres or gaseous contaminants with a density deviating considerably from the room air may also cause a substantial health risk and discomfort and should of course be considered when it occurs.

Transient behaviour with considerable movements takes place when the TSP is judging the perceived air quality, and some results from the wind channel case may also simulate movements and quasi transient conditions. Most of the results, however, arise from steady-state conditions. Therefore, they are mainly applicable for mid-term and long-term exposure assessment in cases where only slight movements occur.

Future perspectives

The author foresees that the development of more advanced personal exposure models will continue with a growing rate in the future. At the same time there will presumably be a growing need for relatively simple models which may be applied for practical engineering design purposes.

The models may be developed both in a direction where the local impact of a person is stronger implemented, but also in a direction where advanced statistical methods are applied in order to take into account the transient behaviour, movements and the various activities performed in a ventilated enclosure where contaminant sources prevail.

The tools for personal exposure assessment presented in this thesis may be improved in different ways. The Computer Simulated Person can be improved by

using a rounded geometry and a low-Reynolds number turbulence model. The boundary conditions in the CFD simulations can also be modified in order to simulate the full-scale measurements better together with a revised grid layout around heat and contaminant sources and at locations where steep gradients occur. Transient behaviour can also be included in the computer calculations.

An obvious new element in the “tool box” may be measurements by means of real people wearing personal exposure monitors. In that way it is possible to consider the transient behaviour and compare with the results and models made under steady-state conditions for validation and further progress.

An other future perspective is the consideration of particles, fibres, and gaseous contaminants with a density deviating from the surrounding room air. Regarding particles etc. the exposure models may also be expanded to “dose models” where, for instance, particle deposition in the upper airways is calculated.

Appendix A

Heat balance for a person

In order to describe how the Breathing Thermal Manikin is controlled, it is necessary to derive a relationship between the skin temperature and the sensible heat loss. To achieve this relationship a total heat balance for the human body is set up.

A.1. Steady-state total heat balance for a person

During steady-state conditions the metabolic heat production, *M*, will normally be almost equal to the total heat loss of a person, Q_m, i.e. the energy flow due to useful, external mechanical work is assumed to be insignificant.

$$Q_m = M = Q_{sk} + Q_{res} \tag{A.1}$$

where

Q_m = Total heat loss from person (W/m^2)
M = Metabolic heat production (W/m^2)
Q_{sk} = Heat loss from skin surface (W/m^2)
Q_{res} = Heat loss by respiration (W/m^2)

The heat loss from the skin and the respiration may be expressed as

$$Q_{sk} = Q_t + E_s \tag{A.2}$$

and, if heat transfer by conduction is assumed to be very small

$$Q_t = R + C \tag{A.3}$$

where

Q_t = Sensible heat loss (W/m^2)
E_s = Latent heat loss (W/m^2)
R = Radiative heat loss (W/m^2)
C = Convective heat loss (W/m^2)

Thus

$$Q_t = Q_m - Q_{res} - E_s \tag{A.4}$$

A.2. Heat loss by respiration

The heat loss by respiration, Q_{res}, consists of a convective part, C_{res}, and an evaporative part, E_{res}.

$$Q_{res} = C_{res} + E_{res} \tag{A.5}$$

Here,

$$C_{res} = \dot{m}_{res} c_p \left(t_{ex} - t_a \right) / A_{Du} \tag{A.6}$$

where the pulmonary ventilation rate (kg/s) may be expressed as (Fanger, 1972)

$$\dot{m}_{res} = K_{res} M = 2.58 \cdot 10^{-6} M \tag{A.7}$$

and c_p is the specific heat of the ambient air (J/kg°C), t_{ex} is the temperature of exhaled air (°C), t_a is the temperature of ambient air (°C) and, finally, A_{Du} is the DuBois area (body surface area in m^2).

The temperature of exhaled air can be expressed as a function of the ambient temperature and the humidity ratio of inhaled air (kg H_2O/kg air) (ASHRAE, 1993). If t_{ex} is evaluated under standard conditions (20°C, 50% rh, sea level), we get an exhaled air temperature of 34°C, and thus

$$C_{res} = 1.43 \cdot 10^{-3} M \left(34 - t_a \right) \tag{A.8}$$

The evaporative part of the respiratory heat loss, E_{res}, can be found as

$$E_{res} = \dot{m}_{res} h_{fg} \left(W_{ex} - W_a \right) / A_{Du} \tag{A.9}$$

where

h_{fg} = Heat of vaporisation of water (e.g. $2.43 \cdot 10^6$ J/kg)
W_{ex} = Humidity ratio of exhaled air (kg H_2O/ kg air)
W_a = Humidity ratio of inhaled (ambient) air (kg H_2O/ kg air)

Here, W_a may be expressed as a function of the water vapour pressure in the ambient air, p_a, and the barometric pressure. If the proper numbers are substituted, we obtain the relation

$$E_{res} = 1.73 \cdot 10^{-3} M \left(5834 - p_a \right) \tag{A.10}$$

where

p_a = Water vapour pressure in the ambient air (Pa).

A.3. Latent heat loss

The latent heat loss may be divided into diffusion through the skin, E_d, and sweating, E_{sw}

$$E_d = h_{fg} m_{p,sk} \left(p_s - p_a \right) \tag{A.11}$$

where

$m_{p,sk}$ = Permeance coefficient of the skin ($1.271 \cdot 10^{-9}$ kg/(m^2 s Pa))
p_s = Saturated water vapour pressure at skin temperature (Pa)

The saturated water vapour pressure may be expressed as a function of the skin temperature, t_s.

$$p_s = 256 t_s - 3373 \tag{A.12}$$

Fanger (1972) found a relationship between the skin temperature and the heat production, which is necessary to achieve a state of thermal comfort

$$t_s = 35.7 + 0.028M \tag{A.13}$$

If t_s is inserted in the expression for p_s and this is applied in the equation for E_d, we obtain the latent heat loss by diffusion through the skin

$$E_d = 3.09 \cdot 10^{-3}\left(5765 - 7.17M - p_a\right) \tag{A.14}$$

Fanger (1972) also found a relationship between E_{sw} and M which is necessary to obtaining thermal comfort

$$E_{sw} = 0.42\left(M - 58.15\right) \tag{A.15}$$

A.4. Skin temperature vs. sensible heat loss

By means of the above expressions it is possible to derive the relationship between the skin temperature and the sensible heat loss. We assume, as mentioned previously, that the total heat loss equals the metabolic heat production, i.e. $Q_m = M$.

To "eliminate" the latent heat in the total heat balance we assume in the equations for Q_{res} and E_s, as a reasonable approximation, that the water vapour pressure in the ambient air is 1500 Pa corresponding to an air temperature of 24°C and a relative humidity of 50% which is equivalent to typical indoor conditions (Tanabe et al., 1994).

$$Q_{res} = 1.43 \cdot 10^{-3} Q_m\left(34 - 24\right) + 1.73 \cdot 10^{-5} Q_m\left(5834 - 1500\right) \tag{A.16}$$

$$Q_{res} = 0.0893 Q_m \tag{A.17}$$

$$E_s = 3.09 \cdot 10^{-3}\left(5765 - 7.17Q_m - 1500\right) + 0.42\left(Q_m - 58.15\right) \quad \text{(A.18)}$$

$$E_s = 0.3978Q_m - 11.2441 \quad \text{(A.19)}$$

If the two equations are inserted in the total heat balance, we get

$$Q_m = 1.95Q_t - 21.92 \quad \text{(A.20)}$$

This equation may be inserted in Fanger´s (1972) thermal comfort relationship between the skin temperature and the total heat loss (the metabolic heat production)

$$t_s = 35.77 - 0.0275Q_m = 35.77 - 0.0275\left(1.95Q_t - 21.92\right) \quad \text{(A.21)}$$

and, finally

$$t_s = 36.4 - 0.054Q_t \quad \text{(A.22)}$$

A.5. Surface temp. vs. insulation value of clothing

The above formula expresses the skin temperature as a function of the sensible heat loss (i.e. radiative and convective heat loss). Often, however, it is the surface temperature of a person that is needed, for instance, when making calculations regarding the natural convective boundary layer etc. The surface temperature of a person will deviate from the skin temperature when s/he is clothed.

In the following an expression of the surface temperature (i.e. the temperature of the clothing),t_{cl}, as a function of the skin temperature, t_s, and the insulation value of the clothing, I_{cl}, is derived.

The sensitive heat flux through the clothing may be expressed as

$$Q_t = \frac{\Delta t}{R_{cl}} = \frac{t_s - t_{cl}}{R_{cl}} \quad \text{(A.23)}$$

where Δt is the temperature difference between the skin and the surface temperature of the clothing, and R_{cl} ($m^2°C/W$) is the thermal resistance against heat loss. When 1 clo = 0.155 $m^2°C/W$ the thermal resistance, R_{cl}, in SI-units becomes

$$R_{cl} = 0.155 I_{cl} \tag{A.24}$$

where I_{cl} is the clothing insulation (in clo). When t_s is expressed as a function of Q_t and the equation above is used, we get

$$Q_t = \frac{36.4 - t_s}{0.054} \tag{A.25}$$

and thus

$$t_{cl} = t_s - Q_t \cdot 0.155 I_{cl} = t_s - \left(\frac{36.4 - t_s}{0.054} \right) \cdot 0.155 I_{cl} \tag{A.26}$$

$$t_{cl} = t_s \left(1 + \frac{0.155}{0.054} \cdot I_{cl} \right) - \frac{36.4 \cdot 0.155}{0.054} \cdot I_{cl} \tag{A.27}$$

If the skin temperature is known and the clothing insulation it is possible to find the surface temperature of the person, t_{cl}.

Appendix B

Surface areas of the BTM

Table B.1. Naked area of the 16 parts of the BTM body.

Part of the body	**Area** (m^2)
Left foot	0.0446
Right foot	0.0437
Left leg	0.0892
Right leg	0.0879
Left thigh	0.1630
Right thigh	0.1670
Crotch	0.1740
Head	0.1100
Left hand	0.0397
Right hand	0.0394
Left arm	0.0490
Right arm	0.0500
Left shoulder	0.0736
Right shoulder	0.0778
Chest	0.1380
Back	0.1270
Total area (A_{Du})	1.4739

Appendix C

Measurement of the convective heat transfer coefficient

To validate the performance of the Breathing Thermal Manikin (BTM) the convective heat transfer coefficient, h_c, is measured and compared with results found in the literature.

C.1. Measurement set-up

The measurements are performed in a displacement ventilated room with a small air change rate and a small vertical temperature gradient.

The dimensions of the room are 8 m x 6 m x 4.5 m (length x width x height). The air flow rate is 0.040 m^3/s corresponding to an air change rate of 0.67 h^{-1}. Heat load is generated by two person simulators (2 x 100 W) and a point heat source (500 W), apart from the manikin itself. The manikin has a surface area of A_{Du} = 1.4739 m^2. In the present measurements it is naked (I_{cl} = 0 clo).

The manikin is suspended from the ceiling so that the feet are raised 0.3 m above the floor to avoid conduction and the relatively high velocities at the floor. In that way the velocity in the surroundings around the manikin is less than 0.05 m/s. Therefore, it is concluded that the flow around the body is free convection (Chapter 2.2.2.2.).

The air temperature and the surface temperature of the surrounding walls, ceiling and floor are measured together with the skin temperature and the total sensible heat loss from the BTM (radiation and convection).

Two cases are examined corresponding to slightly different temperatures of the surroundings. In Table C.1. some of the results from the measurements are presented.

Table C.1. Measurement results from Case 1 and Case 2 used for determination of the convective heat transfer coefficient. Q_t is the total sensible heat loss, t_s is the skin temperature, t_a is the ambient air temperature, and $\bar{t}_r$ is the mean radiant temperature. In Table C.4. results from the 16 individual parts of the body are mentioned together with the calculated local convective heat transfer coefficient.

	Case 1	**Case 2**
Q_t (W/m^2)	76.80	75.77
t_s (°C)	32.3	32.3
t_a (°C)	23.4	22.9
$\bar{t}_r$ (°C)	23.3	23.0

Figure C.1. shows the vertical air temperature profile for the two cases.

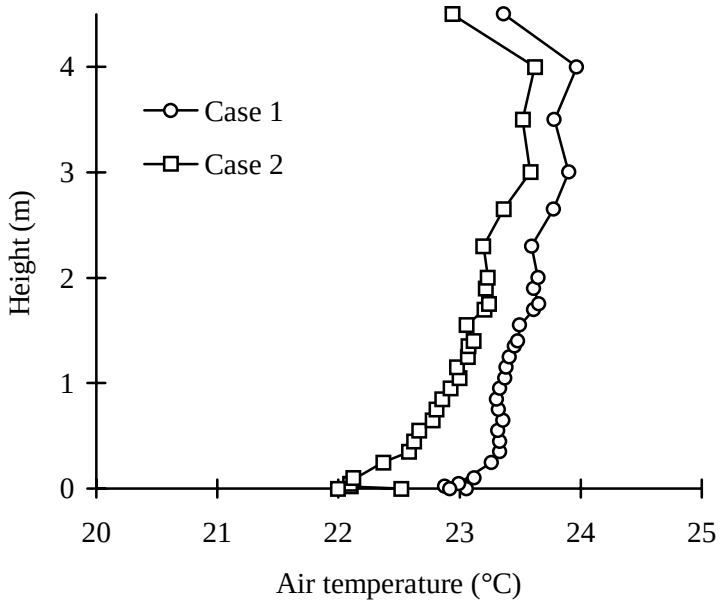

Figure C.1. Vertical temperature profile in the displacement ventilated room during the two measurements of the convective heat transfer coefficient. The local vertical temperature gradient is less than 0.4 °C/m where the manikin is located.

C.2. Radiative heat transfer coefficient

It is only possible to measure the total sensible heat loss directly by means of the manikin. Therefore, it is necessary to calculate the radiative heat loss and afterwards determine the convective heat loss (see Chapter 2.2.2.3. for further explanation of the formulas)

$$R = h_r\left(\bar{t}_r - t_s\right) \tag{C.1}$$

and

$$h_r = 4\varepsilon\sigma f_{eff}\left[273.15 + \frac{t_s + \bar{t}_r}{2}\right]^3 \tag{C.2}$$

Here, f_{eff} = 0.725, ε = 0.95 and σ = 5.669·10^{-8} W/m^{2}K^4, see Table C.2.

Table C.2. Calculation of the linear radiative heat transfer coefficient, h_r, and the radiative heat loss, R, for Case 1 and Case 2.

	Case 1	**Case 2**
h_r (W/m^2°C)	4.26	4.25
R (W/m^2)	38.31	39.53

C.3. Convective heat transfer coefficients

When the total sensible heat loss and the radiative heat loss are found the convective heat transfer coefficient, h_c, may be found from $C = Q_t - R$, see equation (C.3) and Table C.3.

$$h_c = \frac{C}{t_s - t_a} \tag{C.3}$$

Table C.3. Calculation of the convection heat loss, C, and the overall convective heat transfer coefficient, h_c.

	Case 1	**Case 2**
C (W/m^2)	38.47	36.24
h_c (W/m^2°C)	4.32	3.86

The convective part of the sensible heat loss amounts to approximately 50% in both cases.

Table C.4. shows the local convective heat transfer coefficient calculated for each of the 16 parts of the BTM, assuming that 50% of the sensible heat loss comprises convection.

Table C.4. Calculation of the local convective heat transfer coefficient for each part of the BTM. Here, it is assumed that 50% of the sensible heat loss is convective.

Body part	**Case 1**			
	t_s (°C)	t_a (°C)	C (W/m^2)	h_c (W/m^2°C)
Left foot	31.50	23.23	46.25	5,59
Right foot	31.60	23.23	45.25	5,41
Left leg	32.00	23.29	41.50	4.76
Right leg	31.90	23.29	42.75	4.97
Left thigh	32.30	23.36	39.00	4.36
Right thigh	32.30	23.36	38.75	4.33
Crutch	32.65	23.44	35.75	3.87
Head	33.00	23.56	32.50	3.44
Left hand	32.10	23.41	41.00	4.72
Right hand	32.00	23.41	41.50	4.83
Left arm	31.95	23.48	42.00	4.96
Right arm	32.15	23.48	40.00	4.61
Left shoulder	32.50	23.53	36.75	4.10
Right shoulder	32.65	23.53	35.50	3.89
Chest	32.50	23.50	36.75	4.08
Back	32.60	23.50	36.00	3.96

Table continued …

…Table continued

	Case 2			
Body part	t_s (°C)	t_a (°C)	C (W/m^2)	h_c (W/m^2°C)
Left foot	31.33	22.60	47.83	5.48
Right foot	31.50	22.60	46.17	5.19
Left leg	32.03	22.70	41.33	4.43
Right leg	31.97	22.70	41.67	4.50
Left thigh	32.37	22.83	38.33	4.02
Right thigh	32.43	22.83	37.67	3.92
Crutch	32.67	22.97	35.33	3.64
Head	32.90	23.18	33.33	3.43
Left hand	32.27	22.91	39.00	4.17
Right hand	32.30	22.91	38.83	4.14
Left arm	32.27	23.04	39.33	4.26
Right arm	32.43	23.04	37.83	4.03
Left shoulder	32.63	23.12	36.00	3.78
Right shoulder	32.70	23.12	35.17	3.67
Chest	32.53	23.06	36.83	3.89
Back	32.60	23.06	36.33	3.81

The mean value of the overall convective heat transfer coefficients for the two cases is 4.1 W/m^2°C. The result may be compared with a formula adapted by Nielsen & Pedersen (1952) where mean values of skin and ambient temperatures from the measurements are inserted

$$h_c = 2.381\left(t_s - t_a\right)^{0.25} = 2.381(32.3 - 23.15)^{0.25} = 4.1\ \text{W/m}^2\text{°C} \qquad \text{(C.4)}$$

ASHRAE (1993) suggests that h_c = 4.0 W/m^2°C for a standing person in a velocity field below 0.15 m/s. Both references show a close agreement with the measurements.

Appendix D

Measurement of the clothing insulation

In this Appendix the clothing insulation of the Breathing Thermal Manikin (BTM) is determined.

D.1. Theory

According to McCullough et al. (1985) the intrinsic or basic clothing insulation (the insulation from the skin to the surface of the clothing), I_{cl}, is determined as

$$I_{cl} = I_T - \frac{I_a}{f_{cl}} \qquad \text{(D.1)}$$

where

I_{cl} = Intrinsic (basic) clothing insulation (clo)
I_T = Total thermal insulation of clothing plus air layer (clo)
I_a = Insulation of the air layer (clo)
f_{cl} = Clothing area factor (n.d.)

The clothing area factor is defined as the surface area of the clothed body divided by the DuBois surface area of the naked body. f_{cl} is usually expressed as (McCullough et al., 1985)

$$f_{cl} = 1 + 0.3 I_{cl} \qquad \text{(D.2)}$$

The total thermal insulation can be expressed as follows, remembering that 1 clo is equivalent to 0.155 m^2°C/W.

$$I_T = \frac{t_s - t_a}{0.155 Q_t} \tag{D.3}$$

where

t_s = Mean skin temperature (°C)
t_a = Ambient air temperature (°C)
Q_t = Total rate of sensible heat loss (W/m^2)

The BTM is controlled to satisfy the following necessary requirement for achieving thermal comfort applied to sensible heat loss, see Appendix A.

$$t_s = 36.4 - 0.054 Q_t \tag{D.4}$$

Thus, inserting in the first equation gives

$$I_{cl} = \frac{36.4 - 0.054 Q_t - t_a}{0.155 Q_t} - \frac{I_a}{1 + 0.3 I_{cl}} \tag{D.5}$$

where I_{cl} is found by iteration.

The insulation of the air layer, I_a, is easily found by means of a preceding measurement with the naked BTM, where I_{cl} = 0 clo.

$$I_a = \frac{36.4 - 0.054 Q_t - t_a}{0.155 Q_t} \qquad \text{(for } I_{cl} = 0 \text{ clo)} \tag{D.6}$$

D.2. Results

The measurements are performed in an environment satisfying the requirements of ASTM-F1291 (1991) and DS/INSTA 353 (1989).

The clothing ensemble consists of

- Cotton stockings
- Tennis shoes
- Cotton panties
- Cotton vest
- Two pairs of cotton tights
- Two tight-fitting, high-necked cotton blouses with long sleeves

The insulation value of the clothes is found for the manikin standing and the manikin seated on an almost uninsulating chair. Results from the measurements are shown in Table D.1.

Table D.1. Results of measurements where the BTM is applied to determine the clothing insulation in case of standing and seated posture.

	Standing BTM		**Seated BTM**	
	Naked	Clothed	Naked	Clothed
Q_t (W/m^2)	81.2	52.1	82.1	54.1
t_s (°C)	32.0	33.6	32.0	33.5
t_a (°C)	21.40	21.35	21.08	21.18

If the results are inserted in the above equations the different insulation values in Table D.2. are found.

Table D.2. Thermal insulation of the air layer, I_a, and intrinsic (basic) clothing, I_{cl}, of the clothing ensemble mentioned above for the BTM in standing and seated posture.

	Clothing insulation	
	Standing BTM	Seated BTM
I_a (clo)	0.84	0.86
I_{cl} (clo)	0.84	0.77

In this work I_{cl} = 0.8 clo is used in all cases. This clothing insulation correspond well to usual indoor levels found between 0.5 and 1.0 clo.

Appendix E

k - ε transport equations

The turbulent kinetic energy, k, and the rate of dissipation of turbulent kinetic energy, ε, is defined as (Abbott and Basco, 1989)

$$k \equiv \frac{1}{2}\overline{u_i' u_i'} = \frac{1}{2}\left(\overline{u'^2} + \overline{v'^2} + \overline{w'^2}\right) \tag{E.1}$$

$$\varepsilon \equiv -2\nu\overline{s_{ij} s_{ij}} \tag{E.2}$$

where s_{ij} is the strain rate of the fluctuating flow

$$s_{ij} \equiv \frac{1}{2}\left(\frac{\partial u_i'}{\partial x_j} + \frac{\partial u_j'}{\partial x_i}\right) \tag{E.3}$$

Transport equation for turbulent kinetic energy, k

$$\frac{\partial}{\partial x_j}\left(\rho u_j k\right) = \frac{\partial}{\partial x_j}\left(\frac{\mu_{eff}}{\sigma_k}\frac{\partial k}{\partial x_j}\right) + P_k - \rho\varepsilon + S_k \tag{E.4}$$

Transport equation for dissipation of turbulent kinetic energy, ε

$$\frac{\partial}{\partial x_j}\left(\rho u_j \varepsilon\right) = \frac{\partial}{\partial x_j}\left(\frac{\mu_{eff}}{\sigma_\varepsilon}\frac{\partial \varepsilon}{\partial x_j}\right) + \frac{\varepsilon}{k}\left(c_1 P_k - c_2 \rho\varepsilon\right) + S_\varepsilon \tag{E.5}$$

where P_k is the shear production term

$$P_k = \mu_t \left(\frac{\partial u_i}{\partial x_j} + \frac{\partial u_j}{\partial x_i} \right) \frac{\partial u_i}{\partial x_j} \tag{E.6}$$

Constants

c_1 = 1.44 (n.d.)
c_2 = 1.92 (n.d.)
σ_k = 1.0 (n.d.)
σ_ε = 1.3 (n.d.)

Appendix F

t-test

In order to test the following hypothesis, regarding the flow in a displacement ventilated room, a statistical test is performed.: *Concentration assessed after holding the breath is significantly lower than the concentration assessed by the immediate impression*.

Members of a Trained Sensory Panel perceived the air quality both as the "immediate impression" and "after holding the breath". In Table F.1. the differences between the two assessments (in decipol) are summarised for each of the panel members. A paired t-test has been made assuming random sampling and blocking with pairs in persons.

If random sampling is assumed and there are n differences d, then the quantity t_0 is distributed as t with n -1 degrees of freedom (Box et al., 1978)

$$t_0 = \frac{\bar{d} - \delta}{\frac{s_d}{\sqrt{n}}} \tag{F.1}$$

where

$\bar{d}$ = Average of the n differences (decipol)
δ = True mean difference (decipol)

and the null hypothesis is $\delta = 0$. The standard deviation, s_d, is found by

$$s_d{}^2 = \frac{\sum d^2 - \frac{\left(\sum d\right)^2}{n}}{n-1} \tag{F.2}$$

Table F.1. Summarised results of assessments by the members of a Trained Sensory Panel. *A*: Assessment as "immediate impression". *B*: Assessment "after holding the breath". The results are calibrated according to Chapter 2.4.

Person	*B - A*			
	Case 1	**Case 2**	**Case 3**	**No contamination**
1	20.90	5.30	-14.84	-0.53
2	-10.13	-12.91	3.83	-2.59
3	-7.44	-3.42	-2.18	-3.19
4	2.80	-1.12	-2.28	-1.12
5	-8.25	-5.12	-4.04	-2.68
6	-6.69	-3.09	-2.88	-0.84
7	1.24	-1.82	0.89	0.57
8	-6.85	-4.73	-5.10	0.00
9	-5.41	3.23	3.89	-0.82
10	-4.83	-1.10	-0.74	-0.29
11	2.27	none	2.01	-0.92
12	4.29	-4.95	1.38	0.00
n	12	11	12	12
$\bar{d}$	-1.508	-2.703	-1.679	-1.034
$\sum d$	-18.10	-29.73	-20.06	-12.41
$\sum d^2$	840.05	305.30	317.89	28.24
$s_d / \sqrt{n}$	2.4814	1.4300	1.4677	0.3416
t_0	-0.61	-1.89	-1.14	-3.03
$\Pr(t \geq t_0)$	0.28	0.044	0.15	0.0055
Sign. at level	**40 %**	**5 %**	**25 %**	**1 %**

Sammendrag på dansk

Formål

Udgangspunktet for nærværende Ph.D.-afhandling "Personeksponering for forureningskilder i ventilerede rum" er det faktum, at mange mennesker i de industrialiserede lande tilbringer mere end 90% af deres tid i et mere eller mindre kunstigt skabt klima, fx kontorer, fabrikker, offentlige bygninger, hjem, transportmidler, osv.

Indeklimaet er ofte påvirket af forskellige forureningskilder, der influerer på menneskers sundhed og oplevelse af luftkvalitet, hvilket understreger behovet for en korrekt fastsættelse af eksponeringen.

Normalt antager eksponeringsmodeller, at luften og forureningen i det enkelte rum er fuldt opblandet og dermed uden koncentrationsgradienter. På den måde kan eksponeringen fastsættes alene på baggrund af en kildestyrke og en luftmængde.

I praksis vil der dog altid forekomme koncentrationsgradienter i større eller mindre grad, fx tæt på forureningskilderne eller i fortrængningsventilerede rum, hvor lagdeling af strømningen og en vertikal koncentrationsgradient netop anvendes til at forbedre ventilationseffektiviteten.

Når koncentrationsgradienter forekommer i ventilerede rum, vil tilstede-værelsen af personer kunne påvirke det lokale koncentrationsfelt betydeligt, blandt andet på grund af:

… at *kroppens overtemperatur* i forhold til omgivelserne genererer en kon-vektiv opadstigende luftstrøm langs personen. Denne konvektive strømning kan medrive forurening i den nederste del af rummet og transportere den til åndingszonen. Herved kan personen blive eksponeret for koncentrationer, som afviger betydeligt fra den generelle koncentration i indåndingshøjden i andre dele af rummet.

… at personen lokalt kan virke som en *forhindring* for den generelle strømning. Hvis personen er udsat for en strømning bagfra, vil der dannes et kølvand foran

personen. Kølvandet kan medrive forureninger fra horisontale afstande på mere end en halv meter til åndingszonen.

… at personens *bevægelser* kan påvirke strømningsfeltet og forureningsfordelingen betydeligt. Blandt andet vil effekten af grænselagsstrømningen aftage.

Ovenstående diskussion rejser behovet for forbedrede eksponeringsmodeller, der tager hensyn til såvel koncentrationsgradienter som den lokale indflydelse af personer.

Værktøjer til bestemmelse af personeksponering

Tre forskellige værktøjer til bestemmelse af personeksponering er præsenteret

1. En termisk mannequin med åndingsfunktion, hvilket er en opvarmet fuldskalamodel af en kvinde udstyret med en kunstig lunge. Forureningen simuleres med sporgas.

2. En computersimuleret person, hvilket er en numerisk model af en person anvendt i Computational Fluid Dynamics (CFD = numerisk strømnings-dynamik). Her bestemmes strømningsfeltet og forureningstransporten ved hjælp af computersimulering.

3. Et trænet sensorisk panel, hvilket er en gruppe personer trænet til at bedømme luftkvaliteten i sammenligning med referencer, hvor niveauerne af oplevet luftkvalitet er kendte.

De tre værktøjer tager alle hensyn til den lokale effekt af personer, der befinder sig i ventilerede rum med koncentrationsgradienter.

Værktøjerne er anvendt på de to væsentligste principper for rumventilation, nemlig fortrængningsprincippet og opblandingsprincippet. Det sker både for at afprøve værktøjerne på en række cases, men også for at undersøge hvor stor en effekt det har på fastsættelsen af eksponeringen, at der tages hensyn til gradienter og personer ved de to nævnte ventilationsprincipper.

Mannequinen er meget anvendelig ved stationære eksponeringsmålinger, hvor forureningsspredning simuleres med sporgas. Ved hjælp af den kunstige lunge kan forureningskoncentrationen i den inhalerede luft nemt bestemmes.

Det trænede sensoriske panel kan naturligvis benyttes til bestemmelse af den oplevede luftkvalitet, men også til bestemmelse af forureningskoncentrationen i den inhalerede luft, hvis sammenhængen mellem koncentration og oplevet luftkvalitet kendes. Det er tilfældet for referencegassen 2-propanon. For at undgå tilvænning er panelets bedømmelse dog begrænset til én inhalering.

Hvis den computersimulerede person skal anvendes, kræves et godt kendskab til CFD, blandt andet for at bestemme randbetingelser m.v. som er afgørende for et godt resultat af beregningerne.

De tre værktøjer er begrænset til målinger/simuleringer af gasformige forureninger og mindre partikler (< 10 μm), hvor eksponeringen alene finder sted ved respiration gennem mund eller næse.

Målingerne med den termiske mannequin stemmer godt overens med resultater fundet i litteraturen. Der er fundet nogen afvigelse mellem person-eksponeringen bestemt ved hjælp af mannequinen og den computersimulerede person, men alle resultater er dog af samme størrelsesorden, ligesom alle væsentlige strømningsfænomener omkring en person er genfundet ved computermodellen. Simuleringerne viser, at det har stor indflydelse på eksponeringen at udstyre modellen med "ben", især hvis forureningskilden er placeret tæt ved gulvet.

Nye størrelser

Der er defineret to nye størrelser. En ny ventilationseffektivitet: personeksponeringsindekset, ε_e, se ligning (1.4). Personeksponeringsindekset udtrykker den ventilationseffektivitet, som faktisk opleves af en person i et ventileret rum.

Den anden størrelse er: medrivningseffektiviteten i menneskets grænselag, η_e, se ligning (3.1). η_e udtrykker evnen til at tilføre (frisk) luft fra gulvområdet til åndingszonen. Denne størrelse er anvendt i forbindelse med fortrængnings-ventilation og i en eksponeringsmodel for fortrængningsventilation.

Begge størrelser er et resultat af, at den lokale effekt af personen er inkluderet. Målinger og simuleringer har demonstreret deres evne til at udtrykke forskellen mellem den luftkvalitet der reelt eksponeres for og middelventilations-effektiviteten i opholdszonen o.l.

Fortrængningsventilation

Personeksponering i rum ventileret efter fortrængningsprincippet er undersøgt ved hjælp af fuldskalamålinger i to rum og computersimuleringer af forholdene i det ene.

Forureningsfordelingen ved målingerne er genereret af punktkilder. "Varme" forureningskilder anvendes til at skabe den karakteristiske to-zone koncentrationsfordeling, hvor rummet er opdelt i en renere, nedre zone og en øvre, mere forurenet zone. Opadrettede slanger placeret over varmekilder tilfører forureningen (N_2O eller 2-propanon).

En "kold" (passiv) forureningskilde er anvendt til at undersøge indflydelsen af forureningskilder placeret tæt på personer. Denne kilde består af en densitetsneutral blanding af N_2O og He tilført gennem en porøs skumgummibold.

I CFD simuleringerne er der foruden de to nævnte kilder også lavet beregninger med en plan kilde i form af gulvet. Denne kilde har en konstant forureningsemission.

Det er fundet, at den lagdelte strømning og de betydelige koncentrations-gradienter i et fortrængningsventileret rum nødvendiggør en fastsættelse af eksponeringen, som ikke baseres på antagelsen om fuld opblanding.

Strømningen i menneskets grænselag kan i stor udstrækning medrive luft neden for åndingszonen og dermed forbedre kvaliteten af indåndingsluften, når forureningskilderne er "varme".

Luftkvaliteten, som personen oplever i det fortrængningsventilerede rum, er signifikant forbedret i forhold til opblandingsventilation. Forbedringen er både fundet ved stationære kemiske målinger og sensoriske målinger, hvor det trænede panel bedømmer den oplevede luftkvalitet.

Bevægelser forringer luftkvaliteten på grund af forstyrrelser af menneskets termiske grænselag, som er med til at befordre den høje luftkvalitet.

En eksponeringsmodel for fortrængningsventilerede rum er foreslået. Modellen tager højde for koncentrationsgradienter og indflydelsen af menneskets termiske grænselag. Modellen er enkel at anvende ved dimensionering i praksis. Den

forudsætter, at den karakteristiske to-zone koncentrationsfordeling er til stede, og at de tilstedeværende personers bevægelser er forholdsvis begrænsede.

Normalt er medrivning i grænselaget en fordel, men resultaterne viser også en mulig ulempe, når passive forureningskilder forefindes i den nedre del af rummet tæt ved personen. I det tilfælde forbedrer fortrængningsprincippet ikke luftkvaliteten.

Opblandingsventilation

Eksponering i opblandingsventilerede rum er undersøgt ved hjælp af målinger og simuleringer af det ensartede hastighedsfelt omkring en person, der står i en vindkanal. Denne strømning antages at kunne repræsentere det lokale strømningsfelt omkring en person i et opblandingsventileret rum. Desuden er der foretaget computersimuleringer af et opblandingsventileret rum, hvor hele feltet er indbefattet.

Her er forureningen leveret af en passiv punktkilde, og for computer-simuleringerne er også gulvet i et tilfælde simuleret som en plan forurenings-kilde med en konstant emission.

Personeksponering for forureningskilder i det ensartede hastighedsfelt afhænger af både kildeplacering og strømningsretningen i forhold til personen. Hastighedsniveauet er også en betydende faktor.

Hvirvler genereret i kølvandet foran en person, som vender ryggen mod strømningsretningen, har en betydelig evne til at medrive forurening. Denne forurening transporteres til åndingszonen, hvor den forårsager eksponering. Resultaterne viser, at hvirvlerne kan medrive forurening i en horisontal afstand på over en halv meter.

Personeksponering målt ved hjælp af den termiske mannequin stående i vindkanalen med en forureningskilde "i hænderne" kan overstige udsugnings-koncentrationen med en faktor 50. Den samme effekt er fundet ved computersimuleringerne blot med et endnu højere niveau. Dette understreger klart behovet for en forbedret fastsættelse af eksponeringen, når forure-ningskilderne befinder sig i nærheden af personer.

Computersimuleringerne af et opblandingsventileret rum viser, at forureningskoncentrationen i indåndingsluften nemt kan være dobbelt så høj som udsugningskoncentrationen, selvom forureningskilden befinder sig i en stor afstand fra personen.

Målinger og simuleringer viser klart, at det ikke er nok at kende den lokale forureningskoncentration i et "tomt" rum, den lokale effekt af personen er betydelig og bør tages i betragtning ved fastsættelse af personeksponeringen.

References

Abbott, M.B. and Basco, D.R. (1989)
Computational Fluid Dynamics: An Introduction for Engineers, ISBN 0-582-01365-8, Longman Scientific & Technical, 1989.

Air Quality Criteria for Particulate Matter (1969)
National Air Pollution Control Administration Publication No. AP-49, Washington, D.C.

Arpaci, V.S. and Larsen, P.S. (1984)
Convection Heat Transfer, ISBN 0-13-172346-4, Prentice-Hall, Inc.

ASHRAE (1993)
Handbook of Fundamentals, Physiological Principles and Thermal Comfort (Chapter 8).

Asmussen, E. and Nielsen, M. (1989)
Lærebog i menneskets fysiologi, Akademisk Forlag.

ASTM-F1291 (1991)
Standard Test Method for Measuring the Thermal Insulation of Clothing Using a Heated Manikin.

Awbi, H.B. (1991)
Ventilation of Buildings, E & FN Spon, ISBN 0-419-15690-9.

Awbi, H.B. (1996)
A CFD Study of the Air Quality at the Breathing Zone, Proceedings of INDOOR AIR ´96, The 7th International Conference on Indoor Air Quality and Climate, Vol. 2, pp. 1009 - 1014, July 21 - 26, Nagoya, Japan.

Bjørn, E. and Nielsen, P.V. (1995)
Merging Thermal Plumes in the Indoor Environment, Proceedings of Healthy Buildings ´95, Fourth International Conference on Healthy Buildings, Milan, Italy, 11 - 14 September, Vol. 3, pp. 1223 - 1228.

Bjørn, E. and Nielsen, P.V. (1996)
Exposure due to Interacting Air Flows Between Two Persons, Proceedings of ROOMVENT ´96, 5th International Conference on Air Distribution in Rooms, Vol. 1, pp. 107 - 114, July 17 - 19, Yokohama, Japan.

Bluyssen, P.M. and Fanger, P.O. (1991)
Addition of Olfs from Different Pollution Sources, determined by a Trained Panel, Indoor Air, Vol.1, No.4, pp.414-421.

Bluyssen, P.M. and Lemaire, T. (1992)
The Distribution of Perceived Air Quality in an Office Space - Computer Simulations and Sensory Evaluations, Roomvent '92 , Air Distributions in Rooms, Vol.3, pp. 195 - 211, Aalborg, Denmark.

Box, G.E.P., Hunter, W.G. and Hunter, J.S. (1978)
Statistics for Experimenters - An Introduction to Design, Data Analysis, and Model Building, ISBN 0-471-09315-7, John Wiley & Sons.

Brohus, H. (1992)
Air Flow in a Room Ventilated after the Mixing Principle with an Obstacle Placed in the Occupied Zone, Proceedings of Fifth Nordic Seminar on Computational Mechanics, Aalborg, Denmark, pp. 146 - 150.

Brohus, H. and Nielsen, P.V. (1994a)
Contaminant Distribution Around Persons in Rooms Ventilated by Displacement Ventilation, Proceedings of Roomvent '94, Fourth International Conference on Air Distribution in Rooms, Cracow, Poland, Vol.1, pp. 293 - 312.

Brohus, H. and Nielsen, P.V. (1994b)
Personal Exposure in a Ventilated Room with Concentration Gradients, Proceedings of Healthy Buildings '94, 3rd International Conference, 22-25 August, Budapest, Hungary, Vol.2, pp.559 - 564.

Brohus, H. and Nielsen, P.V. (1995)
Personal Exposure to Contaminant Sources in a Uniform Velocity Field, Proceedings of Healthy Buildings ´95, Fourth International Conference on Healthy Buildings, Milan, Italy, 11 - 14 September, Vol. 3, pp. 1555 - 1560.

Brohus, H. and Nielsen, P.V. (1996a)
CFD Models of Persons Evaluated by Full-Scale Wind Channel Experiments, Proceedings of Roomvent ´96, 5th International Conference on Air Distribution in Rooms, July 17 - 19, Yokohama, Japan,Vol.2, pp.137 - 144.

Brohus, H. and Nielsen, P.V. (1996b)
Personal Exposure in Displacement Ventilated Rooms, Indoor Air, Vol. 6, No. 3, pp. 157 - 167.

Brohus, H., Knudsen, H.N., Nielsen, P.V., Clausen, G. and Fanger, P.O. (1996)
Perceived Air Quality in a Displacement Ventilated Room, Proceedings of Indoor Air ´96, The 7th International Conference on Indoor Air Quality and Climate, July 21 - 26, Nagoya, Japan, Vol. 1, pp. 811 - 816.

CEN prENV 1752 (1994)
Ventilation for Buildings: Design Criteria for the Indoor Environment.

Christensen, R. and Stevnhoved, L. (1993)
Private communication, Aalborg University.

Clark, R.P. and Edholm, O.G. (1985)

Man and his Thermal Environment, Edward Arnold (Publishers) Ltd., ISBN 0-7131-4445-9.

Clark, R.P. and Cox, R.N. (1973)
The Generation of Aerosols from the Human Body, In: Airborne Transmission and Airborne Infection. Ed. Hers,J.F.P. & K.C. Winkler, Oosthoek, Holland.

Clark, R.P. and Toy, N. (1975a)
Natural Convection Around the Human Head, J. Physiol. No. 244, pp.283-293.

Clark, R.P. and Toy, N. (1975b)
Forced Convection Around the Human Head, J. Physiol. No. 244, pp.295-302.

Davidson, L. and Nielsen, P.V. (1995)
Calculation of the Two-Dimensional Airflow in Facial Regions and Nasal Cavity using an Unstructured Finite Volume Solver, ISSN 1395-7953 R9539, Dept. of Building Technology and Structural Engineering, Aalborg University.

Davis, J.C. (1986)
Statistics and Data Analysis in Geology, John Wiley & Sons, ISBN 0-471-08079-9.

DS/INSTA 353 (1989)
Beskyttelsesbeklædning, Klæder mod kulde. Termisk dukke til prøvning af varmeisolans.

DuBois, D. and DuBois, E.F. (1916)
A Formula to Estimate Approximate Surface Area, if Height and Weight are known, Archives of Internal Medicine, 17:863-71.

Dunnett, S.J. (1994)
A Numerical Study of the Factors Affecting Worker Exposure to Contaminants, J. Aerosol Science, Vol.25, Suppl.1.

ECA (1991)
European Concerted Action "Indoor Air Quality and its Impact on Man": “Effects of Indoor Air Pollution on Human Health”. Report No. 10, Commission of the European Communities, Luxembourg.

ECA (1992)
European Concerted Action "Indoor Air Quality and its Impact on Man": “Guidelines for Ventilation Requirements in Buildings”. Report No. 11, Commission of the European Communities, Luxembourg.

Etheridge, D.W. and Sandberg, M. (1996)
Building Ventilation: Theory and Measurement, ISBN 0 471 96087 X, John Wiley & Sons Ltd.

Fanger, P.O. (1972)

Thermal Comfort - Analysis and Applications in Environmental Engineering, McGraw-Hill Book Company, ISBN 0-07-019915-9.

Fanger, P.O. (1988)
Introduction of the olf and the decipol Units to Quantify Air Pollution Perceived by Humans Indoors and Outdoors, Energy and Buildings, 12, 1-6.

Fanger, P.O. (1995)
International Trends in Ventilation Standards, Proceedings of Healthy Buildings ´95, Fourth International Conference on Healthy Buildings, Milan, Italy, 11 - 14 September, Vol. 1, pp. 257 - 263.

Fitzner,K. (1996)
Displacement Ventilation and Cooled Ceilings, Results of Laboratory Tests and Practical Installations, Proceedings of Indoor Air ´96, Vol. 1, pp. 41-50, Nagoya, Japan.

Fletcher, B. and Johnson, A.E. (1988)
Comparison of Personal and Area Concentration Measurements, and the use of a Manikin in Sampling, Proceedings of Ventilation '88, New York, Pergamon Press (Ed. Vincent,J.H.), pp.161-167.

Flovent (1994)
FLOVENT Instruction Manual (version 1.4) and FLOVENT Reference Manual (version 1.4), Flomerics Limited, Surrey, England.

Flynn, M.R. and Shelton, W.K. (1990)
Factors Affecting the Design of Local Exhaust Ventilation for the Control of Contaminants from Hand-Held Sources, Appl. Occup. Environ. Hyg. 5(10), pp.707-714.

Flynn, M.R. and George, D.K. (1991)
Aerodynamics and Exposure Variability, Appl. Occup. Environ. Hyg. 6(1), pp. 36-39, January.

Gan, G. (1994)
Numerical Method for a Full Assessment of Indoor Thermal Comfort, Indoor Air, 4, pp. 154-168.

Gan, G., Awbi, H.B. and Croome, D.J. (1993)
CFD Simulation of the Indoor Environment for Ventilation Design, Presented at the ASME 1993 Winter Meeting - Paper No. 93-WA/HT-49, New Orleans, USA.

George, D.K., Flynn, M.R. and Goodman, R. (1990)
The Impact of Boundary Layer Separation on Local Exhaust Design and Worker Exposure, Appl. Occup. Environ. Hyg. 5:501-509.

Heinsohn, R.J. (1991)
Industrial Ventilation: Engineering Principles, ISBN 0-471-63703-3, New York, John Wiley & Sons.

Holman, J.P. (1989)
Heat Transfer, McGraw-Hill Book Co, ISBN 0-07-100487-4.

Holmberg, R.B., Eliasson, L. , Folkesson, K. and Strindehag, O. (1990)
Inhalation-Zone Air Quality Provided by Displacement Ventilation, Proceedings of Roomvent '90, International Conference on Air Distribution in Ventilated Spaces, Oslo, Norway.

Homma, H. and Yakiyama, M. (1988)
Examination Of Free Convection Around Occupant's Body Caused By Its Metabolic Heat, ASHRAE Trans. V.94, Part 1.

Hyldgaard, C.E. (1994)
Humans as a Source of Heat and Air Pollution, Proceedings of Roomvent ´94, Air Distribution in Rooms, Fourth International Conference, Vol.1, pp.413-433, Cracow, Poland.

Ichihara, M., Saitou, M., Nishimura, M. and Tanabe, S. (1996)
Measurements of Convective and Radiative Heat Transfer Coefficients of Standing Human Body by using a Thermal Manikin, Proceedings of INDOOR AIR ´96, The 7th International Conference on Indoor Air Quality and Climate, Vol. 2, pp. 559 - 564, July 21 - 26, Nagoya, Japan.

Iwamoto, S. (1996)
A Study on Numerical Prediction Methods of Thermal Environment around Occupants, Proceedings of INDOOR AIR ´96, The 7th International Conference on Indoor Air Quality and Climate, Vol. 1, pp. 299 - 303, July 21 - 26, Nagoya, Japan.

Jayatilleke, C.L.V. (1969)
The Influence of Prandtl Number and Surface Roughness on the Resistance of the Laminar Sub-layer to Momentum and Heat Transfer, Progress in Heat and Mass Transfer, Vol. 1, pp. 193-329.

Jensen, G.P. and Nielsen, P.V. (1995)
Transfer of Emission Test Data from Small Scale to Full Scale, Proceedings of Healthy Buildings ´95, Fourth International Conference on Healthy Buildings, Milan, Italy, 11 - 14 September, Vol. 1, pp. 851 - 856.

Kato, S., Murakami, S. and Zeng, J. (1996)
Numerical Analysis of Contaminant Distribution around a Human Body, Proceedings of ROOMVENT ´96, 5th International Conference on Air Distribution in Rooms, Vol. 2, pp. 129 - 136, July 17 - 19, Yokohama, Japan.

Kawamura, T., Hiwada, M., Hibino, T., Mabuchi, I. and Kumada, M. (1984)
Flow around a Finite Circular Cylinder on a Flat Plate, Bull. Jpn. Soc. Mech. Eng. 27(232): pp. 2142-2151.

Kerslake, D.M. (1972)
The Stress of Hot Environment, Cambridge University Press, ISBN 0 521

08343 5.

Kim, T. and Flynn, M.R. (1991a)
Airflow Pattern Around a Worker in a Uniform Freestream, Am. Ind. Hyg. Assoc. Journal, 52(7), pp. 287-296.

Kim, T. and Flynn, M.R. (1991b)
Modeling a Worker's Exposure From a Hand-Held Source in a Uniform Freestream, Am. Ind. Hyg. Assoc. J., 52(11), pp.458-463.

Kim, T. and Flynn, M.R. (1992)
The Effect of Contaminant Source Momentum on a Worker´s Breathing Zone Concentration in a Uniform Freestream, Am. Ind. Hyg. Assoc. J. 53(12), pp. 757-766.

Knudsen, H.N. (1994)
Modelling Indoor Air Quality (in Danish), Ph.D.-thesis, Laboratory of Heating, Ventilating and Air Conditioning, Technical University of Denmark.

Knudsen, H.N., Clausen, G. and Fanger, P.O. (1993)
Prediction of Perceived Air Quality in a Space Based on Small-Scale Experiments, Proceedings of the 6th International Conference of Indoor Air Quality and Climate INDOOR AIR ´93, Helsinki, Vol.2, pp.585-590.

Knudsen, H.N., Clausen, G. and Fanger, P.O. (1994)
Characterization of Sensory Emission Rates from Materials, Proceedings of Healthy Buildings, 3rd International Conference, Vol.1, pp.463-468, Budapest, Hungary.

Krühne, H. and Fitzner, K. (1994)
Air Quality in the Breathing Zone in Rooms with Displacement Flow, Proceedings of Roomvent ´94, Air Distribution in Rooms, Fourth International Conference, Vol.2, pp.93-101, Cracow, Poland.

Ljungqvist, B. and Reinmüller, B. (1993)
Interaction Between Air Movements and the Dispersion of Contaminants: Clean Zones with Unidirectional Air Flow, Journal of Parenteral Science and Technology, Vol.47, No.2.

Maroni, M., Seifert, B. and Lindvall, T. (1995)
Indoor Air Quality (Eds.), Elsevier Science B.V., The Netherlands, ISBN 0-444-81642-9.

Martinelli, C.A., Harley, N.H., Lippmann, M. and Cohen, B.S. (1983)
Monitoring Real-time Aerosol Distribution in the Breathing Zone, Am.Ind.Hyg.Assoc.J., 44, 4, pp.280-285.

Mattsson, M. and Sandberg, M. (1994)
Displacement Ventilation -Influence of Physical Activity, Proceedings of Roomvent ´94, Air Distribution in Rooms, Fourth International Conference, Vol.2, pp.77- 92, Cracow, Poland.

McCarthy, J.F., Bearg, D.W. and Spengler, J.D. (1991)
Assessment of Indoor Air Quality, Indoor Air Pollution - A Health Perspective, Ch.4 pp.82-108, Ed. Samet,J.M., Spengler,J.D., ISBN 0-8018-4124-0, The Johns Hopkins University Press.

McCullough, E.A., Jones, B.W. and Huck, J. (1985)
A Comprehensive Data Base for Estimating Clothing Insulation, ASHRAE Transactions, Vol.91, Part 2, pp.29-47.

Mitchell, D. (1974)
Convective heat transfer from man and other animals, Heat loss from animals and man. Ed. by J.L. Monteith & L.E. Mount, Butterworths, London.

Mundt, E. (1994)
Inhaled Air in Displacement Ventilation, Proceedings of Healthy Buildings, 3rd International Conference, Vol.2, pp.355-360, Budapest, Hungary.

Mundt, E. (1996)
The Performance of Displacement Ventilation Systems - Experimental and Theoretical Studies, ISSN 0284 - 141X, ISRN KTH/IT/M--38--SE, Bulletin no 38, Building Services Engineering, Royal Institute of Technology, Stockholm, Sweden.

Murakami, S., Kato, S. and Zeng, J. (1995)
Development of a Computational Thermal Manikin - CFD Analysis of Thermal Environment around Human Body, Proceedings of Tsinghua-HVAC-´95, Beijing, Vol. 2, pp.349 - 354.

Murakami, S., Kato, S. and Zeng, J. (1996)
CFD Analysis of Thermal Environment around Human Body, Proceedings of INDOOR AIR ´96, The 7th International Conference on Indoor Air Quality and Climate, Vol. 2, pp. 479 - 484, July 21 - 26, Nagoya, Japan.

Nickel, J. (1990)
Air Quality in a Conference Room with Tobacco Smoking Ventilated with Mixed or Displacement Ventilation, Proceedings of Roomvent ´90, Engineering Aero- and Thermodynamics of Ventilated Room, Second International Conference, Session D2-4 (64), Oslo, Norway.

Nielsen, P.V. (1981)
Contaminant Distribution in Industrial Areas with Forced Ventilation and Two-Dimensional Flow, IIR-Joint Meeting, Commission E1, Essen, Germany.

Nielsen, P.V. (1990)
Specification of a Two-Dimensional Test Case, International Energy Agency, Energy Conservation in Buildings and Community Systems, Annex 20: Air Flow Pattern Within Buildings, ISSN 0902-7513, R9040, Department of

Building Technology and Structural Engineering, Aalborg Univesity, Denmark.

Nielsen, P.V. (1993)
Displacement Ventilation - theory and design, Department of Building Technology and Structural Engineering, Aalborg University, ISSN 0902-8002 U9306.

Nielsen, P.V. (1996)
Temperature Distribution in a Displacement Ventilated Room, Proceedings of Roomvent ´96, 5th International Conference on Air Distribution in Rooms, July 17 - 19, Yokohama, Japan,Vol.3, pp.323 - 330.

Nielsen, M. and Pedersen, L. (1952)
Studies on the Heat Loss by Radiation and Convection from the Clothed Human Body, Acta Phys. Scandinav., Vol.27, pp.272-294.

Niwa, K., Murakami, S., Kato, S., Kondo, Y. and Kitamura, N. (1996)
Numerical Analysis of Flow and Temperature Fields with Local Air-Conditioning by Supply Jets from the Seats in Hall, Proceedings of ROOMVENT ´96, 5th International Conference on Air Distribution in Rooms, Vol. 2, pp. 307 - 314, July 17 - 19, Yokohama, Japan.

Ott, W.R. (1985)
Total human exposure, Environmental Science and Technology, Vol.19, No.10, pp.880-886.

Patankar, S.V. (1980)
Numerical Heat Transfer and Fluid Flow, Hemisphere Publishing Corporation.

Patankar, S.V. and Spalding, D.B. (1970)
Heat and Mass Transfer in Boundary Layers - a general calculation procedure, International Textbook Company Ltd, ISBN 0 7002 0154 8, London.

Pejtersen, J. and Mayer, E. (1993)
Performance of a Panel Trained to Assess Perceived Air Quality, Proc. 6th. International Conference on Indoor Air Quality and Climate, Indoor Air ´93, Helsinki, Vol.1, pp.95-100.

Pleil, J.D. and Lindstrom, A.B. (1995)
Sampling and Analysis of Exhaled Human Breath as an Exposure Assessment, Proceedings of Healthy Buildings ´95, Fourth International Conference on Healthy Buildings, Milan, Italy, 11 - 14 September, Vol. 1, pp. 507 - 511.

Rapp, G.M. (1973)
Convective heat transfer and convective coefficients of nude man, cylinders and spheres at low air velocities, ASHRAE Transactions, Vol.79, part 1, pp. 75-87.

Rodes, C.E., Kamens, R.M. and Wiener, R.W. (1991)

The Significance and Characteristics of the Personal Activity Cloud on Exposure Assessment Measurement for Indoor Contaminants, Indoor Air, Vol. 2, No. 1, pp.123-145.

Rodes, C.E., Kamens, R.M. and Wiener, R.W. (1995)
Experimental Considerations for the Study of Contaminant Dispersion Near the Body, Am. Ind. Hyg. Assoc. J., 56:535-545.

Rodi, W. (1980)
Turbulence Models and their Application in Hydraulics - A State of the Art Review, University of Karlsruhe, Germany.

Schlichting, H. (1979)
Boundary-Layer Theory, McGraw-Hill Publishing Company, ISBN 0-07-055334-3.

Sexton, K. and Ryan, P.B. (1988)
Assessment of Human Exposure to Air Pollution: Methods, Measurements, and Models, In: . Watson, A.Y., Bates, R.R. and Kennedy, D. (eds) Air Pollution, the Automobile, and Public Health, Washington D.C., National Academy Press, ISBN 0-309-03726-3, pp.207-238.

Skistad, H. (1994)
Displacement Ventilation, ISBN 0 86380 147 1, Research Studies Press Ltd., John Wiley & Sons Inc.

Stymne, H., Sandberg, M. and Mattsson, M. (1991)
Dispersion pattern of contaminants in a displacement ventilated room - implications for demand control, Proceedings of 12th AIVC Conference, Ottawa, Canada.

Surfer (1991)
SURFER, Reference Manual, Version 4, Golden Software, Inc., Golden, Colorado, USA.

Säteri, J.O. (1992a)
Local Ventilation Effectiveness in the Breathing Zone, International Symposium on Room Air Convection and Ventilation Effectiveness, pp. 307 - 312, Tokyo, Japan.

Säteri, J.O. (1992b)
A Breathing Manikin For Measuring Local Thermal Ventilation Effectiveness, Proceedings of Roomvent '92, Air Distribution in Rooms, Third International Conference, Vol.3, pp. 167 - 179, Aalborg, Denmark.

Tanabe, S., Arens, E.A., Bauman, F.S., Zhang, H. and Madsen, T.L. (1994)
Evaluating Thermal Environments by Using a Thermal Manikin with Controlled Skin Surface Temperature, ASHRAE Transactions, 3739, Vol. 100, Part 1, pp.39-48.

Tjelflaat, P.O. (1992)

Evaluation of Ventilation Effectiveness and Worker Exposure at the Design Stage, Proceedings of ISRACVE, pp. 154-164, Tokyo, Japan.

Tjelflaat, P.O. and Knott, R. (1996)
A Simulation Model for Thermal Comfort of a Person in a Large Enclosure, Proceedings of INDOOR AIR ´96, The 7th International Conference on Indoor Air Quality and Climate, Vol. 2, pp. 1015 - 1020, July 21 - 26, Nagoya, Japan.

Turiel, I. (1985)
Indoor Air Quality and Human Health, Stanford University Press, Stanford, California, USA.

Ultman, J.S. (1988)
Transport and Uptake of Inhaled Gases, In: Air Pollution, the Automobile, and Public Health. Eds. A.Y. Watson, R.R. Bates and D. Kennedy, National Academy Press, Washington D.C.,ISBN 0-309-03726-3, pp.323-366.

Wargocki, P., Clausen, G. and Fanger, P.O. (1996)
Field Study on Addition of Indoor Air Sensory Pollution Sources, Proceedings of Indoor Air ´96, The 7th International Conference on Indoor Air Quality and Climate, July 21 - 26, Nagoya, Japan, Vol. 4, pp. 307 - 312.

Wyon, D. and Sandberg, M. (1990)
Thermal Manikin Prediction of Discomfort due to Displacement Ventilation, ASHRAE Transaction 96, 1, 3307, pp.67-75.

Åstrand, P.-O. and Rodahl, K. (1986)
Textbook of Work Physiology - Physiological Bases of Exercise, McGraw-Hill, Inc., ISBN 0-07-100114-X.

Nomenclature

Symbols

c	Concentration (ppm or kg/kg or decipol)
c^*	Dimensionless concentration (c/c_R) (n.d.)
$\bar{c}$	Mean concentration in the room (ppm or kg/kg)
c_e	Personal exposure (ppm or kg/kg or decipol)
c_f	Concentration at the floor (ppm or kg/kg)
c_{oc}	Mean concentration in the occupied zone (ppm or kg/kg)
c_{out}	Perceived air quality of outdoor air (decipol)
c_p	Specific heat at constant pressure (J/kg°C)
c_P	Concentration at point P (ppm or kg/kg)
c_R	Concentration in return opening (ppm or kg/kg)
c_{st}	Average steady-state concentration in recirculation zone (ppm)
d	Difference (decipol)
$\bar{d}$	Average of differences (decipol)
f	Frequency of vortex shedding (s^{-1})
f_{cl}	Clothing area factor (n.d.)
f_{eff}	Effective radiation area factor (n.d.)
f_{res}	Frequency of respiration (min^{-1})
g	Gravitational acceleration (m/s^2)
h_c	Convective heat transfer coefficient ($W/m^2°C$)
h_{fg}	Heat of vaporisation of water (e.g. $2.43 \cdot 10^6$ J/kg)
h_r	Linear radiative heat transfer coefficient ($W/m^2°C$)
k	Thermal conductivity (W/m°C)
k	Turbulent kinetic energy (J/kg)
k_p	Turbulent kinetic energy at first grid node next to surface (J/kg)
$\dot{m}_e$	Dose rate of inhaled contaminant (kg/s)
m_{ed}	Dose of inhaled contaminant (kg)
$m_{p,sk}$	Permeance coefficient of the skin ($1.271 \cdot 10^{-9}$ kg/(m^2 s Pa))
$\dot{m}_r$	Exhaust air flow (m^3/s)
$\dot{m}_{res}$	Pulmonary ventilation rate (kg/s)
n	Air change rate (h^{-1})

n	Number of differences (n.d.)
p	Pressure (Pa or N/m^2)
p_a	Water vapour pressure in the ambient air (Pa)
p_s	Saturated water vapour pressure at skin surface (Pa)
q	Air flow rate (m^3/s or m^3/h or l/(s olf))
q_{out}	Ventilation rate of unpolluted air (m^3/s)
q_{st}	Air flow out of the recirculation zone (m^3/s)
r	Distance from exhaust opening (m)
s_d	Standard deviation (decipol)
s_{ij}	Strain rate of fluctuating flow (s^{-1})
t	Temperature (°C)
t^*	Dimensionless temperature $(t - t_0)/(t_R - t_0)$ (n.d.)
t_0	Supply air temperature (°C)
t_a	Ambient air temperature (°C)
t_{cl}	Mean temperature of outer surface of the clothed body (°C)
t_{ex}	Temperature of exhaled air (°C)
$\overline{t_r}$	Mean radiant temperature (°C)
t_{ref}	Reference temperature (°C)
t_R	Return air temperature (°C)
t_s	Skin temperature (°C)
u, v, w	Mean velocity components of the x, y and z direction (m/s)
u', v', w'	Fluctuating velocity components do. (m/s)
u_i	Mean velocity component of the i direction (m/s)
u_i'	Fluctuating velocity component of the i direction (m/s)
u_r	Velocity at distance r (m/s)
u_τ	Friction velocity (m/s)
u^+, v^+, w^+	Dimensionless velocity (n.d.)
w	Weight function (n.d.)
x, y, z, x_i	Co-ordinate directions (m)
x^+, y^+, z^+	Dimensionless distance to wall in x, y and z directions (n.d.)
y_e	Breathing zone height (m)
y_{oc}	Height of the occupied zone (m)
y_p	Distance from wall to first grid node adjacent to surface (m)
y_P	Vertical location of point P (m)
y_{st}	Stratification height (m)
A_{cl}	Clothed area (m^2)
A_{Du}	DuBois surface area (m^2)
A_{eff}	Effective radiation area (m^2)
A_{Ex}	Exhaust opening (m^2)

Ar	Archimedes number (n.d.), see equation (2.18)
B_i	Volume force in i direction (N/m^3)
C	Rate of convective heat transfer from skin (W/m^2)
C_{res}	Rate of convective heat loss from respiration (W/m^2)
D	Characteristic length (m)
D	Chest width of person (m)
D	Diffusivity (m^2/s)
D_{eff}	Effective diffusivity (m^2/s)
D_t	Turbulent diffusivity (m^2/s)
E_d	Latent heat loss by diffusion through the skin (W/m^2)
E_{res}	Rate of evaporative heat loss from respiration (W/m^2)
E_s	Latent heat loss (W/m^2)
E_{sk}	Rate of total evaporative heat loss from skin (W/m^2)
E_{sw}	Latent heat loss by sweating (W/m^2)
$F_{P\text{-}N}$	Angle factor between a person and surface N (n.d.)
G_{eq}	Source strength of ventilation equipment (olf)
G_k	Buoyancy term (J/m^3 s)
G_n	Pollution source strength regarding source no. n (olf)
Gr	Grashof number (n.d.), see equation (2.7)
H	Room height (m)
H	Height of cylinder or person (m)
I_a	Insulation of air layer around person (clo)
I_{cl}	Intrinsic (basic) clothing insulation (clo)
I_T	Total thermal insulation of clothing plus air layer (clo)
K	Rate of conductive heat transfer from skin (W/m^2)
L	Characteristic length (m)
M	Rate of metabolic heat produced (W/m^2)
Nu	Nusselt number (n.d.), see equation (2.6)
PD	Percentage of dissatisfied (%)
P_j	Jayatilleke´s sub-layer resistance function (n.d.)
P_k	Shear production term (J/m^3 s)
Pr	Prandtl number (laminar) (n.d.), see equation (2.8)
Pr	Probability (n.d.)
Q_m	Total heat loss from person (W/m^2)
Q_{res}	Total rate of heat loss through respiration (W/m^2)
Q_{sk}	Total rate of heat loss through skin (W/m^2)
Q_t	Sensible heat loss (W/m^2)
R	Rate of radiative heat transfer from skin (W/m^2)
R	Straight line distance between mouth and point source (m)
R_{cl}	Thermal resistance of clothing (m^2°C/W)

Re	Reynolds number (n.d.), see equation (2.11)
S	Source strength (m^3/s)
S	Strouhal number (n.d.), see equation (4.3)
S_{body}	Rate of storage in body (W/m^2)
S_c	Source term in concentration equation (kg of species/kg of air·s)
S_k	Source term in k equation (J/m^3 s)
S_{st}	Contaminant flow into the recirculation zone (m^3/s)
S_t	Source term in energy equation (W/m^3)
St	Stanton number (n.d.), see equation (2.54)
S_u	Source term in momentum equation (N/m^3)
S_ε	Source term in ε equation (J/m^3 s^2)
S_ϕ	Source term (general form)
T	Absolute temperature (K)
T_a	Absolute temperature of the ambient air (K)
T_N	Absolute surface temperature of surface N (K)
$\overline{T_r}$	Absolute mean radiant temperature (K)
T_s	Absolute skin temperature (K)
U	Characteristic velocity (m/s)
$\dot{V}_{res}$	Pulmonary ventilation (litre/min)
$\overline{V_T}$	Mean expired tidal volume (litre)
W	Rate of mechanical work accomplished (W/m^2)
W_a	Humidity ratio of exhaled air (kg H_2O/kg air)
W_e	Weight (kg)
W_{ex}	Humidity ratio of exhaled air (kg H_2O/kg air)
α	Thermal diffusivity (m^2/s)
β	Coefficient of cubic expansion / expansivity (1/K)
δ	Boundary layer thickness (m)
δ	True mean difference (decipol)
δ_{ij}	Kronecker delta (equals 1 for $i = j$ and equals 0 for $i \neq j$)
ε	Average emissivity of clothing and body area (n.d.)
ε	Rate of dissipation of turbulent kinetic energy (J/kg s)
$\overline{\varepsilon}$	Mean ventilation effectiveness (n.d.)
ε_e	Personal exposure index (n.d.)
$\varepsilon_{e,n}$	Personal exposure index regarding source no. n (n.d.)
ε_{oc}	Ventilation effectiveness in the occupied zone (n.d.)
ε_P	Local ventilation index (n.d.)
η_e	Effectiveness of entrainment in the human boundary layer (n.d.)

λ_{eff}	Effective conductivity (W/m°C)
λ_l	Laminar thermal conductivity (W/m°C)
λ_t	Turbulent conductivity (W/m°C)
μ_{eff}	Effective viscosity (kg/m s)
μ_l	Laminar dynamic viscosity (kg/m s)
μ_t	Turbulent viscosity (eddy viscosity) (kg/m s)
ν	Kinematic viscosity (m^2/s)
ν_t	Turbulent kinematic viscosity (m^2/s)
ρ	Density (kg/m^3)
σ	Stefan-Boltzmann constant ($5.669 \cdot 10^{-8}$ W/m^2K^4)
σ	Prandtl number (n.d.)
σ_c	Turbulent Schmidt number (n.d.)
σ_k	Turbulent Prandtl number for k (n.d.)
σ_ε	Turbulent Prandtl number for ε (n.d.)
σ_t	Turbulent Prandtl number (n.d.)
τ	Time (s)
τ_s	Start time (s)
τ_e	Stop time (s)
τ_w	Wall shear stress (Pa or N/m^2)
ϕ	Dependent variable (general form)
Γ_ϕ	Diffusion coefficient (general form)
$\Delta\tau$	Time step (s)
Φ	Heat load (W)
Φ_r	Radiative heat loss (W)

Constants

c_1	1.44 (n.d.)
c_2	1.92 (n.d.)
c_μ	0.09 (n.d.)
K_{res}	$2.58 \cdot 10^{-6}$ kg m^2/J
K_{res}'	0.1348 litre $m^2/(W\ min)$
σ_c	0.9 (n.d.)
σ_k	1.0 (n.d.)
σ_t	0.9 (n.d.)
σ_ε	1.3 (n.d.)

Abbreviations

n.d.	Non-dimensional
rh	Relative humidity
BTM	Breathing Thermal Manikin
CFD	Computational Fluid Dynamics
CSP	Computer Simulated Person
TSP	Trained Sensory Panel